UNIVERSITAT ROVIRA I VIRGILI

DIGGING INTO GOLD(I) CATALYSIS: SILVER AND COUNTERION EFFECTS AND TOTAL SYNTHESIS OF NARDOARISTOLONE B.

Anna Homs i Riba

Dipòsit Legal: T 1605-2015

ADVERTIMENT. L'accés als continguts d'aquesta tesi doctoral i la seva utilització ha de respectar els drets de la persona autora. Pot ser utilitzada per a consulta o estudi personal, així com en activitats o materials d'investigació i docència en els termes establerts a l'art. 32 del Text Refós de la Llei de Propietat Intel·lectual (RDL 1/1996). Per altres utilitzacions es requereix l'autorització prèvia i expressa de la persona autora. En qualsevol cas, en la utilització dels seus continguts caldrà indicar de forma clara el nom i cognoms de la persona autora i el títol de la tesi doctoral. No s'autoritza la seva reproducció o altres formes d'explotació efectuades amb finalitats de lucre ni la seva comunicació pública des d'un lloc aliè al servei TDX. Tampoc s'autoritza la presentació del seu contingut en una finestra o marc aliè a TDX (framing). Aquesta reserva de drets afecta tant als continguts de la tesi com als seus resums i índexs.

ADVERTENCIA. El acceso a los contenidos de esta tesis doctoral y su utilización debe respetar los derechos de la persona autora. Puede ser utilizada para consulta o estudio personal, así como en actividades o materiales de investigación y docencia en los términos establecidos en el art. 32 del Texto Refundido de la Ley de Propiedad Intelectual (RDL 1/1996). Para otros usos se requiere la autorización previa y expresa de la persona autora. En cualquier caso, en la utilización de sus contenidos se deberá indicar de forma clara el nombre y apellidos de la persona autora y el título de la tesis doctoral. No se autoriza su reproducción u otras formas de explotación efectuadas con fines lucrativos ni su comunicación pública desde un sitio ajeno al servicio TDR. Tampoco se autoriza la presentación de su contenido en una ventana o marco ajeno a TDR (framing). Esta reserva de derechos afecta tanto al contenido de la tesis como a sus resúmenes e índices.

WARNING. Access to the contents of this doctoral thesis and its use must respect the rights of the author. It can be used for reference or private study, as well as research and learning activities or materials in the terms established by the 32nd article of the Spanish Consolidated Copyright Act (RDL 1/1996). Express and previous authorization of the author is required for any other uses. In any case, when using its content, full name of the author and title of the thesis must be clearly indicated. Reproduction or other forms of for profit use or public communication from outside TDX service is not allowed. Presentation of its content in a window or frame external to TDX (framing) is not authorized either. These rights affect both the content of the thesis and its abstracts and indexes.

Anna Homs i Riba

Digging into Gold(I) Catalysis: Silver and Counterion Effects and Total Synthesis of Nardoaristolone B

DOCTORAL THESIS
Supervised by Prof. Antonio M. Echavarren

Institut Català d'Investigació Química (ICIQ)

UNIVERSITAT ROVIRA I VIRGILI

Tarragona 2015

UNIVERSITAT
ROVIRA I VIRGILI

DEPARTAMENT DE QUIMICA
ANALITICA
I QUIMICA ORGANICA

C/ Marcel.lí Domingo s/n
Campus Sescelades
43007 Tarragona
Tel. 34 977 55 97 69
Fax 34 977 55 84 46
e-mail: secqaqo@urv.net

ICIQ
Institut
Català
d'Investigació
Química

FAIG CONSTAR que aquest treball, titulat “Digging into Gold(I) Catalysis: Silver and Counterion Effects and Total Synthesis of Nardoaristolone B”, que presenta Anna Homs i Riba per a l’obtenció del títol de Doctor, ha estat realitzat sota la meva direcció a l'Institut Català d'Investigació Química i que acompleix els requeriments per poder optar a Menció Internacional.

Tarragona, 26 de novembre de 2014

El director de la tesi doctoral

Antonio M. Echavarren Pablos [

A la meva família i a l'Edu

En solitud, però no solitaris,
reconduïm la vida amb la certesa
que cap esforç no cau en terra eixorca.

Dia vindrà que algú beurà a mans plenes
l'aigua de llum que brolli de les pedres
d'aquest temps nou que ara esculpim nosaltres.

Miquel Martí i Pol

Aquesta tesi doctoral s'ha dut a terme a l'Institut Català d'Investigació Química i ha estat supervisada pel Prof. Antonio M. Echavarren, a qui agraeixo la confiança depositada en mi des del dia que vaig arribar. Així mateix, agraeixo totes les eines i idees que m'ha proporcionat per no deixar d'aprendre contínuament així com per haver-me concedit la beca predoctoral FPI (Formación de Profesorado Investigador, Ministerio de Economía y Competitividad). Part d'aquesta tesi ha estat finançada també per una beca predoctoral ICIQ.

During these four years I spend three-months in Prof. Jin-Quan Yu's lab at The Scripps Research Institute. Thanks for making me feel a member of the group since the day I arrived as well as all the trust in me.

Especial menció també a dos dels puntals del grup; Sònia Gavaldà i Imma Escofet. Sou l'eficiència personificada facilitant totes aquelles tasques que sovint no són gens senzilles amb el valor afegit de fer-ho sempre amb un somriure a la cara. Gràcies de tot cor. Looots of thanks to all the friends I had the pleasure to share the lab with; Yahui Wang (chinese tree), Pilar Calleja (molts ànims a aquesta recta final), Ana Escribano (gracias!), Dr. Michael E. Muratore (for taking over the project, proofreading the manuscript and for your tremendous patince!), Dr. Beatrice Ranieri (you could have started your Post-Doc a bit earlier, though!) and Elena de Orbe. Un gràcies gegantí i molt especial a la Carla Obradors (ja doctora un cop aquesta tesi estigui a l'impremta) i l'Imma Escofet (una altra vegada) amb qui he anat forjant una vertadera amistat dia rere dia i ha estat un plaer compartir aquests 4 i 3 anys, respectivament. Thanks to all the labmates in labs 2.2, 2.3 and 2.10 from 2010 to 2014: Masha Kirillova, Bart Herlé, Núria Huguet, Dr. Paul McGonigal, Dr. David Leboeuf, Zhouting Rong, Araceli Fernández, Laura Amenós, Katya Smirnova, Anthony Pitaval, Dr. Francesco Camponovo, Dr. Óscar de Pablo, Xiang Yin, Dr. Tania Jiménez, Dr. Javier Carreras, Dr. Laura López, Dr. Lorena Riesgo, Dr. Riccarda Miller, Morgane Gaydou, Sofía Ferrer, Ruth Dorel, Madeleine Livendhal, Cristina García, Dr. José M. Muñoz, Ismael Arroyo, Rogelio Solorio, Nicolas Delpont and Lourdes Maestre.

Agrair també a la unitat tècnica de l'ICIQ; espectrometria de masses, ressonància magnètica nuclear, unitat de cromatografia, unitat de cinètica i difracció de Raigs X. Gràcies també al David Pena per solucionar tots aquells problemes informàtics.

Very special thanks to (just Dr.) Asraa Ziadi, the best flatmate one can ever have. The only thing I regret is not moving together earlier (although we might not have slept that much then). Gràcies al David Bastida, al Dr. Toni Moragas i al Dr. Josep Cornellà (merci per les idees i suggeriments durant la tesi) per amenitzar els divendres sovint difícils de passar i per les estones a l'Azu (amb Barça o sense). A la Berta Camafort, Toni Bautista, Xacobe C. Cambeiro, Míriam Sau i a una llista interminable de gent que ha passat per l'ICIQ. Thanks to Dr. Xiaochen Wang (感谢校对), Dr. Navid Dastbaravardeh and Jian He from the Yu's lab for helping me at any time and discovering San Diego together. To Anish, Denis and the pack Ennio and Rita, my flatmates in the US. Lots of thanks to Dr. Christian Borch, who I hope to see very soon!

Gràcies als de la uni (grup "Mikiliterari..."), especialment a l'Àlex Espel, l'Eli Vilella i l'Albert de Aróstegui; perquè amb els seus sopars, viatges o Aplecs, plens d'ironia i sarcasme que tant m'agrada, hagin fet aquests 4 anys més planers. Merci als d'Igualada (o

Aranjuez) per no deixar de preguntar com em va tot. I a la Gemma Ferrer, a qui prometo trucar molt més sovint.

Agrair també al Toni Jorba i a la Glòria Marsal, qui m'ha alimentat durant més del 50% del doctorat. Gràcies a tota la meva immensa (en sentit literal i figurat) família; a l'àvia Quini i als avis Homs, per les seves visites fugaç a Tarragona que sempre acabaven amb un bon arròs. Gràcies al recolzament incondicional dels meus germans, que ha estat clau: a la Maria (i al David), qui no deixo d'admirar profundament cada dia que passa i de qui he intentat imitar el camí, al Pep, qui m'ha encomanat la seva energia desbordant i a la Marta, per fer-me sentir imprescindible (especialment els diumenges al vespre). Al Pep i Quim Mestres els quals de manera sorprenent i amb la seva curta edat, m'han fet tocar de peus a terra més que ningú. Gràcies al pare i a la mare; pel seu continu recolzament en totes les decisions que he pres; per creure i confiar en mi cegament facilitat-me al màxim totes les situacions. Amb vosaltres he après que si treballes, pots anar on vulguis. I finalment, gràcies a l'Edu, qui hauria estat guardonat amb el Nobel de la Paciència i Comprensió durant 4 anys (o potser 7) consecutius. Infinites gràcies per tot.

ICIQ
Institut
Català
d'Investigació
Química

erc
European Research Council
Established by the European Commission

AGAUR
Agència
de Gestió
d'Ajuts
Universitaris
i de Recerca

GOBIERNO
DE ESPAÑA
MINISTERIO
DE ECONOMÍA
Y COMPETITIVIDAD

EXCELENCIA
SEVERO
OCHOA

At the moment of writing this thesis, the results presented herein have been published in:

On the Silver Effect and the Formation of Chloride-Bridged Digold Complexes
Anna Homs, Imma Escofet, Antonio M. Echavarren
Org. Lett. **2013**, *15*, 5782–5785.

Dissecting Anion Effects on Gold(I)-Catalyzed Intermolecular Cycloaddtions
Anna Homs,[+] Carla Obradors,[+] David Leboeuf, Antonio M. Echavarren
Adv. Synth. Catal. **2014**, *356*, 221–228.
[+] These two authors contributed equally to the work.

Meeting the Challenge of Intermolecular Gold(I)-Catalyzed Cycloadditions of Alkynes and Allenes (review)
Michael E. Muratore, Anna Homs, Carla Obradors, Antonio M. Echavarren
Chem. Asian J. **2014**, *9*, 3066–3082.

Enantioselective Total Synthesis of (–)-Nardoaristolone B *via* a Gold(I)-Catalyzed Oxidative Cyclization
Anna Homs,[+] Michal E. Muratore,[+] Antonio M. Echavarren
Org. Lett. **2015**, DOI: 10.1021/ol503531n.
[+] These two authors contributed equally to the work.

Other publications not related to the topic covered in the manuscript are presented below:

Gold for the Generation and Control of Fluxional Barbaralyl Cations
Paul R. McGonigal, Claudia de León, Yahui Wang, Anna Homs, César R. Solorio-Alvarado, Antonio M. Echavarren
Angew. Chem. Int. Ed. **2012**, *51*, 13093–13096.

Mechanistic Aspects of Metal-Catalyzed C,C– and C,X–Bond-Forming Reactions, Chapter 1 in: Metal-Catalyzed Cross-Coupling Reactions and More (DeMeijere; Braese; Oestreich, Eds.) (book chapter)
Antonio M. Echavarren, Anna Homs
Wiley-VCH. **2013**, *1*, 1–64.

Palladium-Catalyzed *ortho*-Selective C–H Deuteration of Arenes: Evidence for Superior Reactivity of Weakly Coordinated Palladacycles
Sandy Ma, Giorgio Villa, Peter S. Thuy-Boun, Anna Homs, Jin-Quan Yu
Angew. Chem. Int. Ed. **2014**, *53*, 734–737.

Ligand-Controlled $C(sp^3)$–H Arylation and Olefination: Synthesis of Novel Chiral α-Amino Acids
Jian He, Suhua Li, Youqian Deng, Haiyan Fu, Brian N. Laforteza, Jillian E. Spangler, Anna Homs, Jin-Quan Yu
Science **2014**, *343*, 1216–1220.

Table of Contents

Prologue 21

List of Abbreviations and Acronyms 23

General Introduction

- Gold as Catalyst 27
- Activation of Gold(I) Complexes to π-Bonds 28
- Nucleophilic Attack 29
- Cycloisomerization of 1,n-Enynes 30
- Nature of Cycloproppyl Gold(I) Carbenes 32
- Gold(I)-Catalyzed Oxidative Cyclizations 34

1. On the Silver Effect and the Formation of Chloride-Bridged Digold Complexes

Introduction 41
- Synthesis of Gold(I) Complexes 41
- Effect of Silver in Gold(I) Catalysis 44
  - "Genuine" Au Catalysis 45
  - Au/Ag Bimetallic Catalysis 46
  - Ag-Assisted Au Catalysis 46

Objectives 48

Results and Discussion 49
- JohnPhosAuCl and AgX in a Non-coordinating Solvents (X = OTf, NTf_2, BF_4, SbF_6) 50
- Relevance of Digoldhalide Cation 56
  - JohnPhosAuCl and AgX with Phenylacetylene 56
  - JohnPhosAuCl and AgX in the [2+2] Intermolecular Cycloaddition Reaction 59
  - JohnPhosAuCl and AgX in the [2+2] Intramolecular Cycloaddition Reaction 60
  - JohnPhosAuCl and AgX in the [4+2] Cycloaddition of Arylenyne **21** 61

Outlook 64

Simultaneous Findings and Further Studies 65

Conclusions 67

Experimental Part 68
- General Information 68
- Synthesis of Mononuclear Gold(I) Complexes 68
- Synthesis of Dinuclear Gold(I) Complexes 70

Synthesis of σ-Mononuclear Gold(I) Complex **F** 74
Synthesis of σ,π-Mononuclear Gold(I) Complex **G** 74
General procedures for Gold(I)-Catalyzed Reactions 76
    [2+2] Intermolecular Cycloaddition of Phenylacetylene and α-Methylstyrene 76
    [2+2] Intramolecular Cycloaddition of 1,6-Enyne **19** 77
    [4+2] Intramolecular Cycloaddition of 1,6-Enyne **21** 78
    X-Ray Tables 80

2. Anion Effects in Intermolecular Gold(I)-Catalyzed Reactions: Use of BAr_4^{F-}

Introduction 117
    Gold(I)-Catalyzed Intermolecular Reactions with Alkynes 117
    Anion Effects in Gold(I)-Catalyzed Reactions 121
    Ion Pairing in Gold(I) Complexes 123
Objectives 124
Results and Discussion 125
    Reactivity of Complex **A2** in Intermolecular Gold(I)-Catalyzed Reactions 125
    Monitoring the [2+2] Cycloadditon Reaction and DFT Modeling 130
    Mechanistic Studies 132
        Order of Reagents 133
        Species Formed in the Reaction Mixture: Counterion Differences 135
        Equilibrium Constants 138
        Formation of σ,π-Digold(I) Complex 140
Conclusions 144
Experimental Part 145
    General Information 145
    Synthesis of Gold(I) Complexes 145
    General Procedure for the Preparation of Cyclobutenes 148
    General Procedure for the Preparation of [3.2.1]-Oxabicycles 151
    General Procedure for the Preparation of Phenols 151
    Monitoring the [2+2] Cycloaddition Reaction 151
    Electrondensity Surfaces 152
    Mechanistic Studies 152
        Order of Reagents 152
        Species Formed in the Reaction Mixture 154
        Additional Experiments 155
        Equilibrium Constants 158

3. Total Synthesis of Nardoaristolone B and an Approach to the Synthesis of (–)-Aristolone and Kanshone H

Introduction 165

Nardoaristolone B 165
(–)-Aristolone 168
Gold(I) Catalysis in Total Synthesis 171
Gold(I)-Catalyzed Oxidative Cyclization of Enynes 173

Objectives 176

Results and Discussion 177
Synthesis of Trialkylated Ketone **42** 178
One-step dialkylation reaction 178
Two or three-steps dialkylation reaction 182
Synthesis of 1,5-Enyne Towards Nardoaristolone B 186
Gold(I)-Catalyzed Cyclization to Access to Nardoaristolone B 187
Allylic Oxidation: Nardoaristolone B 189
Approach to the Synthesis of (–)-Aristolone and Kanshone H: Synthesis of 1,6-Enyne 190
Propargylation and Regioselective Elimination 190
Homologation 191
Horner-Wadsworth-Emmons Reaction 192
Vinyl Bromide Formation and Propargylation 193
Shapiro Reaction and Propargylation 194
Triflation and Cross Coupling 195
Gold(I)-Catalyzed Cyclization to Access to (–)-Aristolone and Kanshone H 201

Outlook 203
Use of Bicyclic Ketone **56** 203
Use of 1,6-Enyne **43** 203

Conclusions 205

Experimental Part 207
General Information 207
Synthesis of Substrates 207

Prologue

This thesis has been divided into four main parts: a general introduction in gold(I)-catalysis and three research chapters. Each chapter contains five sections including a brief and detailed introduction on the research topic, the objectives, the discussion of the results obtained followed by the conclusions and the experimental part.

The general introduction provides the basic principles of homogeneous gold(I) catalysis including the activation of alkynes as well as the basic principles of cyloisomerization of enynes and oxidative gold(I)-catalyzed cyclizations.

In the first research chapter, the so-called "silver effect" in gold(I)-catalyzed reactions has been studied. This work has been done in collaboration with Imma Escofet and thus, for coherency, some of her results have been included. This work was published in *Org. Lett.* **2013**, *15*, 5782–5785.

The second chapter includes the design of a new generation of gold(I)-complexes containing BAr_4^{F-} as counterion, which show better efficiency in intermolecular gold(I)-catalyzed reactions. An extensive mechanistic study on the [2+2] cycloaddition of alkynes and alkenes is exposed. This project was done in collaboration with Carla Obradors and Dr. David Leboeuf and some of their results are also included. The entirely of this work was published in *Adv. Synth. Catal.* **2014**, *356*, 221–228, and some of the most relevant results obtained were highlighted in *Chem. Asian J.* **2014**, *9*, 3066–3082.

The last chapter presents the total synthesis of nardoaristolone B and an approach towards the synthesis of (–)-aristolone and kanshone H, featuring an oxidative gold(I)-catalyzed cyclization as the key step. Dr. Michael Muratore joined me in the project optimizing different reaction conditions. The manuscript summarizing these results has been accepted in *Org. Lett.* **2015**, DOI: 10.1021/ol503531n.

List of Abbreviations and Acronyms

In this manuscript, the abbreviations and acronyms most commonly used in organic and organometallic chemistry have been used following the recommendations of "Guidelines for authors" of *Journal of Organic Chemistry*.

Additional abbreviations and acronyms used in this manuscript are referenced in the list below:

app	Apparent
ATPH	Aluminium tris(2,6-diphenylphenoxide)
BAr_4^{F-}	Tetrakis [3,5-bis(trifluoromethyl)phenylborate]
DA	Diels-Alder
DAD	Diode array detector
dppe	1,2-Bis(diphenylphosphino)ethane
dppf	1,1'-Bis(diphenylphosphino)ferrocene
dppp	1,3-Bis(diphenylphosphino)propane
ESP	Electrostatic potential
GOESY	Gradient enhanced nuclear Overhauser effect spectroscopy
Tf_3H	Tris(trifluoromethyl)sulfonyl)methane
IBX	2-Iodoxybenzoic acid
IMes	1,3-Bis(2,6-diisopropylphenyl)imidazol-2-ylidene
IPr	1,3-Bis(2,4,6-trimethylphenyl)imidazol-2-ylidene
IRMDS	Infrared multiphoton dissociation spectrospray
JohnPhos	(2-Biphenyl)di-*tert*-butylphosphine
NTf_2^-	Bis(trifluoromethyl)imidate
p-TsOH	*para*-Toluene sulfonic acid
SPhos	2-Dicyclohexylphosphino-2',6'-dimethoxybiphenyl
t-BuXPhos	2-(di-*tert*-Butylphosphino)-2',4',6'-triisopropyl-1,1'-biphenyl
tht	Tetrahydrothiophene
tmbn	Trimethoxybenzonitrile
VWD	Variable wavelength detector

General Introduction

Gold As Catalyst

For centuries, gold was considered to be a catalytically inactive metal. Although some gold-catalyzed transformations were discovered around the 70s and 80s,[1] it was not until 1998 that a groundbreaking report was disclosed by the group of Teles describing the first practical gold(I)-catalyzed addition of alcohols to alkynes under mild conditions to form acetals (Scheme 1).[2]

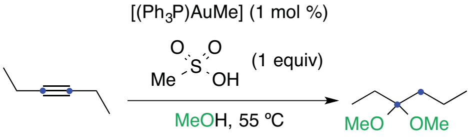

Scheme 1 First practical gold(I)-catalyzed transformation.

Ever since, the use of gold in metal catalysis has grown exponentially. This is mainly due to the high affinity of gold(I) towards π-bonds. This ability to coordinate to unsaturations is rationalized by the so-called relativistic effects.[3] Relativistic effects correspond to the acceleration of the electrons as they orbit closer to a heavy nucleus. As a consequence, the mass of the electron increases whilst the *s* and *p* orbitals are contracted. Indirectly, this implies that the electrons occupying the *d* and *f* orbitals manifest a weaker nuclear attraction. This contraction/expansion phenomenon is significant for metals that have their 4*f* and 5*d* orbitals filled, such as Pt, Au and Hg. In particular, the relativistic effect is maximum for the gold nucleus and hence the contraction of the 6*s* orbital reaches a maximum. Thus, this contraction for gold is significantly more important than for other transition metals.[4] This leads to a substantial expansion of the 5*d* orbitals, minimizing the electron-electron repulsion.

By extension, the Au–L bond is contracted and therefore, the nature of the resulting complexes can be easily modulated by the electronic and steric properties of the ligand used. Gold(I) complexes containing phosphite ligands are much more electrophilic than those bonded to N-heterocyclic carbenes (Figure 1). When bearing phosphines, gold(I) complexes show intermediate electrophilicity. Recently, chiral ligands have been used to induce enantioselectivity in gold(I)-catalyzed reactions.[5]

---

[1] (a) Bond, G. C.; Sermon, P. A.; Webb, G.; Buchanan, D. A.; Wells, P. B. *J. Chem. Soc., Chem. Commun.* **1973**, 444–445. (b) Haruta, M.; Kobayashi, T.; Sano, H.; Yamada, N. *Chem. Lett.* **1987**, *16*, 405–408. (c) Hutchings, G. J. *J. Catal.* **1985**, *96*, 292–295. (d) Ito, Y.; Sawamura, M.; Hayashi, T. *J. Am. Chem. Soc.* **1986**, *108*, 6505–6406. (e) Fukuda, Y.; Utimoto, K. *J. Org. Chem.* **1991**, *56*, 3729–3731.

[2] Teles, H.; Brode, S.; Chabanas, M. *Angew. Chem. Int. Ed.* **1998**, *37*, 1415–1418.

[3] (a) Pyykkö, P. *Angew. Chem. Int. Ed.* **2002**, *41*, 3573–3578. (b) Pyykkö, P. *Angew. Chem. Int. Ed.* **2004**, *43*, 4412–4456. (c) Schwarz, H. *Angew. Chem. Int. Ed.* **2003**, *42*, 4442–4445.

[4] Gorin, D.J.; Toste, F. D. *Nature* **2007**, *446*, 395–403.

[5] For selected reviews see: (a) Widenhoefer, R. A. *Chem.–Eur. J.* **2008**, *14*, 5382–5391. (b) Patil, T. *Chem.–Asian J.* **2012**, *7*, 2186–2194. (c) Wang, Y.-M.; Lackner, A. D.; Toste, F. D. *Acc. Chem. Res.* **2014**, *47,* 889–901 and references therein. (d) Huguet, N.; Echavarren, A. M. Asymmetric Synthesis II, Christman, M.; Bräse, S. Eds. Chapter 26, **2012**, 135–152. Wiley-VCH Verlag GmbH & Co. (e) De Mendoza, P.; Echavarren, A. M. Modern Gold Catalyzed Synthesis, Hashmi, A. S. K.; Toste, F. D. Eds. Chapter 5, **2012**, 205–212. Wiley-VCH Verlag GmbH & Co.

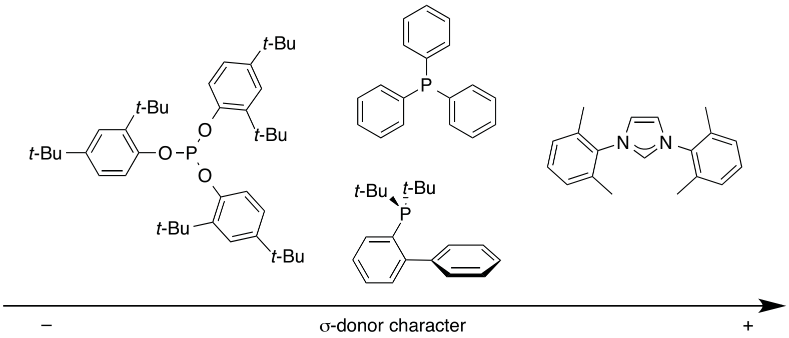

Figure 1 Common ligands used in gold(I) complexes.

The small differences in energy gap between the *s*, *p* or *d* orbitals enhance the *s*/*d* or *s*/*p* hybridizations, which explain the tendency of gold(I) to form linear two-coordinated complexes.[6] Gold(I) complexes are also reluctant to undergo spontaneous oxidative addition or β-hydride elimination.[7]

Gold(III) complexes (or simple gold(III) salts such as $NaAuCl_4$ and $AuCl_3$) are also known to be catalytically active and present a square planar geometry. However, they can be easily reduced to Au(I) and Au(0) by oxidizable substrates.

Activation of π-Bonds with Gold(I) Complexes

The activation of alkynes can be rationalized by the Dewar-Chatt-Duncanson model, which considers the bond as a donor-acceptor interaction between two closed-shell fragments.[8] Thus, the metal-acetylene bonding is described as a combination of a σ-interaction (interaction of the π-bond of the alkyne with the empty orbital on the metal) and a back-bonding π-interaction (donation of the metal to the π* orbitals of the alkyne) (Figure 2).

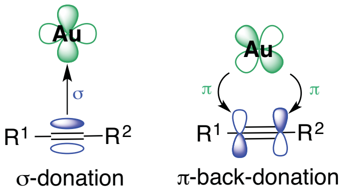

Figure 2 Deward-Chatt Duncanson model.

---

[6] Gimeno, M. C.; Laguna, A. *Chem. Rev.* **1997**, *97*, 511–522.

[7] (a) Lauterbach, T.; Livendahl, M.; Rosellón, A.; Espinet, P.; Echavarren, A. M. *Org. Lett.* **2010**, *12*, 3006–3009. (b) Livendahl, M.; Goehry, C.; Maseras, F.; Echavarren, A. M. *Chem. Commun.* **2014**, *50*, 1533–1536. For oxidative addition of Au(I) complexes, the use of an special system or ligand is required: (c) Guenther, J.; Mallet-Ladeira, S.; Estevez, L.; Miqueu, K.; Amgoune, A.; Bourissou, D. *J. Am. Chem. Soc.* **2014**, *136*, 1778–1781. (d) Joost, M.; Zeineddine, A.; Estévez, L.; Mallet−Ladeira, S.; Miqueu, K.; Amgoune, A.; Bourissou, D. *J. Am. Chem. Soc.* **2014**, *134*, 14654–14657

[8] (a) Dewar, M. J. S. *Bull. Soc. Chim. Fr.* **1951**, *18*, C71–C79. (b) Chatt, J.; Duncanson, L. A. *J. Chem. Soc.* **1953**, 2939–2947.

To gain further insight, several groups have estimated the contributions of these interactions using computational methods.[9] As a conclusion, alkynes are strong two-electron σ-donors but rather weak π-acceptors towards gold(I), although some back-bonding occurs.

Structurally, different η^2-alkyne Au(I) complexes have been characterized by NMR techniques and X-ray diffraction.[9c,10] The metal coordinates symmetrically (e. g. at equal distance of both alkyne carbons) even if the enyne used is not symmetrical (Au–C distances 2.238 and 2.239). However, there is a deviation from linearity, and the ≡C–*t*-Bu and ≡C–Me are bent away from the gold-phosphine fragment (165.6° and 168.1° respectively) substituents (Figure 3).

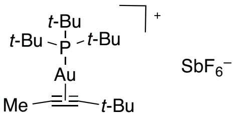

Figure 3 Structure of (η^2-4,4-dimethylpent-2-yne)AuLX. [L = P(*t*-Bu)$_3$ and X = SbF_6^-].

Gold also forms mononuclear two-coordinate π-complexes with alkenes, 1,3-dienes and allenes.[11]

Nucleophilic Attack

The aforementioned interactions result in a transfer of electron density of the unsaturation to the metal turning the resulting metal-alkyne complex into very electrophilic species. Thenceforth, the corresponding η^2-alkyne Au(I) complexes **I** can be attacked in general in an *anti* fashion by a wide range of nucleophiles giving rise to *trans*-alkenyl species **II** (Scheme 2). The *syn* insertion of methyl propiolate into Au–Si bonds has recently been disclosed.[12]

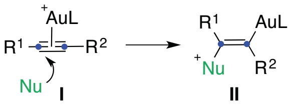

Scheme 2 Formation of *trans*-alkenyl gold(I) species **II** from η^2-alkyne Au(I) complexes **I**.

Different carbon and heteroatom-containing molecules (including arenes,[13] heteroarenes,[14] amines,[15] imines,[16] sulfoxides,[17] *N*-oxides[18] and thiols[19]) have been used as nucleophilic partners in either intra- or intermolecular gold(I) catalyzed reactions. In particular, our group has been mainly focused on the use of alkenes as nucleophiles either intra- or intermolecularly.[20]

---

[9] For selected examples see: (a) Hertwig, R. A.; Koch, W.; Schröder, D.; Schwarz, H.; Hrusak, J.; Schwerdtfeger, P. *J. Phys. Chem.* **1996**, *100*, 12253–12260. (b) Nechaev, M. S.; Rayón, V. M.; Frenking, G. *J. Phys. Chem. A* **2004**, *108*, 3134–3142. (c) Shapiro, N. D.; Toste, F. D. *Proc. Natl. Acad. Sci. U.S.A.* **2007**, *104*, 43569–13573.

[10] For selected examples see: (a) Flügge, S.; Anoop, A.; Goddard, R.; Thiel, W.; Fürstner, A. *Chem.–Eur. J.* **2009**, *15*, 8558–8565. (b) Hooper, N.; Green, M.; Russell, C. A. *Chem. Commun.* **2010**, *46*, 2313–2315. (c) Brown, T. J.; Widenhoefer, R. A. *J. Organomet. Chem.* **2011**, *696*, 1216–1220. (d) Brown, T. J.; Widenhoefer, R. A. *Organometallics*, **2011**, *30*, 6003–6009.

[11] Obradors, C.; Echavarren, A. M. *Chem. Commun.* **2010**, *46*, 2313–2315.

[12] Joost, M.; Gualco, P.; Mallet-Ladeira, S.; Amgoune, A.; Bourissou, D. *Angew. Chem. Int. Ed.* **2013**, *52*, 7160–7163

[13] (a) Hashmi, A. S. K; Haufe, P.; Schmid, C.; Rivas Nass, A.; Frey, W. *Chem.–Eur. J.* **2006**, *12*, 5376–5382. (b) Ferrer C.; Echavarren, A. M. *Angew. Chem. Int. Ed.* **2006**, *45*, 1105–1109.

Cycloisomerization of 1,n-Enynes

Gold(I) complexes do not coordinate selectively to alkynes over alkenes.[21] However, the addition occurs exclusively to the η^2-alkyne Au(I) complexes since it presents a lower LUMO than its alkene analogue. Thus, after coordination of the metal to the alkyne, the reaction with the alkene takes place forming the proposed cyclopropyl gold(I) carbene-like intermediates **IV** and **IX** deriving from an *anti*-5-*exo*-dig cyclization or a 6-*endo*-dig cyclization (Scheme 3). The nature of these intermediates is determined by the substitution pattern of the alkyne or alkene moieties as well as the ligand used.

Cyclopropyl gold(I) carbene intermediates **IV** (*exo*) can further rearrange forming 1,3-dienes **VI** through a process known as a single cleavage rearrangement in which the external carbon of the alkene moiety migrates to the terminal carbon of the alkyne. A double cleavage rearrangement can also take place, resulting in the formal insertion of the terminal alkene carbon into the alkyne (**VII**). A final α-proton elimination of the carbene formed **VII** gives rise to 1,3-enyne **VIII**. Bicyclo[4.1.0]hept-2-ene substrates **X** can also be obtained by an α-proton elimination of the cyclopropyl gold(I) intermediate **IX** followed by protodeauration.[22] However, **IX** can also rearrange to **XI**, which upon protodemetalation affords **XII**. Although these strained bicyclic structures have been isolated in few cases in the cycloisomerization of 1,6-enynes,[23] they are more common

---

[14] (a) Mizushima, E.; Sato, K.; Hayashi, T.; Tanaka, M. *Angew. Chem. Int. Ed.* **2002**, *41*, 4563–4565. (b) Krauter, C. M.; Hashmi A. S. K.; Pernpointner, M. *ChemCatChem* **2010**, *2*, 1226–1230.

[15] (a) Istrate, F. M.; Gagosz, F. *Org. Lett.* **2007**, *9*, 3181–3184. (b) Qian, J.; Liu, Y.; Cui, J.; Xu, Z. *J. Org. Chem.* **2012**, *77*, 4484–4490.

[16] (a) Kusama, H.; Miyashita, Y.; Takay, J.; Iwasawa, N. *Org. Lett.* **2006**, *8*, 289–292. (b) Benedetti, E.; Lemière, G.; Chapellet, L. L.; Penoni, A.; Palmisano, G.; Malacria, M.; Goddard, J. P.; Fensterbank, L. *Org. Lett.* **2010**, *12*, 4396–4399.

[17] (a) Shapiro, N. D.; Toste, F. D. *J. Am. Chem. Soc.* **2007**, *129*, 4160–4161. (b) Davies, P. W.; Albrecht, S. J. C. *Angew. Chem. Int. Ed.* **2009**, *48*, 8372–8375. (c) Shi, S.; Wang, T.; Yang, W.; Rudolph, M.; Hashmi, A. S. K. *Chem.–Eur. J.* **2013**, *19*, 6576–6580.

[18] Ye, L.; Cui, L.; Zhang, G.; Zhang, L. *J. Am. Chem. Soc.* **2010**, *132*, 3258–3259.

[19] (a) Nakamura, I.; Sato, T.; Yamamoto, Y. *Angew. Chem. Int. Ed.* **2006**, *45*, 4473–4475. (b) Nakamura, I.; Sato, T.; Terada, M.; Yamamoto, Y. *Org. Lett.* **2007**, *9*, 4081–4083.

[20] (a) Jiménez-Núñez, E.; Echavarren, A. M. *Chem. Rev.* **2008**, *108*, 3326–3350. (b) Obradors, C.; Echavarren, A. M. *Acc. Chem. Res.* **2014**, *47*, 902–912.

[21] García-Mota, M.; Cabello, N.; Maseras, F.; Echavarren, A. M.; Pérez-Ramírez, J.; López, N. *ChemPhysChem* **2008**, *9*, 1624–1629.

[22] (a) Nieto-Oberhuber, C.; López, S.; Echavarren, A. M. *J. Am. Chem. Soc.* **2005**, *127*, 6178–6179. (b) Nieto-Oberhuber, C.; Muñoz, M. P.; López, S.; Jiménez-Núñez, E.; Nevado, C.; Herrero-Gómez, E.; Raducan, M.; Echavarren, A. M. *Chem.–Eur. J.* **2006**, *12*, 1677–1693. (c) Nieto-Oberhuber, C.; Pérez-Galán, P.; Herrero-Gómez, E.; Lauterbach, T.; Rodríguez, C.; López, S.; Bour, C.; Rosellón, A.; Cárdenas, D. J.; Echavarren, A. M. *J. Am. Chem. Soc.* **2008**, *130*, 269–279. (d) Lee, Y. T.; Kang, Y. K.; Chung, Y. K. *J. Org. Chem.* **2009**, *74*, 7922–7934.

[23] (a) Lee, S. I.; Kim, S. M.; Choi, M. R.; Kim, S. Y.; Chung, Y. K. *J. Org. Chem.* **2006**, *71*, 9366–9372. (b) Escribano-Cuesta, A.; Pérez-Galán, P.; Herrero-Gómez, E.; Sekine, M.; Braga, A. A. C.; Maseras, F.; Echavarren, A. M. *Org. Biomol. Chem.* **2012**, *10*, 6105–6111. (c) Brooner, R. E. M.; Brown, T. J.; Widenhoefer, R. A. *Angew. Chem. Int. Ed.* **2013**, *52*, 6259–6261. For DFT calculations see: (d) Nieto-Oberhuber, C.; López, S.; Muñoz, M. P.; Cárdenas, D. J.; Buñuel, E.; Nevado, C.; Echavarren, A. M. *Angew. Chem. Int. Ed.* **2005**, *44*, 6146–6148.

products in the cyclization of higher 1,n-enynes (n ≥ 7).[23c,23d,24] Interestingly, cyclobutenes are obtained in the intermolecular reaction between alkynes and alkenes.[25] Isomerization and demetalation of **XI** gives rise to **XIII**.[22a] Interestingly, the product of a single cleavage rearrangement **VI** can also originate from the ring opening of **XI**. 1,5-[26] and 1,7-enynes[23d,27] follow a very similar reactivity trend as the one observed for 1,6-enynes.

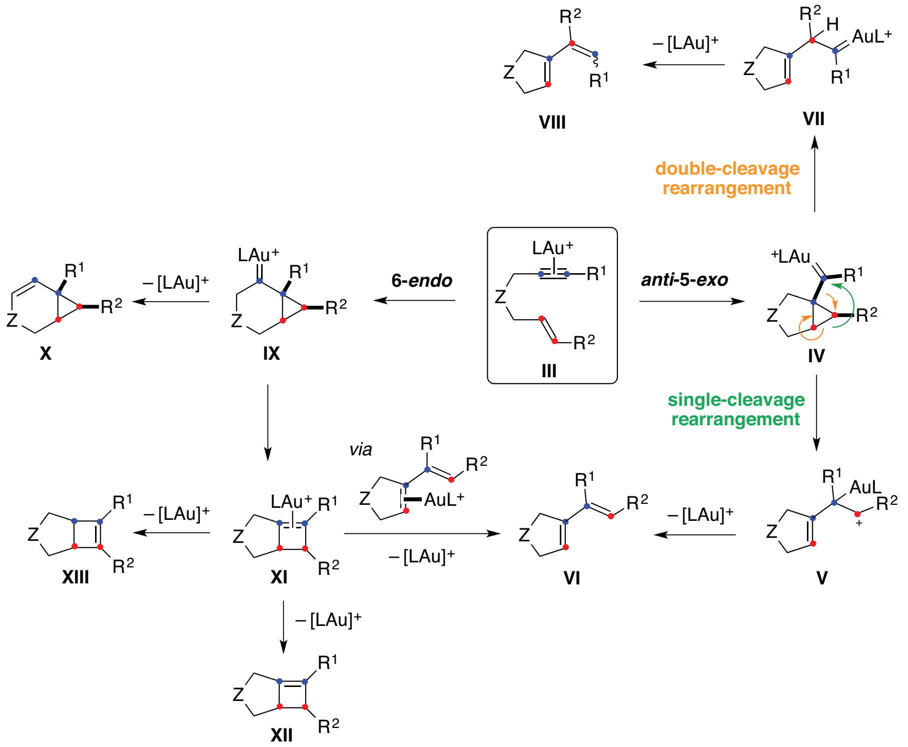

Scheme 3 Gold(I)-catalyzed cyclosiomerization of 1,6-enynes.

These transformations have been widely explored because of the diversity of the products that are formed.[20] Indeed, in the presence of other nucleophiles (e.g. alcohols or water) the resulting cyclopropyl gold(I) carbene can be further attacked giving products of alkoxy- or heterocyclization.[22b,28] On the other hand, when the alkyne is substituted with an aryl ring, a formal [4+2] cycloaddition reaction takes place, giving rise to tricyclic products **XVIII** (Scheme 4).[22a] Once the cyclopropyl gold(I) carbene **XV** is formed, a Friedel–Crafts-type

---

[24] (a) Odabachian, Y.; Gagosz, F. *Adv. Synth. Catal.* **2009**, *351*, 379–386. (b) Obradors, C.; Leboeuf, D.; Aydin, J.; Echavarren, A. M. *Org. Lett.* **2013**, *15*, 1576–1579.

[25] López-Carrillo, V.; Echavarren, A. M. *J. Am. Chem. Soc.* **2010**, *132*, 9292–9294.

[26] (a) Zhang, L.; Kozmin, S. *J. Am. Chem. Soc.* **2004**, *126*, 11806–11807. (b) Sun, J.; Conley, M.; Zhang, L.; Kozmin, S. *J. Am. Chem. Soc.* **2006**, *128*, 9705–9710. (c) López-Carrillo, V.; Huguet, N.; Mosquera, Á.; Echavarren, A. M. *Chem.–Eur. J.* **2011**, *17*, 10972–10978.

[27] Cabello, N.; Rodríguez, C.; Echavarren, A. M. *Synlett* **2007**, 1753–1758.

[28] For some examples in gold(I)-catalyzed intramolecular reactions: (a) Fürstner, A.; Morency, L. *Angew. Chem. Int. Ed.* **2008**, *47*, 5030–5033. (b) Zhang, L.; Kozmin, S. A. *J. Am. Chem. Soc.* **2005**, *127*, 6962–6963. For some examples in gold(I)-catalyzed intermolecular reactions: (c) Chao, C.-M.; Toullec, P. Y.; Michelet, V. *Tetrahedron Lett.* **2009**, *50*, 3719–3722. (d) Buzas, A. K.; Istrate, F. M.; Gagosz, F. *Angew. Chem. Int. Ed.* **2007**, *46*, 1141–1144.

reaction takes place giving **XVI**. Final aromatization and protodemetalation give access to tricyclic products **XVIII**.

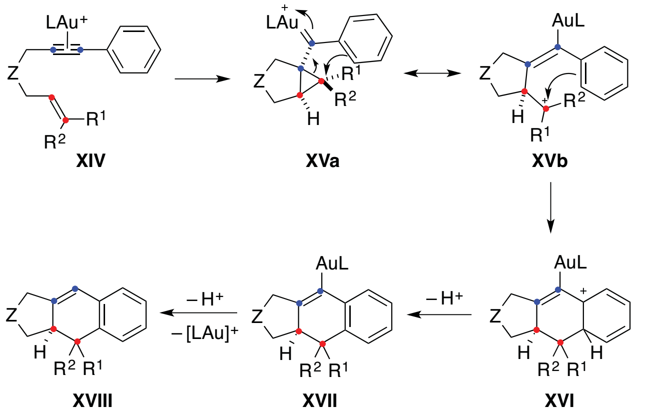

Scheme 4 Proposed mechanism for the formal [4+2] cycloaddition reaction of 1,6-enynes bearing an arene at the alkyne moiety.

Nature of cyclopropyl gold(I) carbenes

The proposed cyclopropyl gold(I) carbene species are highly distorted structures and can also be represented as cyclopropyl gold-stabilized homoallylic carbocations (**XIX**). DFT calculations have proved that the more cationic or carbenic character depends on the substitution pattern of the enyne as well as the nature of the ligand.[23d,29] Therefore, if R = H or Me, the best representation of the intermediate is **XIXc** (longest bond is **b**), whereas for R = cyclopropyl it is the carbocationic form **XIXb** (Table 1).

Table 1 Bond distances for cyclopropyl gold carbene determined by DFT.

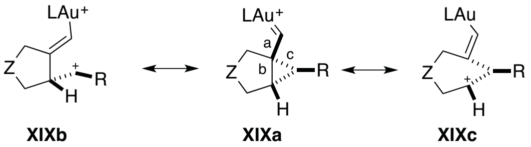

R	a	b	c
H	1.378	1.742	1.569
Me	1.372	1.720	1.622
cyclopropyl	1.356	1.586	1.987

An example of this dualism was observed in the single-cleavage rearrangement of enynes **1** and **2**, which was found to be a non-stereospecific process (Scheme 5). Both *E* and *Z* isomers generated the same product.[30]

---

[29] (a) Cabello, N.; Jiménez-Núñez, E.; Buñuel, E.; Cárdenas, D. J.; Echavarren, A. M. *Eur. J. Org. Chem.* **2007**, 4217–4223. (b) Seidel, G.; Mynott, R.; Fürstner, A. *Angew. Chem. Int. Ed.* **2009**, *48*, 2510–2513. (c) Pérez-Galán, P.; Martin, N. J. A.; Campaña, A. G.; Cárdenas, D. J.; Echavarren, A. M. *Chem. Asian. J.* **2011**, *6*, 482–486.

[30] Jiménez-Núñez, E.; Claverie, C. K.; Bour, C.; Cárdenas, D. J.; Echavarren, A. M. *Angew. Chem. Int. Ed.* **2008**, *47*, 7892–7895.

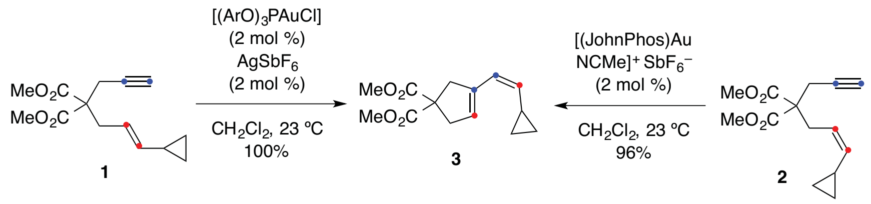

Scheme 5 *Cis*-selective single-cleavage rearrangements of **1** and **2**.

Another example that highlights how the carbenic or cationic character of the intermediate gold(I) species formed can be tuned is the addition of indoles onto 1,6-enynes, which gives products **5** and **6** in different ratios depending on the ligand (Scheme 6).[31] The use of electron donating NHC ligands enhances the carbene-like nature of the intermediate **XX**. Thus, the nucleophilic attack takes place at the carbenic carbon giving **5** as the major product, which corresponds to the trapping of the gold(I) carbene-like intermediate with an indole. On the other hand, using [(JohnPhos)AuNCMe]SbF$_6$ as catalyst favors the attack of the indole at the carbocation-like intermediate.

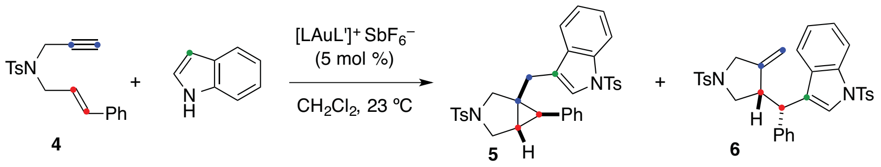

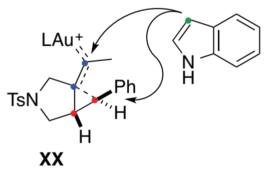

[LAuL']	5:6 (yield)
[(IPr)AuNCPh]	75:25 (57%)
[(JohnPhos)AuNCMe]	20:80 (74%)

Scheme 6 Nucleophilic addition of indole to cyclopropylgold(I) carbene **XX**.

Although cyclopropyl gold(I) carbenes have never been characterized spectroscopically, their intermediacy has been confirmed in several other cases. Alkenes have also been reported to trap these species *via* intra-[32] or intermolecular[33] pathways giving rise to cyclopropane derivatives (Scheme 7).

---

[31] Amijs, C. H. M.; Ferrer, C.; Echavarren, A. M. *Chem. Commun.* **2007**, 698–700.

[32] (a) Nieto-Oberhuber, C.; Muñoz, M. P.; Buñuel, E.; Nevado, C.; Cárdenas, D. J.; Echavarren, A. M. *Angew. Chem. Int. Ed.* **2004**, *43*, 2402–2406. (b) Nieto-Oberhuber, C.; López, S.; Muñoz, M. P.; Jiménez-Núñez, E.; Buñuel, E.; Cárdenas, D. J.; Echavarren, A. M. *Chem.–Eur. J.* **2006**, *12*, 1694–1702. (c) Kim, S. M.; Park, J. H.; Choi, S. Y.; Chung, Y. K. *Angew. Chem. Int. Ed.* **2007**, *46*, 6172–6175.

[33] (a) López, S.; Herrero-Gómez, E.; Pérez-Galán, P.; Nieto-Oberhuber, C.; Echavarren, A. M. *Angew. Chem. Int. Ed.* **2006**, *45*, 6029–6032. (b) Pérez-Galán, P.; Herrero-Gómez, E.; Hog, D. T.; Martin, N. J. A.; Maseras, F.; Echavarren, A. M. *Chem. Sci.* **2011**, *2*, 141–149.

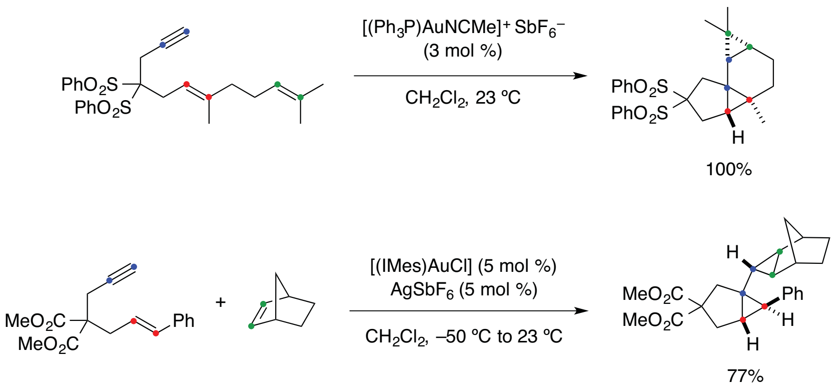
[(Ph$_3$P)AuNCMe]$^+$ SbF$_6^-$
(3 mol %)
CH$_2$Cl$_2$, 23 °C
PhO$_2$S
PhO$_2$S
H
100%
[(IMes)AuCl] (5 mol %)
AgSbF$_6$ (5 mol %)
CH$_2$Cl$_2$, –50 °C to 23 °C
MeO$_2$C
MeO$_2$C
Ph
+
H
77%

Scheme 7 Intra- and intermolecular cyclopropanation of 1,6-enynes, respectively.

Carbenes have also been trapped by oxidation to the corresponding aldehydes upon addition of Ph$_2$SO (Scheme 8).[34] 1,6-Enynes were rearranged under gold(I)-catalyzed conditions using stoichiometric amounts of Ph$_2$SO to give bicyclic products **8** with a pendant aldehyde. This finding corresponds to the first gold(I)-catalyzed oxidative cyclization.

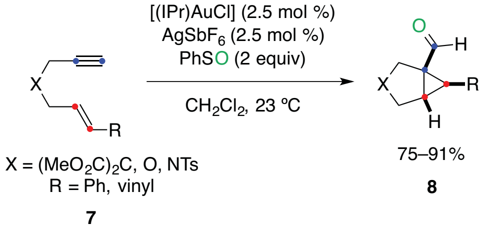
[(IPr)AuCl] (2.5 mol %)
AgSbF$_6$ (2.5 mol %)
PhSO (2 equiv)
CH$_2$Cl$_2$, 23 °C
X
R
O
H
X = (MeO$_2$C)$_2$C, O, NTs
R = Ph, vinyl
7
75–91%
8

Scheme 8 First gold(I)-catalyzed oxidative rearrangement of 1,6-enynes.

Oxidative Gold(I)-Catalyzed Reactions

Interestingly, only two other examples of gold(I)-catalyzed cyclizations of enynes using an external oxidant have been reported.[35] The lack of other reports is probably due to the inability of organic oxidants to produce oxidative cyclization products from most enynes. Thus, 1,5-,[35a] 1,6-[35] and 1,7-enynes[35b] could be cyclized and oxidized in a one-pot sequence using pyridine-*N*-oxides as additives giving rise to [n.1.0]bicyclic frameworks (Scheme 9).

---

[34] Witham, C. A.; Mauleón, P.; Shapiro, N. D.; Sherry, B. D.; Toste, F. D. *J. Am. Chem. Soc.* **2007***, 129,* 5838–5839.

[35] (a) Vasu, D.; Hung, H.-H.; Bhunia, S.; Gawade, S. A.; Das, A.; Liu, R.-S. *Angew. Chem. Int. Ed.* **2011**, *50*, 6911–6914. (b) Qian, D.; Zhang, J. *Chem. Commun.* **2011**, *47*, 11152–11154.

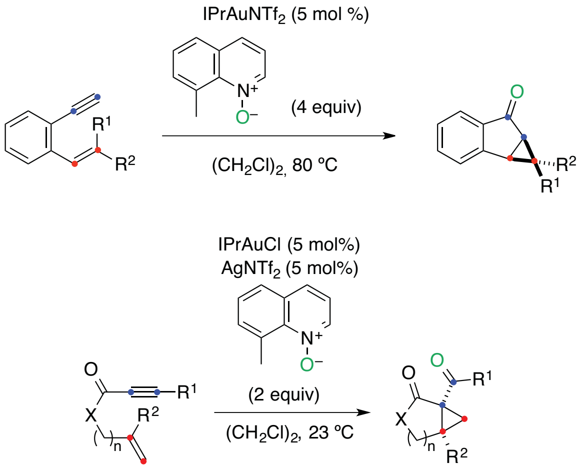
IPrAuNTf$_2$ (5 mol %)
N+
O−
(4 equiv)
(CH$_2$Cl)$_2$, 80 °C
R1
R2
O
R2
R1
IPrAuCl (5 mol%)
AgNTf$_2$ (5 mol%)
(2 equiv)
(CH$_2$Cl)$_2$, 23 °C
X
n

Scheme 9 Gold(I)-catalyzed intramolecular oxidation–cyclopropanation of 1,5-, 1,6- and 1,7-enynes.

However, the mechanism proposed in both reactions does not involve a cyclization followed by the trapping of the carbene with the oxidant (**XXI**) but the initial formation of an α-oxo gold(I) carbene intermediate (**XXII**) that undergoes intramolecular cyclopropanation to give the bicyclic product (Figure 3).[36]

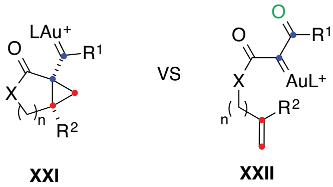
LAu+
O
R1
X
n
R2
XXI
VS
O
O
R1
X
AuL+
R2
n
XXII

Figure 3 Possible intermediates in the gold(I)-catalyzed oxidative cyclization of 1,6- or 1,7-enynes.

Indeed, the use of oxidants in gold(I)-catalysis is a common procedure to access to α-oxo gold carbenes *via* gold-catalyzed alkyne oxidation (Scheme 10).[37] Thus, alkynes can be surrogates for α-diazo carbonyl compounds.

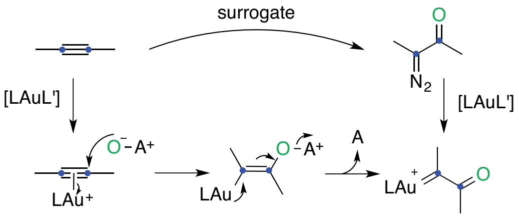
surrogate
O
N$_2$
[LAuL']
[LAuL']
O−A+
LAu+
LAu
O−A+
A
LAu
O

Scheme 10 Gold(I)-catalyzed intermolecular oxidation of an alkyne.

---

[36] The enantioselective version of this reaction was reported while this manuscript was in preparation: Qian, D.; Hu, H.; Liu, F.; Tang, B.; Ye, W.; Wang, Y.; Zhang, J. *Angew. Chem. Int. Ed.* **2014**, doi: 10.1002/anie.201407717.

[37] (a) Zhang, L. *Acc. Chem. Res.* **2014**, *47*, 877–888. (b) Yeom, H.-S.; Shin, S. *Acc. Chem. Res.* **2014**, *47*, 966–977.

An important number of publications have been reported on the intramolecular trapping of α-oxo gold carbenes by formal O–H,[38] N–H[39] and C–H[40] insertions or by addition of other nucleophilic partners.[41]

Nonetheless, the intermediacy of gold(I) α-oxo carbenes has been questioned in several intramolecular reactions.[42] Indeed, a recent mechanistic study on the oxidation reactions of alkynes catalyzed by gold(I) complexes by exploring these reactions applying tandem mass spectrometry, infrared multiphoton dissociation spectrospray (IRMDS) and density functional theory (DFT) suggested that the formation of naked α-oxo carbenes as the key intermediates is rather unlikely.[43]

---

[38] (a) Ye, L.; Cui, L.; Zhang, G.; Zhang, L. *J. Am. Chem. Soc.* **2010**, *132*, 3258–3259. (b) Ye, L.; He, W.; Zhang, L. *J. Am. Chem. Soc.* **2010**, *132*, 8550–8551.

[39] Ye, L.; He, W.; Zhang, L. *Angew. Chem. Int. Ed.* **2011**, *50*, 3236 –3239.

[40] (a) Henrion, G.; Chavas, T. E. J.; Le Goff, X.; Gagosz, F. *Angew. Chem. Int. Ed.* **2013**, *52*, 6277–6282. (b) Lu, B.; Li, C.; Zhang, L. *J. Am. Chem. Soc.* **2010**, *132*, 14070–14072. (c) Yang, L.-Q.; Wang, K.-B.; Li, C.-Y. *Eur. J. Org. Chem.* **2013**, 2775–2779.

[41] (a) Davies, P. W.; Cremonesi, A.; Martin, N. *Chem. Commun.* **2011**, *47*, 379–381. (b) Xu, C.-F.; Xu, M.; Jia, Y.-X.; Li, C.-Y. *Org. Lett.* **2011**, *13*, 1556–1559. (c) He, W.; Li, C.; Zhang, L. *J. Am. Chem. Soc.* **2011**, *133*, 8482–8485. (d) Luo, Y.; Ji, K.; Li, Y.; Zhang, L. *J. Am. Chem. Soc.* **2012**, *134*, 17412–17415.

[42] (a) Noey, E. L.; Luo, Y.; Zhang, L.; Houk, K. N. *J. Am. Chem. Soc.* **2012**, *134*, 1078–1084. (b) Lu, B.; Li, Y.; Wang, Y.; Aue, D. H.; Luo, Y.; Zhang, L.; *J. Am. Chem. Soc.* **2013**, *135*, 8512–8524. (c) Henrion, G.; Chavas, T. E. J.; Le Goff, X.; Gagosz, F. *Angew. Chem. Int. Ed.* **2013**, *52*, 6277–6278.

[43] Schulz, J.; Jašíková, L.; Škríba, A.; Roithová, J. *J. Am. Chem. Soc.* **2014**, *136*, 11513–11523.

Chapter 1: On the Silver Effect and the Formation of Chloride-Bridged Digold Complexes

Introduction

Gold(I)-catalyzed reactions are initiated by the coordination of a bicoordinated gold(I) to an unsaturated substrate (mainly alkynes, allenes and alkenes). The substitution of one of the ligands on the metal by the substrate proceeds through associative processes.[44] Recently, several studies have addressed the catalytically relevant ligand substitution of alkenes and alkynes with cationic gold(I) complexes.[45]

Synthesis of Gold(I) Complexes

In order to be catalytically active, gold(I) complexes should be coordinated with one weakly coordinating ligand, which is replaced by the substrate in an associative reaction. Complexes containing two neutral nitrogen donors that fulfill this characteristic are $[Au(NCR)_2]X$ (R = alkyl, aryl)[46] and related complexes containing ammonia $[Au(NH_3)_2]X$ (Figure 1).[47] Nonetheless, these species themselves are not active. Other $[AuL_2]X$ species are known to be so unstable that they undergo disproportionation to form gold(III) complexes as well as metallic gold.

$$\left[H_3N\text{-}Au\text{-}NH_3\right]^+ \; X^- \qquad \left[RCN\text{-}Au\text{-}NCR\right]^+ \; X^-$$

R = alkyl, aryl

Figure 1 Sources of gold(I) cation.

The aforementioned species have mainly been utilized as precatalysts in gold(I) chemistry that could play a role similar to that of $Pd_2(dba)_3$ in palladium chemistry. Whilst $[Au(NCMe)_2]X$ was not found to be attractive due to the harsh conditions or the special equipment required for its synthesis,[48] the use of the benzonitrile or hexanenitrile analogues proved to be more successful.[49] However, these complexes are unstable to air and moisture and decompose very easily. Thus, our group reported the synthesis of a more robust complex using 2,4,6-trimethoxybenzonitrile (tmbn) as ligand (Scheme 1).[50]

---

[44] (a) Pacheco, E. A.; Tiekink, E. R. T; Whitehouse, M. W. Gold Chemistry: Applications and Future Directions in the Life Sciences, Mohr, F. Ed. Chapter 6, **2009**, 283–287. Willey-VCH Verlag, GmbH & Co. (b) Schmidbaur, H.; Schier, A. *Organometallics* **2010**, *29*, 2–23. (c) Dickson, P. N.; Wehrli, A.; Geier, G. *Inor. Chem.* **1988**, *27*, 2921–2925.

[45] (a) Brown, T. J.; Dickens, M. G.; Widenhoefer, R. A. *J. Am. Chem. Soc.* **2009**, *131*, 6350–6351. (b) Hooper, T. N.; Green, M.; McGrady, J. E.; Patela, J. R.; Russell, C. A. *Chem. Commun.* **2009**, 3877–3879. (c) Brooner, R. E. M.; Brown, T. J.; Widenhoefer, R. A. *Chem.–Eur. J.* **2013**, *19*, 8276–8284.

[46] (a) Bonati, F.; Minghetti, G. *Gazz. Chim. Ital.* **1973**, *103*, 373–386. (b) Mingos, D. M. P.; Yau, J. *J. Organomet. Chem.* **1994**, *479*, C16–C17.

[47] Mingos, D. M. P.; Yau, J.; Menzer, S.; Wiliams, D. J. *J. Chem. Soc., Dalton Trans.* **1995**, 319–320.

[48] (a) Bergerhoff, G. *Z. Anorg. Allg. Chem.* **1964**, *327*, 139–142. (b) Kissner, R.; Latal, P.; Geier, G. *J. Chem. Soc., Chem. Commun.* **1993**, 136–137.

[49] (a) Yau, J.; Mingos, D. M. P. *J. Chem. Soc., Dalton Trans.* **1997**, 1103–1111. (b) Ito, Y.; Sawamura, M.; Hayashi, T. *J. Am. Chem. Soc.* **1986**, *108*, 6405–6406.

[50] Raducan, M.; Rodríguez-Escrich, C.; Cambeiro, X. C.; Escudero-Adán, E. C.; Pericàs, M. A.; Echavarren, A. M. *Chem. Commun.* **2011**, *47*, 4893–4895.

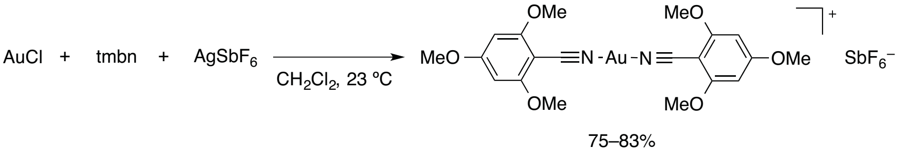

Scheme 1 Preparation of [Au(tmbn)$_2$]SbF$_6$.

Any of these homoleptic complexes can be mixed with one equiv of a ligand with sufficient donor capacity and generate a heteroleptic Au(I) complex after ligand exchange (Scheme 2). The reactivity of the complexes newly formed can be modulated by changing the coordination sphere around gold. Thus, an increase in the electron density of the d^{10} metal center is observed by moving from electron-withdrawing (e. g. phosphites) to electron-donating ligands (e. g. NHC carbenes).

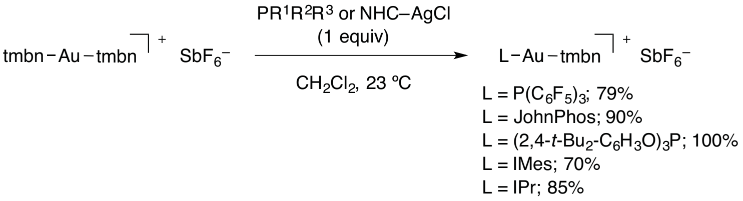

Scheme 2 Synthesis of cationic [LAu(tmbn)]SbF$_6$ starting from [Au(tmbn)$_2$]SbF$_6$.

The first practical gold(I)-catalyzed reaction reported by the group of Teles used [(Ph$_3$P)AuMe] as the catalyst source.[2] However, the complex itself was not active due to the strong donor capacity of both ligands. Therefore, in order to generate the active cationic species the addition of a Brønsted acid, namely, methanesulfonic acid (CH_3SO_3H) was necessary. Other Brønsted acids such as fluoroboric acid (HBF_4), phosphotungstic acid trihydrate ($H_3PW_{12}O_{40}$) or trifluoroacetic acid (TFA) can also be used.[22b]

The synthesis of [(Ph$_3$P)AuMe] relies on the addition of methyl magnesium iodide to (triphenylphosphine)gold(I) chloride (Scheme 3).[51] The resulting complex could be isolated through a filtration process albeit in moderate yield. (Triphenylphosphine)gold(I) chloride –and any other LAuCl source– could be easily accessed by reacting PPh$_3$ and (tht)AuCl, an air stable salt prepared by reduction of $HAuCl_4 \cdot nH_2O$ with tetrahydrothiophene.

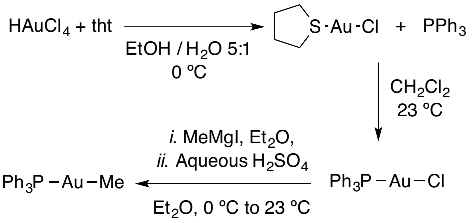

Scheme 3 Synthesis of methyl(triphenylphosphine)gold(I).

A useful alternative employs (triphenylphosphine)gold(I) chloride as the starting complex, and then the active Au(I) species in gold(I)-catalyzed transformations are generated *in* situ by addition of silver salts to form insoluble AgCl.[52] Our group pioneered the preparation of well defined cationic gold(I) complexes by reacting different LAuCl with silver salts featuring non-coordinating anions in the presence of nitriles.[53] Thus, a new protocol for the synthesis of air-stable cationic gold(I) complexes was disclosed (Scheme 4). Remarkably, their preparation, storage and handling did not require any special equipment and they could be directly used as catalysts. It is important to stress that cations $[LAu]^+$ with only mono-coordinated gold atoms are not stable.[54]

---

[51] Tamaki, A.; Kochi, J. K. *J. Organomet. Chem.* **1973**, *61*, 441–450.

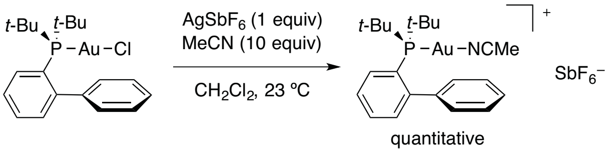

Scheme 4 Procedure to synthetize cationic $[(JohnPhos)AuNCMe]SbF_6$.

Independently, the group of Gagosz presented a new class of stable catalysts $LAuNTf_2$ with the weakly coordinating bistriflimide (Scheme 5).[55] The resulting structures were reminiscent of bis(trimethylsilyl)imide $[(Ph_3P)AuN(SiMe_3)_2]$ reported in 1970.[56] More recently, copper salts were used generate cationic gold(I).[57]

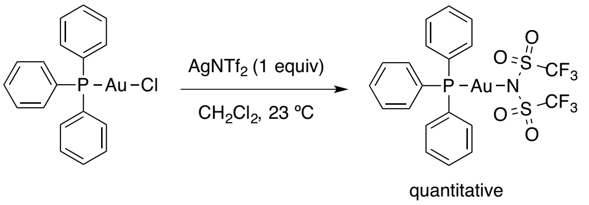

Scheme 5 Procedure to synthesize neutral $[(Ph_3P)AuNTf_2]$.

Despite all the advanced protocols to isolate active gold(I) species, the *in situ* generation of cationic species through the addition of a silver salt in gold(I)-catalyzed reaction is still the preferred option for most experimental chemists. Nonetheless, over the years, different papers have claimed the "non-innocent" role of these silver salts in gold(I)-catalyzed reactions. In addition, there is no single common procedure to set-up reactions catalyzed by Au(I): the order of addition of the different components of a reaction mixture (silver salt, gold precatalyst, substrate, additives…) varies from one report to another.

---

[52] For the isolation of a silver intermediate in the activation of gold precatalyst, see: Weber, S. G.; Rominger, F.; Straub, B. F. *Eur. J. Inorg. Chem.* **2012**, 2863–2867.

[53] (a) Herrero-Gómez, E.; Nieto-Oberhuber, C.; López, S.; Benet-Buchholz, J.; Echavarren, A. M. *Angew. Chem. Int. Ed.* **2006**, *45*, 5455–5459. (b) Amijs, C. H. M.; López-Carrillo, V.; Raducan, M.; Pérez-Galán, P.; Ferrer, C.; Echavarren, A. M. *J. Org. Chem.* **2008**, *73*, 7721–7730.

[54] A report claimed the formation of $[(IPr)Au]BArF_{24}$ with the bulky ligand IPr = 1,3-bis(2,4,6-trimethylphenyl)imidazol-2-ylidene, although no structural proof was provided: Weber, S. D.; Zahner, D.; Rominger, F.; Straub, B. F. *Chem. Commun.* **2012**, *48*, 11325–11327.

[55] (a) Mézailles, N.; Ricard, L.; Gagosz, F. *Org. Lett.* **2005**, *7*, 4133–4136. (b) Ricard, L.; Gagosz, F. *Organometallics* **2007**, *26*, 4704–4707.

[56] Shiotani, A.; Schmidbaur, H. *J. Am. Chem. Soc.* **1970**, *92*, 7003–7004.

[57] Guérinot, A.; Fang, W.; Sircoglou, M.; Bour, C.; Bezzenine-Lafollée, S.; Gandon, V. *Angew. Chem. Int. Ed.* **2013**, *52*, 5848–5852.

Effect of Silver in Gold(I) Catalysis

In 2005, our group observed that the outcome of a reaction changed depending on the mode of generation of the cationic Au(I) catalyst (addition of protic acid vs. silver salt).[58] 2,3-Dimethoxyphenol propargyl ether (**1**) reacted with [(Ph_3P)AuCl] and HBF_4 giving selectively 6,7-dimethoxy-2*H*-chromene (**2**) in 70% yield (Table 1, entry 1). When the protic acid was replaced by $AgSbF_6$, dimer **3** was also isolated as a byproduct. Indeed, chromene **2** was shown to dimerize under Ag(I)-catalyzed process (Table 1, entry 3).

Table 1 Au(I)-catalyzed reaction of 2,3-dimethoxyphenol propargyl ether.

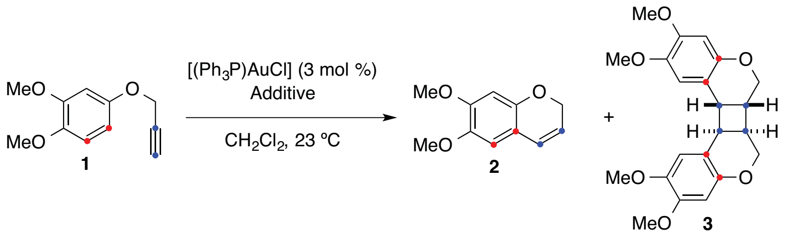

Additive	Yield 2	Yield 3
HBF_4 (6 mol %)	70%	-
$AgSbF_6$ (3 mol %)	72%	18%
$AgSbF_6$ (15 mol %)[a]	-	40%

[a] [(Ph_3P)AuCl] not added; reaction heated at 40 °C.

Later, the group of Gagné reported a similar finding.[59] They designed a new dinuclear Au(I)-catalyst using (*R*)-3,5-xylyl-binap as ligand. Interestingly, the levels of enantioselectivity in the cycloisomerization of enallenes (e. g. **4**) varied depending on the mode of activation of the catalyst (Scheme 6). If the reaction was initiated by [(*R*)-3,5-xylyl-binap($AuOTf)_2$] (isolated catalyst), the product was obtained slowly and with lower levels of *ee* than if the catalyst was generated *in situ* using [(*R*)-3,5-xylyl-binap($AuCl)_2$] and AgOTf.

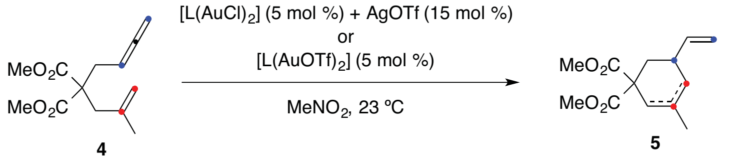

In situ; 16 h reaction, 72% *ee*
Isolated; > 24 h reaction, 21% *ee*

Scheme 6 Cycloisomerization of enallene **4** catalyzed by Au(I) complexes.
[L = (*R*)-3,5-xylyl-binap].

Another experiment performed by the same group showed that silver ions could have an influence on a gold(I)-catalyzed reaction by intercepting key organogold intermediates

---

[58] Nevado, C.; Echavarren, A. M. *Chem.–Eur. J.* **2005**, *11*, 3155–3164.

[59] Tarselli, M. A.; Chianese, A. R.; Lee, S. J.; Gagné, M. R. *Angew. Chem. Int. Ed.* **2007**, *46*, 6670–6673.

(Scheme 7).[60] Dinuclear gold–silver species were isolated as the resting state of this gold(I)-catalyzed hydroarylation of allenes.

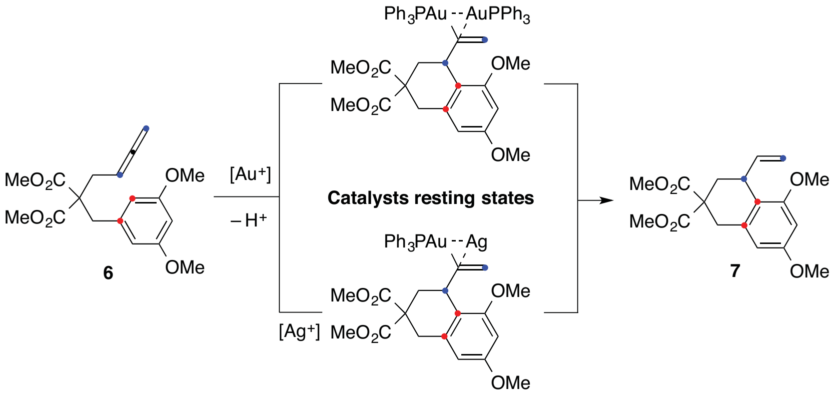

Scheme 7 Catalysts resting states in the hydroarylation of allene **6**.

The group of Shi then examined the so-called "silver-effect" in gold(I) catalysis.[61] Various reported gold(I)-catalyzed reactions were reexamined under three different conditions: "only gold" (silver free reaction)", "only silver" and "gold and silver". Mixing LAuCl with the silver salt and filtrating the resulting crude through Celite gave the "only gold conditions",[62] whereas the "only silver conditions" included the addition of the silver salt as the only catalyst. The last conditions consisted in the typical reaction set-up with no prior filtration of the bimetallic mixture through Celite. The results led them to classify the reactions into three different types: a)"genuine" Au catalysis, b) Au/Ag bimetallic catalysis and c) Ag-assisted gold catalysis.

"Genuine" Au Catalysis

This group accounted for the type of reactions catalyzed by the "only gold" conditions. However only two examples were reported and in both, the silver salt with the more coordinating anion NTf_2^- was used (Table 2).

Table 2 Selected example of the "genuine Au catalysis" type.

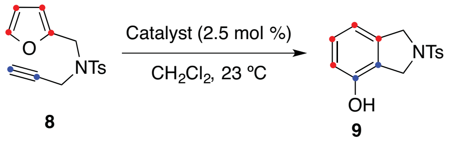

	"only Au"	"only Ag"	Au + Ag
catalyst	[XPhosAuCl + $AgNTf_2$] + Celite filtration	$AgNTf_2$	[XPhosAuCl + $AgNTf_2$]
yield	88%	0%	89%

---

[60] Weber, D.; Gagné, M. R. *Org. Lett.* **2009**, *11*, 4962–4965.

[61] Wang, D.; Cai, R.; Sharma, S.; Jirak, J.; Thummanapelli, S. K.; Akhmedov, N. G.; Zhang, H.; Liu, X.; Petersen, J. L.; Shi, X. *J. Am. Chem. Soc.* **2012**, *134*, 9012–9019.

[62] XPS analysis showed no traces of silver mixing [$(Ph_3P)AuCl$] and $AgSbF_6$.

Au/Ag Bimetallic Catalysis

The transformations belonging to this group were only effective in the presence of both metals. Filtering the mixture LAuCl + AgX through Celite resulted in no reactivity. However, with no filtration, the bimetallic mixture proved to be effective (Table 3).

Table 3 Selected example of the "Au/Ag bimetallic catalysis" type.

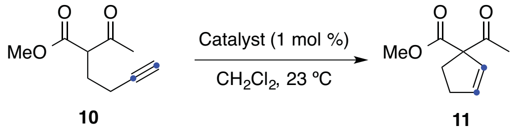

	"only Au"	**"only Ag"**	**Au + Ag**
catalyst	[Ph$_3$PAuCl + AgSbF$_6$] + Celite filtration	AgSbF$_6$ [a]	[Ph$_3$PAuCl + AgSbF$_6$]
yield	24 h, 0%	24 h, 0%	30 min, 88%

[a] 5 mol % used.

Ag-Assisted Au Catalysis

Reactions that could be promoted by both the "only gold" and "gold and silver" conditions belonged to that group. However, the yields obtained using the bimetallic mixture were significantly higher and the transformation required shorter reaction times. The substrates did not react using only silver as catalyst (Table 4).

Table 4 Selected example of the "Ag-assisted Au catalysis" type.

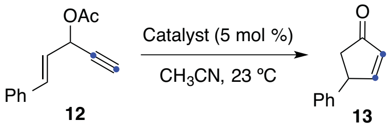

	"only Au"	**"only Ag"**	**Au + Ag**
catalyst	[(Ph$_3$P)AuCl + AgSbF$_6$] + Celite filtration	AgSbF$_6$	[(Ph$_3$P)AuCl + AgSbF$_6$]
yield	24 h, 45%	24 h, 0%	6 h, 77%

In addition, transformations that could be catalyzed by "only gold" or "only silver" were also included in this group (Table 5).

Table 5 Selected example of the "Ag-assisted Au catalysis" type.

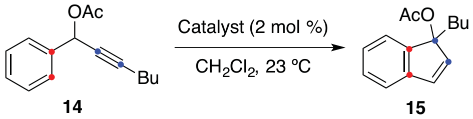

	"only Au"	**"only Ag"**	**Au + Ag**
catalyst	[IPrAuCl + $AgBF_4$] + Celite filtration	$AgBF_4$	[IPrAuCl + $AgBF_4$]
yield	10 min, 87%	6 h, 83%	10 min, 90%

Based on these surprising results, the group concluded that the so far assumed mechanisms in gold(I)-catalyzed reactions could be much more complex. They ruled out any reactivity from the formed AgCl.

Objectives

With the so-called "silver effect" previously described, we realized that there was not a universal procedure to perform gold(I) catalyzed reactions. Whilst in some cases the silver salt was the last reagent added in the reaction, in some others, the Au(I) and Ag(I) sources were mixed first and then added to the substrate, regardless of the coordinating abilities of the solvent or anion of the silver salt used.

Due to the absence of monocoordinated species reported in the literature, we were particularly interested in the real species formed when mixing LAuCl and AgX, especially when this was done in a non-coordinating solvent and/or when silver was ion-paired with a non-coordinating anion.

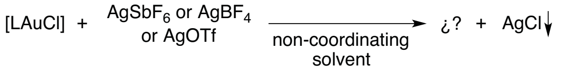

$$[\mathrm{LAuCl}] + \begin{matrix}\mathrm{AgSbF_6}\text{ or }\mathrm{AgBF_4}\\ \text{or }\mathrm{AgOTf}\end{matrix} \xrightarrow[\text{non-coordinating solvent}]{} ¿? + \mathrm{AgCl}\downarrow$$

Scheme 9 Reaction between [LAuCl] and silver salts featuring non-coordinating anions in a non-coordinating solvent.

Therefore, we decided to study how the order of addition of the silver salts could influence the outcome of the gold(I)-catalyzed methodologies we previously reported.

Results and Discussion

The initial experiments were performed using [(Ph_3P)AuCl] and were monitored by ^{31}P NMR. The first silver salt used was AgOTf in order to assess the coordinating ability of the triflate anion. [(Ph_3P)AuCl] was mixed with 0.2 equiv of AgOTf and the ^{31}P NMR spectrum was acquired after 20 min stirring at 23 ºC. To the same reaction mixture, 0.2 more equiv of the silver salt were introduced and the resulting mixture was examined by ^{31}P NMR (Figure 2). This process was repeated until 2 equiv of silver salt were added.

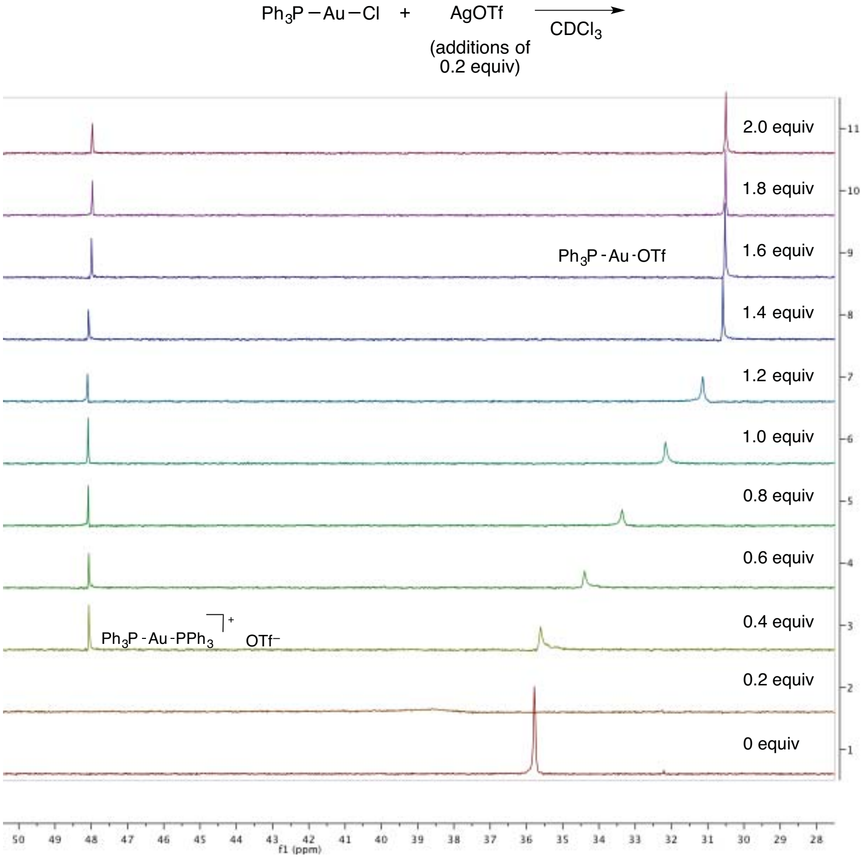

Figure 2 ^{31}P NMR of [(Ph_3P)AuCl] and [n × 0.2 equiv AgOTf].

It is generally accepted that the more cationic character of the complexes generated, the more upfield the ^{31}P NMR signals. The broad signal observed upon addition of 0.2 equiv sharpened with the addition of AgOTf. The equilibrium was observed after 1.4 equiv of AgOTf were added. We could distinguish the species at 48 ppm as the bisphosphine complex [(Ph_3P)$_2$Au]OTf. The traces of excess PPh_3 that the starting material contained, bind to the metal center much faster than the triflate anion itselfs.[63] The sharp signal at 30.5 ppm was consistent with the formation of [(Ph_3P)AuOTf]. We suspected that within the range of 0.2 equiv to 1.4 equiv, this covalent complex was in equilibrium with other unknown species. Attempts to crystallize any of the new species formed proved unsuccessful. Schmibaur had observed that above –20 ºC, [(Ph_3P)AuOTf] was not stable in the solid state, although they were able to crystallize its *o*-tolyl analogue.[64] Nonetheless, the group of Yu has supported this hypothesis by showing that triphenylphosphine gold triflate was very prone to hydration when analytical grade CH_2Cl_2 was used.[65] Therefore, we decided to switch to the more stable JohnPhos (2-biphenyl-*t*-Bu_2P) ligand.

---

[63] Although the signal corresponding to free PPh_3 could not be observed by ^{31}P NMR of [(Ph_3P)AuCl], elemental analysis indicated that a slight excess of PPh_3 was present.

JohnPhosAuCl and AgX in a Non-coordinating Solvent (X = OTf, NTf_2, BF_4, SbF_6)

A very similar trend was observed using this bulky phosphine. Mixing 1 equiv of [(JohnPhos)AuCl] (**A**) with 1 equiv of AgOTf a rather sharp signal was observed in the ^{31}P NMR spectrum. The crystallization of the crude mixture led to the isolation of the unexpected dinuclear chloride bridged [((JohnPhos)Au)$_2$Cl]OTf (**B1**) (Scheme 9) that could be fully characterized by X-ray diffraction (Figure 3).

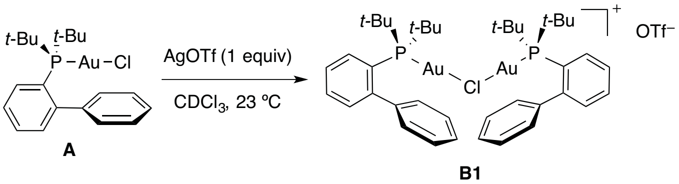

Scheme 9 Formation of [((JohnPhos)Au)$_2$Cl]OTf (**B1**).

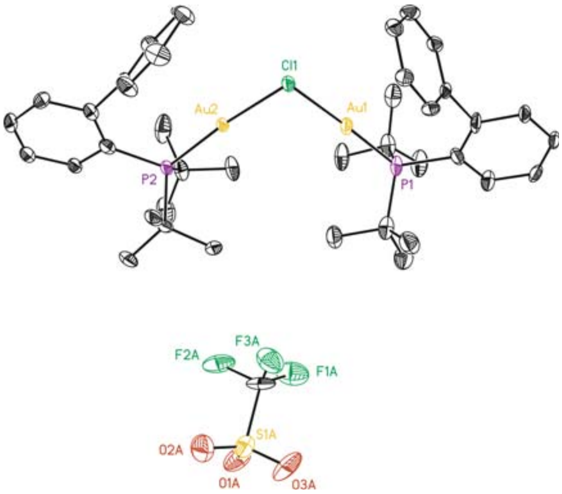

Figure 3 X-ray crystal structure of complex **B1**. ORTEP plots (50% thermal ellipsoids). Hydrogen atoms and solvent molecules omitted for clarity.

We hypothesized that the equilibrium previously observed in the case of [(Ph_3P)AuCl] also took place between [(JohnPhos)AuOTf] (**C1**), [((JohnPhos)Au)$_2$Cl]OTf (**B1**) and

---

[64] Preisenberger, M.; Schier, A.; Schmidbaur, H. *J. Chem. Soc., Dalton Trans.* **1999**, 1645–1650.
[65] Tang, Y.; Yu, B. *RSC Adv.* **2012**, *2*, 12686–12689.

[(JohnPhos)AuCl] (**A**). The sharp ^{31}P NMR signal observed after addition of 1.6 equiv of silver salt corresponded to the neutral complex [(JohnPhos)AuOTf]. [(JohnPhos)AuOTf] was cleanly formed upon the addition of 5 equiv of the silver salt (Scheme 10 and Figure 4).

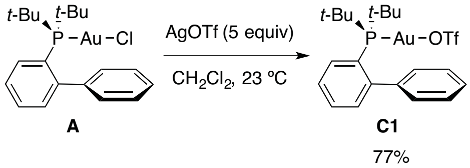
t-Bu
t-Bu
P–Au–Cl
AgOTf (5 equiv)
CH2Cl2, 23 °C
t-Bu
t-Bu
P–Au–OTf
A
C1
77%

Scheme 10 Formation of neutral complex [(JohnPhos)AuOTf] (**C1**).

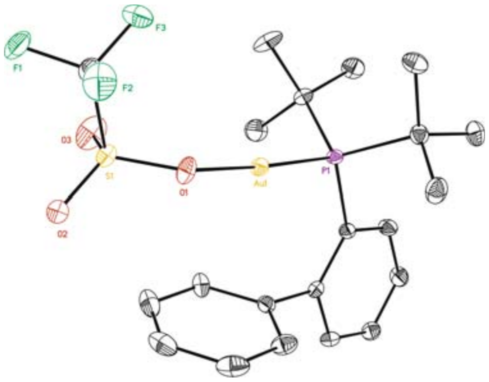
F1
F2
F3
O3
S1
O1
Au1
P1
O2

Figure 4 X-ray crystal structure of complex **C1**. ORTEP plots (50% thermal ellipsoids). Hydrogen atoms and solvent molecules omitted for clarity.

The stronger coordinating character of the triflimide anion was evidenced when a 1:1 mixture of [(JohnPhos)AuCl] (**A**) and AgNTf$_2$ gave a 1:1 mixture of the monocationic species [((JohnPhos)Au)$_2$Cl]NTf$_2$ (**B2**) and the neutral complex [(JohnPhos)AuNTf$_2$] (**C2**) (Scheme 11 and Figure 5). The formation of dinuclear complex **B2** could be avoided by using either excess or slow addition of the silver salt.

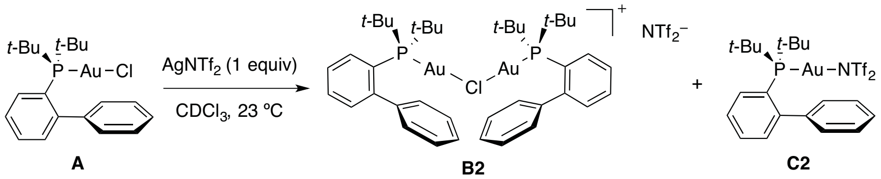
t-Bu
t-Bu
P–Au–Cl
AgNTf2 (1 equiv)
CDCl3, 23 °C
t-Bu
t-Bu
P
Au
Cl
Au
P
t-Bu
t-Bu
+
NTf2–
+
t-Bu
t-Bu
P–Au–NTf2
A
B2
C2

Scheme 11 Formation of [((JohnPhos)Au)$_2$Cl]NTf$_2$ (**B2**) and [(JohnPhos)AuNTf$_2$] (**C2**).

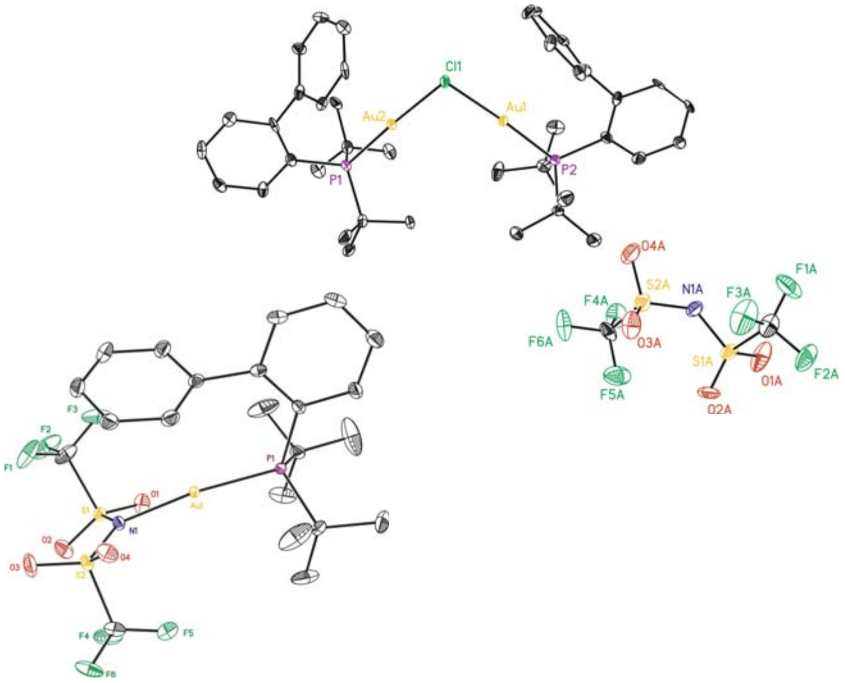
Cl1
Au2
Au1
P1
P2
O4A
S2A
N1A
F1A
F3A
F4A
F6A
O3A
S1A
O1A
F2A
F5A
O2A
F3
F2
F1
O1
S1
N1
Au1
P1
O2
O3
O4
S2
F4
F5
F6

Figure 5 X-ray crystal structure of complexes **B2** and **C2**. ORTEP plots (50% thermal ellipsoids). Hydrogen atoms and solvent molecules omitted for clarity.

Finally, mixing [(JohnPhos)AuCl] (**A**) with the non-coordinating silver salts $AgBF_4$ or $AgSbF_6$ gave the dinuclear monocation complexes **B3** and **B4**, respectively (Scheme 12 and Figure 6). Interestingly, addition of up to 10 equiv of either silver salts was not enough to break the resulting dinuclear complexes apart.

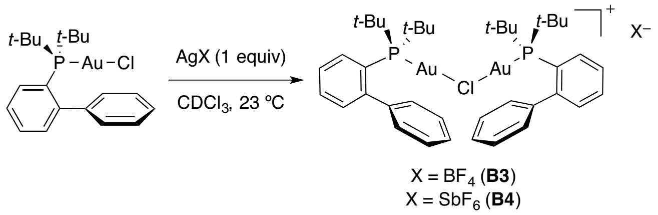
t-Bu
t-Bu
P–Au–Cl
AgX (1 equiv)
CDCl3, 23 °C
t-Bu
t-Bu
P
Au
Cl
Au
P
t-Bu
t-Bu
+
X−
X = BF4 (B3)
X = SbF6 (B4)

Scheme 12 Formation of $[((JohnPhos)Au)_2Cl]X$ ($X = BF_4^-$ or SbF_6^-).

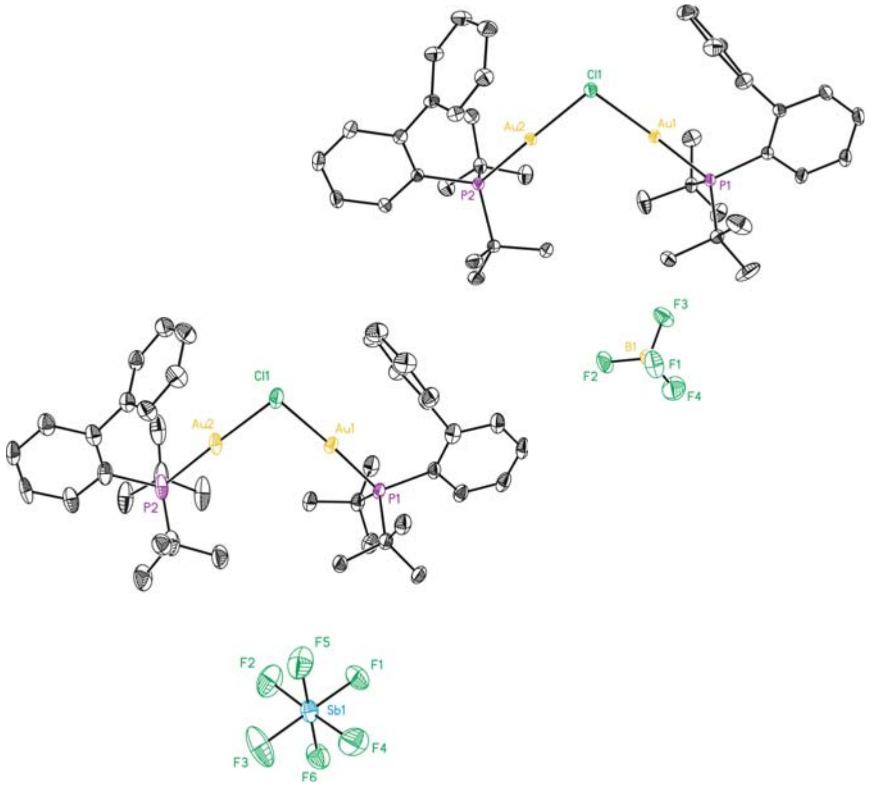

Figure 6 X-ray crystal structure of complexes **B3** and **B4**. ORTEP plots (50% thermal ellipsoids). Hydrogen atoms and solvent molecules omitted for clarity.

All the crystalline dinuclear complexes [((JohnPhos)Au)$_2$Cl]X (**B**) showed weak aurophilic interactions (Au–Au distances = 3.48–3.54 Å, Au–Cl–Au angles = 94.7–97.5º).[66] Interestingly, Usón[67] and Schmidbaur[68] had already reported the synthesis of similar digoldhalide cations employing triphenyl- and triethylphosphine as ligands in a 1:2 ratio of silver:gold. Their reactivity was later tested in the first example of an intermolecular reaction of an alkyne and a furan.[69]

The bimetallic complexes **B** were then synthesized quantitatively using 0.5 equiv of the silver salt in a 1:1 mixture of CH_2Cl_2 and THF (Scheme 13). Under these optimized conditions and using SbF_6^- as counterion and PPh_3 as ligand, the group of Schmidbaur observed the formation of tetranuclear dications through a self-assembly of two dinuclear monocations.[70] In our case, the steric bulk of the JohnPhos ligand did not allow this association process to take place. The formation of these dinuclear complexes was also viable when treating [(JohnPhos)AuBr] and [(JohnPhos)AuI] with silver salts that have non-coordinating anions.[71]

---

[66] (a) Schmidbaur, H.; Schier, A. *Chem. Soc. Rev.* **2012**, *41*, 370–412. (b) Schmidbaur, H.; Schier, A. *Chem. Soc. Rev.* **2008**, *37*, 1931–1951.

[67] Usón, R.; Laguna, A.; Castrillo, M. B. *Synth. React. Inorg–Met.–Org. Chem.* **1979**, *9*, 317–324.

[68] Bayler, A.; Bauer, A.; Schmidbaur, H. *Chem. Ber.* **1997**, *130*, 115–118.

[69] (a) Hashmi, A. S. K.; Blanco, M. C.; Kurpejović, E.; Frey, W.; Bats, J. W. *Adv. Synth. Catal.* **2006**, *348*, 709–713. (b) Hashmi, A. S. K.; Blanco, M. C. *Eur. J. Org. Chem.* **2006**, 4340–4342. Our group reported later more efficient conditions for this reaction: (c) Huguet, N.; Leboeuf, D.; Echavarren, A. M. *Chem.–Eur. J.* **2013**, *19*, 6581–6585.

[70] Schmidbaur, H.; Hamel, A.; Mitzel, N. W.; Schier, A.; Nogai, S. *Proc. Natl. Acad. Sci. USA* **2002**, *99*, 4916–4921.

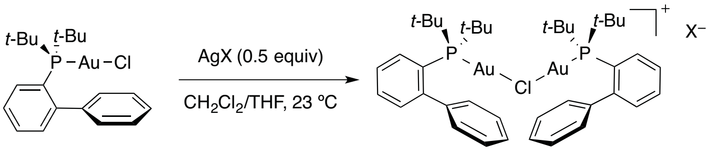

X = OTf (**B1**) X = BF$_4$ (**B3**)
X = NTf$_2$ (**B2**) X = SbF$_6$ (**B4**)
80–96%

Scheme 13 Optimized synthesis of [(JohnPhos)$_2$AuCl]X (X = NTf$_2^-$, OTf$^-$, BF$_4^-$ or SbF$_6^-$).

To evaluate the stability of these monocationic species and study if the equilibrium between the monocoordinated Au complex ([(JohnPhos)Au]$^+$) and [(JohnPhosAu)Cl] was possible, we examined their ^{1}H and ^{31}P NMR spectra while lowering the temperature. No equilibrium could be observed for the species featuring BF$_4^-$ or SbF$_6^-$ as counterions. Interestingly, the ^{1}H and ^{31}P NMR spectra of the above-mentioned crude mixtures (1:1 mixture of [(JohnPhosAu)Cl] and AgX) were studied before and after filtration through Celite in the range from –80 ºC to 25 ºC. Digoldchloride cations were the major species at –80 ºC in the case of AgSbF$_6$ and AgBF$_4$ (in agreement with the chemical shifts observed in the ^{31}P NMRs) (Figure 7). Filtration of the crude mixture involving the BF$_4^-$ anion, gave 17% of hydrated dinuclear cation **D** that could be fully characterized by X-ray diffraction (Figure 8). The group of Nolan also reported analogous gold species using carbenes as ligands.[72]

---

[71] For further information, see experimental part.

[72] Gaillard, S.; Bosson,J.; Ramón, R. S.; Nun, P.; Slawin, A. M. Z.; Nolan, S. P. *Chem.–Eur. J.* **2010**, *16*, 13729–13740.

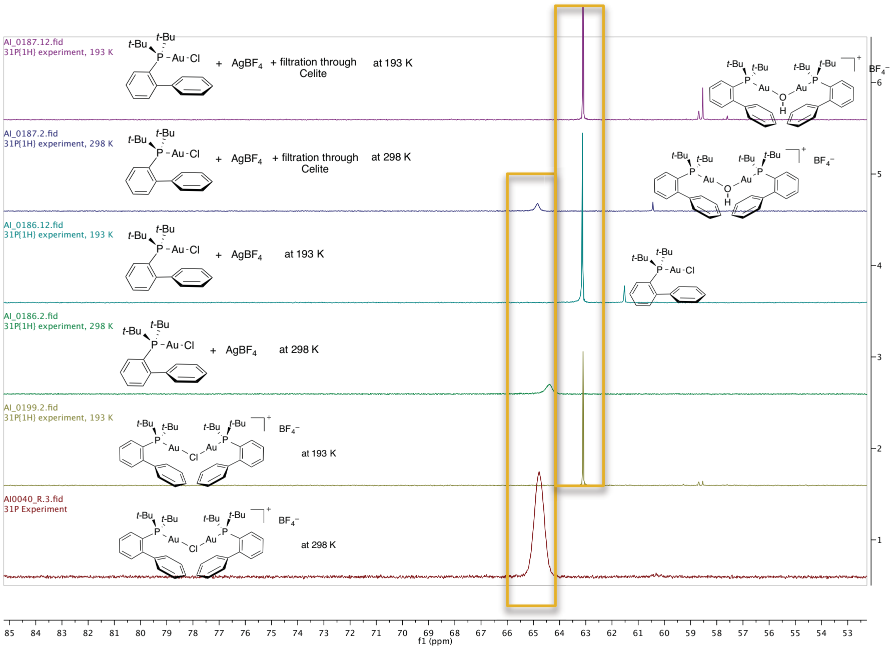

Figure 7 ^{31}P NMR of [((JohnPhos)Au)$_2$Cl]BF$_4$ (**B3**) or [(JohnPhos)AuCl] (**A**) + AgBF$_4$.

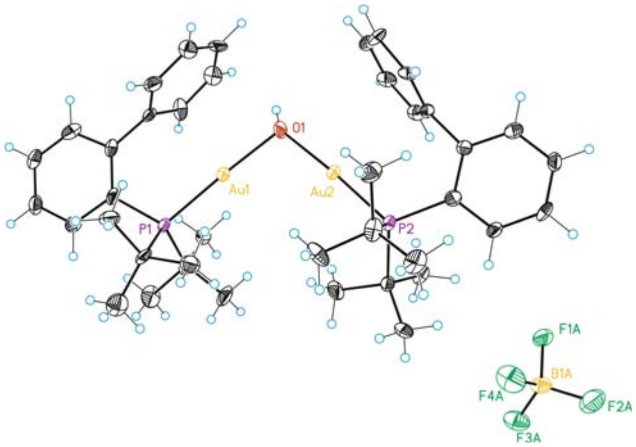

Figure 8 X-ray crystal structure of complex **D**. ORTEP plots (50% thermal ellipsoids). Hydrogen atoms and solvent molecules omitted for clarity.

The rather broad signal at 65.1 ppm, observed after filtering the crude mixture of [(JohnPhos)AuCl] (**A**) and AgOTf, further split into the corresponding [((JohnPhos)Au)$_2$Cl]OTf (**B1**) and [(JohnPhos)AuOTf] (**C1**). In contrast, without filtration, the dinuclear chloride species [((JohnPhos)Au)$_2$Cl]OTf (**B1**) was the only one observed. Interestingly, filtering through Celite the mixture of [((JohnPhos)Au)$_2$Cl]NTf$_2$ (**B2**) and [(JohnPhos)AuNTf$_2$] (**C2**) obtained by reaction of [(JohnPhos)AuCl] (**A**) and AgNTf$_2$ afforded only [(JohnPhos)AuNTf$_2$] (**C2**) (Figure 9).

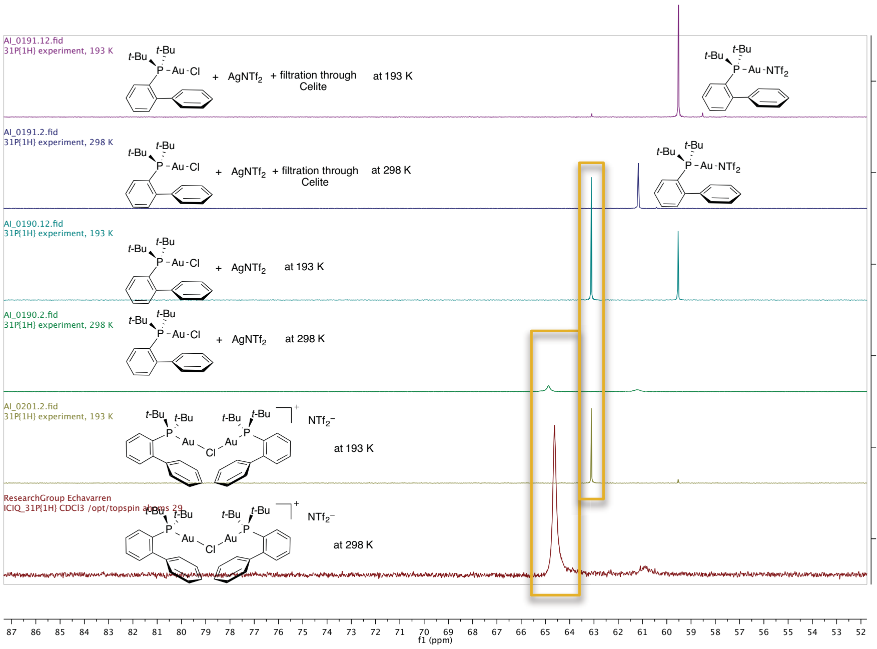

Figure 9 ^{31}P NMR of [((JohnPhos)Au)$_2$Cl]NTf$_2$ (**B2**) or [(JohnPhos)AuCl] (**A**) + AgNTf$_2$.

Given the differences observed in the experimental procedures of different gold(I)-catalyzed reactions regarding the order of addition of the reagents, we examined if these dinuclear complexes could be indeed generated when the Au(I) and Ag(I) sources were initially mixed in a non-coordinating solvent. Therefore, to determine the relevance of the formation of the bimetallic complexes, we performed the gold(I)-catalyzed reactions under three different conditions: a) *in situ* generation of the catalyst in the presence of the substrate(s), b) *in situ* generation of the catalyst followed by the addition of the substrate(s) and c) filtration through Celite after the *in situ* generation of the catalyst followed by the addition of the substrate(s). We performed this last experiment to remove the precipitate of AgCl, and see if there was any effect on the outcome of the reaction.

Relevance of Digoldhalide Cation

JohnPhosAuCl and AgX with Phenylacetylene

The mixture of phenylacetylene and [(*t*-BuXPhos)AuNCMe]SbF$_6$ is known to produce digold complex **E**.[73] The π-coordination of the acetylene moiety to the metal increases the acidity of the terminal proton of the triple bond, generating σ-coordinated species **F** with release of HSbF$_6$. Complex **F**, in turn, coordinates to another molecule of the Au(I) source, giving rise to σ,π-digold complex **E** (Scheme 14).

---

[73] Obradors, C.; Echavarren, A. M. *Chem.–Eur. J.* **2013**, *29*, 3547–3551.

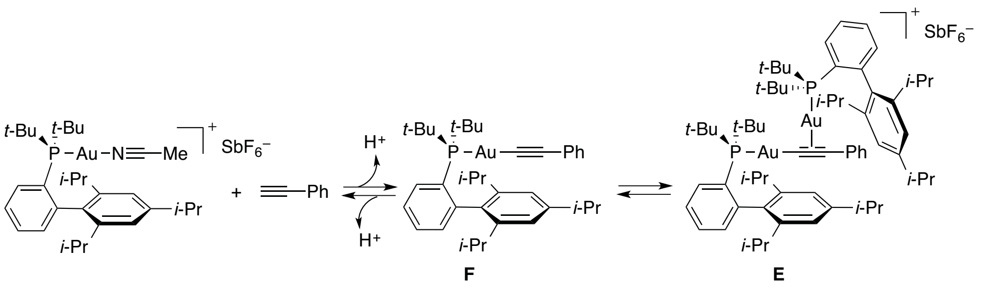

Scheme 14 Formation of digold complex **E**.

We first synthesized and fully characterized the σ,π-digold species **G** (analogous to **E** but bearing JohnPhos as ligand instead of *t*-BuXPhos) following a described procedure,[73] to prove its formation under the conditions studied. Then, we carefully examined the species formed under the aforementioned conditions.

a) In situ generation of the catalyst in the presence of phenylacetylene

To perform this experiment, we used the usual ratio of catalyst/substrate for gold(I)-catalyzed reactions. Thus, 3 mol % of [(JohnPhos)AuCl] were added to a solution of phenylacetylene in CD_2Cl_2. The subsequent addition of 3 mol % of any of the silver salts gave exclusively the formation the digold complexes **G** (Scheme 15).

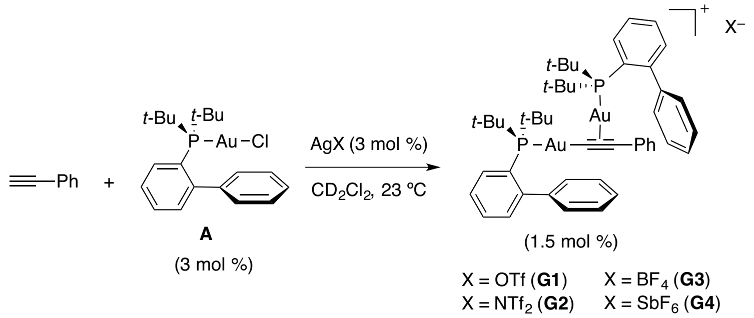

Scheme 15 *In situ* generation of the catalyst from in the presence of phenylacetylene.

b) In situ generation of the catalyst followed by the addition of phenylacetylene

The same species were observed when phenylacetylene was added to a 1:1 mixture of 3 mol % of [(JohnPhos)AuCl] (**A**) and any of the silver salts. We postulated that after combining the two metal sources, digoldchloride species **B**, AgX and AgCl (1:1:1 ratio) would be the predominant species in solution. Phenylacetylene could then coordinate to one of the gold centers of the chloride bridged species **B** and through an associative mechanism, [(JohnPhos)AuCl] (**A**) would be eliminated. This neutral complex can further coordinate to phenylacetylene in the presence of the residual AgX (Scheme 16).

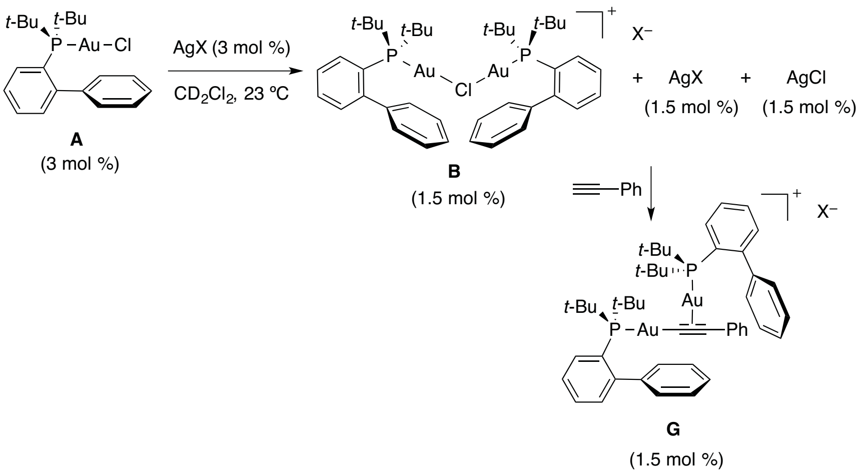

Scheme 16 *In situ* generation of the catalyst followed by the addition of phenylacetylene. (X = NTf_2^-, OTf^-, BF_4^-, SbF_6^-).

c) Filtration through Celite after the in situ generation of the catalyst followed by the addition of the substrate(s)

In this case, the mixture containing digoldchloride species **B**, AgX and AgCl (presumably in equimolar amount) was filtered through Celite. We proposed that insoluble AgCl and part of the AgX would remain on Celite. Addition of phenylacetylene led to the formation of digold species **G** as well as neutral [(JohnPhos)AuCl] (**A**). Interestingly, the ratio of σ,π-digold complexes **G** and [(JohnPhos)AuCl] (**A**) depended on the nature of the silver salt used. Thus, whereas $AgNTf_2$ gave only traces of **A**, 14% of unreacted [(JohnPhos)AuCl] was observed when using AgOTf, and much higher quantities were observed for $AgBF_4$ (61%) and $AgSbF_6$ (30%).

Examining the reaction between $[(JohnPhos)_2AuCl]X$ (**B**) and phenylacetylene at –80 ºC, we could detect an equilibrium between **B** + phenylacetylene and [(JohnPhos)AuCl] + σ,π-digold complexes **G** (Scheme 17).

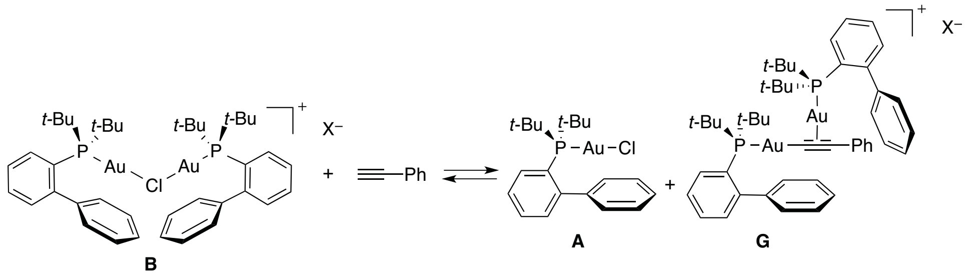

Scheme 17 Equilibrium between $[(JohnPhos)_2AuCl]X$ (**B**) + phenylacetylene and σ,π-digold complexes **G** + [(JohnPhos)AuCl] (**A**).

With these results in hand, we sough to study the gold(I)-catalyzed [2+2] inter-[25] and intramolecular[22c] cycloaddition reactions already reported in our group.

JohnPhosAuCl and AgX in the [2+2] Intermolecular Cycloaddition of Phenylacetylene and α-Methylstyrene

The intermolecular reaction between phenylacetylene and α-methylstyrene gives cyclobutene **18** in 60% yield in the presence of [JohnPhosAu(MeCN)]SbF_6 as catalyst.[25] We studied the reaction under the different conditions previously stated to determine the effect of the silver salts (Table 6).

Table 6 Formation of cyclobutene **18** by gold(I)-catalyzed [2+2] intermolecular cycloaddition.

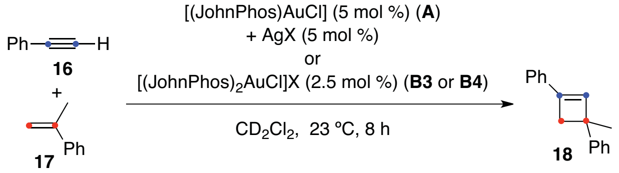
Ph
H
16
+
17
Ph
[(JohnPhos)AuCl] (5 mol %) (A)
+ AgX (5 mol %)
or
[(JohnPhos)2AuCl]X (2.5 mol %) (B3 or B4)
CD2Cl2, 23 °C, 8 h
Ph
18
Ph

Conditions	X = SbF_6^-	X = BF_4^-
In situ generation of the catalyst in the presence of the substrates	0%	31%
In situ generation of the catalyst and addition of the substrates	0%	34%
In situ generation of the catalyst, filtration and addition of the substrates	26%	30%
[$(JohnPhos)_2AuCl$]X	46%	11%
[$(JohnPhos)_2AuCl$]X + AgX	0%	34%
AgX	Alkene polimerization	0%

Yields determined by ^1H NMR using diphenylmethane as internal standard.

When a solution of the alkyne, the alkene and [(JohnPhos)AuCl] was added to the silver salt, after stirring for 8 h, no traces of the expected cyclobutene were formed whilst decomposition was detected. Decomposition was also observed when a solution of α-methylstyrene and phenylacetylene was added to a solution of [(JohnPhos)AuCl] and the silver salt. However, filtration through Celite of the *in situ* formed complex, gave the cyclobutene in 26% yield. Finally, the reaction proceeded in 46% yield using [$((JohnPhos)Au)_2Cl$]SbF_6 (**B4**). No cyclization took place after the addition of both starting materials to [$((JohnPhos)Au)_2Cl$]SbF_6 (**B4**) with 2.5 mol % of silver salt. We then discovered that the alkene underwent oligomerization or polymerization in the presence of $AgSbF_6$. Thus, under all the conditions in which the alkene was in contact with the silver salt, only decomposition was observed. The fact that the filtration of the *in situ* generated complex through Celite gave less cyclobutene than using [$((JohnPhos)Au)_2Cl$]SbF_6 supported the assumption that not all the $AgSbF_6$ was removed by filtration.

The results obtained with $AgBF_4$ were different. In this case, the silver salt did not polymerize any of the substrates and did not catalyze the reaction either. The same amount of cyclobutene (around 31% yield) was formed when the addition of the substrate was done either prior or after the formation of the catalyst. Filtration of the *in situ* generated catalyst did not result in any drop in the yield, presumably because most of the silver salt went through the Celite. Only 11% of cyclobutene was formed when using

[((JohnPhos)Au)$_2$Cl]BF$_4$ (**B3**) as catalyst, although the addition of 2.5 mol % of the silver salt increased the yield to 34%.

Since phenylacetylene –as it was previously observed– was able to associate one of the gold centers of the digoldhalide cations species, in principle, the order of addition of the silver salts should not have had any effect on the outcome of the reaction. However, it proved to be significant for AgSbF$_6$, since decomposition of the starting materials was observed with this specific silver salt.

JohnPhosAuCl and AgX in the [2+2] Intramolecular Cycloaddition of Enyne 19

The intramolecular gold(I)-catalyzed [2+2] cycloaddition of 1,6-enyne **19** giving rise to bicyclo[3.2.0]hept-6-ene derivative was reported for the first time by our group.[22] Similar cyclobutenes related to **20** had been generated by the group of Trost using palladacyclopentadienes as catalysts.[74] Later, Fürstner also described its synthesis of this type of compounds through a Pt(II)-catalyzed transformation under CO atmosphere.[75]

Table 7 Formation of cyclobutene **20** by gold(I)-catalyzed [2+2] intramolecular cycloaddition.

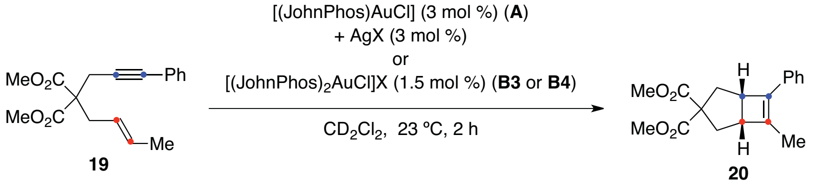
MeO2C
MeO2C
Ph
Me
19
[(JohnPhos)AuCl] (3 mol %) (A)
+ AgX (3 mol %)
or
[(JohnPhos)2AuCl]X (1.5 mol %) (B3 or B4)
CD2Cl2, 23 °C, 2 h
MeO2C
MeO2C
H
H
Ph
Me
20

Conditions	X = SbF$_6^-$	X = BF$_4^-$
In situ generation of the catalyst in the presence of the substrates	77%	17%
In situ generation of the catalyst and addition of the substrates	12%	0%
In situ generation of the catalyst, filtration and addition of the substrates	0%	0%
[(JohnPhos)$_2$AuCl]X	0%	0%
[(JohnPhos)$_2$AuCl]X + AgX	67%	26%
AgX	0%	0%

Yields determined by ^{1}H NMR using diphenylmethane as internal standard.

When the silver salt was added to a solution containing the enyne and [(JohnPhos)AuCl] (**A**), the bicyclic product **20** was formed in 77% yield after 2 h. However, only 12% of **20** was formed (along with unreacted starting material) with the *in situ* generation of the catalyst after this reaction time. No reaction took place filtering the *in situ* formed catalyst with Celite. The reaction also failed using [(JohnPhos)$_2$AuCl]SbF$_6$ (**B4**) as catalyst. The yield raised to 67% after the addition of 1 equiv of $AgSbF_6$ to $[(JohnPhos)_2AuCl]SbF_6$ (**B4**) and the substrate.

---

[74] (a) Trost, B. M.; Tanoury, G. J. *J. Am. Chem. Soc.* **1988**, *110*, 1636–1638. (b) Trost, B. M.; Trost, M. K. *Tetrahedron Lett.* **1991**, *32*, 3647–3650.

[75] Fürstner, A.; Davies, P. W.; Gress, T. *J. Am. Chem. Soc.* **2005**, *127*, 8244–8245.

The reaction was found to be much less effective when using $AgBF_4$. Even increasing the amount of gold(I) complex to 5 mol % and leaving the reaction for 18 h, **20** was formed in only 17% yield. No reaction took place when the catalyst was generated *in situ*, neither did it occur using $[(JohnPhos)_2AuCl]BF_4$ (**B3**). However, the effectiveness of this last catalyst was recovered after adding $AgBF_4$.

Presumably, since the 1,6-enyne is not able to associate to the cationic metal of the digoldchloride species, generated from reaction of LAuCl and AgX, under these conditions, the order of addition of the reagents had a tremendous impact on the outcome of the reaction. Therefore, the reaction proceeded more efficiently when the addition of the metal sources was last.

JohnPhosAuCl and AgX in the [4+2] Cycloaddition of Arylenyne 21

The intramolecular gold(I)-catalyzed [4+2] cycloaddition reaction of 1,6-enyne **21** forming the tricyclic derivative **22** was reported by our group (Scheme 18).[22] The cycloisomerization proceeds stepwise by the initial formation of a cyclopropylgold(I)-carbene that is further attacked by the aryl ring in a Friedel–Crafts type reaction.

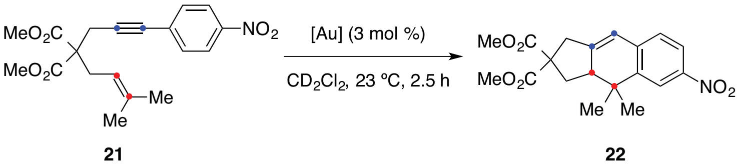

Scheme 18 Gold(I)-catalyzed [4+2] cycloaddition of arylenyne **21**.

The reaction of **21** was performed under different conditions, whilst formation of product **22** was monitored by ^1H NMR (Figure 10).

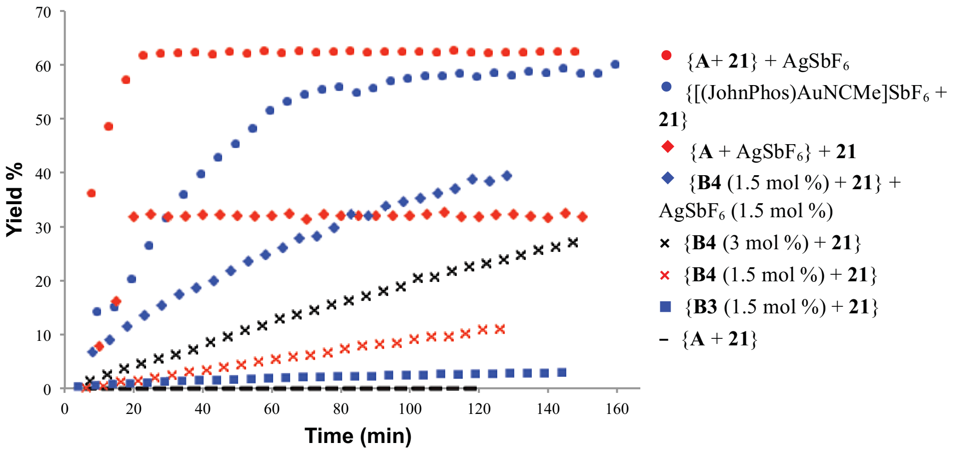

Figure 10 Cycloisomerization of 1,6-enyne **21** to form **22**. Yields determined by ^{1}H NMR using diphenylmethane as internal standard.[76]

The reaction afforded the same amount of product after 2.5 h when treating the enyne either with [(JohnPhos)AuCl] and AgSbF$_6$ (●) or [(JohnPhos)AuNCMe]SbF$_6$ (●). However, it was slower in the presence of acetonitrile since replacement of the acetonitrile by the enyne is a slow process. Indeed, the ^{31}P NMR after 5 min reaction showed two signals corresponding to the coordination of the unsaturated moieties to the gold for the *in situ* generation procedure (●) (Figure 11). Contrarily, the only signal observed for conditions ● was the corresponding to the complex [(JohnPhos)AuNCMe]SbF$_6$.

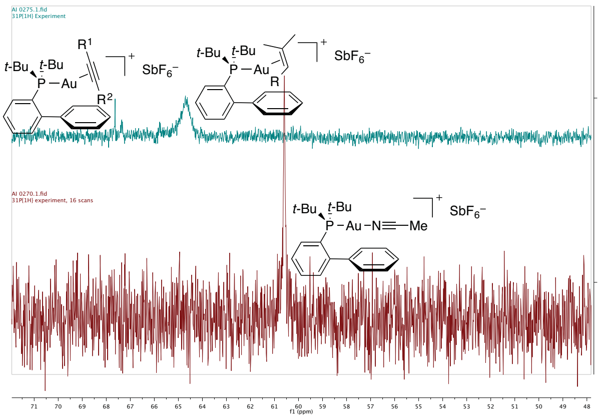

Figure 11 ^{31}P NMRs of {**A** + **21**} + AgSbF$_6$ (●) and {[(JohnPhos)AuNCMe]SbF$_6$ + **21**} (●) taken after 5 min reaction.

As expected, no reaction took place with [(JohnPhos)AuCl] (–). Initial mixing of [(JohnPhos)AuCl] and AgSbF$_6$, followed by the addition of the enyne, gave the tricyclic product in 32% yield after 2.5 h (◆). We were rather surprised of the fast formation of the product, which reached its maximum after 20 min reaction. The slope observed during this period was very similar to that of the reaction with {[(JohnPhos)AuCl] + **21**} + $AgSbF_6$. This would have suggested the non-influence of the order of addition of the silver salts if the efficiency of the reaction had not changed. This first trend in the graph can be explained if some of [(JohnPhos)AuCl] remain intact after the initial mixture of the two metal sources. Upon the addition of the enyne and in the presence of $AgSbF_6$, the formation of tricyclic product is fast. However, the major complex formed is $[((JohnPhos)Au)_2Cl]SbF_6$ (**B4**), which is much less reactive as observed (see figure 10, × and ×). Indeed, the enyne can coordinate to one of the metal centers of digoldchloride complex very slowly through an associative process. ^{31}P NMR measured after 5 min reaction between $[((JohnPhos)Au)_2Cl]BF_4$ (**B3**) and the enyne showed mainly digoldchloride species but also traces of enyne coordinated to one gold center (either through the alkene or the alkyne) (Figure 12).

---

[76] Kinetics performed by Imma Escofet.

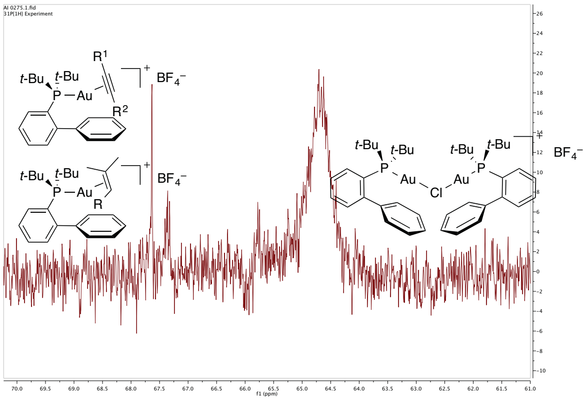

Figure 12 ^{31}P NMRs of {**A** + **21**} + $AgSbF_6$ (●) and {$[(JohnPhos)AuNCMe]SbF_6$ + **21**} (●) taken after 5 min reaction.

It is worth mentioning, that the tricyclic product was formed after 24 h reaction in 70%, 69% and 52% yield after mixing {[(JohnPhos)AuCl] + $AgSbF_6$} + enyne (◆), {$[((JohnPhos)Au)_2Cl]SbF_6$ + enyne} (×) and {$[((JohnPhos)Au)_2Cl]SbF_6$ (1.5 mol %) + enyne} (×), respectively.

The reaction was found to be faster after the addition of $AgSbF_6$ to a mixture of $[((JohnPhos)Au)_2Cl]SbF_6$ (◆) and the enyne **21** but not as fast as the addition of the silver salt to [(JohnPhos)AuCl] and the enyne (●). These results illustrate the high stability of the digoldchloride cations formed as well as the difficulties of the substrates to rapidly associate to one of the gold centers.

Outlook

We are rather reluctant to classify the reactions studied into the categories proposed by the group of Shi[61] since in our experience, there are too many variables to consider in gold(I)-catalyzed reactions. As it has been shown, the outcome of a particular reaction can dramatically change when different procedures were used to generate the active catalyst. The coordinating character of both the solvent and the counterion of the silver salt used as well as the order of addition of the reagents are parameters that can have detrimental effects.

Herein, we expose some guidelines to consider when performing a gold(I)-catalyzed reaction starting from a LAuCl precatalyst. First, a blank experiment using the silver salt as the sole catalyst should be performed. If the substrate(s) decompose(s) or polymerize(s) giving side products, the isolated cationic or neutral gold(I) complexes should be used as catalysts (see introduction part).[53,55] However, if the substrate(s) remain(s) unchanged, the active species can be generated *in situ* in the reaction mixture and thus the order of addition of the metals has to be considered if the reaction is performed in a non-coordinating solvent.

To avoid the formation of the stable and less efficient digoldchloride cations when using silver salts with non-coordinating counterions, the silver salt should be added last. Although the results in terms of efficiency or yield would be the same if the substrate is highly coordinating to one of the gold centers, a dramatic effect can be seen if the process is slow or does not occur at all. When the silver salt has a coordinating counterion (e.g. triflimide), then the order of mixture of the two metal sources is inconsequential as the dinuclear gold complexes will not be formed.[77]

---

[77] To obtain the covalent complex as the sole product, the silver salt has to be added slowly to the L–Au–Cl.

Simultaneous Findings and Further Studies

While the manuscript of this project was in preparation, the group of Jones reported a new trinuclear complex incorporating silver and gold coordinated to a central chloride anion.[78] Cooling the crude mother liquor (filtered through Celite) of 1 equiv of [(JohnPhos)AuCl] with 1 equiv of $AgSbF_6$ in CH_2Cl_2 gave crystals of **H** (Figure 13).

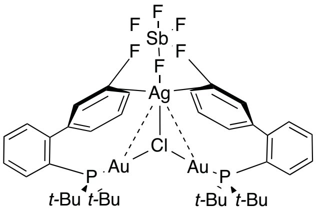

Figure 13 Structure of Au–Ag–Au trinuclear complex **H**.

We never observed the formation of this complex, neither by ^{31}P NMR, nor by X-ray analysis. However, the authors concluded that "*in the presence of substrate, silver incorporation is likely minimal*". They described the complex obtained as a snapshot of the chloride abstraction process.[52]

During the same period, the group of Albrecht observed a different outcome in the reaction when mixing [(NHC)AuCl] and silver salts in a non-coordinating environment.[79] Under these conditions, homoleptic bis(carbene) gold(I) complexes were obtained from the corresponding carbene gold chloride analogues and $AgBF_4$ (Scheme 19). Carbenes could be easily transferred by dissociation to another Au center. This process was accelerated in the presence of Ag^+ cations.

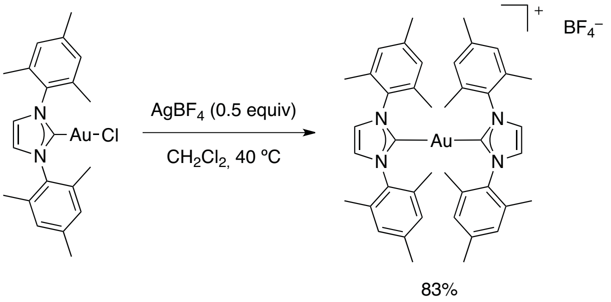

Scheme 19 Formation of homoleptic Bis(IMes) gold complex via carbene transfer.

We hypothesized that the formation of such species is very specific of NHC ligands due to its facile transfer in the presence of silver(I) salts.[79] However, this is not the case when using bulky phosphines as ligands.

---

[78] Zhu, Y.; Day, C. S.; Zhang, L.; Hauser, K. J.; Jones, A. C. *Chem. Eur.–J.* **2013**, *19*, 12264–12271.

[79] Canseco-Gonzalez, D.; Petronilho, A.; Mueller-Bunz, H.; Ohmatsu, K.; Ooi, T.; Albrecht, M. *J. Am. Chem. Soc.* **2013**, *135*, 13193–13203.

With these results, chemists were prompted to investigate other ways to generate the cationic active species circumventing the use of silver salts. Thus, the group of Gandon reported the use of Lewis acids of the transition and main group (Cu(I), Cu(II), Zn(II), In(III), Si(IV), Bi(III)) avoiding the use of silver salts.[80] However, the limited set of gold-catalyzed reactions tested using this method as well as the lesser efficiency observed with respect to the conventional procedure, makes this protocol not particularly attractive.

Following a similar approach, the groups of Hammond and Bo offered another way to generate gold(I) active species by using Brønsted or Lewis acid assisted activation of imidogold precatalysts (L–Au–Phth, Phth = phthalimide; L = PPh_3, JohnPhos, IPr).[81] This system was applied to several described Au(I)-catalyzed reactions and the most efficient additive to activate L–Au–Phth was found to be Tf_3CH, a very strong acid in aqueous solution and although its pK_a has not been determined, it is estimated to lie between concentrated HNO_3 and $HOSO_2F$.[82]

Very recently, the group of Michon has reported the crystal structure of a digold complex coordinated to tetrafluoroborate.[83] This is the first time that this weakly coordinating anion binds to a gold center. Interestingly, crystals were grown in toluene and no η^1/η^2 coordination of the arene solvent and the metal was observed, as was shown with JohnPhos[53a] or NHC[84] as ligands.

---

[80] Fang, W.; Presset, M.; Guérinot, A.; Bour, C.; Bezzenine-Lafollée, S.; Gandon, V. *Chem.–Eur. J.* **2014**, *20*, 5439–5446.

[81] Han, J.; Shimizu, N.; Lu, Z.; Amii, H.; Hammond, G. B.; Xu, B. *Org. Lett.* **2014**, *16*, 3500–3503.

[82] Turowsky, L.; Seppelt, K. *Inorg. Chem.* **1988**, *27*, 2135–2137.

[83] Abadie, M.-A.; Trivelli, X.; Medina, F.; Capet, F.; Roussel, P; Agbossou-Niedercorn, F.; Michon, C. *Chem.Cat.Chem.* **2014**, *6*, 2235–2239.

[84] Lavallo, V.; Frey, G. D.; Kousar, S.; Donnadieu, B.; Bertrand, G. *Proc. Natl. Acad. Sci. USA* **2007**, *104*, 13569–13573.

Conclusions

We have shown that the formation of robust chloride-bridged dinuclear gold(I) complexes [((JohnPhos)Au)$_2$Cl]X occurs readily when mixing [(JohnPhos)AuCl] precatalyst with silver salts with a non-coordinating anion in the absence of the substrate in non-coordinating solvents such as CH_2Cl_2 (Scheme 20).

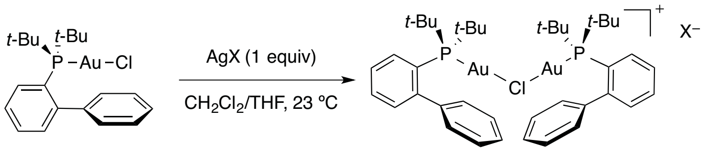

X = OTf, BF_4 or SbF_6

Scheme 20 Formation of bridged dinuclear gold(I) complexes [((JohnPhos)Au)$_2$Cl]X (**B**).

These dinuclear gold(I) complexes are significantly less active than cationic complexes [(JohnPhos)Au(NCMe)]X. The formation of these dinuclear gold(I) complexes can be avoided if the silver salt is the last reagent added into the reaction mixture. Based on these results, we have proposed some guidelines to follow when generating *in situ* the active gold species starting from [LAuCl] precatalysts.

Experimental Part

General Information

Unless otherwise stated, reactions were carried out under argon atmosphere in solvents dried by passing through an activated alumina column on a PureSolv^{TM} solvent purification system (Innovative Technologies, Inc., MA). Analytical thin layer chromatography was carried out using TLC-aluminium sheets with 0.2 mm of silica gel (Merck GF$_{234}$) using UV light as the visualizing agent and an acidic solution of vanillin in ethanol as the developing agent. Chromatograpy purifications were carried out using flash grade silica gel (SDS Chromatogel 60 ACC, 40-60 mm) or automated flash chromatographer CombiFlash Companion. Preparative TLC was performed on 20 cm × 20 cm silica gel plates (2.0 mm thick, catalogue number 02015, Analtech). If indicated, preparative TLC was performed on 20 cm x 20 cm aluminium oxide plates (0.25 mm thick, 90066, Fluka). Organic solutions were concentrated under reduced pressure on a Büchi rotary evaporator. NMR spectra was recorded at 298 K on a Bruker Avance 400 Ultrashield and Bruker Avance 500 Ultrashield apparatus. Mass spectra were recorded on a Waters Micromass LCT Premier (ESI), Waters Micromass GCT (EI, CI) and Bruker Daltonics Autoflex (MALDI) spectrometers. Elemental analyses were performed on a LECO CHNS 932 micro-analyzer at the Universidad Complutense de Madrid. Melting points were determined using a Büchi melting point apparatus.

Crystal structure determinations were carried out using a Bruker-Nonius diffractomer equipped with an APPEX 2 4K CCD area detector, a FR591 rotating anode with MoK$_a$ radiation, Montel mirrors as monochromator and a Kryoflex low temperature device (T = –173 ºC). Full-sphere data collection was used with w and j scans. *Programs used*: Data collection APEX-2, data reduction Bruker Saint V/.60A and absorption correction SADABS. Structure Solution and Refinement: Crystal structure solution was achieved using direct methods as implement in SHELXTL and visualized using the program XP. Missing atoms were subsequently located from difference Fourier synthesis and added to the atom list. Least-squares refinement on F2 using all measured intensities was carried out using the program SHELXTL. All non-hydrogen atoms were refined including anisotropic displacement parameters.

Synthesis of Mononuclear Gold(I) Complexes

Chloro[(1,1′-biphenyl-2-yl)di-*tert*-butylphosphine]gold(I) (A)

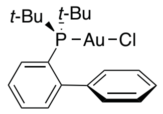

To a solution of $NaAuCl_4 \cdot 2H_2O$ (398 mg, 1 mmol) in 10 mL H_2O in an ice bath, thiodiethanol (312 µL, 3.01 mmol) was added. After stirring for 45 min, [(1,1′ -biphenyl-2-yl)di-tert butylphosphine] (299 mg, 1 mmol) in 10 mL EtOH were added to the mixture. After 4 h stirring, the white solid was filtered (with a porous filter), washed with MeOH and dried under vacuum.

504 mg (0.949 mmol) of [(JohnPhos)AuCl] (**A**) were isolated in 95% yield.

^{1}H NMR (500 MHz, CD_2Cl_2) δ_H 7.89 (td, *J* = 7.6, 1.4 Hz, 1H), 7.56 – 7.47 (m, 3H), 7.39 (t, *J* = 7.7 Hz, 2H), 7.29 (dt, *J* = 4.7, 2.3 Hz, 1H), 7.15 (dd, *J* = 8.5, 1.5 Hz, 2H), 1.40 (d, *J* = 15.6 Hz, 18H). **^{13}C NMR** (125 MHz, CD_2Cl_2) δ_C 150.4 (d, *J* (^{13}C-^{31}P) = 13.4 Hz), 142.1

(d, J (^{13}C-^{31}P) = 6.7 Hz), 134.1 (d, J (^{13}C-^{31}P) = 2.9 Hz), 133.5 (d, J (^{13}C-^{31}P) = 7.5 Hz), 130.9 (d, J (^{13}C-^{31}P) = 2.9 Hz), 129.7, 128.9, 128.3, 127.2, 126.4 (d, J (^{13}C-^{31}P) = 45.1 Hz), 38.1 (d, J (^{13}C-^{31}P) =25.6 Hz), 31.1 (d, J (^{13}C-^{31}P) = 6.7 Hz). **^{31}P {^{1}H} NMR** (202 MHz, CD_2Cl_2) δ_P 63.2.

Trifluoromethanesulfonate[(1,1′-biphenyl-2-yl)di-*tert*-butylphosphine]gold(I) (C1)

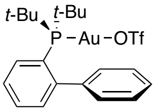

Silver trifluoromethanesulfonate (121 mg, 0.471 mmol) was added to a solution of chloro[(1,1′-biphenyl-2-yl)di-*tert*-butylphosphine]gold(I) (50 mg, 0.094 mmol) in dry CH_2Cl_2 (1 mL). After stirring the reaction mixture for 2 h at 23 ºC, the crude was filtered through a pad of Celite and cotton at the top of the pipette and Teflon filters (2 x 0.22 μm). The resulting colorless solution was evaporated to dryness under vacuum to give the neutral complex as a white solid. White crystals were grown by crystallization with CH_2Cl_2/pentane.

47 mg (0.073 mmol) of trifluoromethanesulfonate [(1,1′-biphenyl-2-yl)di-*tert*-butylphosphine]gold(I) (**C1**) were obtained in 77% yield.

^{1}H NMR (400 MHz, CD_2Cl_2) δ_H 7.89 (td, J = 7.8, 1.4 Hz, 1H), 7.63 – 7.43 (m, 5H), 7.38 – 7.32 (m, 1H), 7.22 – 7.16 (m, 2H), 1.40 (d, J = 16.2 Hz, 18H). **^{13}C NMR** (126 MHz CD_2Cl_2) δ_C 150.1 (d, J (^{13}C-^{31}P) = 11.7 Hz), 133.5 (d, J (^{13}C-^{31}P) = 4.2 Hz), 131.7 (d, J (^{13}C-^{31}P) = 2.4 Hz), 129.9, 129.2, 128.9, 127.7 (d, J (^{13}C-^{31}P) = 7.8 Hz), 124.4 (d, J (^{13}C-^{31}P) = 51.0 Hz), 121.9, 119.4, 38.6 (d, J (^{13}C-^{31}P) = 28.0 Hz), 31.1 (d, J (^{13}C-^{31}P) = 6.1 Hz). **^{31}P {^{1}H} NMR** (162 MHz, CD_2Cl_2) δ_P 60.4. **^{19}F NMR** (376 MHz, CD_2Cl_2) δ_F –77.7. **HRMS** (ESI+) calculated for $[C_{22}H_{27}AuP]^+$ (M^+–CF_3O_3S): 495.1511, found *m/z* 495.1511. Structure confirmed by **X-ray** diffraction.

Triflimide[(1,1′-biphenyl-2-yl)di-*tert*-butylphosphine]gold(I) (C2)

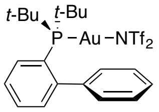

Silver bis(trifluoromethanesulfonyl)imide (181 mg, 0.471 mmol) was added to a solution of chloro[(1,1′-biphenyl-2-yl)di-*tert*-butylphosphine]gold(I) (50 mg, 0.094 mmol) in dry CH_2Cl_2 (1 mL). After stirring the reaction mixture for 2 h at 23 ºC, the crude was filtered through a pad of Celite and cotton at the top of the pipette and Teflon filters (2 x 0.22 μm). The resulting colorless solution was evaporated to dryness under vacuum to give the neutral complex as a white solid. Crystals were grown by crystallization with CH_2Cl_2/pentane.

58.4 mg (0.075 mmol) of triflimide[(1,1′-biphenyl-2-yl)di-*tert*-butylphosphine]gold(I) (**C2**) were obtained (80% yield).

^{1}H NMR (400 MHz, CD_2Cl_2) δ_H 7.94 –7.88 (m, 1H), 7.61 – 7.44 (m, 5H), 7.32 – 7.26 (m, 1H), 7.24 – 7.18 (m, 2H), 1.41 (d, J = 16.1 Hz, 18H). **^{13}C NMR** (101 MHz, CD_2Cl_2) δ_C 149.6 (d, J (^{13}C-^{31}P) = 11.8 Hz), 141.9 (d, J (^{13}C-^{31}P) = 7.2 Hz), 133.5 (d, J (^{13}C-^{31}P) = 7.5 Hz), 133.3 (d, J (^{13}C-^{31}P) = 4.0 Hz), 131.1 (d, J (^{13}C-^{31}P) = 2.5 Hz), 129.2, 129.0, 128.2, 127.5 (d, J (^{13}C-^{31}P) = 7.6 Hz), 124.3 (d, J (^{13}C-^{31}P) = 49.2 Hz), 38.1 (d, J (^{13}C-^{31}P) = 26.2 Hz), 30.7 (d, J (^{13}C-^{31}P) = 6.3 Hz). **^{31}P {^{1}H} NMR** (162 MHz, CD_2Cl_2) δ_P 60.8. **^{19}F NMR** (376 MHz, CD_2Cl_2) δ_F –74.4. **HRMS** (ESI+) calculated for $[C_{22}H_{27}AuP]^+$ (M^+–$C_2F_6NO_4S_2$): 495.1511, found *m/z* 495.1512. Structure confirmed by **X-ray** diffraction.

Bromo[(1,1′-biphenyl-2-yl)di-*tert*-butylphosphine]gold(I)

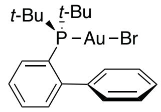

To a stirred solution of chloro[(1,1′-biphenyl-2-yl)di-*tert*-butylphosphine]gold(I) (60 mg, 0.113 mmol) in 1.4 mL $CHCl_3$, was added a 3.2 mL sat. solution of NaBr in a 1:1 mixture of EtOH/H_2O (v/v). The mixture was stirred for 2 h at 23 ºC, after which organic solvents were removed under vacuum. The organic fraction was extracted with CH_2Cl_2 (x3), dried over Na_2SO_4 and solvent was evaporated.

60 mg (0.104 mmol) of bromo[(1,1′-biphenyl-2-yl)di-*tert*-butylphosphine]gold(I) were isolated in 92% yield.

^{1}**H NMR** (400 MHz, $CDCl_3$) δ_H 7.87 (td, J = 7.3, 1.6 Hz, 1H), 7.59 – 7.45 (m, 3H), 7.40 (t, J = 7.8 Hz, 2H), 7.33 – 7.27 (m, 1H), 7.11 (dd, J = 8.2, 1.3 Hz, 2H), 1.41 (d, J = 15.6 Hz, 18H). ^{13}**C NMR** (101 MHz, CD_2Cl_2) δ_C 150.3 (d, J (^{13}C-^{31}P) = 14.1 Hz), 142.1 (d, J (^{13}C-^{31}P) = 6.8 Hz), 134.7 (d, J (^{13}C-^{31}P) = 2.4 Hz), 133.4 (d, J (^{13}C-^{31}P) = 7.3 Hz), 130.7 (d, J (^{13}C-^{31}P) = 2.2 Hz), 129.3, 128.9, 128.4, 126.8 (d, J (^{13}C-^{31}P) = 6.6 Hz), 38.1 (d, J (^{13}C-^{31}P) = 24.6 Hz), 31.0 (d, J (^{13}C-^{31}P) = 6.9 Hz) (one ^{13}C is missing due to overlapping). ^{31}**P {^{1}H} NMR** (202 MHz, $CDCl_3$) δ_P 64.9. **HRMS** (ES+) calculated for $[C_{22}H_{26}AuPBr]^+$ (M^+–H): 597.0621, found *m/z* 597.0626.

Iodo[(1,1′-biphenyl-2-yl)di-*tert*-butylphosphine]gold(I)

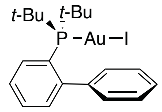

KI (338 mg, 2.04 mmol) was suspended in a solution of chloro[(1,1′-biphenyl-2-yl)di-*tert*-butylphosphine]gold(I) (60 mg, 0.113 mmol) in 5 mL THF. After 48 h stirring at 23 ºC, solvent was removed under reduced pressure.

66 mg (0.106 mmol) of iodo[(1,1′-biphenyl-2-yl)di-*tert*-butylphosphine]gold(I) were isolated in 94% yield.

^{1}**H NMR** (500 MHz, CD_2Cl_2) δ_H 7.90 (td, J = 7.1, 1.8 Hz, 1H), 7.57 – 7.47 (m, 3H), 7.37 (t, 2H), 7.29 – 7.25 (m, 1H), 7.12 (dd, J = 8.2, 1.2 Hz, 1H), 1.41 (d, J = 15.6 Hz, 18H). ^{13}**C NMR** (126 MHz, CD_2Cl_2) δ_C 150.6, 143.2 (d, J (^{13}C-^{31}P) = 6.9 Hz), 134.7 (d, J (^{13}C-^{31}P) = 2.0 Hz), 133.8 (d, J (^{13}C-^{31}P) = 7.3 Hz), 131.1 (d, J (^{13}C-^{31}P) = 2.3 Hz), 129.8, 129.6, 128.7, 127.4 (d, J (^{13}C-^{31}P) = 6.4 Hz), 127.0 (d, J (^{13}C-^{31}P) = 41.7 Hz), 38.7 (d, J (^{13}C-^{31}P) = 22.9 Hz), 31.2 (d, J (^{13}C-^{31}P) = 6.9 Hz). ^{31}**P {^{1}H} NMR** (202 MHz, CD_2Cl_2) δ_P 67.8. **HRMS** (ES+) calculated for $[C_{22}H_{26}AuPI]^+$ (M^+–H): 645.0483, found *m/z* 645.0483.

Synthesis of Dinuclear Gold(I) Complexes

Although the initial isolation of the dinuclear gold(I) complexes was accomplished using 1:1 ratio of Au:Ag in CH_2Cl_2 , its synthesis was proven to be more efficient following a modified procedure of Schmidbaur.[70]

Chloro bis{[(1,1′-biphenyl-2-yl)di-*tert*-butylphosphine]gold(I)} trifluoromethane sulfonate (B1)

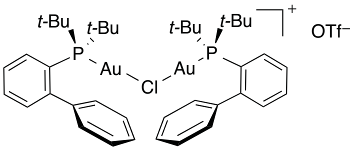

A solution of chloro[(1,1′-biphenyl-2-yl)di-*tert*-butylphosphine]gold(I) (205 mg, 0.389 mmol) in dry CH_2Cl_2 (10 mL) was added to a solution of silver trifluoromethanesulfonate (50 mg, 0.195 mmol) in 10 mL of dry THF at 23 ºC. After stirring the reaction mixture for 2 h at the same temperature, the

crude was filtered through a pad of Celite and cotton at the top of the pipette and the resulting colorless solution was evaporated to dryness under vacuum. White crystals were obtained after crystallization from CH_2Cl_2/pentane (1:1).
206 mg (0.175 mmol) of **B1** were obtained in 90% yield.
^{1}H NMR (500 MHz, CD_2Cl_2) δ_H 7.92–7.85 (m, 2H), 7.63–7.56 (m, 4H), 7.55–7.50 (m, 2H), 7.43–7.36 (m, 4H), 7.34–7.29 (m, 2H), 7.16–7.11 (m, 4H), 1.40 (d, *J* = 16.1 Hz, 36H). **^{13}C NMR** (126 MHz CD_2Cl_2) δ_C 149.7 (d, *J* (^{13}C-^{31}P) = 12.2 Hz), 143.1 (d, *J* (^{13}C-^{31}P) = 6.9 Hz), 133.9 (d, *J* (^{13}C-^{31}P) = 7.9 Hz), 133.8 (d, *J* (^{13}C-^{31}P) = 4.0 Hz), 131.9 (d, *J* (^{13}C-^{31}P) = 2.6 Hz), 130.0, 129.3, 128.8, 128.1 (d, *J* (^{13}C-^{31}P) = 7.4 Hz), 124.9 (d, *J* (^{13}C-^{31}P) = 49.0 Hz), 38.7 (d, *J* (^{13}C-^{31}P) = 26.0 Hz), 31.2 (d, *J* (^{13}C-^{31}P) = 6.4 Hz). **^{31}P {^{1}H} NMR** (202 MHz, CD_2Cl_2) δ_P 64.6; δ_P (193 K) 63.1. **^{19}F NMR** (376 MHz, CD_2Cl_2) δ_F –78.7. **HRMS** (ESI+) calculated for $[C_{40}H_{54}Au_2ClP_2]^+$ (M^+–CF_3O_3S): 1025.2710, found *m/z* 1025.2704. Structure confirmed by **X-ray** diffraction.

Chloro bis{[(1,1′-biphenyl-2-yl)di-*tert*-butylphosphine]gold(I)} triflimide (B2)

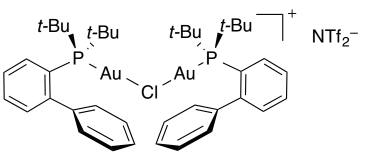

A solution of chloro[(1,1′ -biphenyl-2-yl)di-tert butylphosphine]gold(I) (205 mg, 0.387 mmol) in dry CH_2Cl_2 (10 mL) is added to a solution of silver bis(trifluoromethanesulfonyl)
imide (75 mg, 0.193 mmol) in 10 mL of dry THF at 23 ºC. After stirring the reaction mixture for 2h at the same temperature, the crude was filtered through a pad of Celite and cotton at the top of the pipette and the resulting colorless solution was evaporated to dryness under vacuum. White crystals were obtained after crystallization from CH_2 Cl_2/pentane (1:1).
216.3 mg (0.166 mmol) of **B2** were obtained in 86% yield.
^{1}H NMR (400 MHz, CD_2Cl_2) δ_H 7.93 – 7.84 (m, 2H), 7.65 – 7.54 (m, 4H), 7.56 – 7.45 (m, 2H), 7.43 – 7.35 (m, 4H), 7.34 – 7.26 (m, 2H), 7.18 – 7.08 (m, 4H), 1.39 (d, *J* = 16.0 Hz, 36H). **^{13}C NMR** (126 MHz CD_2Cl_2) δ_C 149.6 (d, *J* (^{13}C-^{31}P) = 12.3 Hz), 143.1 (d, *J* (^{13}C-^{31}P) = 6.8 Hz), 133.8 (d, *J* (^{13}C-^{31}P) = 7.2 Hz), 133.8 (d, *J* (^{13}C-^{31}P) = 3.3 Hz), 131.9 (d, *J* (^{13}C-^{31}P) = 2.5 Hz), 130.0, 129.3, 128.8, 128.1 (d, *J* (^{13}C-^{31}P) = 7.4 Hz), 124.9 (d, *J* (^{13}C-^{31}P) = 49.1 Hz), 38.7 (d, *J* (^{13}C-^{31}P) = 26.2 Hz), 31.2 (d, *J* (^{13}C-^{31}P) = 6.4 Hz). **^{31}P {^{1}H} NMR** (202 MHz, CD_2Cl_2) δ_P 64.6; δ_P (193 K) 63.1. **^{19}F NMR** (376 MHz, CD_2Cl_2) δ_F –78.8. **HRMS** (ESI+) calculated for $[C_{40}H_{54}Au_2ClP_2]^+$ (M^+–$C_2F_6NO_4S_2$): 1025.2715 found *m/z* 1025.2744. Structure confirmed by **X-ray** diffraction.

Chloro bis{[(1,1′-biphenyl-2-yl)di-*tert*-butylphosphine]gold(I)} tetrafluoroborate (B3)

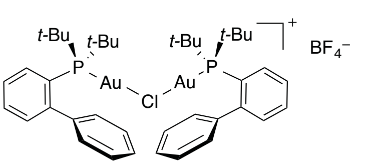

A solution of chloro[(1,1′-biphenyl-2-yl)di-*tert*-butylphosphine]gold(I) (205 mg, 0.380 mmol) in dry CH_2Cl_2 (10 mL) is added to a solution of silver tetrafluoroborate (37 mg, 0.190 mmol) in 10 mL of THF at 23 ºC. After stirring the reaction mixture for 2 h at the same temperature, the crude was filtered through a pad of Celite and cotton at the top of the pipette and the resulting colorless solution was evaporated to dryness under vacuum. White crystals were obtained after crystallization from CH_2Cl_2/*n*-pentane (1:1).
171 mg (0.154 mmol) of **B3** were obtained in 81% yield.
^{1}H NMR (400 MHz, CD_2Cl_2) δ_H 7.92 – 7.85 (m, 2H), 7.63 – 7.56 (m, 4H), 7.55 – 7.49 (m,

2H), 7.40 – 7.35 (m, 4H), 7.34 – 7.28 (m, 2H), 7.17 – 7.10 (m, 4H), 1.39 (d, *J* = 16.0 Hz, 36H). **^{13}C NMR** (126 MHz CD_2Cl_2) δ_C 149.1 (d, *J* (^{13}C-^{31}P) = 12.5 Hz), 142.5 (d, *J* (^{13}C-^{31}P) = 6.9 Hz), 133.4 (d, *J* (^{13}C-^{31}P) = 7.7 Hz), 133.3 (d, *J* (^{13}C-^{31}P) = 3.6 Hz), 131.4 (d, *J* (^{13}C-^{31}P) = 2.5 Hz), 129.5, 128.7, 128.2, 127.5 (d, *J* (^{13}C-^{31}P) = 7.6 Hz), 124.3 (d, *J* (^{13}C-^{31}P) = 49.2 Hz), 38.1 (d, *J* (^{13}C-^{31}P) = 26.2 Hz), 30.7 (d, *J* (^{13}C-^{31}P) = 6.3 Hz). **^{31}P {^{1}H} NMR** (202 MHz, CD_2Cl_2) δ_P 64.8; δ_P (193 K) 63.1. **^{19}F NMR** (376 MHz, CD_2Cl_2) δ_F –153.6. **HRMS** (ESI+) calculated for $[C_{40}H_{54}Au_2ClP_2]^+$ (M^+–BF_4): 1025.2715 found *m/z* 1025.2747. Structure confirmed by **X-ray** diffraction.

Chloro bis{[(1,1′-biphenyl-2-yl)di-*tert*-butylphosphine]gold(I)} hexafluoroantimonate (B4)

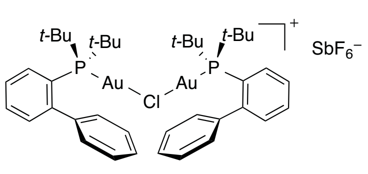

A solution of chloro[(1,1′-biphenyl-2-yl)di-*tert*-butylphosphine]gold(I) (205 mg, 0.378 mmol) in dry CH_2Cl_2 (10 mL) is added to a solution of silver hexafluoroantimonate (65 mg, 0.189 mmol) in 10 mL of THF at 23 ºC. After stirring the reaction mixture for 2 h at the same temperature, the crude was filtered through a pad of Celite and cotton at the top of the pipette and the resulting colorless solution was evaporated to dryness under vacuum. White crystals were obtained after crystallization from CH_2Cl_2/pentane (1:1).

210 mg (0.166 mmol) of **B4** were obtained in 88% yield.

^{1}H NMR (400 MHz, CD_2Cl_2) δ_H 7.96–7.89 (m, 2H), 7.67–7.59 (m, 4H), 7.59–7.52 (m, 2H), 7.47–7.39 (m, 4H), 7.38–7.31 (m, 2H), 7.22–7.13 (m, 4H), 1.43 (d, *J* = 16.2 Hz, 36H). **^{13}C NMR** (101 MHz CD_2Cl_2) δ_C 149.8 (d, *J* (^{13}C-^{31}P) = 12.2 Hz), 143.1 (d, *J* (^{13}C-^{31}P) = 6.7 Hz), 133.9 (d, *J* (^{13}C-^{31}P) = 7.9 Hz), 133.8 (d, *J* (^{13}C-^{31}P) = 3.7 Hz), 131.9 (d, *J* (^{13}C-^{31}P) = 2.4 Hz), 130.0, 129.3, 128.8, 128.1 (d, *J* (^{13}C-^{31}P) = 7.4 Hz), 124.8 (d, *J* (^{13}C-^{31}P) = 49.0 Hz), 38.7 (d, *J* (^{13}C-^{31}P) = 26.0 Hz), 31.2 (d, *J* (^{13}C-^{31}P) = 6.3 Hz). **^{31}P {^{1}H} NMR** (202 MHz, CD_2Cl_2) δ_P 64.8; δ_P (193 K) 63.1. **HRMS** (ESI+) calculated for $[C_{40}H_{54}Au_2ClP_2]^+$ (M^+–BF_4): 1025.2715, found *m/z* 1025.2719. Structure confirmed by **X-ray** diffraction.

Hydroxy bis{[(1,1′-biphenyl-2-yl)di-*tert*-butylphosphine]gold(I)} tetrafluoroborate (D)

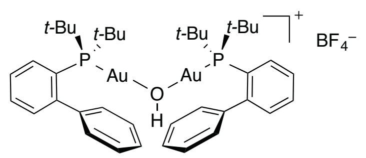

This complex was prepared according to the procedure used for the synthesis of [(JohnPhosAu)$_2$(OH)]SbF$_6$.[85] [(JohnPhos)AuNCMe]BF$_4$ (40 mg, 0.065 mmol) was suspended in water (1 mL) and stirred at 60 ºC for 72 h under air. The reaction mixture was extracted with CH_2Cl_2 and the organic layer was washed three times with a large excess of water and dried over Na_2SO_4. The mixture was filtered and solvent was removed under reduced pressure. White crystals were obtained after crystallization from CH_2Cl_2/*n*-pentane (1:1).

35 mg of **D** (0.032 mmol) were obtained in 98% yield.

---

[85] Adriaenssens, L.; Escribano-Cuesta, A.; Homs, A.; Echavarren, A. M.; Ballester, P. *Eur. J. Org. Chem.* **2013**, 1494–1500.

^{1}H NMR (500 MHz, $CDCl_3$) δ_H 7.91 – 7.77 (m, 2H), 7.61 – 7.52 (m, 6H), 7.47 (t, *J* = 7.6 Hz, 4H), 7.34 – 7.27 (m, 2H), 7.24 – 7.17 (m, 4H), 1.38 (d, *J* = 15.9 Hz, 36H). **^{13}C NMR** (125 MHz, $CDCl_3$) δ_C 149.5 (d, *J* (^{13}C-^{31}P) = 15.5 Hz), 144.32 (d, *J* (^{13}C-^{31}P) = 8.1 Hz), 133.8 (d, *J* (^{13}C-^{31}P) = 4.9 Hz), 133.5 (d, *J* (^{13}C-^{31}P) = 9.9 Hz), 130.7 (d, *J* (^{13}C-^{31}P) = 2.3 Hz), 130.7, 128.9, 128.0 (d, *J* (^{13}C-^{31}P) = 9.5 Hz), 127.7, 125.4 (d, *J* (^{13}C-^{31}P) = 61.7 Hz), 38.2 (d, *J* (^{13}C-^{31}P) = 34.7 Hz), 31.1 (d, *J* (^{13}C-^{31}P) = 7.7 Hz). **^{31}P {^{1}H} NMR** (202 MHz, $CDCl_3$) δ_P 60.6. Structure confirmed by **X-ray** diffraction.

Bromo bis{[(1,1′-biphenyl-2-yl)di-*tert*-butylphosphine]gold(I)} hexafluoroantimonate

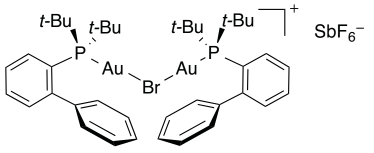

A solution of chloro[(1,1′-biphenyl-2-yl)di-*tert*-butylphosphine]gold(I) (60 mg, 0.105 mmol) in dry CH_2Cl_2 (3 mL) was added to a solution of silver hexafluoroantimonate (18 mg, 0.052 mmol) in 3 mL of THF at 23 ºC. After stirring the reaction mixture for 2 h at the same temperature, the crude was filtered through a pad of Celite and cotton at the top of the pipette and the resulting colorless solution was evaporated to dryness under vacuum. White crystals were obtained after crystallization from CH_2Cl_2/pentane (1:1). 67 mg (0.051 mmol) of $[((JohnPhos)Au)_2Br]SbF_6$ were obtained in 98% yield.

^{1}H NMR (500 MHz, CD_2Cl_2) δ_H 7.90 (ddd, *J* = 7.9, 6.7, 2.8 Hz, 2H), 7.63–7.55 (m, 4H), 7.53 (t, *J* = 7.6 Hz, 2H), 7.38 (app t, *J* = 7.7 Hz, 4H), 7.30 (ddd, *J* = 6.5, 4.5, 2.9 Hz, 2H), 7.13 (dd, *J* = 8.2, 1.3 Hz, 4H), 1.40 (d, *J* = 16.1 Hz, 36H). **^{13}C NMR** (126 MHz, CD_2Cl_2) δ_C 149.8 (d, *J* (^{13}C-^{31}P) = 13.0 Hz), 143.2 (d, *J* (^{13}C-^{31}P) = 6.8 Hz), 134.0 (d, *J* (^{13}C-^{31}P) = 3.3 Hz), 133.8 (d, *J* (^{13}C-^{31}P) = 7.5 Hz), 131.8 (d, *J* (^{13}C-^{31}P) = 2.5 Hz), 130.0, 129.4, 128.7, 128.0 (d, *J* (^{13}C-^{31}P) = 7.3 Hz), 125.4 (d, *J* (^{13}C-^{31}P) = 47.2 Hz), 38.8 (d, *J* (^{13}C-^{31}P) = 25.0 Hz), 31.3 (d, *J* (^{13}C-^{31}P) = 6.4 Hz). **^{31}P {^{1}H} NMR** (202 MHz, CD_2Cl_2) δ_P 66.9. **HRMS** (MALDI) calculated for $[C_{40}H_{54}Au_2BrP_2]^+$ (M^+–SbF_6): 1069.2210, found *m/z* 1069.2150. Structure confirmed by **X-ray** diffraction.

Iodo bis{[(1,1'-biphenyl-2-yl)di-*tert*-butylphosphine]gold(I)} hexafluoroantimonate

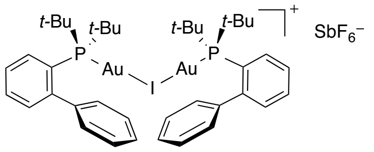

A solution of chloro[(1,1′-biphenyl-2-yl)di-*tert*-butylphosphine]gold(I) (58 mg, 0.093 mmol) in dry CH_2Cl_2 (1 mL) is added to a solution of silver hexafluoroantimonate (16 mg, 0.047 mmol) in 1 mL of THF at 23 ºC. After stirring the reaction mixture for 2 h at the same temperature, the crude was filtered through a pad of Celite and cotton at the top of the pipette and the resulting colorless solution was evaporated to dryness under vacuum. White crystals were obtained after crystallization from CH_2Cl_2/pentane (1:1).

60 mg (0.044 mmol) of $[((JohnPhos)Au)_2I]SbF_6$ were obtained in 95% yield.

^{1}H NMR (500 MHz, CD_2Cl_2) δ_H 7.90 (td, *J* = 7.5, 2.0 Hz, 2H), 7.62 – 7.54 (m, 4H), 7.52 (tt, *J* = 7.2, 1.3 Hz, 2H), 7.37 (app t, *J* = 7.5 Hz, 4H), 7.31 – 7.23 (m, 2H), 7.12 (dd, *J* = 8.1, 1.3 Hz, 4H), 1.40 (d, *J* = 16.0 Hz, 36H). **^{13}C NMR** (126 MHz, CD_2Cl_2) δ 149.7 (d, *J* (^{13}C-^{31}P) = 13.6 Hz), 143.49 (d, *J* (^{13}C-^{31}P) = 6.9 Hz), 134.3 (d, *J* (^{13}C-^{31}P) = 2.7 Hz), 133.9 (d, *J* (^{13}C-^{31}P) = 7.5 Hz), 131.7 (d, *J* (^{13}C-^{31}P) = 2.4 Hz), 130.1, 129.8, 128.7, 128.03 (d, *J* (^{13}C-^{31}P) = 6.9 Hz), 125.6 (d, *J* (^{13}C-^{31}P) = 45.0 Hz), 39.0 (d, *J* (^{13}C-^{31}P) = 23.5 Hz), 31.3 (d, *J* (^{13}C-^{31}P) = 6.7 Hz). **^{31}P {^{1}H} NMR** (202 MHz, CD_2Cl_2) δ_P 69.4. **HRMS (**MALDI) calculated for $[C_{40}H_{54}Au_2IP_2]^+$ (M^+–SbF_6): 1117.2071, found *m/z* 1117.2055. Structure confirmed by **X-ray** diffraction.

Synthesis of σ-Mononuclear Gold(I) Complex F

[(1,1'-biphenyl-2-yl)di-*tert*-butylphosphine](2-phenylethynyl)gold(I)

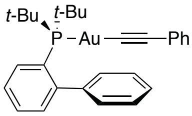

Lithium bis(trimethylsilyl)amide (165 mg, 0.989 mmol) was dissolved in THF (10 mL) and cooled to 0 ºC. Phenylacetylene (109 μl, 0.989 mmol) was added and the solution was stirred for 30 min. Afterwards, complex **A** (500 mg, 0.942 mmol) dissolved in THF (7.5 mL) was added and the solution was stirred overnight at 23 ºC. The crude was concentrated, dissolved in CH_2Cl_2 and filtered through Teflon pad. Solvent was removed under reduced pressure and the σ-gold complex was used without further purification.

549 mg of **F** (0.920 mmol) were isolated in 98% yield.

^{1}H NMR (400 MHz, CD_2Cl_2) δ_H 7.90 (dt, *J* = 6.8, 2.0 Hz, 1H), 7.54 – 7.44 (m, 5H), 7.37 – 7.32 (m, 2H), 7.30 – 7.13 (m, 6H), 1.42 (d, *J* = 14.9 Hz, 18H). **^{13}C NMR** (101 MHz, CD_2Cl_2) δ 150.7 (d, *J* (^{13}C-^{31}P) = 15.1 Hz), 143.3 (d, *J* (^{13}C-^{31}P) = 5.9 Hz), 136.5 (d, *J* (^{13}C-^{31}P) = 132.0 Hz), 135.2 (d, (^{13}C-^{31}P) = 1.0 Hz), 133.5 (d, *J* (^{13}C-^{31}P) = 7.4 Hz), 132.2, 130.8 (d, *J* (^{13}C-^{31}P) = 2.4 Hz), 129.8, 129.4, 128.5, 128.4, 127.9 (d, *J* (^{13}C-^{31}P) = 39.8 Hz), 127.3 (d, *J* (^{13}C-^{31}P) = 5.9 Hz), 127.2 (d, *J* (^{13}C-^{31}P) = 2.8 Hz), 126.4, 101.9 (d, *J* (^{13}C-^{31}P) = 23.6 Hz), 38.0 (d, *J* (^{13}C-^{31}P) = 22.6 Hz), 31.4 (d, *J* (^{13}C-^{31}P) = 7.0 Hz). **^{31}P {^{1}H} NMR** (162 MHz, CD_2Cl_2) δ_P 67.5. **HRMS (**ESI+) calculated for $[C_{28}H_{33}AuP]^+$ (M^++H): 597.1980 found *m/z* 597.1982.

Synthesis of σ,π-Dinuclear Gold(I) Complexes G

{Phenylethynyl[(1,1'-biphenyl-2-yl)di-*tert*-butylphosphine]gold(I)}[(1,1'-biphenyl-2-yl)di-*tert*-butylphosphine]gold(I) trifluoromethane sulfonate (G1)

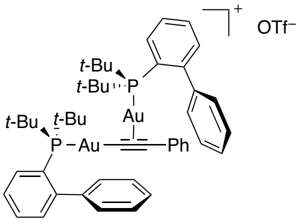

G1

Chloro[(1,1’-biphenyl-2-yl)di-tert-butylphosphine] gold(I) (55 mg, 0.104 mmol) and [(1,1’-biphenyl-2-yl)di-tertbutylphosphine](2-phenylethynyl)gold(I) (62 mg, 0.104 mmol) were dissolved in CH_2Cl_2 (9.4 mL). Then, (((trifluoromethyl)sulfonyl)oxy)silver (27 mg, 0.104 mmol) was added and the reaction mixture was stirred at 23 ºC for 30 min. The crude was filtered through Celite and concentrated. Finally, it was filtered through Teflon and washed with CH_2Cl_2. The solvent was removed to afford a white powder.

129 mg of **G1** (0.104 mmol) were isolated in 100% yield.

^{1}H NMR (400 MHz, CD_2Cl_2) δ_H 7.92 – 7.87 (m, 2H), 7.59 – 7.55 (m, 5H), 7.46 (d, *J* = 1.6 Hz, 4H), 7.39 – 7.30 (m, 6H), 7.28 – 7.24 (m, 2H), 7.12 (dd, *J* = 8.0, 1.6 Hz, 4H), 1.42 (d, *J* = 15.7 Hz, 36H). **^{13}C NMR** (101 MHz, CD_2Cl_2) δ_C 149.8 (d, *J* (^{13}C-^{31}P) = 14.0 Hz), 143.3 (d, *J* (^{13}C-^{31}P) = 7.0 Hz), 134.5, 133.8 (d, *J* (^{13}C-^{31}P) = 8.0 Hz), 133.3, 131.7, 130.7, 129.9, 129.6, 129.3, 128.6, 128.3 (d, *J* (^{13}C-^{31}P) = 6.9 Hz), 125.7 (d, *J* (^{13}C-^{31}P) = 45.0 Hz), 121.5, 38.5 (d, *J* (^{13}C-^{31}P) = 24.1 Hz), 31.4 (d, *J* (^{13}C-^{31}P) = 7.0 Hz). Two signals missing due to overlapping. **^{31}P {^{1}H} NMR** (162 MHz, CD_2Cl_2) δ_P 65.8. **^{19}F NMR** (376 MHz,

CD_2Cl_2) δ –79.6. **HRMS (**ESI+) calculated for $[C_{48}H_{59}Au_2P_2]^+$ (M^+–CF_3O_3S): 1091.3481, found *m/z* 1091.3429.

{Phenylethynyl[(1,1'-biphenyl-2-yl)di-*tert*-butylphosphine]gold(I)}[(1,1'-biphenyl-2-yl)di-*tert*-butylphosphine]gold(I) triflimide (G2)

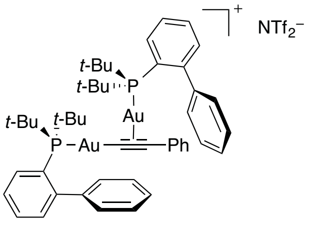

G2

Chloro[(1,1'-biphenyl-2-yl)di-tert-butylphosphine] gold(I) (55 mg, 0.104 mmol) and [(1,1'-biphenyl-2-yl)di-tertbutylphosphine](2-phenylethynyl)gold(I) (62 mg, 0.104 mmol) were dissolved in CH_2Cl_2 (9.4 mL). Then, (1,1,1-trifluoro-N-((trifluoromethyl)sulfonyl)methyl sulfonamido)silver (27 mg, 0.104 mmol) was added and the reaction mixture was stirred at 23 ºC for 30 min. The crude was filtered through Celite and concentrated. Finally, it was filtered through Teflon and washed with CH_2Cl_2. The solvent was removed to afford a white powder.

129 mg of **G2** (0.094 mmol) were isolated in 90% yield.

^{1}H NMR (400 MHz, CD_2Cl_2) δ_H 7.94 – 7.86 (m, 2H), 7.57 (m, 4H), 7.51 – 7.42 (m, 5H), 7.41 – 7.29 (m, 6H), 7.29 – 7.23 (m, 2H), 7.17 – 7.08 (m, 4H), 1.42 (d, *J* = 15.7 Hz, 36H). **^{13}C NMR** (101 MHz, CD_2Cl_2) δ_C 149.8 (d, *J* (^{13}C-^{31}P) = 14.1 Hz), 143.3 (d, *J* (^{13}C-^{31}P) = 6.6 Hz), 134.5, 133.8 (d, *J* (^{13}C-^{31}P) = 7.8 Hz), 133.3, 131.7 (d, *J* (^{13}C-^{31}P) = 1.9 Hz), 130.7, 129.9, 129.6, 129.2, 128.6, 128.0 (d, *J* (^{13}C-^{31}P) = 6.8 Hz), 125.7 (d, *J* (^{13}C-^{31}P) = 45.0 Hz), 121.4, 38.5 (d, *J* (^{13}C-^{31}P) = 24.0 Hz), 31.4 (d, *J* (^{13}C-^{31}P) = 7.1 Hz). **^{31}P {^{1}H} NMR** (162 MHz, CD_2Cl_2) δ_P 65.8. **^{19}F NMR** (376 MHz, CD_2Cl_2) δ_F –79.0. **HRMS (**ESI+) calculated for $[C_{48}H_{59}Au_2P_2]^+$ (M^+– $C_2F_6NO_4S_2$): 1091.3481, found *m/z* 1091.3432.

{Phenylethynyl[(1,1'-biphenyl-2-yl)di-*tert*-butylphosphine]gold(I)}[(1,1'-biphenyl-2-yl)di-*tert*-butylphosphine]gold(I) tetrafluoroborate (G3)

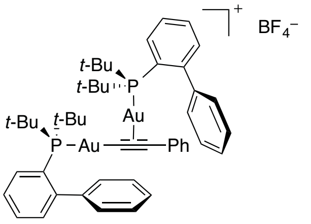

G3

Chloro[(1,1'-biphenyl-2-yl)di-tert-butylphosphine] gold(I) (55 mg, 0.104 mmol) and [(1,1'-biphenyl-2-yl)di-tertbutylphosphine](2-phenylethynyl)gold(I) (62 mg, 0.104 mmol) were dissolved in CH_2Cl_2 (9.4 mL). Then, silver tetrafluoroborate (20 mg, 0.104 mmol) was added and the reaction mixture was stirred at 23 ºC for 30 min. The crude was filtered through Celite and concentrated. Finally, it was filtered through Teflon and washed with CH_2Cl_2. The solvent was removed to afford a white powder.

120 mg of **G3** (0.102 mmol) were isolated in 98% yield.

^{1}H NMR (400 MHz, CD_2Cl_2) δ_H 7.94 – 7.85 (m, 2H), 7.61 – 7.53 (m, 4H), 7.51 – 7.42 (m, 5H), 7.40 – 7.30 (m, 6H), 7.29 – 7.24 (m, 2H), 7.17 – 7.08 (m, 4H), 1.42 (d, *J* = 15.7 Hz, 36H). **^{13}C NMR** (101 MHz, CD_2Cl_2) δ_C 149.8 (d, *J* (^{13}C-^{31}P) = 14.1 Hz), 143.3 (d, *J* (^{13}C-^{31}P) = 6.9 Hz), 134.5, 133.8 (d, *J* (^{13}C-^{31}P) = 7.6 Hz), 133.3, 131.7, 130.7, 129.9, 129.6, 129.3, 128.6, 128.0 (d, *J* (^{13}C-^{31}P) = 6.8 Hz), 125.7 (d, *J* (^{13}C-^{31}P) = 45.0 Hz), 121.5, 38.5 (d, *J* (^{13}C-^{31}P) = 23.9 Hz), 31.4 (d, *J* (^{13}C-^{31}P) = 7.0 Hz). Two signals missing due to overlapping. **^{31}P {^{1}H} NMR** (162 MHz, CD_2Cl_2) δ_P 65.8. **^{19}F NMR** (376 MHz, CD_2Cl_2) δ_F –153.6. **HRMS (**ESI+) calculated for $[C_{48}H_{59}Au_2P_2]^+$ (M^+– BF_4): 1091.3481, found *m/z* 1091.3384.

{Phenylethynyl[(1,1'-biphenyl-2-yl)di-*tert*-butylphosphine]gold(I)}[(1,1'-biphenyl-2-yl)di-*tert*-butylphosphine]gold(I) hexafluoroantimonate (G4)

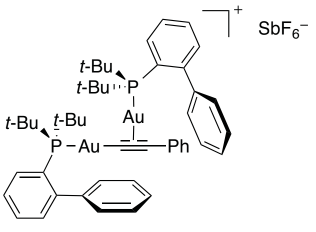

G4

Chloro[(1,1'-biphenyl-2-yl)di-tert-butylphosphine] gold(I) (55 mg, 0.104 mmol) and [(1,1'-biphenyl-2-yl)di-tertbutylphosphine](2-phenylethynyl)gold(I) (62 mg, 0.104 mmol) were dissolved in CH_2Cl_2 (9.4 mL). Then, silver hexafluoroantimonate (36 mg, 0.104 mmol) was added and the reaction mixture was stirred at 23 ºC for 30 min. The crude was filtered through Celite and concentrated. Finally, it was filtered through Teflon and washed with CH_2Cl_2. The solvent was removed to afford a white powder.

132 mg of **G4** (0.099 mmol) were isolated in 96% yield.

^{1}H NMR (400 MHz, CD_2Cl_2) δ_H 7.94 – 7.86 (m, 2H), 7.62 – 7.52 (m, 4H), 7.50 – 7.42 (m, 5H), 7.41 – 7.29 (m, 6H), 7.29 – 7.24 (m, 2H), 7.17 – 7.07 (m, 4H), 1.42 (d, J = 15.7 Hz, 36H). **^{13}C NMR** (101 MHz, CD_2Cl_2) δ_C 149.8 (d, J (^{13}C-^{31}P) = 13.7 Hz), 143.3 (d, J (^{13}C-^{31}P) = 6.6 Hz), 134.5, 133.8 (d, J (^{13}C-^{31}P) = 7.7 Hz), 133.3, 131.6 (d, J (^{13}C-^{31}P) = 2.2 Hz), 130.7, 129.9, 129.6, 129.2, 128.6, 128.0 (d, J (^{13}C-^{31}P) = 7.2 Hz), 125.7 (d, J (^{13}C-^{31}P) = 45.0 Hz), 121.5, 38.5 (d, J (^{13}C-^{31}P) = 24.1 Hz), 31.4 (d, J (^{13}C-^{31}P) = 7.0 Hz). Two signals missing due to overlapping. **^{31}P {^{1}H} NMR** (162 MHz, CD_2Cl_2) δ 65.8. **HRMS (**ESI+) calculated for $[C_{48}H_{59}Au_2P_2]^+$ (M^+– SbF_6): 1091.3481, found *m/z* 1091.3392.

General Procedures for Gold(I)-Catalyzed Reactions

[2+2] Intermolecular Cycloaddition Reaction of Phenylacetylene and α-Methylsyrene

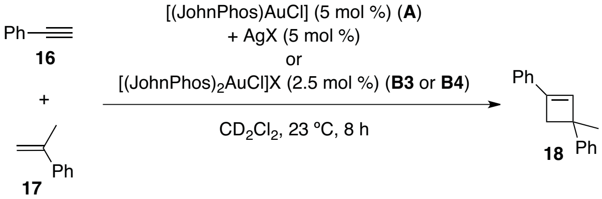
Ph
16
+
Ph
17
[(JohnPhos)AuCl] (5 mol %) (A)
+ AgX (5 mol %)
or
[(JohnPhos)$_2$AuCl]X (2.5 mol %) (B3 or B4)
CD_2Cl_2, 23 °C, 8 h
Ph
Ph
18

The cyclobutene was prepared according to the previous described procedure.[25] **^{1}H NMR** (400 MHz, $CDCl_3$) δ_H 7.39 (d, J = 7.2 Hz, 4H), 7.32 (dd, J = 13.7, 7.2 Hz, 4H), 7.27–7.22 (m, 1H), 7.21–7.15 (m, 1H), 6.72 (s, 1H), 2.93 (q, J = 12.5 Hz, 2H), 1.62 (s, 3H). **^{13}C NMR** (100 MHz, $CDCl_3$) δ_C 147.8, 143.9, 134.8, 133.9, 128.4, 128.2, 127.9, 126.0, 125.8, 124.7, 46.1, 44.4, 27.7.

In situ generation of the catalyst in the presence of the substrates

Phenylacetylene (19 μL, 0.169 mmol), α-methylstyrene (44 μL, 0.338 mmol) and diphenylmethane (14 μL, 0.085 mmol) dissolved in 0.7 mL of CD_2Cl_2 were introduced in a NMR tube. JohnPhosAuCl (4.5 mg, 8.45 μmol) and AgX (8.45 μmol) were then added and the resulting mixture was stirred for 8 h at 23 ºC. The reaction was monitored by ^{1}H NMR and ^{31}P NMR.

In situ generation of the catalyst and addition of the substrates

JohnPhosAuCl (4.5 mg, 8.45 μmol) and AgX (8.45 μmol) were dissolved in 0.7 mL

CD$_2$Cl$_2$ and introduced in a NMR tube. After 10 min stirring, phenylacetylene (19 μL, 0.169 mmol), α-methylstyrene (44 μL, 0.338 mmol) and diphenylmethane (14 μL, 0.085 mmol) were added. The resulting mixture was stirred for 8 h at 23 ºC and monitored by ^{1}H NMR and ^{31}P NMR.

In situ generation of the catalyst, filtration through Celite and addition of the substrates

In a vial, JohnPhosAuCl (4.5 mg, 8.45 μmol) and AgX (8.45 μmol) were dissolved in 0.7 mL CD$_2$Cl$_2$. After 10 min stirring, the slurry mixture was filtered through a pipette containing Celite and cotton (top and bottom). The resulting solution was introduced in a NMR tube along with phenylacetylene (19 μL, 0.169 mmol), α-methylstyrene (44 μL, 0.338 mmol) and diphenylmethane (14 μL, 0.085 mmol). The resulting mixture was stirred for 8 h at 23 ºC and monitored by ^{1}H NMR and ^{31}P NMR.

Reaction using [(JohnPhos)Au$_2$Cl]X (X = SbF$_6^-$, BF$_4^-$)

Phenylacetylene (19 μL, 0.169 mmol), α-methylstyrene (44 μL, 0.338 mmol) and diphenylmethane (14 μL, 0.085 mmol) dissolved in 0.7 mL of CD$_2$Cl$_2$ were introduced in a NMR tube. Complex **B3** or **B4** (4.23 μmol) was then added and the resulting mixture was stirred for 8 h at 23 ºC. The reaction was monitored by ^{1}H NMR and ^{31}P NMR.

Reaction using [(JohnPhos)Au$_2$Cl]X and AgX (X = SbF$_6^-$, BF$_4^-$)

Phenylacetylene (19 μL, 0.169 mmol), α-methylstyrene (44 μL, 0.338 mmol) and diphenylmethane (14 μL, 0.085 mmol) dissolved in 0.7 mL of CD$_2$Cl$_2$ were introduced in a NMR tube. Complex **B3** or **B4** (4.23 μmol) and AgX (4.23 μmol) were then added and the resulting mixture was stirred for 8 h at 23 ºC. The reaction was monitored by ^{1}H NMR and ^{31}P NMR.

[2+2] Intramolecular Cycloaddition of 1,6-Enyne 19

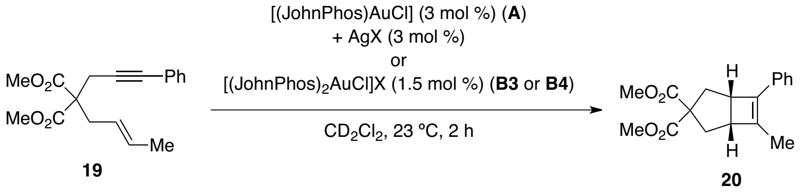
[(JohnPhos)AuCl] (3 mol %) (**A**)
+ AgX (3 mol %)
or
[(JohnPhos)2AuCl]X (1.5 mol %) (**B3** or **B4**)
CD2Cl2, 23 °C, 2 h
MeO2C
MeO2C
Ph
Me
H
H
19
20

Cycloisomerized product **20** was prepared according to the previous described procedure.[22c] **^{1}H NMR** (400 MHz, CDCl$_3$) δ_H 7.33–7.25 (m, 4H), 7.21–7.15 (m, 1H), 3.68 (s, 3H), 3.50–3.45 (m, 1H), 3.22 (s, 3H), 3.15–3.11 (m, 1H), 2.72 (dd, J = 28.8, 13.3 Hz, 1H), 2.02 (dd, J = 13.4, 7.2 Hz, 1H), 1.86 (dd, J = 13.2, 7.6 Hz, 1H), 1.85 (dd, J = 2.8, 1.4 Hz, 3H).

In situ generation of the catalyst in the presence of the substrate

Enyne **19** (30 mg, 0.1 mmol) and diphenylmethane (8.3 μL, 0.05 mmol) dissolved in 0.7 mL of CD$_2$Cl$_2$ were introduced in a NMR tube. JohnPhosAuCl (1.6 mg, 3 μmol) and AgX (3 μmol) were then added and the resulting mixture was stirred for 2 h at 23 ºC. The reaction was monitored by ^{1}H NMR and ^{31}P NMR.

In situ generation of the catalyst and addition of the substrate
JohnPhosAuCl (1.6 mg, 3 µmol) and AgX (3 µmol) were dissolved in 0.7 mL CD$_2$Cl$_2$ and introduced in a NMR tube. After 10 min stirring, enyne **19** (30 mg, 0.1 mmol) and diphenylmethane (8.3 µL, 0.05 mmol) were added. The resulting mixture was stirred for 2 h at 23 ºC and monitored by ^{1}H NMR and ^{31}P NMR.

In situ generation of the catalyst, filtration through Celite and addition of the substrates
In a vial, JohnPhosAuCl (1.6 mg, 3 µmol) and AgX (3 µmol) were dissolved in 0.7 mL CD$_2$Cl$_2$. After 10 min stirring, the slurry mixture was filtered through a pipette containing Celite and cotton (top and bottom). The resulting solution was introduced in a NMR tube along with enyne **19** (30 mg, 0.1 mmol) and diphenylmethane (8.3 µL, 0.05 mmol). The resulting mixture was stirred for 2 h at 23 ºC and monitored by ^{1}H NMR and ^{31}P NMR.

Reaction using [(JohnPhos)Au$_2$Cl]X (X = SbF$_6^-$, BF$_4^-$)
Enyne **19** (30 mg, 0.1 mmol) and diphenylmethane (8.3 µL, 0.05 mmol) dissolved in 0.7 mL of CD$_2$Cl$_2$ were introduced in a NMR tube. Complex **B3** or **B4** (4.23 µmol) was then added and the resulting mixture was stirred for 8 h at 23 ºC. The reaction was monitored by ^{1}H NMR and ^{31}P NMR.

Reaction using [(JohnPhos)Au$_2$Cl]X and AgX (X = SbF$_6^-$, BF$_4^-$)
Enyne **19** (30 mg, 0.1 mmol) and diphenylmethane (14 µL, 0.085 mmol) dissolved in 0.7 mL of CD$_2$Cl$_2$ were introduced in a NMR tube. Complex **B3** or **B4** (4.23 µmol) and AgX (4.23 µmol) were then added and the resulting mixture was stirred for 8 h at 23 ºC. The reaction was monitored by ^{1}H NMR and ^{31}P NMR.

[4+2] Intramolecular cycloaddition of 1,6-enyne 21

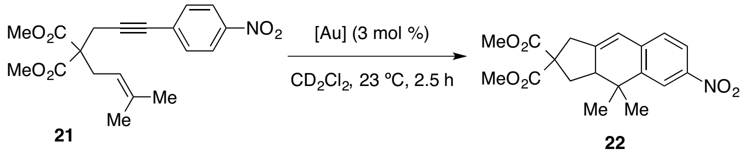

The tricyclic product **22** was prepared according to the previous described procedure.[22a] **^{1}H NMR** (400 MHz, CDCl$_3$) δ_H 8.14 (d, *J* = 2.2 Hz, 1H), 8.02 (dd, *J* = 8.4, 2.3 Hz, 1H), 7.12 (d, *J* = 8.4 Hz, 1H), 6.45 (bs, 1H), 3.78 (s, 3H), 3.74 (s, 3H), 3.34 (d, *J* = 18.7 Hz, 1H), 3.03 (dt, *J* = 18.6, 3.0 Hz, 1H), 2.80–2.71 (m, 1H), 2.63 (ddd, *J* = 12.6, 7.6, 1.3 Hz, 1H), 2.18 (t, *J* = 12.6 Hz, 1H), 1.49 (s, 3H), 0.95 (s, 3H).

Enyne **21** (40 mg, 0.111 mmol) and diphenylmethane (9.3 µL, 0.056 mmol) were dissolved in 0.7 mL CD$_2$Cl$_2$ and introduced in a NMR tube. JohnPhosAuCl (1.8 mg, 3.34 µmol) was then added and the resulting mixture was monitored by ^{1}H NMR at 23 ºC every 5 min during 2.5 h.

Enyne **21** (40 mg, 0.111 mmol) and diphenylmethane (9.3 µL, 0.056 mmol) were dissolved in 0.7 mL CD$_2$Cl$_2$ in a vial. JohnPhosAuCl (1.8 mg, 3.34 µmol) was then added and the mixture was introduced in a NMR tube. AgSbF$_6$ (1.2 mg, 3.34 µmol) was then added and the resulting mixture was monitored by ^{1}H NMR at 23 ºC every 5 min during

2.5 h. Then the sample was analyzed again after 6 h and 24 h.

JohnPhosAuCl (1.8 mg, 3.34 µmol) was dissolved in 0.7 mL CD_2Cl_2 in a vial and added to $AgSbF_6$ (1.2 mg, 3.34 µmol). The resulting mixture was shaken during 3 min and added to enyne **21** (40 mg, 0.111 mmol) and diphenylmethane (9.3 µL, 0.056 mmol). The mixture resulting mixture was introduced in a NMR tube and monitored by ^{1}H NMR at 23 ºC every 5 min during 2.5 h. The sample was analyzed again after 9 h and 24 h.

Enyne **21** (40 mg, 0.111 mmol) and diphenylmethane (9.3 µL, 0.056 mmol) were dissolved in 0.7 mL CD_2Cl_2 and introduced in a NMR tube. Complex **B4** (2.1 mg, 1.67 µmol) was then added and the resulting mixture was monitored by ^{1}H NMR at 23 ºC every 5 min during 2.5 h. Then the sample was analyzed again after 23 h.

Enyne **21** (40 mg, 0.111 mmol) and diphenylmethane (9.3 µL, 0.056 mmol) were dissolved in 0.7 mL CD_2Cl_2 and introduced in a NMR tube. Complex **B3** (1.8 mg, 1.67 µmol) was then added and the resulting mixture was monitored by ^{1}H NMR at 23 ºC every 5 min during 2.5 h. Then the sample was analyzed again after 9 h and 24 h.

Enyne **21** (40 mg, 0.111 mmol) and diphenylmethane (9.3 µL, 0.056 mmol) were dissolved in 0.7 mL CD_2Cl_2 and introduced in a NMR tube. Complex **B4** (4.2 mg, 3.34 µmol) was then added and the resulting mixture was monitored by ^{1}H NMR at 23 ºC every 5 min during 2.5 h. Then the sample was analyzed again after 9 h and 25h.

Enyne **21** (40 mg, 0.111 mmol) and diphenylmethane (9,31 µL, 0.056 mmol) were dissolved in 0.7 mL CD_2Cl_2 and introduced in a NMR tube. Complex **B4** (2.1 mg, 1.67 µmol) was added and the resulting mixture was shaken for 3 min. Then, $AgSbF_6$ (0.5 mg, 1.67 µmol) was added and the resulting mixture was monitored by ^{1}H NMR at 23 ºC every 5 min during 2 h. Then the sample was analyzed again after 6 h and 21h.

Enyne **21** (40 mg, 0.111 mmol) and diphenylmethane (9.31 µL, 0.056 mmol) were dissolved in 0.7 mL CD_2Cl_2 and introduced in a NMR tube. [(JohnPhos)AuNCMe]SbF_6 cationic complex (2.6 mg, 3.34 mmol) was then added and the resulting mixture was monitored by ^{1}H NMR at 23 ºC every 5 min during 2.5 h. The sample was analyzed again after 6 h and 24 h

Enyne **21** (40 mg, 0.111 mmol) and diphenylmethane (9.31 µL, 0.056 mmol) were dissolved in 0.7 mL CD_2Cl_2 and introduced in a NMR tube. [(*t*-BuXPhos)AuNCMe]SbF_6 complex (3.0 mg, 3.34 mmol) was then added and the resulting mixture was monitored by ^{1}H NMR at 23 ºC every 5 min during 2.5 h. The sample was analyzed again after 4 h and 24 h.

X-Ray Tables

Trifluoromethanesulfonate[(1,1′-biphenyl-2-yl)di-*tert*-butylphosphine]gold(I) (C1)

Table S1 Crystal data and structure refinement for **C1**.

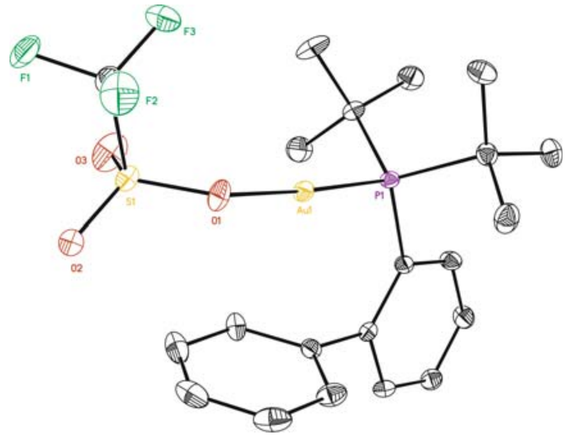

Identification code	mo_AI002512_0m
Empirical formula	C21 H27 Au F3 O3 P S
Formula weight	644.42
Temperature	100(2) K
Wavelength	0.71073 Å
Crystal system	Monoclinic
Space group	P2(1)/c
Unit cell dimensions	
a = 14.2158(12) Å	α= 90.00 °.
b = 9.9549(9) Å	β = 97.068(3) °.
c = 16.0881(13) Å	γ = 90.00 °.
Volume	2259.4(3) Å^3
Z	4
Density (calculated)	1.894 Mg/m^3
Absorption coefficient	6.719 mm^{-1}
F(000)	1256
Crystal size	0.15 x 0.10 x 0.10 mm^3
Theta range for data collection	1.44 to 36.41 °.
Index ranges	-18 <=h<=23 ,-13 <=k<=16 ,-26 <=l<=22
Reflections collected	27299
Independent reflections	10995 [R(int) = 0.0377]
Completeness to theta =36.41 °	99.6%
Absorption correction	Empirical
Max. and min. transmission	0.5531 and 0.4322
Refinement method	Full-matrix least-squares on F^2
Data / restraints / parameters	10995 / 0 / 277
Goodness-of-fit on F^2	1.041
Final R indices [I>2sigma(I)]	R1 = 0.0274 , wR2 = 0.0671
R indices (all data)	R1 = 0.0362 , wR2 = 0.0749

Largest diff. peak and hole	2.667 and -2.383 e.Å^{-3}

Table S2 Bond lengths [Å] and angles [°] for **C1**.

Bond lengths

Au1-O1	2.1133(17)	C13-C16	1.531(3)
Au1-P1	2.2294(6)	C13-C15	1.530(3)
C1-C2	1.400(3)	C13-C14	1.530(3)
C1-C6	1.410(3)	C13-P1	1.876(2)
C1-P1	1.836(2)	C17-C19	1.536(3)
C2-C3	1.390(3)	C17-C20	1.534(3)
C3-C4	1.377(3)	C17-C18	1.534(3)
C4-C5	1.383(3)	C17-P1	1.877(2)
C5-C6	1.403(3)	C22-F2	1.321(3)
C6-C7	1.491(3)	C22-F3	1.322(3)
C7-C12	1.391(3)	C22-F1	1.332(3)
C7-C8	1.398(3)	C22-S1	1.829(2)
C8-C9	1.390(4)	O1-S1	1.4791(17)
C9-C10	1.386(4)	O2-S1	1.423(2)
C10-C11	1.388(4)	O3-S1	1.429(2)
C11-C12	1.391(3)		

Angles

O1-Au1-P1	174.20(5)	C15-C13-P1	109.39(17)
C2-C1-C6	118.27(18)	C14-C13-P1	107.29(16)
C2-C1-P1	118.70(16)	C19-C17-C20	109.01(19)
C6-C1-P1	123.03(16)	C19-C17-C18	108.45(19)
C3-C2-C1	122.0(2)	C20-C17-C18	108.99(19)
C4-C3-C2	119.3(2)	C19-C17-P1	116.32(16)
C3-C4-C5	120.1(2)	C20-C17-P1	108.39(15)
C4-C5-C6	121.5(2)	C18-C17-P1	105.47(16)
C5-C6-C1	118.8(2)	F2-C22-F3	108.4(2)
C5-C6-C7	115.71(19)	F2-C22-F1	108.1(2)
C1-C6-C7	125.45(19)	F3-C22-F1	108.6(2)
C12-C7-C8	119.4(2)	F2-C22-S1	111.17(17)
C12-C7-C6	121.1(2)	F3-C22-S1	111.12(18)
C8-C7-C6	119.4(2)	F1-C22-S1	109.29(16)
C9-C8-C7	120.3(2)	S1-O1-Au1	123.77(10)
C8-C9-C10	120.0(2)	C1-P1-C17	106.16(10)
C9-C10-C11	119.9(2)	C1-P1-C13	106.88(10)
C10-C11-C12	120.5(2)	C17-P1-C13	114.34(10)
C7-C12-C11	119.9(2)	C1-P1-Au1	114.53(7)
C16-C13-C15	108.0(2)	C17-P1-Au1	106.75(7)
C16-C13-C14	110.0(2)	C13-P1-Au1	108.38(7)
C15-C13-C14	107.3(2)	O2-S1-O3	118.03(13)
C16-C13-P1	114.70(16)	O2-S1-O1	112.78(11)

O3-S1-O1	114.18(12)	O3-S1-C22	104.42(12)
O2-S1-C22	103.76(12)	O1-S1-C22	101.06(10)

Table S3 Torsion angles [º] for **C1**.

Torsion angles			
C6-C1-C2-C3	-1.7(3)	C18-C17-P1-C1	-69.30(17)
P1-C1-C2-C3	178.13(19)	C19-C17-P1-C13	-66.66(19)
C1-C2-C3-C4	1.0(4)	C20-C17-P1-C13	56.53(19)
C2-C3-C4-C5	0.1(4)	C18-C17-P1-C13	173.13(15)
C3-C4-C5-C6	-0.4(4)	C19-C17-P1-Au1	173.49(15)
C4-C5-C6-C1	-0.3(3)	C20-C17-P1-Au1	-63.31(17)
C4-C5-C6-C7	-179.5(2)	C18-C17-P1-Au1	53.28(15)
C2-C1-C6-C5	1.4(3)	C16-C13-P1-C1	-79.26(19)
P1-C1-C6-C5	-178.47(16)	C15-C13-P1-C1	159.26(18)
C2-C1-C6-C7	-179.5(2)	C14-C13-P1-C1	43.19(19)
P1-C1-C6-C7	0.6(3)	C16-C13-P1-C17	37.9(2)
C5-C6-C7-C12	-99.6(3)	C15-C13-P1-C17	-83.6(2)
C1-C6-C7-C12	81.3(3)	C14-C13-P1-C17	160.35(17)
C5-C6-C7-C8	75.7(3)	C16-C13-P1-Au1	156.83(16)
C1-C6-C7-C8	-103.4(3)	C15-C13-P1-Au1	35.34(19)
C12-C7-C8-C9	-0.4(4)	C14-C13-P1-Au1	-80.73(17)
C6-C7-C8-C9	-175.8(2)	O1-Au1-P1-C1	141.7(5)
C7-C8-C9-C10	-0.6(4)	O1-Au1-P1-C17	24.5(5)
C8-C9-C10-C11	1.3(4)	O1-Au1-P1-C13	-99.1(5)
C9-C10-C11-C12	-1.0(4)	Au1-O1-S1-O2	132.28(13)
C8-C7-C12-C11	0.7(4)	Au1-O1-S1-O3	-6.07(18)
C6-C7-C12-C11	176.0(2)	Au1-O1-S1-C22	-117.54(13)
C10-C11-C12-C7	0.0(4)	F2-C22-S1-O2	52.95(19)
P1-Au1-O1-S1	129.1(4)	F3-C22-S1-O2	173.80(17)
C2-C1-P1-C17	-62.2(2)	F1-C22-S1-O2	-66.3(2)
C6-C1-P1-C17	117.66(18)	F2-C22-S1-O3	177.18(18)
C2-C1-P1-C13	60.2(2)	F3-C22-S1-O3	-62.0(2)
C6-C1-P1-C13	-119.90(19)	F1-C22-S1-O3	57.9(2)
C2-C1-P1-Au1	-179.72(15)	F2-C22-S1-O1	-64.06(19)
C6-C1-P1-Au1	0.1(2)	F3-C22-S1-O1	56.79(19)
C19-C17-P1-C1	50.91(19)	F1-C22-S1-O1	176.68(18)
C20-C17-P1-C1	174.10(16)		

Triflimide [(1,1′-biphenyl-2-yl)di-*tert*-butylphosphine]gold(I) (C2)

Table S4 Crystal data and structure refinement for **C2**.

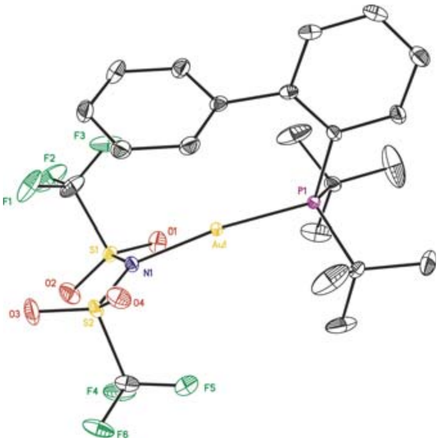

Identification code	mo_AI0035_0m
Empirical formula	C22 H27 Au F6 N O4 P S2
Formula weight	775.50
Temperature	100(2) K
Wavelength	0.71073 Å
Crystal system	Triclinic
Space group	P1
Unit cell dimensions	
a = 9.5483(8) Å	α= 98.149(4) °.
b = 10.0082(12) Å	β = 96.743(3) °.
c = 15.3039(14) Å	γ = 107.426(4) °.
Volume	1361.3(2) Å^3
Z	2
Density (calculated)	1.892 Mg/m^3
Absorption coefficient	5.686 mm^{-1}
F(000)	756
Crystal size	0.30 x 0.20 x 0.10 mm^3
Theta range for data collection	1.36 to 30.29 °.
Index ranges	-13 <=h<=13 ,-13 <=k<=14 ,-21 <=l<=20
Reflections collected	16807
Independent reflections	7077 [R(int) = 0.0685]
Completeness to theta =30.29 °	86.799995%
Absorption correction	Empirical
Max. and min. transmission	0.6002 and 0.2803
Refinement method	Full-matrix least-squares on F^2
Data / restraints / parameters	7077 / 0 / 340
Goodness-of-fit on F^2	1.078
Final R indices [I>2sigma(I)]	R1 = 0.0319 , wR2 = 0.0795
R indices (all data)	R1 = 0.0345 , wR2 = 0.0803
Largest diff. peak and hole	2.945 and -4.094 e.Å^{-3}

Table S5 Bond lengths [Å] and angles [°] for **C2**.

Bond lengths

Au1-N1	2.113(3)	C8-H8	0.9300
Au1-P1	2.2445(9)	C9-C10	1.388(6)
S1-O1	1.418(3)	C9-H9	0.9300
S1-O2	1.419(3)	C10-C11	1.384(7)
S1-N1	1.636(3)	C10-H10	0.9300
S1-C21	1.829(4)	C11-C12	1.394(5)
S2-O3	1.424(3)	C11-H11	0.9300
S2-O4	1.428(3)	C12-H12	0.9300
S2-N1	1.621(3)	C13-C16	1.520(6)
S2-C22	1.848(4)	C13-C14	1.530(6)
P1-C1	1.825(4)	C13-C15	1.535(7)
P1-C17	1.874(4)	C14-H14	0.9600
P1-C13	1.885(4)	C14-H14B	0.9600
F1-C21	1.328(6)	C14-H14C	0.9600
F2-C21	1.325(5)	C15-H15	0.9600
F3-C21	1.327(6)	C15-H15B	0.9600
F4-C22	1.325(5)	C15-H15C	0.9600
F5-C22	1.327(5)	C16-H16	0.9600
F6-C22	1.321(5)	C16-H16B	0.9600
C1-C2	1.409(5)	C16-H16C	0.9600
C1-C6	1.418(5)	C17-C20	1.517(6)
C2-C3	1.384(5)	C17-C19	1.537(6)
C2-H2A	0.9300	C17-C18	1.538(6)
C3-C4	1.385(6)	C18-H18	0.9600
C3-H3A	0.9300	C18-H18B	0.9600
C4-C5	1.382(5)	C18-H18C	0.9600
C4-H4A	0.9300	C19-H19	0.9600
C5-C6	1.395(5)	C19-H19B	0.9600
C5-H5	0.9300	C19-H19C	0.9600
C6-C7	1.490(5)	C20-H20	0.9600
C7-C8	1.392(5)	C20-H20B	0.9600
C7-C12	1.394(5)	C20-H20C	0.9600
C8-C9	1.396(5)		

Angles

N1-Au1-P1	170.77(9)	O4-S2-N1	107.25(17)
O1-S1-O2	121.0(2)	O3-S2-C22	106.3(2)
O1-S1-N1	108.11(17)	O4-S2-C22	103.84(19)
O2-S1-N1	113.46(19)	N1-S2-C22	103.06(18)
O1-S1-C21	104.6(2)	C1-P1-C17	104.99(18)
O2-S1-C21	105.3(2)	C1-P1-C13	107.10(18)
N1-S1-C21	102.30(19)	C17-P1-C13	116.35(18)
O3-S2-O4	121.2(2)	C1-P1-Au1	117.01(12)
O3-S2-N1	113.22(19)	C17-P1-Au1	105.68(13)

C13-P1-Au1	106.17(12)	C13-C14-H14C	109.5
S2-N1-S1	122.48(19)	H14-C14-H14C	109.5
S2-N1-Au1	118.77(18)	H14B-C14-H14C	109.5
S1-N1-Au1	118.16(17)	C13-C15-H15	109.5
C2-C1-C6	117.9(3)	C13-C15-H15B	109.5
C2-C1-P1	118.1(3)	H15-C15-H15B	109.5
C6-C1-P1	123.9(3)	C13-C15-H15C	109.5
C3-C2-C1	122.2(4)	H15-C15-H15C	109.5
C3-C2-H2A	118.9	H15B-C15-H15C	109.5
C1-C2-H2A	118.9	C13-C16-H16	109.5
C2-C3-C4	119.5(4)	C13-C16-H16B	109.5
C2-C3-H3A	120.3	H16-C16-H16B	109.5
C4-C3-H3A	120.3	C13-C16-H16C	109.5
C5-C4-C3	119.2(4)	H16-C16-H16C	109.5
C5-C4-H4A	120.4	H16B-C16-H16C	109.5
C3-C4-H4A	120.4	C20-C17-C19	109.6(4)
C4-C5-C6	122.7(4)	C20-C17-C18	107.7(5)
C4-C5-H5	118.6	C19-C17-C18	106.6(4)
C6-C5-H5	118.6	C20-C17-P1	117.3(3)
C5-C6-C1	118.4(3)	C19-C17-P1	109.9(3)
C5-C6-C7	115.4(3)	C18-C17-P1	105.2(3)
C1-C6-C7	126.2(3)	C17-C18-H18	109.5
C8-C7-C12	118.7(3)	C17-C18-H18B	109.5
C8-C7-C6	121.5(3)	H18-C18-H18B	109.5
C12-C7-C6	119.2(3)	C17-C18-H18C	109.5
C7-C8-C9	120.6(4)	H18-C18-H18C	109.5
C7-C8-H8	119.7	H18B-C18-H18C	109.5
C9-C8-H8	119.7	C17-C19-H19	109.5
C10-C9-C8	120.0(4)	C17-C19-H19B	109.5
C10-C9-H9	120.0	H19-C19-H19B	109.5
C8-C9-H9	120.0	C17-C19-H19C	109.5
C11-C10-C9	119.9(4)	H19-C19-H19C	109.5
C11-C10-H10	120.0	H19B-C19-H19C	109.5
C9-C10-H10	120.0	C17-C20-H20	109.5
C10-C11-C12	120.0(4)	C17-C20-H20B	109.5
C10-C11-H11	120.0	H20-C20-H20B	109.5
C12-C11-H11	120.0	C17-C20-H20C	109.5
C7-C12-C11	120.8(4)	H20-C20-H20C	109.5
C7-C12-H12	119.6	H20B-C20-H20C	109.5
C11-C12-H12	119.6	F2-C21-F3	108.4(4)
C16-C13-C14	109.8(4)	F2-C21-F1	108.8(4)
C16-C13-C15	108.0(4)	F3-C21-F1	108.1(4)
C14-C13-C15	108.0(5)	F2-C21-S1	109.4(3)
C16-C13-P1	109.4(3)	F3-C21-S1	110.9(3)
C14-C13-P1	116.3(3)	F1-C21-S1	111.2(3)
C15-C13-P1	104.8(3)	F6-C22-F4	109.6(4)
C13-C14-H14	109.5	F6-C22-F5	108.8(4)
C13-C14-H14B	109.5	F4-C22-F5	108.5(4)
H14-C14-H14B	109.5	F6-C22-S2	108.5(3)

F4-C22-S2	111.5(3)	F5-C22-S2	109.8(3)

Table S6 Torsion angles [º] for **C2**.

Torsion angles			
N1-Au1-P1-C1	173.9(6)	C8-C9-C10-C11	0.2(7)
N1-Au1-P1-C17	57.5(6)	C9-C10-C11-C12	-0.7(7)
N1-Au1-P1-C13	-66.7(6)	C8-C7-C12-C11	0.3(6)
O3-S2-N1-S1	-30.1(3)	C6-C7-C12-C11	-171.7(4)
O4-S2-N1-S1	-166.5(2)	C10-C11-C12-C7	0.5(7)
C22-S2-N1-S1	84.3(2)	C1-P1-C13-C16	180.0(3)
O3-S2-N1-Au1	158.8(2)	C17-P1-C13-C16	-63.0(4)
O4-S2-N1-Au1	22.4(2)	Au1-P1-C13-C16	54.2(3)
C22-S2-N1-Au1	-86.8(2)	C1-P1-C13-C14	-54.9(5)
O1-S1-N1-S2	-151.0(2)	C17-P1-C13-C14	62.1(5)
O2-S1-N1-S2	-13.9(3)	Au1-P1-C13-C14	179.3(4)
C21-S1-N1-S2	98.9(3)	C1-P1-C13-C15	64.3(4)
O1-S1-N1-Au1	20.1(2)	C17-P1-C13-C15	-178.7(3)
O2-S1-N1-Au1	157.25(19)	Au1-P1-C13-C15	-61.5(3)
C21-S1-N1-Au1	-89.9(2)	C1-P1-C17-C20	57.0(4)
P1-Au1-N1-S2	105.7(6)	C13-P1-C17-C20	-61.2(5)
P1-Au1-N1-S1	-65.8(6)	Au1-P1-C17-C20	-178.7(4)
C17-P1-C1-C2	-63.7(4)	C1-P1-C17-C19	-177.0(3)
C13-P1-C1-C2	60.6(4)	C13-P1-C17-C19	64.8(3)
Au1-P1-C1-C2	179.5(3)	Au1-P1-C17-C19	-52.7(3)
C17-P1-C1-C6	112.1(4)	C1-P1-C17-C18	-62.6(3)
C13-P1-C1-C6	-123.6(3)	C13-P1-C17-C18	179.2(3)
Au1-P1-C1-C6	-4.6(4)	Au1-P1-C17-C18	61.7(3)
C6-C1-C2-C3	-1.1(7)	O1-S1-C21-F2	73.0(4)
P1-C1-C2-C3	175.0(4)	O2-S1-C21-F2	-55.5(4)
C1-C2-C3-C4	-0.7(7)	N1-S1-C21-F2	-174.3(4)
C2-C3-C4-C5	1.9(7)	O1-S1-C21-F3	-46.5(4)
C3-C4-C5-C6	-1.3(7)	O2-S1-C21-F3	-175.0(3)
C4-C5-C6-C1	-0.5(6)	N1-S1-C21-F3	66.1(4)
C4-C5-C6-C7	179.8(4)	O1-S1-C21-F1	-166.8(3)
C2-C1-C6-C5	1.7(6)	O2-S1-C21-F1	64.7(4)
P1-C1-C6-C5	-174.2(3)	N1-S1-C21-F1	-54.1(4)
C2-C1-C6-C7	-178.7(4)	O3-S2-C22-F6	-58.1(4)
P1-C1-C6-C7	5.5(6)	O4-S2-C22-F6	70.8(3)
C5-C6-C7-C8	-103.0(4)	N1-S2-C22-F6	-177.4(3)
C1-C6-C7-C8	77.3(5)	O3-S2-C22-F4	62.7(4)
C5-C6-C7-C12	68.8(5)	O4-S2-C22-F4	-168.4(3)
C1-C6-C7-C12	-110.9(5)	N1-S2-C22-F4	-56.6(3)
C12-C7-C8-C9	-0.8(6)	O3-S2-C22-F5	-177.0(3)
C6-C7-C8-C9	171.0(4)	O4-S2-C22-F5	-48.0(3)
C7-C8-C9-C10	0.5(6)	N1-S2-C22-F5	63.7(3)

Chloro bis{[(1,1′-biphenyl-2-yl)di-*tert*-butylphosphine]gold(I)} trifluoromethanesulfonate (B1)

Table S7 Crystal data and structure refinement for **B1**.

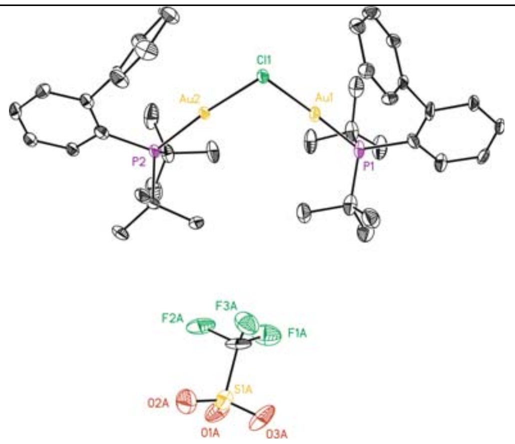

Empirical formula	C44 H61 Au2 Cl2 F3 O3 P2 S
Identification code	mo_AI002512B_0m
Formula weight	1253.76
Temperature	100(2) K
Wavelength	0.71073 Å
Crystal system	Triclinic
Space group	P-1
Unit cell dimensions	
a = 11.5811(13) Å	α= 68.918(2) °.
b = 15.0678(16) Å	β = 77.341(2) °.
c = 15.1920(17) Å	γ = 72.311(2) °.
Volume	2338.6(4) Å^3
Z	2
Density (calculated)	1.781 Mg/m^3
Absorption coefficient	6.543 mm^{-1}
F(000)	1228
Crystal size	0.40 x 0.001 x 0.001 mm^3
Theta range for data collection	2.88 to 35.10 °.
Index ranges	-18 <=h<=18 ,-24 <=k<=19 ,-24 <=l<=24
Reflections collected	27698
Independent reflections	18809 [R(int) = 0.0285]
Completeness to theta =35.10 °	90.7%
Absorption correction	Empirical
Max. and min. transmission	0.9935 and 0.1794
Refinement method	Full-matrix least-squares on F^2
Data / restraints / parameters	18809 / 86 / 564
Goodness-of-fit on F^2	1.035
Final R indices [I>2sigma(I)]	R1 = 0.0488 , wR2 = 0.1270
R indices (all data)	R1 = 0.0803 , wR2 = 0.1518
Largest diff. peak and hole	3.185 and -4.483 e.Å^{-3}

Table S8 Bond lengths [Å] and angles [°] for **B1**.

Bond lengths			
Au1-P1	2.2545(14)	C25-C26	1.395(8)
Au1-Cl1	2.3623(14)	C26-C27	1.513(8)
Au2-P2	2.2537(14)	C27-C32	1.386(8)
Au2-Cl1	2.3438(14)	C27-C28	1.398(8)
C1-C6	1.400(8)	C28-C29	1.388(9)
C1-C2	1.419(8)	C29-C30	1.392(9)
C1-P1	1.815(5)	C30-C31	1.388(9)
C2-C3	1.379(8)	C31-C32	1.390(9)
C3-C4	1.375(9)	C33-C36	1.532(9)
C4-C5	1.382(8)	C33-C35	1.540(10)
C5-C6	1.383(8)	C33-C34	1.548(9)
C6-C7	1.527(8)	C33-P2	1.882(6)
C7-C12	1.392(8)	C37-C39	1.516(10)
C7-C8	1.402(7)	C37-C40	1.538(10)
C8-C9	1.381(8)	C37-C38	1.550(9)
C9-C10	1.391(9)	C37-P2	1.891(6)
C10-C11	1.401(8)	C1B-F1B	1.324(9)
C11-C12	1.374(8)	C1B-F2B	1.342(9)
C13-C16	1.503(9)	C1B-F3B	1.363(10)
C13-C14	1.527(9)	C1B-S1B	1.797(8)
C13-C15	1.540(9)	O1B-S1B	1.432(5)
C13-P1	1.902(7)	O2B-S1B	1.444(5)
C17-C18	1.535(8)	O3B-S1B	1.423(5)
C17-C20	1.541(9)	Cl1S-C1S#1	1.64(2)
C17-C19	1.545(9)	Cl2S-C1S#1	1.94(2)
C17-P1	1.879(6)	C1S-Cl1S#2	1.64(2)
C21-C26	1.387(8)	C1S-Cl2S#2	1.94(2)
C21-C22	1.405(8)	C1R-C2R	1.511(10)
C21-P2	1.830(6)	C2R-C3R	1.539(10)
C22-C23	1.399(8)	C3R-C4R	1.549(10)
C23-C24	1.378(8)	C4R-C5R	1.542(10)
C24-C25	1.401(8)		

Angles			
P1-Au1-Cl1	178.01(5)	C1-C6-C7	123.2(5)
P2-Au2-Cl1	175.08(5)	C12-C7-C8	119.3(5)
C6-C1-C2	116.7(5)	C12-C7-C6	120.2(5)
C6-C1-P1	125.3(4)	C8-C7-C6	120.2(5)
C2-C1-P1	117.9(4)	C9-C8-C7	119.5(5)
C3-C2-C1	122.0(5)	C8-C9-C10	121.1(5)
C4-C3-C2	119.6(5)	C9-C10-C11	119.1(5)
C3-C4-C5	119.9(5)	C12-C11-C10	119.9(5)
C4-C5-C6	120.9(5)	C11-C12-C7	121.0(5)
C5-C6-C1	120.8(5)	C16-C13-C14	109.0(6)
C5-C6-C7	116.0(5)	C16-C13-C15	108.6(6)

C14-C13-C15	109.5(5)	C39-C37-C38	107.5(5)
C16-C13-P1	108.5(4)	C40-C37-C38	106.9(6)
C14-C13-P1	115.7(5)	C39-C37-P2	116.9(5)
C15-C13-P1	105.3(5)	C40-C37-P2	106.9(4)
C18-C17-C20	108.4(5)	C38-C37-P2	107.5(4)
C18-C17-C19	109.1(5)	Au2-Cl1-Au1	96.76(5)
C20-C17-C19	109.7(5)	C1-P1-C17	105.8(3)
C18-C17-P1	115.7(4)	C1-P1-C13	106.5(3)
C20-C17-P1	105.8(4)	C17-P1-C13	115.0(3)
C19-C17-P1	108.0(4)	C1-P1-Au1	114.06(18)
C26-C21-C22	119.0(5)	C17-P1-Au1	107.78(19)
C26-C21-P2	123.3(4)	C13-P1-Au1	107.93(19)
C22-C21-P2	117.6(4)	C21-P2-C33	103.8(3)
C23-C22-C21	121.3(5)	C21-P2-C37	108.2(3)
C24-C23-C22	119.1(5)	C33-P2-C37	114.4(3)
C23-C24-C25	120.1(5)	C21-P2-Au2	115.97(18)
C26-C25-C24	120.7(5)	C33-P2-Au2	106.3(2)
C21-C26-C25	119.8(5)	C37-P2-Au2	108.4(2)
C21-C26-C27	125.2(5)	F1B-C1B-F2B	106.9(7)
C25-C26-C27	114.9(5)	F1B-C1B-F3B	107.0(7)
C32-C27-C28	119.0(5)	F2B-C1B-F3B	106.5(6)
C32-C27-C26	120.4(5)	F1B-C1B-S1B	113.7(5)
C28-C27-C26	120.5(5)	F2B-C1B-S1B	112.9(5)
C29-C28-C27	120.2(6)	F3B-C1B-S1B	109.4(6)
C28-C29-C30	120.4(6)	O3B-S1B-O1B	115.1(4)
C31-C30-C29	119.4(6)	O3B-S1B-O2B	115.1(3)
C30-C31-C32	120.2(6)	O1B-S1B-O2B	115.7(3)
C27-C32-C31	120.8(5)	O3B-S1B-C1B	102.7(4)
C36-C33-C35	108.8(6)	O1B-S1B-C1B	102.4(3)
C36-C33-C34	110.1(5)	O2B-S1B-C1B	103.1(4)
C35-C33-C34	109.0(6)	Cl1S#2-C1S-Cl2S#2	107.2(11)
C36-C33-P2	114.9(5)	C1R-C2R-C3R	112.8(13)
C35-C33-P2	105.9(4)	C2R-C3R-C4R	106.0(11)
C34-C33-P2	108.0(5)	C5R-C4R-C3R	110.2(11)
C39-C37-C40	110.8(6)		

Table S9 Torsion angles [º] for **B1**.

Torsion angles			
C6-C1-C2-C3	0.2(9)	P1-C1-C6-C5	174.4(4)
P1-C1-C2-C3	-176.2(5)	C2-C1-C6-C7	178.7(5)
C1-C2-C3-C4	1.2(9)	P1-C1-C6-C7	-5.2(8)
C2-C3-C4-C5	-1.0(9)	C5-C6-C7-C12	95.2(6)
C3-C4-C5-C6	-0.5(9)	C1-C6-C7-C12	-85.1(7)
C4-C5-C6-C1	1.8(9)	C5-C6-C7-C8	-78.0(7)
C4-C5-C6-C7	-178.5(5)	C1-C6-C7-C8	101.6(7)
C2-C1-C6-C5	-1.7(8)	C12-C7-C8-C9	0.4(8)

C6-C7-C8-C9	173.7(5)
C7-C8-C9-C10	-0.4(9)
C8-C9-C10-C11	0.6(10)
C9-C10-C11-C12	-0.7(9)
C10-C11-C12-C7	0.7(9)
C8-C7-C12-C11	-0.5(8)
C6-C7-C12-C11	-173.8(5)
C26-C21-C22-C23	1.6(8)
P2-C21-C22-C23	-175.2(4)
C21-C22-C23-C24	1.2(9)
C22-C23-C24-C25	-2.9(9)
C23-C24-C25-C26	1.7(9)
C22-C21-C26-C25	-2.8(8)
P2-C21-C26-C25	173.9(4)
C22-C21-C26-C27	172.8(5)
P2-C21-C26-C27	-10.5(8)
C24-C25-C26-C21	1.2(8)
C24-C25-C26-C27	-174.8(5)
C21-C26-C27-C32	-75.7(7)
C25-C26-C27-C32	100.0(6)
C21-C26-C27-C28	108.8(7)
C25-C26-C27-C28	-75.4(7)
C32-C27-C28-C29	1.6(9)
C26-C27-C28-C29	177.1(6)
C27-C28-C29-C30	-1.7(11)
C28-C29-C30-C31	1.6(11)
C29-C30-C31-C32	-1.4(10)
C28-C27-C32-C31	-1.5(9)
C26-C27-C32-C31	-177.0(5)
C30-C31-C32-C27	1.4(9)
P2-Au2-Cl1-Au1	-31.3(6)
P1-Au1-Cl1-Au2	-23.5(15)
C6-C1-P1-C17	-111.2(5)
C2-C1-P1-C17	64.9(5)
C6-C1-P1-C13	126.0(5)
C2-C1-P1-C13	-57.9(5)
C6-C1-P1-Au1	7.1(6)
C2-C1-P1-Au1	-176.9(4)
C18-C17-P1-C1	-51.1(5)
C20-C17-P1-C1	68.9(4)
C19-C17-P1-C1	-173.7(4)
C18-C17-P1-C13	66.1(5)
C20-C17-P1-C13	-173.8(4)
C19-C17-P1-C13	-56.5(5)
C18-C17-P1-Au1	-173.5(4)
C20-C17-P1-Au1	-53.4(4)
C19-C17-P1-Au1	63.9(5)
C16-C13-P1-C1	-162.5(4)
C14-C13-P1-C1	74.6(5)
C15-C13-P1-C1	-46.4(5)
C16-C13-P1-C17	80.7(5)
C14-C13-P1-C17	-42.2(6)
C15-C13-P1-C17	-163.2(4)
C16-C13-P1-Au1	-39.6(5)
C14-C13-P1-Au1	-162.5(4)
C15-C13-P1-Au1	76.4(4)
Cl1-Au1-P1-C1	-166.5(14)
Cl1-Au1-P1-C17	-49.4(15)
Cl1-Au1-P1-C13	75.3(15)
C26-C21-P2-C33	-100.7(5)
C22-C21-P2-C33	76.0(5)
C26-C21-P2-C37	137.5(5)
C22-C21-P2-C37	-45.9(5)
C26-C21-P2-Au2	15.5(5)
C22-C21-P2-Au2	-167.8(4)
C36-C33-P2-C21	-55.4(6)
C35-C33-P2-C21	64.7(5)
C34-C33-P2-C21	-178.7(5)
C36-C33-P2-C37	62.2(6)
C35-C33-P2-C37	-177.7(4)
C34-C33-P2-C37	-61.1(5)
C36-C33-P2-Au2	-178.2(5)
C35-C33-P2-Au2	-58.1(4)
C34-C33-P2-Au2	58.5(5)
C39-C37-P2-C21	83.5(5)
C40-C37-P2-C21	-41.2(5)
C38-C37-P2-C21	-155.7(5)
C39-C37-P2-C33	-31.5(6)
C40-C37-P2-C33	-156.2(5)
C38-C37-P2-C33	89.3(5)
C39-C37-P2-Au2	-150.0(4)
C40-C37-P2-Au2	85.3(4)
C38-C37-P2-Au2	-29.2(5)
Cl1-Au2-P2-C21	-161.8(6)
Cl1-Au2-P2-C33	-47.1(7)
Cl1-Au2-P2-C37	76.4(6)
F1B-C1B-S1B-O3B	60.0(8)
F2B-C1B-S1B-O3B	-62.1(6)
F3B-C1B-S1B-O3B	179.5(5)
F1B-C1B-S1B-O1B	179.6(7)
F2B-C1B-S1B-O1B	57.6(7)
F3B-C1B-S1B-O1B	-60.8(6)
F1B-C1B-S1B-O2B	-59.9(8)
F2B-C1B-S1B-O2B	178.0(6)
F3B-C1B-S1B-O2B	59.6(6)
C1R-C2R-C3R-C4R	106(2)
C2R-C3R-C4R-C5R	163.4(16)

Chloro bis{[(1,1′-biphenyl-2-yl)di-*tert*-butylphosphine]gold(I)} triflimide (B2)

Table S10 Crystal data and structure refinement for **B2**.

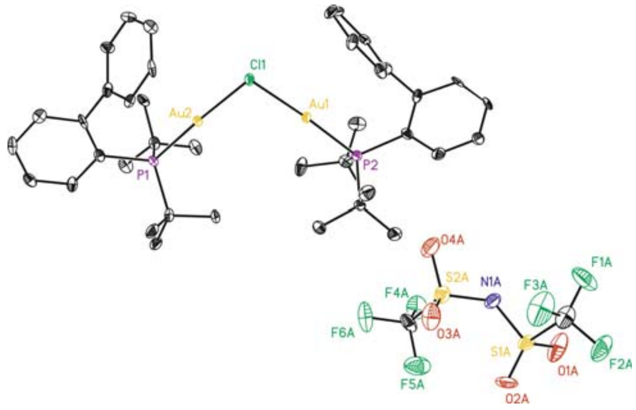

Identification code	mo_AI046Fb_1_0m
Empirical formula	C43 H56 Au2 Cl3 F6 N O4 P2 S2
Formula weight	1391.23
Temperature	100(2) K
Wavelength	0.71073 Å
Crystal system	Triclinic
Space group	P-1
Unit cell dimensions	
a = 11.4925(5) Å	α= 65.585(2) °.
b = 14.9454(6) Å	β = 81.287(2) °.
c = 16.7159(8) Å	γ = 72.405(2) °.
Volume	2490.90(19) Å^3
Z	2
Density (calculated)	1.855 Mg/m^3
Absorption coefficient	6.255 mm^{-1}
F(000)	1356
Crystal size	0.3 x 0.1 x 0.03 mm^3
Theta range for data collection	1.34 to 30.30 °.
Index ranges	-15 <=h<=15 ,-13 <=k<=21 ,-19 <=l<=23
Reflections collected	19961
Independent reflections	12629 [R(int) = 0.0355]
Completeness to theta =30.30 °	84.5%
Absorption correction	Empirical
Max. and min. transmission	0.8345 and 0.2555
Refinement method	Full-matrix least-squares on F^2
Data / restraints / parameters	12629 / 0 / 580
Goodness-of-fit on F^2	1.022
Final R indices [I>2sigma(I)]	R1 = 0.0405 , wR2 = 0.0821
R indices (all data)	R1 = 0.0656 , wR2 = 0.1020
Largest diff. peak and hole	1.071 and -1.092 e.Å^{-3}

Table S11 Bond lengths [Å] and angles [°] for **B2**.

Bond lengths

Au1-P2	2.2542(16)	C20-C21	1.374(9)
Au1-Cl1	2.3524(14)	C21-C22	1.381(9)
Au2-P1	2.2616(15)	C22-C23	1.352(9)
Au2-Cl1	2.3548(14)	C23-C24	1.407(8)
P1-C13	1.830(6)	C25-C38	1.507(9)
P1-C26	1.880(7)	C25-C40	1.525(9)
P1-C28	1.884(6)	C25-C39	1.549(8)
P2-C1	1.807(6)	C26-C30	1.530(8)
P2-C25	1.882(6)	C26-C31	1.537(8)
P2-C27	1.889(6)	C26-C29	1.551(9)
C1-C6	1.417(8)	C27-C35	1.504(9)
C1-C2	1.425(8)	C27-C36	1.515(9)
C2-C3	1.382(8)	C27-C37	1.561(9)
C2-C7	1.508(8)	C28-C32	1.527(9)
C3-C4	1.380(9)	C28-C33	1.536(8)
C4-C5	1.365(9)	C28-C34	1.550(8)
C5-C6	1.404(9)	F1A-C1A	1.288(9)
C7-C8	1.400(8)	F2A-C1A	1.334(9)
C7-C12	1.405(9)	F3A-C1A	1.336(9)
C8-C9	1.395(9)	F4A-C2A	1.303(8)
C9-C10	1.393(9)	F5A-C2A	1.308(9)
C10-C11	1.388(9)	F6A-C2A	1.323(8)
C11-C12	1.392(8)	S1A-O2A	1.396(5)
C13-C18	1.413(9)	S1A-O1A	1.442(5)
C13-C14	1.419(8)	S1A-N1A	1.590(6)
C14-C15	1.387(9)	S1A-C1A	1.826(8)
C15-C16	1.396(9)	S2A-O3A	1.414(5)
C16-C17	1.410(9)	S2A-O4A	1.441(6)
C17-C18	1.393(8)	S2A-N1A	1.582(6)
C18-C19	1.481(8)	S2A-C2A	1.831(7)
C19-C24	1.397(8)	Cl1S-C1S	1.746(7)
C19-C20	1.424(9)	Cl2S-C1S	1.738(8)

Angles

P2-Au1-Cl1	176.83(6)	C25-P2-Au1	107.01(19)
P1-Au2-Cl1	175.92(5)	C27-P2-Au1	108.3(2)
Au1-Cl1-Au2	97.49(5)	C6-C1-C2	116.9(6)
C13-P1-C26	109.1(3)	C6-C1-P2	118.5(5)
C13-P1-C28	103.5(3)	C2-C1-P2	124.6(5)
C26-P1-C28	115.0(3)	C3-C2-C1	120.1(6)
C13-P1-Au2	114.8(2)	C3-C2-C7	116.3(6)
C26-P1-Au2	107.8(2)	C1-C2-C7	123.6(5)
C28-P1-Au2	106.7(2)	C4-C3-C2	121.1(6)
C1-P2-C25	105.1(3)	C5-C4-C3	121.1(6)
C1-P2-C27	106.2(3)	C4-C5-C6	119.0(6)
C25-P2-C27	115.7(3)	C5-C6-C1	121.7(6)
C1-P2-Au1	114.7(2)	C8-C7-C12	119.7(6)

C8-C7-C2	121.0(6)	C35-C27-C37	108.3(6)
C12-C7-C2	119.1(6)	C36-C27-C37	106.5(5)
C9-C8-C7	120.1(6)	C35-C27-P2	106.1(4)
C10-C9-C8	119.4(6)	C36-C27-P2	117.0(5)
C11-C10-C9	121.1(6)	C37-C27-P2	108.0(4)
C10-C11-C12	119.6(6)	C32-C28-C33	109.7(5)
C11-C12-C7	120.0(6)	C32-C28-C34	109.9(5)
C18-C13-C14	118.6(5)	C33-C28-C34	110.1(5)
C18-C13-P1	123.5(5)	C32-C28-P1	105.3(4)
C14-C13-P1	117.7(4)	C33-C28-P1	109.2(4)
C15-C14-C13	121.5(6)	C34-C28-P1	112.6(4)
C14-C15-C16	120.1(6)	O2A-S1A-O1A	120.0(4)
C15-C16-C17	118.5(6)	O2A-S1A-N1A	117.1(3)
C18-C17-C16	122.3(6)	O1A-S1A-N1A	107.8(3)
C17-C18-C13	118.7(6)	O2A-S1A-C1A	106.1(4)
C17-C18-C19	115.4(6)	O1A-S1A-C1A	101.7(4)
C13-C18-C19	125.8(5)	N1A-S1A-C1A	101.4(3)
C24-C19-C20	118.6(6)	O3A-S2A-O4A	119.1(4)
C24-C19-C18	120.0(6)	O3A-S2A-N1A	117.3(3)
C20-C19-C18	121.1(6)	O4A-S2A-N1A	106.5(3)
C21-C20-C19	119.5(6)	O3A-S2A-C2A	105.9(3)
C20-C21-C22	121.0(7)	O4A-S2A-C2A	103.4(3)
C23-C22-C21	120.5(6)	N1A-S2A-C2A	102.5(3)
C22-C23-C24	120.6(6)	S2A-N1A-S1A	123.8(4)
C19-C24-C23	119.6(6)	F1A-C1A-F2A	107.7(7)
C38-C25-C40	109.6(5)	F1A-C1A-F3A	110.0(7)
C38-C25-C39	109.3(5)	F2A-C1A-F3A	105.9(7)
C40-C25-C39	107.3(5)	F1A-C1A-S1A	112.4(6)
C38-C25-P2	108.7(5)	F2A-C1A-S1A	110.0(5)
C40-C25-P2	115.9(4)	F3A-C1A-S1A	110.5(6)
C39-C25-P2	105.8(4)	F4A-C2A-F5A	107.9(7)
C30-C26-C31	107.3(5)	F4A-C2A-F6A	107.5(6)
C30-C26-C29	108.2(5)	F5A-C2A-F6A	108.5(6)
C31-C26-C29	109.9(6)	F4A-C2A-S2A	112.5(5)
C30-C26-P1	108.1(4)	F5A-C2A-S2A	110.7(5)
C31-C26-P1	116.4(4)	F6A-C2A-S2A	109.5(5)
C29-C26-P1	106.7(4)	Cl2S-C1S-Cl1S	112.6(5)
C35-C27-C36	110.6(6)		

Table S12 Torsion angles [º] for **B2**.

Torsion angles			
P2-Au1-Cl1-Au2	-23.0(10)	Cl1-Au1-P2-C1	-167.3(10)
P1-Au2-Cl1-Au1	-23.7(8)	Cl1-Au1-P2-C25	-51.1(10)
Cl1-Au2-P1-C13	-171.1(8)	Cl1-Au1-P2-C27	74.3(10)
Cl1-Au2-P1-C26	67.1(9)	C25-P2-C1-C6	68.0(6)
Cl1-Au2-P1-C28	-57.0(9)	C27-P2-C1-C6	-55.1(6)

Au1-P2-C1-C6	-174.7(4)
C25-P2-C1-C2	-114.1(6)
C27-P2-C1-C2	122.8(6)
Au1-P2-C1-C2	3.2(6)
C6-C1-C2-C3	-3.6(9)
P2-C1-C2-C3	178.5(5)
C6-C1-C2-C7	178.9(6)
P2-C1-C2-C7	1.0(9)
C1-C2-C3-C4	2.6(10)
C7-C2-C3-C4	-179.7(6)
C2-C3-C4-C5	0.3(10)
C3-C4-C5-C6	-2.2(10)
C4-C5-C6-C1	1.0(10)
C2-C1-C6-C5	1.8(10)
P2-C1-C6-C5	179.8(5)
C3-C2-C7-C8	-82.9(8)
C1-C2-C7-C8	94.7(8)
C3-C2-C7-C12	92.1(7)
C1-C2-C7-C12	-90.3(8)
C12-C7-C8-C9	-0.1(9)
C2-C7-C8-C9	174.9(6)
C7-C8-C9-C10	-0.3(10)
C8-C9-C10-C11	0.8(10)
C9-C10-C11-C12	-0.9(10)
C10-C11-C12-C7	0.6(9)
C8-C7-C12-C11	-0.1(9)
C2-C7-C12-C11	-175.2(6)
C26-P1-C13-C18	138.4(5)
C28-P1-C13-C18	-98.6(6)
Au2-P1-C13-C18	17.3(6)
C26-P1-C13-C14	-47.1(6)
C28-P1-C13-C14	75.9(5)
Au2-P1-C13-C14	-168.3(4)
C18-C13-C14-C15	2.3(9)
P1-C13-C14-C15	-172.4(5)
C13-C14-C15-C16	1.9(10)
C14-C15-C16-C17	-2.0(10)
C15-C16-C17-C18	-2.2(10)
C16-C17-C18-C13	6.4(9)
C16-C17-C18-C19	-171.9(6)
C14-C13-C18-C17	-6.3(9)
P1-C13-C18-C17	168.1(5)
C14-C13-C18-C19	171.8(6)
P1-C13-C18-C19	-13.9(9)
C17-C18-C19-C24	110.0(7)
C13-C18-C19-C24	-68.1(9)
C17-C18-C19-C20	-64.7(8)
C13-C18-C19-C20	117.2(7)
C24-C19-C20-C21	0.0(9)
C18-C19-C20-C21	174.8(6)
C19-C20-C21-C22	-0.3(10)
C20-C21-C22-C23	1.3(11)
C21-C22-C23-C24	-2.0(10)
C20-C19-C24-C23	-0.6(9)
C18-C19-C24-C23	-175.5(5)
C22-C23-C24-C19	1.7(9)
C1-P2-C25-C38	-176.0(4)
C27-P2-C25-C38	-59.2(5)
Au1-P2-C25-C38	61.6(4)
C1-P2-C25-C40	-52.1(5)
C27-P2-C25-C40	64.7(5)
Au1-P2-C25-C40	-174.5(4)
C1-P2-C25-C39	66.7(4)
C27-P2-C25-C39	-176.5(4)
Au1-P2-C25-C39	-55.7(4)
C13-P1-C26-C30	-160.8(4)
C28-P1-C26-C30	83.4(5)
Au2-P1-C26-C30	-35.5(4)
C13-P1-C26-C31	78.3(5)
C28-P1-C26-C31	-37.5(6)
Au2-P1-C26-C31	-156.4(4)
C13-P1-C26-C29	-44.7(5)
C28-P1-C26-C29	-160.5(4)
Au2-P1-C26-C29	80.6(4)
C1-P2-C27-C35	-46.5(5)
C25-P2-C27-C35	-162.7(4)
Au1-P2-C27-C35	77.2(5)
C1-P2-C27-C36	77.4(6)
C25-P2-C27-C36	-38.8(6)
Au1-P2-C27-C36	-158.9(5)
C1-P2-C27-C37	-162.5(5)
C25-P2-C27-C37	81.3(5)
Au1-P2-C27-C37	-38.8(5)
C13-P1-C28-C32	64.1(5)
C26-P1-C28-C32	-176.9(4)
Au2-P1-C28-C32	-57.4(4)
C13-P1-C28-C33	-178.1(4)
C26-P1-C28-C33	-59.2(5)
Au2-P1-C28-C33	60.3(5)
C13-P1-C28-C34	-55.6(5)
C26-P1-C28-C34	63.4(5)
Au2-P1-C28-C34	-177.1(4)
O3A-S2A-N1A-S1A	-23.4(6)
O4A-S2A-N1A-S1A	-159.7(4)
C2A-S2A-N1A-S1A	92.1(5)
O2A-S1A-N1A-S2A	-17.4(6)
O1A-S1A-N1A-S2A	-156.2(4)
C1A-S1A-N1A-S2A	97.5(5)

O2A-S1A-C1A-F1A	177.7(6)	O3A-S2A-C2A-F4A	178.2(5)
O1A-S1A-C1A-F1A	-56.1(7)	O4A-S2A-C2A-F4A	-55.9(6)
N1A-S1A-C1A-F1A	54.9(6)	N1A-S2A-C2A-F4A	54.8(6)
O2A-S1A-C1A-F2A	-62.3(7)	O3A-S2A-C2A-F5A	57.3(6)
O1A-S1A-C1A-F2A	63.9(7)	O4A-S2A-C2A-F5A	-176.7(5)
N1A-S1A-C1A-F2A	174.9(6)	N1A-S2A-C2A-F5A	-66.1(6)
O2A-S1A-C1A-F3A	54.3(7)	O3A-S2A-C2A-F6A	-62.3(6)
O1A-S1A-C1A-F3A	-179.5(6)	O4A-S2A-C2A-F6A	63.6(6)
N1A-S1A-C1A-F3A	-68.5(7)	N1A-S2A-C2A-F6A	174.3(5)

Chloro bis{[(1,1′-biphenyl-2-yl)di-*tert*-butylphosphine]gold(I)} tetrafluoroborate (B3)

Table S13 Crystal data and structure refinement for **B3**.

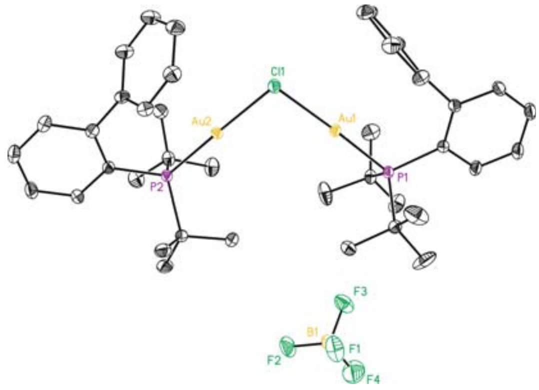

Identification code	AI0047_0m
Empirical formula	C42 H56 Au2 B Cl7 F4 P2
Formula weight	1351.70
Temperature	100(2) K
Wavelength	0.71073 Å
Crystal system	Monoclinic
Space group	P2(1)/c
Unit cell dimensions	
a = 11.4730(5) Å	α= 90.00 °.
b = 16.4087(8) Å	β = 95.4410(10) °.
c = 26.3794(11) Å	γ = 90.00 °.
Volume	4943.7(4) Å^3
Z	4
Density (calculated)	1.816 Mg/m^3
Absorption coefficient	6.416 mm^{-1}
F(000)	2624
Crystal size	0.18 x 0.08 x 0.04 mm^3
Theta range for data collection	2.48 to 39.50 °.
Index ranges	-6 <=h<=20 ,-28 <=k<=29 ,-46 <=l<=22

Reflections collected	52894
Independent reflections	23036 [R(int) = 0.0201]
Completeness to theta =39.50 °	77.5%
Absorption correction	Empirical
Max. and min. transmission	0.7834 and 0.3913
Refinement method	Full-matrix least-squares on F^2
Data / restraints / parameters	23036 / 122 / 571
Goodness-of-fit on F^2	0.938
Final R indices [I>2sigma(I)]	R1 = 0.0229 , wR2 = 0.0576
R indices (all data)	R1 = 0.0306 , wR2 = 0.0609
Largest diff. peak and hole	2.659 and -1.124 e.Å^{-3}

Table S14 Bond lengths [Å] and angles [°] for **B3**.

Bond lengths			
Au1-P1	2.2544(4)	C9-C8	1.394(3)
Au1-Cl1	2.3478(4)	C11-C10	1.396(3)
Au2-P2	2.2558(4)	C21-C26	1.405(2)
Au2-Cl1	2.3512(4)	C21-C22	1.417(2)
P1-C1	1.8355(16)	C22-C23	1.394(2)
P1-C17	1.873(2)	C22-C27	1.496(2)
P1-C13	1.8801(19)	C23-C24	1.391(3)
P2-C21	1.8327(16)	C26-C25	1.390(2)
P2-C33	1.876(2)	C27-C32	1.392(3)
P2-C37	1.890(2)	C27-C28	1.396(3)
C1S-Cl3S	1.745(2)	C28-C29	1.390(3)
C1S-Cl1S	1.755(2)	C29-C30	1.391(3)
C1S-Cl2S	1.756(2)	C30-C31	1.386(3)
Cl2Y-C1Y	1.763(2)	C32-C31	1.392(3)
Cl3Y-C1Y	1.766(2)	C33-C36	1.537(3)
Cl1Y-C1Y	1.766(2)	C33-C35	1.537(3)
C13-C15	1.527(3)	C33-C34	1.539(3)
C13-C14	1.535(3)	C37-C39	1.537(2)
C13-C16	1.545(3)	C37-C38	1.538(3)
C17-C20	1.530(3)	C37-C40	1.539(3)
C17-C18	1.531(3)	C4-C5	1.385(3)
C17-C19	1.532(3)	C4-C3	1.385(3)
C1-C6	1.404(2)	C24-C25	1.385(3)
C1-C2	1.410(2)	B1-F1'	1.343(7)
C2-C3	1.390(2)	B1-F2'	1.378(7)
C6-C5	1.405(2)	B1-F3	1.382(3)
C6-C7	1.494(2)	B1-F4	1.385(4)
C7-C12	1.393(3)	B1-F1	1.391(3)
C7-C8	1.396(3)	B1-F4'	1.395(6)
C12-C11	1.393(3)	B1-F2	1.394(3)
C9-C10	1.386(3)	B1-F3'	1.439(7)

Angles			
P1-Au1-Cl1	176.388(16)	C26-C21-C22	118.51(15)
P2-Au2-Cl1	177.015(14)	C26-C21-P2	117.75(13)
Au1-Cl1-Au2	97.015(15)	C22-C21-P2	123.53(12)
C1-P1-C17	106.12(9)	C23-C22-C21	118.93(16)
C1-P1-C13	106.38(8)	C23-C22-C27	115.77(16)
C17-P1-C13	116.16(9)	C21-C22-C27	125.27(15)
C1-P1-Au1	113.90(6)	C24-C23-C22	121.50(18)
C17-P1-Au1	108.61(6)	C25-C26-C21	121.63(17)
C13-P1-Au1	105.91(6)	C32-C27-C28	118.95(17)
C21-P2-C33	104.80(8)	C32-C27-C22	120.39(19)
C21-P2-C37	107.87(8)	C28-C27-C22	120.29(18)
C33-P2-C37	114.97(9)	C29-C28-C27	120.14(19)
C21-P2-Au2	114.35(6)	C28-C29-C30	120.5(2)
C33-P2-Au2	106.91(6)	C31-C30-C29	119.57(19)
C37-P2-Au2	108.13(6)	C31-C32-C27	120.8(2)
Cl3S-C1S-Cl1S	111.15(12)	C36-C33-C35	110.10(16)
Cl3S-C1S-Cl2S	110.55(13)	C36-C33-C34	108.99(16)
Cl1S-C1S-Cl2S	109.77(11)	C35-C33-C34	108.24(18)
Cl2Y-C1Y-Cl3Y	110.58(14)	C36-C33-P2	108.48(15)
Cl2Y-C1Y-Cl1Y	110.49(11)	C35-C33-P2	114.87(14)
Cl3Y-C1Y-Cl1Y	109.39(11)	C34-C33-P2	105.96(12)
C15-C13-C14	108.29(17)	C39-C37-C38	107.61(15)
C15-C13-C16	108.46(17)	C39-C37-C40	108.09(17)
C14-C13-C16	108.62(19)	C38-C37-C40	110.19(16)
C15-C13-P1	117.20(15)	C39-C37-P2	108.47(13)
C14-C13-P1	108.79(13)	C38-C37-P2	116.07(16)
C16-C13-P1	105.20(13)	C40-C37-P2	106.17(12)
C20-C17-C18	108.05(19)	C5-C4-C3	119.22(16)
C20-C17-C19	110.1(2)	C4-C5-C6	121.87(17)
C18-C17-C19	108.03(19)	C4-C3-C2	119.94(17)
C20-C17-P1	115.50(15)	C25-C24-C23	119.89(16)
C18-C17-P1	109.45(15)	C24-C25-C26	119.47(17)
C19-C17-P1	105.47(15)	C30-C31-C32	120.0(2)
C6-C1-C2	118.27(15)	F1'-B1-F2'	113.6(5)
C6-C1-P1	123.56(12)	F1'-B1-F3	152.5(4)
C2-C1-P1	118.16(13)	F2'-B1-F3	79.4(4)
C3-C2-C1	121.59(17)	F1'-B1-F4	70.5(4)
C1-C6-C5	119.09(16)	F2'-B1-F4	155.7(5)
C1-C6-C7	125.14(14)	F3-B1-F4	108.1(2)
C5-C6-C7	115.76(15)	F1'-B1-F1	50.6(4)
C12-C7-C8	119.05(17)	F2'-B1-F1	89.4(4)
C12-C7-C6	120.43(16)	F3-B1-F1	108.3(2)
C8-C7-C6	120.27(18)	F4-B1-F1	109.1(3)
C11-C12-C7	120.49(18)	F1'-B1-F4'	110.7(5)
C10-C9-C8	120.20(19)	F2'-B1-F4'	112.2(5)
C12-C11-C10	120.1(2)	F3-B1-F4'	83.9(4)
C9-C8-C7	120.5(2)	F4-B1-F4'	48.1(3)
C9-C10-C11	119.64(18)	F1-B1-F4'	157.1(4)

F1'-B1-F2	94.6(4)	F2'-B1-F3'	109.3(5)
F2'-B1-F2	46.1(4)	F3-B1-F3'	44.6(4)
F3-B1-F2	110.7(3)	F4-B1-F3'	90.9(4)
F4-B1-F2	110.9(2)	F1-B1-F3'	76.2(4)
F1-B1-F2	109.7(2)	F4'-B1-F3'	102.1(5)
F4'-B1-F2	82.5(4)	F2-B1-F3'	152.9(5)
F1'-B1-F3'	108.2(5)		

Table S15 Torsion angles [º] for **B3**.

Torsion angles			
P1-Au1-Cl1-Au2	29.8(3)	C2-C1-C6-C7	179.46(19)
P2-Au2-Cl1-Au1	-45.0(4)	P1-C1-C6-C7	-1.5(3)
Cl1-Au1-P1-C1	138.4(3)	C1-C6-C7-C12	-90.7(2)
Cl1-Au1-P1-C17	-103.6(3)	C5-C6-C7-C12	88.7(2)
Cl1-Au1-P1-C13	21.8(3)	C1-C6-C7-C8	95.0(2)
Cl1-Au2-P2-C21	-151.1(3)	C5-C6-C7-C8	-85.5(2)
Cl1-Au2-P2-C33	-35.6(4)	C8-C7-C12-C11	-0.4(3)
Cl1-Au2-P2-C37	88.7(4)	C6-C7-C12-C11	-174.72(16)
C1-P1-C13-C15	62.04(18)	C7-C12-C11-C10	-0.2(3)
C17-P1-C13-C15	-55.78(17)	C10-C9-C8-C7	-0.8(3)
Au1-P1-C13-C15	-176.43(14)	C12-C7-C8-C9	0.9(3)
C1-P1-C13-C14	-174.76(16)	C6-C7-C8-C9	175.25(17)
C17-P1-C13-C14	67.42(18)	C8-C9-C10-C11	0.2(3)
Au1-P1-C13-C14	-53.23(17)	C12-C11-C10-C9	0.3(3)
C1-P1-C13-C16	-58.54(14)	C33-P2-C21-C26	70.78(18)
C17-P1-C13-C16	-176.36(12)	C37-P2-C21-C26	-52.17(19)
Au1-P1-C13-C16	62.99(13)	Au2-P2-C21-C26	-172.49(14)
C1-P1-C17-C20	-65.2(2)	C33-P2-C21-C22	-103.87(18)
C13-P1-C17-C20	52.7(2)	C37-P2-C21-C22	133.18(17)
Au1-P1-C17-C20	171.94(18)	Au2-P2-C21-C22	12.9(2)
C1-P1-C17-C18	172.61(14)	C26-C21-C22-C23	-2.5(3)
C13-P1-C17-C18	-69.43(16)	P2-C21-C22-C23	172.08(16)
Au1-P1-C17-C18	49.76(15)	C26-C21-C22-C27	175.5(2)
C1-P1-C17-C19	56.61(17)	P2-C21-C22-C27	-9.9(3)
C13-P1-C17-C19	174.58(15)	C21-C22-C23-C24	2.5(3)
Au1-P1-C17-C19	-66.23(16)	C27-C22-C23-C24	-175.7(2)
C17-P1-C1-C6	-114.01(18)	C22-C21-C26-C25	0.5(3)
C13-P1-C1-C6	121.71(18)	P2-C21-C26-C25	-174.38(17)
Au1-P1-C1-C6	5.4(2)	C23-C22-C27-C32	-69.4(2)
C17-P1-C1-C2	64.99(18)	C21-C22-C27-C32	112.5(2)
C13-P1-C1-C2	-59.29(19)	C23-C22-C27-C28	103.6(2)
Au1-P1-C1-C2	-175.57(14)	C21-C22-C27-C28	-74.5(2)
C6-C1-C2-C3	-0.8(3)	C32-C27-C28-C29	-1.8(3)
P1-C1-C2-C3	-179.86(18)	C22-C27-C28-C29	-174.91(16)
C2-C1-C6-C5	0.0(3)	C27-C28-C29-C30	-0.6(3)
P1-C1-C6-C5	179.00(16)	C28-C29-C30-C31	1.9(3)

C28-C27-C32-C31	2.9(3)	C33-P2-C37-C38	-38.08(16)
C22-C27-C32-C31	176.02(18)	Au2-P2-C37-C38	-157.42(12)
C21-P2-C33-C36	-175.99(14)	C21-P2-C37-C40	-44.40(14)
C37-P2-C33-C36	-57.75(15)	C33-P2-C37-C40	-160.90(12)
Au2-P2-C33-C36	62.27(14)	Au2-P2-C37-C40	79.76(12)
C21-P2-C33-C35	-52.33(17)	C3-C4-C5-C6	-0.6(3)
C37-P2-C33-C35	65.91(17)	C1-C6-C5-C4	0.7(3)
Au2-P2-C33-C35	-174.07(14)	C7-C6-C5-C4	-178.8(2)
C21-P2-C33-C34	67.11(13)	C5-C4-C3-C2	-0.2(3)
C37-P2-C33-C34	-174.65(11)	C1-C2-C3-C4	0.9(4)
Au2-P2-C33-C34	-54.64(12)	C22-C23-C24-C25	-0.4(3)
C21-P2-C37-C39	-160.35(13)	C23-C24-C25-C26	-1.7(3)
C33-P2-C37-C39	83.15(15)	C21-C26-C25-C24	1.6(3)
Au2-P2-C37-C39	-36.19(14)	C29-C30-C31-C32	-0.8(3)
C21-P2-C37-C38	78.42(15)	C27-C32-C31-C30	-1.6(3)

Chloro bis{[(1,1′-biphenyl-2-yl)di-*tert*-butylphosphine]gold(I)} hexafluoroantimonate (B4)

Table S16 Crystal data and structure refinement for **B4**.

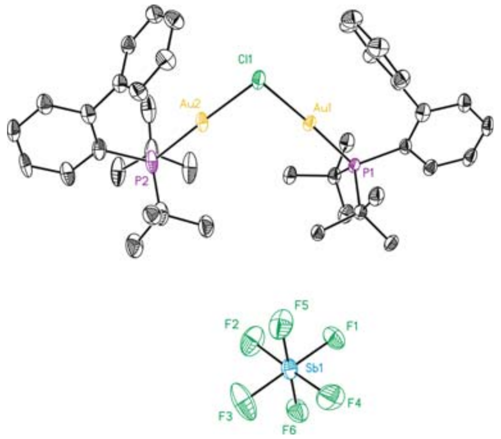

Identification code	AHR30022_0m
Empirical formula	C41.50 H55.50 Au2 Cl5.50 F6 P2 Sb
Formula weight	1440.96
Temperature	100(2) K
Wavelength	0.71073 Å
Crystal system	Triclinic
Space group	P-1
Unit cell dimensions	
a = 11.5465(4) Å	α= 69.5680(10) °.
b = 14.7971(5) Å	β = 80.2880(10) °.
c = 15.8602(6) Å	γ = 72.5010(10) °.

Volume	2415.63(15) Å^3
Z	2
Density (calculated)	1.981 Mg/m^3
Absorption coefficient	7.037 mm^{-1}
F(000)	1382
Crystal size	0.15 x 0.05 x 0.03 mm^3
Theta range for data collection	1.52 to 29.96 °.
Index ranges	-16 <=h<=15 ,-20 <=k<=20 ,-22 <=l<=22
Reflections collected	89373
Independent reflections	12847 [R(int) = 0.0336]
Completeness to theta =29.96 °	0.914 %
Absorption correction	Empirical
Max. and min. transmission	0.8166 and 0.4183
Refinement method	Full-matrix least-squares on F^2
Data / restraints / parameters	12847 / 150 / 650
Goodness-of-fit on F^2	1.166
Final R indices [I>2sigma(I)]	R1 = 0.0305 , wR2 = 0.0689
R indices (all data)	R1 = 0.0394 , wR2 = 0.0723
Largest diff. peak and hole	2.418 and -1.354 e.Å^{-3}

Table S17 Bond lengths [Å] and angles [°] for **B4**.

Bond lengths			
Au1-P1	2.2519(11)	C11-C12	1.380(7)
Au1-Cl1	2.3560(11)	C13-C15	1.529(6)
Au2-P2	2.2517(12)	C13-C16	1.534(6)
Au2-Cl1	2.3802(11)	C13-C14	1.536(6)
P1-C1	1.825(4)	C17-C20	1.531(7)
P1-C13	1.875(4)	C17-C18	1.538(6)
P1-C17	1.889(5)	C17-C19	1.541(6)
P2-C37	1.81(2)	C21-C26	1.398(7)
P2-C21	1.826(5)	C21-C22	1.402(6)
P2-C33'	1.85(3)	C22-C23	1.382(7)
P2-C33	1.892(10)	C23-C24	1.364(8)
P2-C37'	1.98(3)	C24-C25	1.386(7)
C1-C2	1.399(6)	C25-C26	1.398(6)
C1-C6	1.406(6)	C26-C27	1.509(6)
C2-C3	1.390(6)	C27-C32	1.396(6)
C3-C4	1.376(7)	C27-C28	1.399(6)
C4-C5	1.391(7)	C28-C29	1.384(6)
C5-C6	1.384(6)	C29-C30	1.391(6)
C6-C7	1.520(6)	C30-C31	1.391(6)
C7-C8	1.386(6)	C31-C32	1.382(6)
C7-C12	1.401(6)	C33-C34	1.533(10)
C8-C9	1.388(7)	C33-C36	1.535(13)
C9-C10	1.383(7)	C33-C35	1.539(9)
C10-C11	1.387(7)	C33'-C36'	1.530(8)

C33'-C34'	1.537(8)	C1X-Cl2X	1.724(13)
C33'-C35'	1.541(8)	C1X-Cl1X	1.761(12)
C37-C38	1.527(17)	C1X-Cl3X	1.779(12)
C37-C40	1.542(16)	C1X-Cl1X#1	2.195(15)
C37-C39	1.556(16)	Cl1X-Cl2X#1	1.481(6)
C37'-C40'	1.530(8)	Cl1X-C1X#1	2.195(15)
C37'-C38'	1.537(8)	Cl1X-Cl1X#1	2.288(10)
C37'-C39'	1.540(8)	Cl2X-Cl1X#1	1.481(6)
Sb1-F3	1.846(4)	Cl3X-C1S	1.829(18)
Sb1-F6	1.865(3)	C1S-Cl2S	1.71(2)
Sb1-F2	1.866(3)	C1S-Cl1S	1.730(14)
Sb1-F5	1.867(4)	C1V-Cl1V	1.739(12)
Sb1-F1	1.868(3)	C1V-Cl2V	1.746(10)
Sb1-F4	1.869(3)	C1V-Cl3V	1.786(10)

Angles			
P1-Au1-Cl1	176.92(4)	C5-C6-C7	115.9(4)
P2-Au2-Cl1	178.17(4)	C1-C6-C7	123.3(4)
Au1-Cl1-Au2	94.67(4)	C8-C7-C12	118.9(4)
C1-P1-C13	104.26(18)	C8-C7-C6	121.9(4)
C1-P1-C17	107.21(19)	C12-C7-C6	119.0(4)
C13-P1-C17	114.8(2)	C7-C8-C9	120.6(4)
C1-P1-Au1	116.30(15)	C10-C9-C8	120.3(4)
C13-P1-Au1	106.67(14)	C9-C10-C11	119.5(5)
C17-P1-Au1	107.84(14)	C12-C11-C10	120.5(4)
C37-P2-C21	104.3(7)	C11-C12-C7	120.2(4)
C37-P2-C33'	114.9(12)	C15-C13-C16	109.8(4)
C21-P2-C33'	106.0(10)	C15-C13-C14	108.3(4)
C37-P2-C33	119.5(7)	C16-C13-C14	108.8(4)
C21-P2-C33	105.0(3)	C15-C13-P1	115.0(3)
C33'-P2-C33	4.8(13)	C16-C13-P1	109.2(3)
C37-P2-C37'	6.7(12)	C14-C13-P1	105.5(3)
C21-P2-C37'	109.1(8)	C20-C17-C18	107.6(4)
C33'-P2-C37'	108.5(12)	C20-C17-C19	110.7(4)
C33-P2-C37'	113.1(8)	C18-C17-C19	107.8(4)
C37-P2-Au2	106.4(6)	C20-C17-P1	116.1(3)
C21-P2-Au2	114.76(17)	C18-C17-P1	107.5(3)
C33'-P2-Au2	110.5(10)	C19-C17-P1	106.9(3)
C33-P2-Au2	107.2(3)	C26-C21-C22	118.5(4)
C37'-P2-Au2	107.8(8)	C26-C21-P2	123.6(3)
C2-C1-C6	117.1(4)	C22-C21-P2	117.8(4)
C2-C1-P1	118.5(3)	C23-C22-C21	121.2(5)
C6-C1-P1	124.2(3)	C24-C23-C22	120.0(4)
C3-C2-C1	122.0(5)	C23-C24-C25	120.2(4)
C4-C3-C2	119.6(4)	C24-C25-C26	120.7(5)
C3-C4-C5	119.7(4)	C25-C26-C21	119.4(4)
C6-C5-C4	120.6(5)	C25-C26-C27	115.7(4)
C5-C6-C1	120.8(4)	C21-C26-C27	124.9(4)

C32-C27-C28	119.3(4)
C32-C27-C26	119.8(4)
C28-C27-C26	120.5(4)
C29-C28-C27	119.9(4)
C28-C29-C30	120.9(4)
C31-C30-C29	118.9(4)
C32-C31-C30	120.9(4)
C31-C32-C27	120.1(4)
C34-C33-C36	110.6(7)
C34-C33-C35	108.9(7)
C36-C33-C35	108.1(7)
C34-C33-P2	108.3(8)
C36-C33-P2	105.3(6)
C35-C33-P2	115.6(7)
C36'-C33'-C34'	107.8(8)
C36'-C33'-C35'	110.6(8)
C34'-C33'-C35'	108.1(8)
C36'-C33'-P2	104(2)
C34'-C33'-P2	109(3)
C35'-C33'-P2	118(2)
C38-C37-C40	109.9(12)
C38-C37-C39	108.0(10)
C40-C37-C39	106.3(12)
C38-C37-P2	107.4(13)
C40-C37-P2	114.1(15)
C39-C37-P2	111.0(17)
C40'-C37'-C38'	108.0(8)
C40'-C37'-C39'	110.6(8)
C38'-C37'-C39'	108.0(8)
C40'-C37'-P2	119.0(19)
C38'-C37'-P2	105.2(17)
C39'-C37'-P2	105(3)
F3-Sb1-F6	89.43(19)
F3-Sb1-F2	90.4(2)
F6-Sb1-F2	89.21(18)
F3-Sb1-F5	90.9(2)
F6-Sb1-F5	179.42(19)
F2-Sb1-F5	90.32(18)
F3-Sb1-F1	178.67(18)
F6-Sb1-F1	89.29(15)
F2-Sb1-F1	89.16(18)
F5-Sb1-F1	90.36(17)
F3-Sb1-F4	91.4(2)
F6-Sb1-F4	91.18(18)
F2-Sb1-F4	178.11(19)
F5-Sb1-F4	89.28(18)
F1-Sb1-F4	88.99(17)
Cl2X-C1X-Cl1X	112.0(8)
Cl2X-C1X-Cl3X	111.7(6)
Cl1X-C1X-Cl3X	109.0(6)
Cl2X-C1X-Cl1X#1	42.3(4)
Cl1X-C1X-Cl1X#1	69.7(5)
Cl3X-C1X-Cl1X#1	128.1(6)
Cl2X-Cl1X-C1X#1	161.9(6)
Cl2X#1-Cl1X-C1X#1	51.6(3)
C1X-Cl1X-C1X#1	110.3(5)
Cl2X#1-Cl1X-Cl1X#1	97.8(3)
C1X-Cl1X-Cl1X#1	64.1(5)
C1X#1-Cl1X-Cl1X#1	46.2(3)
Cl1X-Cl2X-C1X#1	86.1(5)
C1X-Cl3X-C1S	92.3(7)
Cl2S-C1S-Cl1S	112.9(10)
Cl2S-C1S-Cl3X	110.5(9)
Cl1S-C1S-Cl3X	107.3(9)
Cl1V-C1V-Cl2V	111.0(6)
Cl1V-C1V-Cl3V	110.1(6)
Cl2V-C1V-Cl3V	109.6(6)

Hydroxy bis{[(1,1′-biphenyl-2-yl)di-*tert*-butylphosphine]gold(I)} tetrafluoroborate (D)

Table S18 Crystal data and structure refinement for **D**.

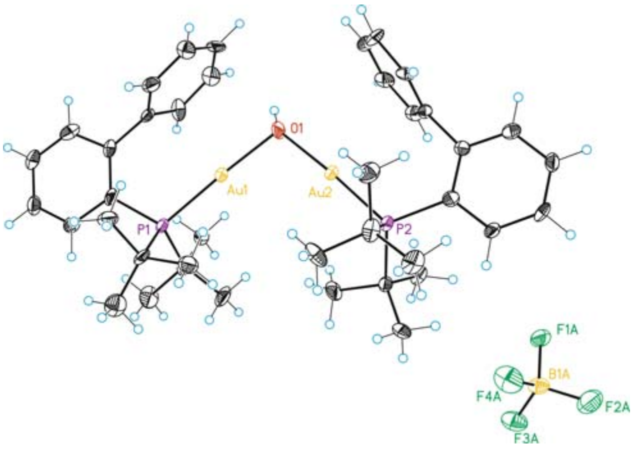

Identification code	mo_AHR30016_0m
Empirical formula	C42.50 H57.50 Au2 B Cl7.50 F4 O P2
Formula weight	1392.94
Temperature	100(2) K
Wavelength	0.71073 Å
Crystal system	Monoclinic
Space group	P2(1)/n
Unit cell dimensions	
a = 11.9239(16) Å	á= 90.00 °.
b = 26.260(3) Å	â = 92.182(4) °.
c = 16.336(2) Å	ã = 90.00 °.
Volume	5111.4(11) Å^3
Z	4
Density (calculated)	1.810 Mg/m^3
Absorption coefficient	6.235 mm^{-1}
F(000)	2708
Crystal size	0.30 x 0.05 x 0.03 mm^3
Theta range for data collection	1.88 to 25.44 °.
Index ranges	-14 <=h<=14 ,-31 <=k<=31 ,-19 <=l<=19
Reflections collected	47708
Independent reflections	9380 [R(int) = 0.0811]
Completeness to theta =25.44 °	0.992 %
Absorption correction	Empirical
Max. and min. transmission	0.8350 and 0.2563
Refinement method	Full-matrix least-squares on F^2
Data / restraints / parameters	9380 / 90 / 625
Goodness-of-fit on F^2	1.184
Final R indices [I>2sigma(I)]	R1 = 0.0753 , wR2 = 0.1865
R indices (all data)	R1 = 0.0891 , wR2 = 0.1920

Largest diff. peak and hole	3.106 and -2.321 e.Å^{-3}

Table S19 Bond lengths [Å] and angles [°] for **D**.

Bond lengths

Au1-O1	2.049(10)	C24-C25	1.382(18)
Au1-P1	2.235(3)	C25-C26	1.378(18)
Au1-Au2	3.2781(7)	C26-C27	1.521(17)
Au2-O1	2.083(10)	C27-C28	1.366(18)
Au2-P2	2.234(3)	C27-C32	1.385(18)
P1-C1	1.850(13)	C28-C29	1.404(18)
P1-C13	1.877(13)	C29-C30	1.370(19)
P1-C17	1.899(14)	C30-C31	1.41(2)
P2-C21	1.829(13)	C31-C32	1.424(18)
P2-C40	1.868(14)	C33-C40	1.550(18)
P2-C36	1.897(12)	C34-C40	1.552(19)
C1-C2	1.410(19)	C35-C40	1.540(19)
C1-C6	1.431(18)	C36-C39	1.513(18)
C2-C3	1.389(18)	C36-C37	1.545(18)
C3-C4	1.38(2)	C36-C38	1.564(17)
C4-C5	1.39(2)	C1T-Cl2T	1.78(3)
C5-C6	1.404(18)	C1T-Cl1T	1.78(3)
C6-C7	1.468(18)	C1T-Cl3T	1.78(3)
C7-C8	1.385(18)	Cl3T-Cl1U	1.980(10)
C7-C12	1.416(18)	C1T'-Cl2'	1.73(4)
C8-C9	1.38(2)	C1T'-Cl3'	1.74(4)
C9-C10	1.381(19)	C1S-Cl3"	1.59(2)
C10-C11	1.387(19)	C1S-Cl1S	1.69(2)
C11-C12	1.387(19)	C1S-Cl2S	1.70(2)
C13-C15	1.51(2)	C1S-Cl1"	1.76(2)
C13-C14	1.546(17)	C1S-Cl2"	1.90(2)
C13-C16	1.552(18)	C1S-Cl3S	1.93(2)
C17-C19	1.48(2)	C1U-Cl2U	1.785(9)
C17-C18	1.52(2)	C1U-Cl1U	1.786(9)
C17-C20	1.539(19)	C1U-Cl3U	1.790(9)
C21-C22	1.406(18)	B1A-F2A	1.357(18)
C21-C26	1.427(18)	B1A-F3A	1.384(18)
C22-C23	1.386(18)	B1A-F1A	1.387(17)
C23-C24	1.365(19)	B1A-F4A	1.400(17)

Angles

O1-Au1-P1	177.3(3)	Au1-O1-Au2	105.0(5)
O1-Au1-Au2	37.9(3)	C1-P1-C13	108.2(6)
P1-Au1-Au2	139.47(8)	C1-P1-C17	105.6(6)
O1-Au2-P2	175.7(3)	C13-P1-C17	114.2(6)
O1-Au2-Au1	37.1(3)	C1-P1-Au1	112.8(4)
P2-Au2-Au1	139.37(9)	C13-P1-Au1	109.9(4)

C17-P1-Au1	106.3(5)	C32-C27-C26	119.2(11)
C21-P2-C40	104.5(6)	C27-C28-C29	121.1(12)
C21-P2-C36	108.7(6)	C30-C29-C28	118.6(13)
C40-P2-C36	113.3(6)	C29-C30-C31	121.8(12)
C21-P2-Au2	113.3(4)	C30-C31-C32	118.1(13)
C40-P2-Au2	107.9(4)	C27-C32-C31	119.2(13)
C36-P2-Au2	109.2(4)	C39-C36-C37	109.6(11)
C2-C1-C6	119.4(11)	C39-C36-C38	110.4(10)
C2-C1-P1	117.7(10)	C37-C36-C38	107.2(11)
C6-C1-P1	122.9(9)	C39-C36-P2	115.7(9)
C3-C2-C1	120.3(13)	C37-C36-P2	107.8(8)
C4-C3-C2	121.2(13)	C38-C36-P2	105.8(9)
C3-C4-C5	119.0(12)	C35-C40-C33	111.3(12)
C4-C5-C6	122.8(13)	C35-C40-C34	108.5(11)
C5-C6-C1	117.3(12)	C33-C40-C34	108.0(11)
C5-C6-C7	117.0(12)	C35-C40-P2	108.0(9)
C1-C6-C7	125.7(11)	C33-C40-P2	115.0(9)
C8-C7-C12	117.9(12)	C34-C40-P2	105.7(10)
C8-C7-C6	123.4(11)	Cl2T-C1T-Cl1T	111.3(15)
C12-C7-C6	118.3(11)	Cl2T-C1T-Cl3T	109.2(14)
C9-C8-C7	121.8(13)	Cl1T-C1T-Cl3T	110.7(14)
C10-C9-C8	119.3(13)	C1T-Cl3T-Cl1U	171.2(10)
C9-C10-C11	120.8(13)	Cl2'-C1T'-Cl3'	112(3)
C12-C11-C10	119.5(12)	Cl3"-C1S-Cl1S	130.5(16)
C11-C12-C7	120.6(12)	Cl3"-C1S-Cl2S	98.4(11)
C15-C13-C14	110.0(11)	Cl1S-C1S-Cl2S	117.8(12)
C15-C13-C16	109.0(11)	Cl3"-C1S-Cl1"	126.0(15)
C14-C13-C16	106.0(11)	Cl1S-C1S-Cl1"	6.7(8)
C15-C13-P1	117.9(10)	Cl2S-C1S-Cl1"	116.6(12)
C14-C13-P1	105.2(8)	Cl3"-C1S-Cl2"	111.2(11)
C16-C13-P1	108.1(9)	Cl1S-C1S-Cl2"	104.1(11)
C19-C17-C18	107.7(13)	Cl2S-C1S-Cl2"	13.9(5)
C19-C17-C20	112.6(12)	Cl1"-C1S-Cl2"	103.4(10)
C18-C17-C20	108.4(13)	Cl3"-C1S-Cl3S	29.3(6)
C19-C17-P1	106.3(10)	Cl1S-C1S-Cl3S	103.9(13)
C18-C17-P1	114.8(10)	Cl2S-C1S-Cl3S	106.6(11)
C20-C17-P1	107.1(10)	Cl1"-C1S-Cl3S	98.4(12)
C22-C21-C26	117.2(12)	Cl2"-C1S-Cl3S	114.9(11)
C22-C21-P2	119.1(10)	Cl2U-C1U-Cl1U	104.5(6)
C26-C21-P2	123.6(9)	Cl2U-C1U-Cl3U	109.5(8)
C23-C22-C21	121.3(12)	Cl1U-C1U-Cl3U	102.6(6)
C24-C23-C22	121.1(11)	C1U-Cl1U-Cl3T	175.4(6)
C23-C24-C25	118.5(12)	F2A-B1A-F3A	111.6(11)
C26-C25-C24	122.8(13)	F2A-B1A-F1A	107.9(12)
C25-C26-C21	119.0(12)	F3A-B1A-F1A	109.9(12)
C25-C26-C27	115.7(11)	F2A-B1A-F4A	110.0(13)
C21-C26-C27	125.3(11)	F3A-B1A-F4A	109.2(12)
C28-C27-C32	121.1(11)	F1A-B1A-F4A	108.1(11)
C28-C27-C26	119.5(11)		

Bromo bis{[(1,1′-biphenyl-2-yl)di-*tert*-butylphosphine]gold(I)} hexafluoroantimonate

Table S20 Crystal data and structure refinement for bromo bis{[(1,1′-biphenyl-2-yl)di-*tert*-butylphosphine]gold(I)} hexafluoroantimonate.

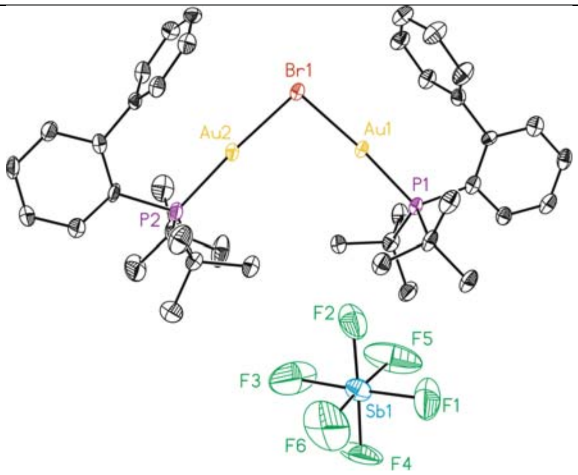

Identification code	mo_AHR3_0081_0m
Empirical formula	C42.75 H60 Au2 Br Cl3 F6 P2 Sb
Formula weight	1451.79
Temperature	100(2) K
Wavelength	0.71073 Å
Crystal system	Triclinic
Space group	P-1
Unit cell dimensions	
a = 11.7124(8) Å	α= 69.359(2) °.
b = 14.7716(10) Å	β = 78.298(2) °.
c = 15.6969(11) Å	γ = 72.557(2) °.
Volume	2410.1(3) Å^3
Z	2
Density (calculated)	2.001 Mg/m^3
Absorption coefficient	7.743 mm^{-1}
F(000)	1391
Crystal size	0.35 x 0.15 x 0.15 mm^3
Theta range for data collection	1.83 to 29.94 °.
Index ranges -15 <=h<=15 ,-20 <=k	

Table S21 Bond lengths [Å] and angles [°] for bromo bis{[(1,1′-biphenyl-2-yl)di-*tert*-butylphosphine]gold(I)} hexafluoroantimonate.

Bond lengths			
Au1-P1	2.2648(8)	C1-C6	1.420(5)
Au1-Br1	2.4588(3)	C1-P1	1.817(3)
Au2-P2	2.2637(9)	C2-C3	1.378(4)
Au2-Br1	2.4605(3)	C3-C4	1.386(5)
C1-C2	1.394(4)	C4-C5	1.393(5)

C5-C6	1.383(4)	C31-C32	1.396(5)
C6-C7	1.516(4)	C33-C35	1.523(7)
C7-C8	1.379(5)	C33-C36	1.527(5)
C7-C12	1.401(5)	C33-C34	1.541(5)
C8-C9	1.377(5)	C33-P2	1.880(4)
C9-C10	1.391(6)	C37-C39	1.515(6)
C10-C11	1.386(5)	C37-C38	1.531(5)
C11-C12	1.378(5)	C37-C40	1.539(6)
C13-C14	1.526(6)	C37-P2	1.884(5)
C13-C15	1.537(4)	Sb1-F6	1.814(4)
C13-C16	1.544(6)	Sb1-F3	1.822(4)
C13-P1	1.878(3)	Sb1-F4	1.830(3)
C17-C19	1.527(5)	Sb1-F1	1.842(4)
C17-C20	1.533(5)	Sb1-F5	1.850(4)
C17-C18	1.538(5)	Sb1-F2	1.865(3)
C17-P1	1.868(4)	Cl1S-C1S	1.777(6)
C21-C26	1.398(5)	Cl1S-C1S'	1.783(8)
C21-C22	1.400(5)	C1S-C1P	1.611(8)
C21-P2	1.809(3)	C1S-Cl2S	1.757(5)
C22-C23	1.376(5)	Cl2S-C1P	1.856(8)
C23-C24	1.363(6)	C1S'-Cl2'	1.780(7)
C24-C25	1.384(5)	C1T-Cl1T	1.789(9)
C25-C26	1.395(4)	C1T-Cl2T	1.794(7)
C26-C27	1.511(5)	C1D-Cl2D	1.789(4)
C27-C32	1.391(5)	C1D-Cl1D	1.796(4)
C27-C28	1.402(4)	C1P-C2P	1.541(4)
C28-C29	1.386(5)	C2P-C3P	1.539(4)
C29-C30	1.389(6)	C3P-C4P	1.539(4)
C30-C31	1.390(5)	C4P-C5P	1.540(4)

Angles			
P1-Au1-Br1	174.83(2)	C8-C9-C10	120.9(4)
P2-Au2-Br1	176.00(2)	C11-C10-C9	118.8(3)
Au1-Br1-Au2	96.093(13)	C12-C11-C10	120.5(3)
C2-C1-C6	116.7(3)	C11-C12-C7	120.2(3)
C2-C1-P1	119.6(3)	C14-C13-C15	107.1(3)
C6-C1-P1	123.6(2)	C14-C13-C16	110.5(3)
C3-C2-C1	123.2(3)	C15-C13-C16	107.7(3)
C2-C3-C4	119.4(3)	C14-C13-P1	116.5(3)
C3-C4-C5	119.2(3)	C15-C13-P1	107.4(2)
C6-C5-C4	121.3(3)	C16-C13-P1	107.2(2)
C5-C6-C1	120.2(3)	C19-C17-C20	108.8(3)
C5-C6-C7	115.8(3)	C19-C17-C18	109.0(3)
C1-C6-C7	124.0(2)	C20-C17-C18	109.5(3)
C8-C7-C12	119.2(3)	C19-C17-P1	105.6(3)
C8-C7-C6	122.8(3)	C20-C17-P1	114.9(2)
C12-C7-C6	117.8(3)	C18-C17-P1	108.9(2)
C9-C8-C7	120.3(3)	C26-C21-C22	116.8(3)

C26-C21-P2	124.2(3)	C21-P2-C33	104.24(15)
C22-C21-P2	118.9(3)	C21-P2-C37	107.28(18)
C23-C22-C21	122.3(4)	C33-P2-C37	115.91(19)
C24-C23-C22	120.0(4)	C21-P2-Au2	114.53(12)
C23-C24-C25	119.7(3)	C33-P2-Au2	107.93(13)
C24-C25-C26	120.5(4)	C37-P2-Au2	107.21(11)
C25-C26-C21	120.6(3)	F6-Sb1-F3	90.0(3)
C25-C26-C27	115.2(3)	F6-Sb1-F4	88.9(2)
C21-C26-C27	124.1(3)	F3-Sb1-F4	88.8(2)
C32-C27-C28	118.7(3)	F6-Sb1-F1	90.2(2)
C32-C27-C26	121.7(3)	F3-Sb1-F1	177.5(2)
C28-C27-C26	119.2(3)	F4-Sb1-F1	93.6(2)
C29-C28-C27	120.8(4)	F6-Sb1-F5	175.6(2)
C28-C29-C30	120.0(3)	F3-Sb1-F5	94.1(3)
C29-C30-C31	119.9(3)	F4-Sb1-F5	89.85(18)
C30-C31-C32	120.0(4)	F1-Sb1-F5	85.7(2)
C27-C32-C31	120.6(3)	F6-Sb1-F2	91.7(2)
C35-C33-C36	108.7(4)	F3-Sb1-F2	88.67(19)
C35-C33-C34	110.1(4)	F4-Sb1-F2	177.4(2)
C36-C33-C34	109.4(4)	F1-Sb1-F2	88.86(19)
C35-C33-P2	105.5(3)	F5-Sb1-F2	89.71(18)
C36-C33-P2	115.6(3)	C1S-Cl1S-C1S'	22.2(3)
C34-C33-P2	107.5(3)	C1P-C1S-Cl2S	66.7(4)
C39-C37-C38	108.3(3)	C1P-C1S-Cl1S	107.5(8)
C39-C37-C40	111.1(4)	Cl2S-C1S-Cl1S	109.5(3)
C38-C37-C40	107.2(3)	C1S-Cl2S-C1P	52.9(3)
C39-C37-P2	116.5(3)	Cl2'-C1S'-Cl1S	106.4(4)
C38-C37-P2	108.3(3)	Cl1T-C1T-Cl2T	110.0(6)
C40-C37-P2	105.0(3)	Cl2D-C1D-Cl1D	104.3(3)
C1-P1-C17	104.01(15)	C2P-C1P-C1S	145.3(8)
C1-P1-C13	107.65(15)	C2P-C1P-Cl2S	152.4(7)
C17-P1-C13	114.97(17)	C1S-C1P-Cl2S	60.4(3)
C1-P1-Au1	115.77(12)	C3P-C2P-C1P	111.6(5)
C17-P1-Au1	106.56(10)	C2P-C3P-C4P	111.7(4)
C13-P1-Au1	108.12(11)	C3P-C4P-C5P	111.3(5)

Table S22 Torsion angles [°] for bromo bis{[(1,1′-biphenyl-2-yl)di-*tert*-butylphosphine]gold(I)} hexafluoroantimonate.

Torsion angles			
P1-Au1-Br1-Au2	-25.2(2)	C4-C5-C6-C7	-174.2(3)
P2-Au2-Br1-Au1	6.8(4)	C2-C1-C6-C5	-3.5(5)
C6-C1-C2-C3	1.6(5)	P1-C1-C6-C5	171.7(3)
P1-C1-C2-C3	-173.7(3)	C2-C1-C6-C7	173.0(3)
C1-C2-C3-C4	1.3(6)	P1-C1-C6-C7	-11.9(5)
C2-C3-C4-C5	-2.4(6)	C5-C6-C7-C8	-74.1(5)
C3-C4-C5-C6	0.5(6)	C1-C6-C7-C8	109.3(4)
C4-C5-C6-C1	2.5(5)	C5-C6-C7-C12	99.7(4)

C1-C6-C7-C12	-76.9(5)
C12-C7-C8-C9	2.1(6)
C6-C7-C8-C9	175.9(3)
C7-C8-C9-C10	-1.3(6)
C8-C9-C10-C11	0.9(6)
C9-C10-C11-C12	-1.3(6)
C10-C11-C12-C7	2.2(5)
C8-C7-C12-C11	-2.6(5)
C6-C7-C12-C11	-176.6(3)
C26-C21-C22-C23	0.5(6)
P2-C21-C22-C23	-175.5(3)
C21-C22-C23-C24	1.4(7)
C22-C23-C24-C25	-2.4(6)
C23-C24-C25-C26	1.5(6)
C24-C25-C26-C21	0.4(6)
C24-C25-C26-C27	-177.2(3)
C22-C21-C26-C25	-1.4(5)
P2-C21-C26-C25	174.4(3)
C22-C21-C26-C27	176.0(3)
P2-C21-C26-C27	-8.2(5)
C25-C26-C27-C32	-79.5(4)
C21-C26-C27-C32	103.0(4)
C25-C26-C27-C28	93.4(4)
C21-C26-C27-C28	-84.1(4)
C32-C27-C28-C29	-0.4(5)
C26-C27-C28-C29	-173.6(3)
C27-C28-C29-C30	1.5(5)
C28-C29-C30-C31	-1.9(5)
C29-C30-C31-C32	1.2(5)
C28-C27-C32-C31	-0.3(4)
C26-C27-C32-C31	172.7(3)
C30-C31-C32-C27	-0.1(5)
C2-C1-P1-C17	74.5(3)
C6-C1-P1-C17	-100.5(3)
C2-C1-P1-C13	-47.9(3)
C6-C1-P1-C13	137.1(3)
C2-C1-P1-Au1	-168.9(2)
C6-C1-P1-Au1	16.1(3)
C19-C17-P1-C1	65.0(2)
C20-C17-P1-C1	-54.9(3)
C18-C17-P1-C1	-178.1(2)
C19-C17-P1-C13	-177.57(19)
C20-C17-P1-C13	62.6(3)
C18-C17-P1-C13	-60.7(3)
C19-C17-P1-Au1	-57.8(2)
C20-C17-P1-Au1	-177.7(2)
C18-C17-P1-Au1	59.1(3)
C14-C13-P1-C1	81.0(3)
C15-C13-P1-C1	-158.9(3)
C16-C13-P1-C1	-43.4(3)
C14-C13-P1-C17	-34.3(3)
C15-C13-P1-C17	85.8(3)
C16-C13-P1-C17	-158.7(2)
C14-C13-P1-Au1	-153.2(3)
C15-C13-P1-Au1	-33.1(3)
C16-C13-P1-Au1	82.4(2)
Br1-Au1-P1-C1	-165.0(2)
Br1-Au1-P1-C17	-49.9(3)
Br1-Au1-P1-C13	74.2(3)
C26-C21-P2-C33	-109.3(3)
C22-C21-P2-C33	66.4(4)
C26-C21-P2-C37	127.2(3)
C22-C21-P2-C37	-57.1(3)
C26-C21-P2-Au2	8.4(4)
C22-C21-P2-Au2	-175.9(3)
C35-C33-P2-C21	67.0(3)
C36-C33-P2-C21	-53.1(4)
C34-C33-P2-C21	-175.6(3)
C35-C33-P2-C37	-175.4(2)
C36-C33-P2-C37	64.6(4)
C34-C33-P2-C37	-57.9(4)
C35-C33-P2-Au2	-55.2(2)
C36-C33-P2-Au2	-175.2(3)
C34-C33-P2-Au2	62.3(4)
C39-C37-P2-C21	74.8(3)
C38-C37-P2-C21	-162.9(2)
C40-C37-P2-C21	-48.6(3)
C39-C37-P2-C33	-41.1(4)
C38-C37-P2-C33	81.2(3)
C40-C37-P2-C33	-164.5(2)
C39-C37-P2-Au2	-161.7(3)
C38-C37-P2-Au2	-39.4(3)
C40-C37-P2-Au2	74.9(2)
Br1-Au2-P2-C21	168.2(4)
Br1-Au2-P2-C33	-76.2(4)
Br1-Au2-P2-C37	49.3(4)
C1S'-Cl1S-C1S-C1P	67.4(8)
C1S'-Cl1S-C1S-Cl2S	-3.5(5)
Cl1S-C1S-Cl2S-C1P	101.2(9)
C1S-Cl1S-C1S'-Cl2'	81.7(7)
Cl2S-C1S-C1P-C2P	-166(3)
Cl1S-C1S-C1P-C2P	90(3)
Cl1S-C1S-C1P-Cl2S	-104.2(4)
C1S-Cl2S-C1P-C2P	163(3)
C1S-C1P-C2P-C3P	145(2)
Cl2S-C1P-C2P-C3P	-8(3)
C1P-C2P-C3P-C4P	94.1(9)
C2P-C3P-C4P-C5P	115.3(8)

Iodo bis{[(1,1′-biphenyl-2-yl)di-*tert*-butylphosphine]gold(I)} hexafluoroantimonate

Table S23 Crystal data and structure refinement for iodo bis{[(1,1′-biphenyl-2-yl)di-*tert*-butylphosphine]gold(I)} hexafluoroantimonate.

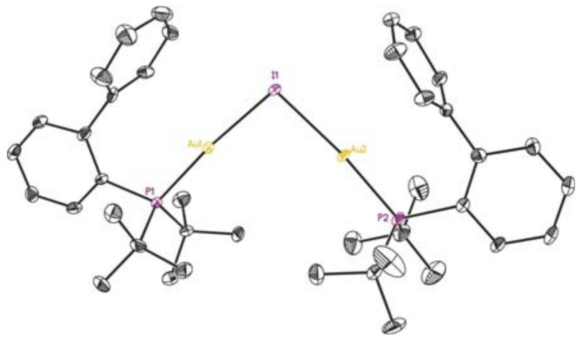

Identification code	mo_AHR3_0092R2_0m
Empirical formula	C41 H58 Au2 Cl2 F6 I O P2 Sb
Formula weight	1456.30
Temperature	100(2) K
Wavelength	0.71073 Å
Crystal system	Triclinic
Space group	P-1
Unit cell dimensions	
a = 11.7778(8) Å	α= 68.501(4) °.
b = 14.9330(12) Å	β = 76.809(4) °.
c = 15.7163(12) Å	γ = 72.286(4) °.
Volume	2428.6(3) Å^3
Z	2
Density (calculated)	1.991 Mg/m^3
Absorption coefficient	7.443 mm^{-1}
F(000)	1384
Crystal size	0.30 x 0.20 x 0.15 mm^3
Theta range for data collection	1.83 to 37.35 °.
Index ranges	-20 <=h<=19 ,-20 <=k<=25 ,-26 <=l<=26
Reflections collected	40115
Independent reflections	21806 [R(int) = 0.0597]
Completeness to theta =37.35 °	0.861 %
Absorption correction	Empirical
Max. and min. transmission	0.4015 and 0.2136
Refinement method	Full-matrix least-squares on F^2
Data / restraints / parameters	21806 / 23 / 550
Goodness-of-fit on F^2	0.996
Final R indices [I>2sigma(I)]	R1 = 0.0581 , wR2 = 0.1555
R indices (all data)	R1 = 0.0858 , wR2 = 0.1801
Largest diff. peak and hole	4.702 and -3.183 e.Å^{-3}

Table S24 Torsion angles [º] for iodo bis{[(1,1′-biphenyl-2-yl)di-*tert*-butylphosphine]gold(I)} hexafluoroantimonate

Bond lengths			
Au1-P1	2.2804(13)	C21-C26	1.404(8)
Au1-I1	2.6016(4)	C22-C23	1.41(8)
Au2-P2	2.2701(14)	C23-C24	1.384(10)
Au2-I1	2.5894(4)	C24-C25	1.381(9)
P1-C1	1.823(5)	C25-C26	1.428(7)
P1-C13	1.87(6)	C26-C27	1.48(8)
P1-C17	1.872(5)	C27-C32	1.362(7)
P2-C21	1.829(5)	C27-C28	1.405(7)
P2-C33	1.888(6)	C28-C29	1.418(8)
P2-C37	1.889(6)	C29-C30	1.373(8)
C1-C2	1.407(7)	C30-C31	1.391(9)
C1-C6	1.42(7)	C31-C32	1.406(8)
C2-C3	1.385(7)	C33-C36	1.502(10)
C3-C4	1.385(8)	C33-C35	1.53(9)
C4-C5	1.392(8)	C33-C34	1.534(11)
C5-C6	1.385(7)	C37-C38	1.447(10)
C6-C7	1.5(7)	C37-C39	1.535(8)
C7-C8	1.382(8)	C37-C40	1.587(9)
C7-C12	1.413(8)	Sb1-F2	1.849(5)
C8-C9	1.396(8)	Sb1-F5	1.849(5)
C9-C10	1.376(9)	Sb1-F4	1.86(5)
C10-C11	1.413(10)	Sb1-F6	1.86(5)
C11-C12	1.385(9)	Sb1-F1	1.87(5)
C13-C14	1.539(8)	Sb1-F3	1.879(5)
C13-C15	1.544(7)	C1S-Cl1S	1.746(8)
C13-C16	1.562(8)	C1S-Cl2'	1.775(8)
C17-C18	1.506(8)	C1S-Cl2S	1.776(7)
C17-C19	1.526(8)	Cl2S-Cl2'	1.646(14)
C17-C20	1.54(8)	O1W"-O1W"#1	1.38(3)
C21-C22	1.397(8)		

Angles			
P1-Au1-I1	174.09(3)	C33-P2-Au2	107.4(2)
P2-Au2-I1	173.83(4)	C37-P2-Au2	106.34(18)
Au2-I1-Au1	96.347(13)	C2-C1-C6	118.5(4)
C1-P1-C13	108.7(2)	C2-C1-P1	118.4(4)
C1-P1-C17	104.3(2)	C6-C1-P1	123.0(4)
C13-P1-C17	113.7(3)	C3-C2-C1	122.0(5)
C1-P1-Au1	115.28(17)	C2-C3-C4	119.4(5)
C13-P1-Au1	107.89(17)	C3-C4-C5	119.1(5)
C17-P1-Au1	107.13(17)	C6-C5-C4	122.9(5)
C21-P2-C33	104.7(3)	C5-C6-C1	118.1(5)
C21-P2-C37	107.9(3)	C5-C6-C7	116.9(5)
C33-P2-C37	115.6(3)	C1-C6-C7	124.7(4)
C21-P2-Au2	115.17(19)	C8-C7-C12	119.0(5)

C8-C7-C6	119.3(4)	C30-C31-C32	119.3(5)
C12-C7-C6	121.4(5)	C27-C32-C31	121.1(5)
C7-C8-C9	121.5(5)	C36-C33-C35	109.1(6)
C10-C9-C8	118.9(5)	C36-C33-C34	110.2(6)
C9-C10-C11	121.3(6)	C35-C33-C34	108.1(6)
C12-C11-C10	118.9(6)	C36-C33-P2	115.5(5)
C11-C12-C7	120.4(6)	C35-C33-P2	108.3(5)
C14-C13-C15	107.7(4)	C34-C33-P2	105.4(4)
C14-C13-C16	108.3(5)	C38-C37-C39	111.1(6)
C15-C13-C16	107.6(5)	C38-C37-C40	110.9(7)
C14-C13-P1	117.5(4)	C39-C37-C40	105.4(5)
C15-C13-P1	107.6(4)	C38-C37-P2	106.5(5)
C16-C13-P1	107.7(4)	C39-C37-P2	108.8(4)
C18-C17-C19	110.0(5)	C40-C37-P2	114.1(5)
C18-C17-C20	109.2(5)	F2-Sb1-F5	89.8(3)
C19-C17-C20	108.2(5)	F2-Sb1-F4	179.1(3)
C18-C17-P1	109.5(4)	F5-Sb1-F4	91.0(3)
C19-C17-P1	114.7(4)	F2-Sb1-F6	89.5(3)
C20-C17-P1	105.0(4)	F5-Sb1-F6	178.7(3)
C22-C21-C26	120.6(5)	F4-Sb1-F6	89.7(3)
C22-C21-P2	117.8(4)	F2-Sb1-F1	90.0(2)
C26-C21-P2	121.6(4)	F5-Sb1-F1	89.3(3)
C21-C22-C23	120.2(6)	F4-Sb1-F1	90.5(2)
C24-C23-C22	119.9(6)	F6-Sb1-F1	89.7(3)
C25-C24-C23	120.0(5)	F2-Sb1-F3	89.9(2)
C24-C25-C26	121.5(6)	F5-Sb1-F3	92.0(3)
C21-C26-C25	117.7(5)	F4-Sb1-F3	89.6(2)
C21-C26-C27	127.8(4)	F6-Sb1-F3	89.0(3)
C25-C26-C27	114.5(5)	F1-Sb1-F3	178.7(3)
C32-C27-C28	120.5(5)	Cl1S-C1S-Cl2'	113.2(5)
C32-C27-C26	119.0(5)	Cl1S-C1S-Cl2S	107.9(4)
C28-C27-C26	120.4(5)	Cl2'-C1S-Cl2S	55.2(5)
C27-C28-C29	117.8(5)	Cl2'-Cl2S-C1S	62.3(4)
C30-C29-C28	121.4(5)	Cl2S-Cl2'-C1S	62.4(4)
C29-C30-C31	119.7(5)		

Chapter 2: Anion Effects in Intermolecular Gold(I)-Catalyzed Reactions: Use of BAr_4^{F-}

Introduction

As was emphasized in the general introduction section, the initial development of gold(I)-catalyzed reactions mainly focused on intramolecular reactions of 1,n-enynes.[20] Intermolecular reactions between alkynes and alkenes have been less studied because these processes pose additional challenges. On one hand, both substrates compete to bind to the metal making the nucleophilic attack less likely to happen.[86] On the other hand, alkenes have been shown to polymerize by a cationic mechanism in the presence of inherently acidic gold complexes.[87]

Gold(I)-Catalyzed Intermolecular Reactions with Alkynes

The intermolecular cycloadditions reactions involving an alkyne as one of the partners are challenging processes. Our group described the first cycloaddition reaction between alkynes and alkenes giving rise to cyclobutenes in a regioselective way (Scheme 1).[25] Aryl acetylenes and ethynylcyclopropane could cyclize with di- and trisubstituted alkenes in the presence of the bulky [(*t*BuXPhos)Au(NCMe)]SbF_6 (**A1**) as catalyst. The reaction did not proceed when internal alkynes were used.

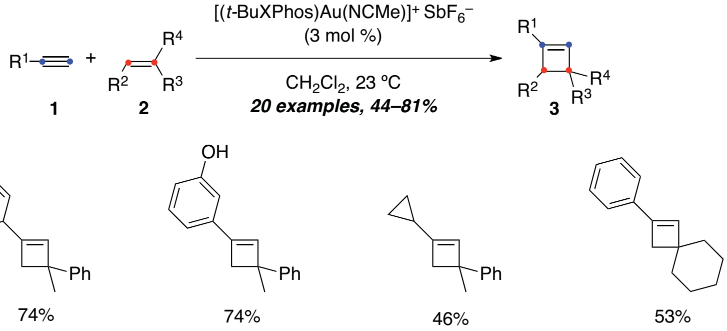

Scheme 1 Gold(I)-catalyzed [2+2] cycloaddition of terminal alkynes (**1**) and alkenes (**2**).

The reaction was proposed to proceed by an initial activation of the alkyne by the gold(I) complex forming π-gold(I)-acetylene complexes **I** (Scheme 2). These electrophilic species react with the alkene generating cyclopropyl gold(I) carbenes **II** as intermediates, that undergo ring-expansion to form intermediates **III**. Final metal elimination gives access to cyclobutenes **3**.

---

[86] (a) Brown, T. J.; Dickens, M. G.; Widenhoefer, R. A. *J. Am. Chem. Soc.* **2009**, *131*, 6350–6351. (b) Brown, T. J.; Dickens, M. G.; Widenhoefer, R. A. *Chem. Commun.* **2009**, 6451–6453.

[87] Urbano, J.; Hormigo, A. J.; de Frémont, P.; Nolan, S. P; Díaz-Requejo, M. M.; Pérez, P. J. *Chem. Commun.* **2008**, 759–761.

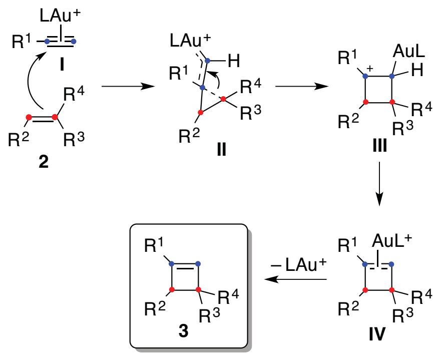

Scheme 2 Mechanistic proposal for the formation of cyclobutenes **3**.

Later, other methodologies showed that the outcome of the reaction depended greatly on the substitution pattern of the alkyne moiety. When the terminal proton of the arylacetylene was replaced by an amine, [4+2] annulations were observed, whereas reacting terminal ynamides with enol ethers, intermolecular [2+2+2] cycloadditions with two molecules of alkene occurred.[88] Additionally, if the phenyl group was replaced by a carboxylic acid or ester, α,β-unsaturated lactones or 1,3-dienes resulting from a metathesis-type reaction were obtained.[89]

Our group further expanded the intermolecular reaction of arylacetylenes **1** with gold(I) using oxoalkenes and furans. Thus, when oxoalkenes **4** were used, [3.2.1]-oxabicycles **5** were readily obtained using conditions similar to the ones developed for the [2+2] cycloaddition reaction (Scheme 3).[73] The reaction tolerated different substitutions at the aryl ring of the electrophile as well as hetero- and polyaromatic rings. The intramolecular version of this reaction had already been studied by our group.[90] The formation of the two new C–C bonds and one C–O bond was proposed to proceed through a formal [2+2+2] cycloaddition reaction. This methodology was later applied as a key step for the total synthesis of (+)-orientalol F[91] and (–)-englerin A.[92]

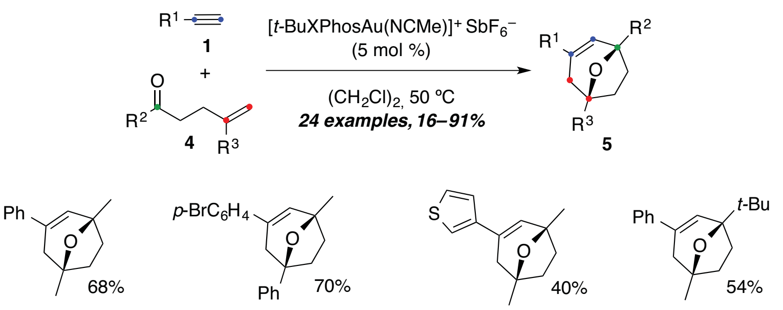

Scheme 3 Gold(I)-catalyzed [2+2+2] cycloaddition of terminal alkynes (**1**) and oxoalkenes (**4**).

---

[88] Dateer, R. B.; Shaibu, B. S.; Liu, R.-S. *Angew. Chem. Int. Ed.* **2012**, *51*, 113–117.

[89] Yeom, H.-S.; Koo, J.; Park, H.-S.; Wang, Y.; Liang, Y.; Yu, Z.-X.; Shin, S. *J. Am. Chem. Soc.* **2012**, *134*, 208–211.

[90] Jiménez-Núñez, E.; Claverie, C. K.; Nieto-Oberhuber, C.; Echavarren, A. M. *Angew. Chem. Int. Ed.* **2006**, *45*, 5452–5455.

[91] Jiménez-Núñez, E.; Molawi, K.; Echavarren, A. M. *Chem. Commun.* **2009**, 7327–7329.

[92] Molawi, K.; Delpont, N.; Echavarren, A. M. *Angew. Chem. Int. Ed.* **2010**, *49*, 3517–3519.

The suggested mechanism commences as the one previously described. However, once cyclopropyl gold(I) carbene **V** is formed, the regioselective nucleophilic attack of the ketone takes place instead of the ring-expansion. The resulting oxonium cation **VI** undergoes a Prins-type cyclization affording **VII**. Final demetalation gives rise to the oxabicyclic products **5** (Scheme 4).

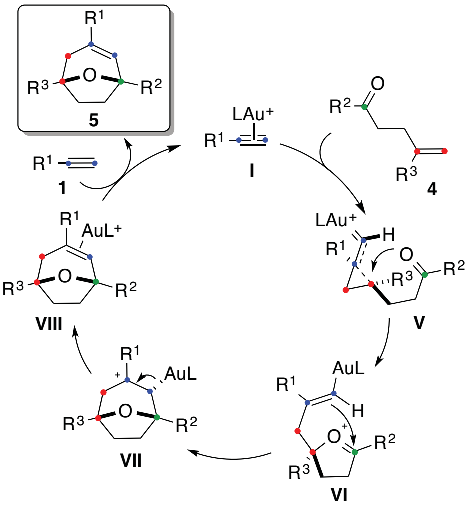

Scheme 4 Mechanistic proposal for the formation of [3.2.1]-oxabicycles **5**.

Although this proposal was supported by DFT calculations, the isolation of σ,π-digold(I) complexes from the crude mixture was an indication of a more complex mechanism (Scheme 5). Their formation originated from the deprotonation of the active π-gold(I)-acetylene complex and they were found to be unreactive under the aforementioned reaction conditions. Other groups have recently reported the formation of similar digold(I) complexes and their influence on the reactivity in catalytic transformations.[93]

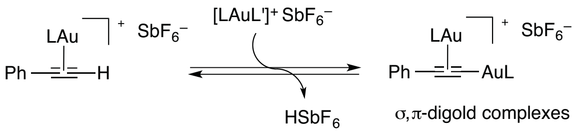

Scheme 5 Formation of σ,π-digold(I) complex from π-gold(I)-acetylene complex (L = *t*-BuXPhos).

---

[93] (a) Wei, C.; Li, C. J. *J. Am. Chem. Soc.* **2003**, *125*, 9584–9585. (b) Cheong, P. H. Y.; Morganelli, P.; Luzung, M. R.; Houk, K. N.; Toste, F. D. *J. Am. Chem. Soc.* **2008**, *130*, 4517–4526. (c) Hooper, T. N.; Green, M.; Russell, C. A. *Chem. Commun.* **2010**, *46*, 2313–2315. (d) Simonneau, A.; Jaroschik, F.; Lesage, D.; Karanik, M.; Guillot, R.; Malacria, M.; Tabet, J.-C.; Goddard, J.-P.; Fensterbank, L.; Gandon, V.; Gimbert, Y. *Chem. Sci.* **2011**, *2*, 2417–2422. (e) Grirrane, A.; Garcia, H.; Corma, A.; Álvarez, E. *ACS Catal.* **2011**, *1*, 1647–1653. (f) Brown, T. J.; Widenhoefer, R. A. *Organometallics* **2011**, *30*, 6003–6009. (g) Raducan, M.; Moreno, M.; Bour, C.; Echavarren, A. M. *Chem. Commun.* **2012**, *48*, 52–54. (h) Hashmi, A. S. K.; Lauterbach, T.; Nçsel, P.; Vilhelmsen, M. H.; Rudolph, M.; Rominger, F. *Chem.–Eur. J.* **2013**, *19*, 1058–1065. (i) Gómez-Surez, A.; Dupuis, S.; Slawin, A. M. Z.; Nolan, S. P. *Angew. Chem. Int. Ed.* **2013**, *52*, 938–942. (j) Zhdanko, A.; Strçbele, M.; Maier, M. E. *Chem.–Eur. J.* **2012**, *18*, 14732–14744. (k) Hashmi, A. S. K.; Braun, I.; Nçsel, P.; Schädlich, J.; Wieteck, M.; Rudolph, M.; Rominger, F. *Angew. Chem. Int. Ed.* **2012**, *51*, 4456–4460. (l) Rubial, B.; Ballesteros, A.; González, J. M. *Adv.Synth. Catal.* **2013**, *355*, 3337–3343.

Trisubstituted phenols **7** could be readily accessed from the reaction of terminal alkynes **1** and furans **6** in the presence of [(IPr)Au(NCPh)]SbF_6 (**B1**) (Scheme 6).[69c] In this reaction, both alkyl and aryl acetylenes bearing different substituents could be used as reaction partners. The reaction proceeded satisfactorily for symmetric furans, although non-symmetrical furans gave phenols with low to good regioselectivities. Interestingly, the use of the non-coordinating tetrakis[3,5-bis(trifluoromethyl)phenyl]borate (BAr_4^{F-}) counterion instead of SbF_6^- improved the yields of some substrates.

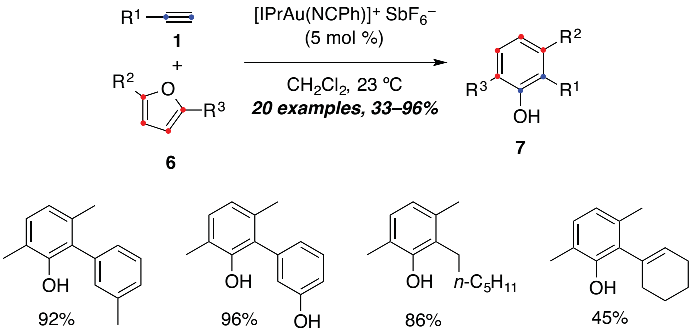
R1
1
+
R2
O
R3
6
[IPrAu(NCPh)]+ SbF6−
(5 mol %)
CH2Cl2, 23 °C
20 examples, 33–96%
R2
R3
R1
OH
7
OH
92%
OH
96%
OH
OH
86%
n-C5H11
OH
45%

Scheme 6 Gold(I)-catalyzed cyclization of terminal alkynes (**1**) and furans (**6**).

After activation of the alkyne with the metal, nucleophilic attack of the furan takes place, generating cyclopropyl gold(I) carbene **IX**. Ring opening leads to a new gold(I) carbene **X** that further cyclizes to generate oxonium cation **XI**. Final elimination of the gold complex gives rise to oxepin **XII** whose tautomeric form is arene oxide **XIII**. Phenols are finally obtained by opening of the epoxide **XIII** (Scheme 7). Again, σ,π-digold(I) species were observed in the reaction mixture.

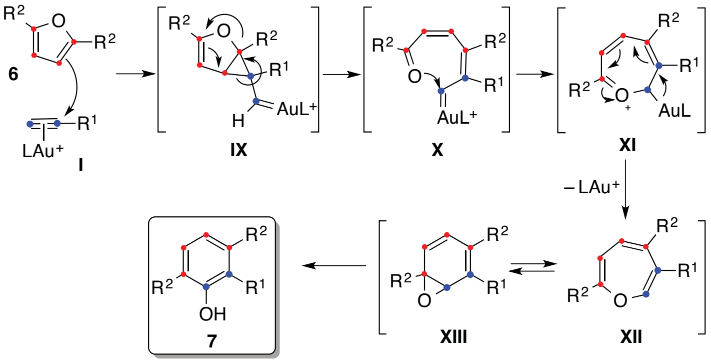
R2
O
R2
6
R1
LAu+
I
R2
O
R2
R1
H
AuL+
IX
R2
R2
O
R1
AuL+
X
R2
R1
R2
O
+
AuL
XI
– LAu+
R2
R1
R2
O
XII
R2
R2
O
R1
XIII
R2
R2
R1
OH
7

Scheme 7 Mechanistic proposal for the formation of trisubstituted phenols **7**.

Anion Effects in Gold(I)-Catalyzed Reactions

The effect of the counterion on the reaction pathway was discovered since the beginning of the gold(I) rush, affecting the reactivity, regioselectivity and stereoselectivity.[94] In a seminal work from the group of Toste, a highly enantioselective gold(I)-catalyzed reaction was achieved by using a chiral counterion (Scheme 8).[95]

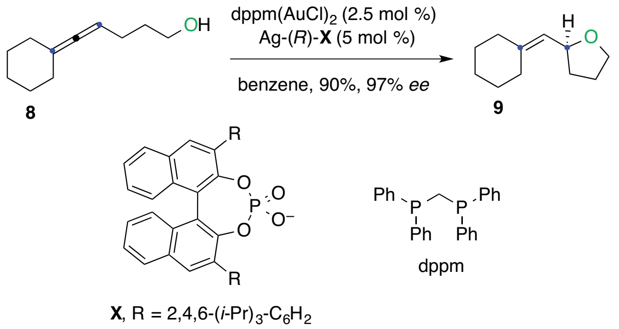

Scheme 8 Counterion-mediated enantioselective hydroalkoxylation of allene **8**.

The group of Davies demonstrated that the outcome of the reaction aryl substituted *N*-tosyl alkynyl aziridines **10** depended on the counterion used.[96] Thus, substrates **10** underwent ring expansion to afford 2,4-disubstituted pyrrole products (**11**) using [(Ph_3P)AuCl + AgOTf], whereas 2,5-disubstituted pyrroles (**12**) were obtained when AgOTs was used (Scheme 9).

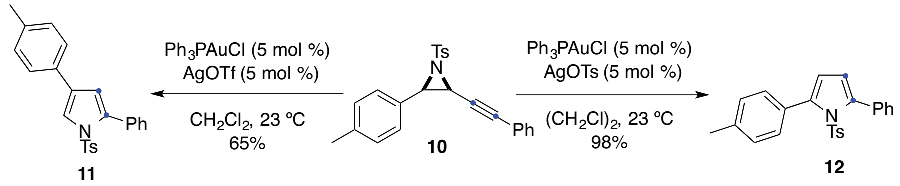

Scheme 9 Gold(I)-catalyzed synthesis of 2,5- or 2,4-disubstituted pyrroles depending on the counterion used.

Although a deeper mechanistic understanding is lacking, the authors proposed that the results obtained could be correlated with the basicity of the counterion. Thus, if a sufficiently basic counterion was used (e.g. tosylate), proton elimination and atom transfer were proposed to occur. However, if the basicity of the counterion was too low, a 1,2-aryl shift took place.

---

[94] For selected examples see: (a) Lemière, G.; Gandon, V.; Agenet, N.; Goddard, J.-P.; de Kozak, A.; Aubert, C.; Fensterbank, L; Malacria, M. *Angew. Chem., Int. Ed.* **2006**, *45*, 7596–7599. (b) Schelwies, M.; Dempwolff, A. L.; Rominger, F.; Helmchen, G. *Angew. Chem. Int. Ed.* **2007**, *46*, 5598–5601. (c) Lin, G.-Y; Yang, C.-Y; Liu, R.-S. *J. Org. Chem.* **2007**, *72*, 6753–6757. (d) LaLonde, R. L.; Sherry, B. D.; Kang, E. J.; Toste, F. D. *J. Am. Chem. Soc.* **2007**, *129*, 2452–2453. (e) Zhang, Z.; Wiedenhofer, R. A. *Org. Lett.* **2008**, *10*, 2079–2081. (f) Xia, Y.; Dudnik, A. S.; Gevorgyan V.; Li, Y. *J. Am. Chem. Soc.* **2008**, *130*, 6940–6941. Some theoretical studies include (g) Bandini, M.; Bottoni, A.; Chiarucci, M.; Cera, G.; Miscione, G. P. *J. Am. Chem. Soc.* **2014**, *134*, 20690–20700. (h) Zhou, T.; Xu, L.; Xia, Y. *Org. Lett.* **2013**, *15*, 6074–6077. (i) Zhou, T.; Xia, Y. *Organometallics* **2014**, *33*, 4230–4239.

[95] Hamilton, G. L.; Kang, E. J.; Mba, M.; Toste, F. D. *Science*, **2007**, *317*, 496–499.

[96] Davies, P. W.; Martin, N. *Org. Lett.* **2009**, *11*, 2293–2296.

Significant differences were also observed in the gold(I)-catalyzed tandem reaction of multifunctionalized cyclopentanes. The proposed mechanism involved a tandem regioselective 1,2-alkyl migration of the phenyl-substituted ketone, which depending on the silver salt used (AgOMs or $AgPF_6$), resulted in heterocyclization or oxygen-transfer (Scheme 10).[97]

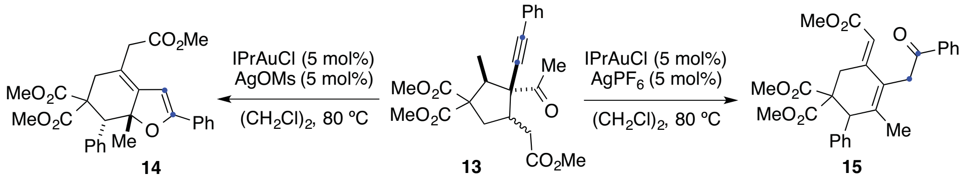

Scheme 10 Gold(I)-catalyzed transformation of multifunctionalized cyclopentane **13**.

Another important example is the cyclization of enyne-urea derivatives that underwent chemo- and regioselective 6-*endo-dig* cyclization to afford either the *O*- or *N*- cyclized products depending on the silver salt used.[98]

More recently, the group of Hashmi has designed a new generation of σ,π-dinuclear gold propyne acetylide complexes that can serve as precatalysts in various gold(I)-catalyzed transformations.[99] Again, the selectivity and the rate of the reaction depended on the counterion of the propyne catalyst. PF_6^- was found to be the most effective counterion followed by BF_4^- and NTf_2^-, among others, whereas SbF_6^- was the least efficient (Figure 1). No rationalization was provided for these results.

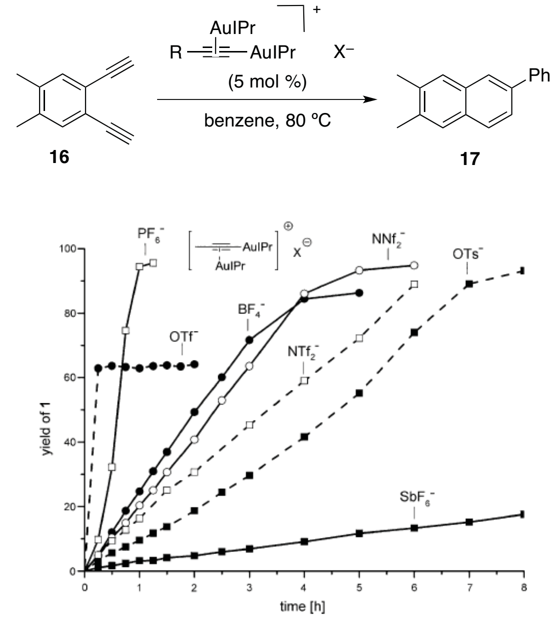

Figure 1 Yields of **17** depending on the counterion used in the σ,π-dinuclear gold propyne acetylide complex.

---

[97] Li, W.; Li, Y.; Zhang, J. *Chem.–Eur. J.* **2010**, *16*, 6447–6450.

[98] Gupta, S.; Koley, D.; Ravikumar, K.; Kundu, B. *J. Org. Chem.* **2013**, *78*, 8624–8633.

[99] Hashmi, A. S. K.; Lauterbach, T.; Nösel, P.; Vilhelmsen, M. H.; Rudolph, M.; Rominger, F. *Chem.–Eur. J.* **2013**, *19*, 1058–1065.

Although there is a lack of studies on the influence of the counterion on the reaction pathways in gold(I)-catalyzed reactions, ion pairing[100] was recognized to be responsible for part of the counterion effects by DFT calculations[101] and experiments (NMR and conductimetric techniques).[102]

Ion Pairing in Gold(I) Complexes

The group of Macchioni has been the main player on the study of ion pairing of gold(I) complexes. They determined the location of the counterion BF_4^- in two different systems $[(Ph_3P)Au(4\text{-Me-styrene})]$ and [IPrAu(4-Me-styrene)] by nOe (^{19}F–^{1}H HOESY) NMR measurements and theoretical modeling (Figure 2). The positive charge is redistributed on the ligand and the metal center whereas the preferential position of the anion is determined by the ancillary ligand. For the phosphine gold(I) complex, the anion appears to be close to the styrene whereas for NHC gold complex, it is located on the side of the carbene making the counterion effects less pronounced. A study on the effect of the carbene backbone on the ion pair structure has recently been disclosed.[103]

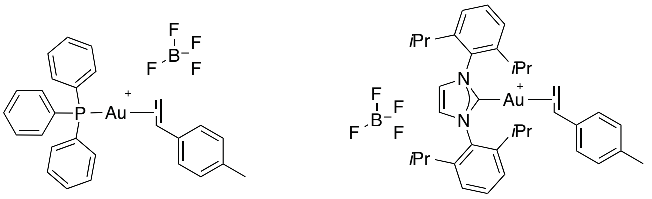

Figure 2 The most stable ion-pair configuration for $[(Ph_3P)Au(4\text{-Me-styrene})]$ and [IPrAu(4-Me-styrene)]. For clarity, the positive charge has been drawn on the metal center although it is delocalized on the substrate as well.

The study was later extended to other phosphine and phosphite ligands with 3-hexyne. As previously stated, the exact position of the anion in solution can be modulated by the donor ability of the phosphorous donor.[104]

---

[100] For a review on ion-pair concepts see: Macchioni, A. *Chem. Rev.* **2005**, *105*, 2039–2073.

[101] (a) Kovàcs, G.; Ujaque, G.; Lledàs, A. *J. Am. Chem. Soc.* **2008**, *130*, 853–864. (b) Gourlaouen, C.; Marion, N.; Nolan, S. P.; Maseras, F. *Org. Lett.* **2009**, *11*, 81–84.

[102] (a) Ciancaleoni, G.; Zuccaccia, C.; Zuccaccia, D.; Macchioni, A. *Organometallics*, **2007**, *26*, 3624–3626. (b) Zuccaccia, D.; Belpassi, L.; Tarantelli, F.; Macchioni, A. *J. Am. Chem. Soc.* **2009**, *131*, 3170–3171.

[103] Ciancaleoni, G.; Biasiolo, L.; Bistoni, G.; Macchioni, A.; Tarantelli, F.; Zuccaccia, D.; Belpassi, L. *Organometallics* **2013**, *32*, 4444–4447.

[104] Ciancaleoni, G.; Belpassi, L.; Tarantelli, F.; Zuccaccia, D.; Macchioni, A. *Dalton Trans.* **2013**, *22*, 4122–4131.

Objectives

Considering the significant effect that the counterion can have on a reaction pathway, we decided to design a new generation of catalysts containing BAr_4^{F-} as counterion and explore their effectiveness in the gold(I)-catalyzed intermolecular reactions reported by our group (Figure 3). We envisioned that the use of this bulky, non-coordinating and less basic counterion would minimize the formation of σ,π-digold(I) complexes.

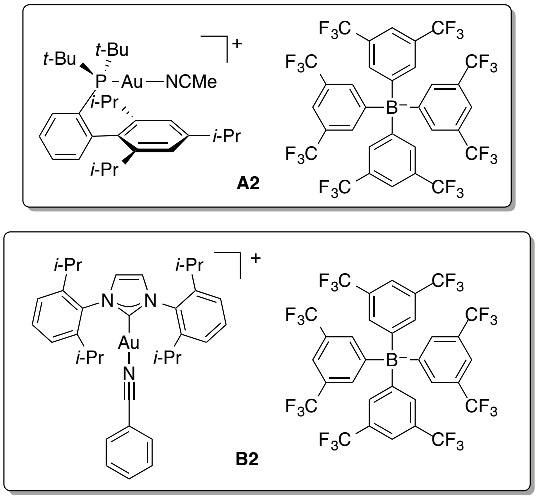

Figure 3 New generation of gold(I) complexes containing BAr_4^{F-} as counterion.

Mechanistic studies were performed to understand the influence of the counterion.

Results and Discussion

To check the effectiveness of the newly designed complexes in the reported gold(I)-catalyzed intermolecular reactions and compare them with other cationic catalyst with different counterions, we first prepared [(*t*-BuXPhos)AuNCMe]BAr_4^F (**A2**).[105] This complex was formed in quantitative yield following a procedure analogous to the synthesis of cationic gold(I) complexes (Scheme 11).[22d,53]

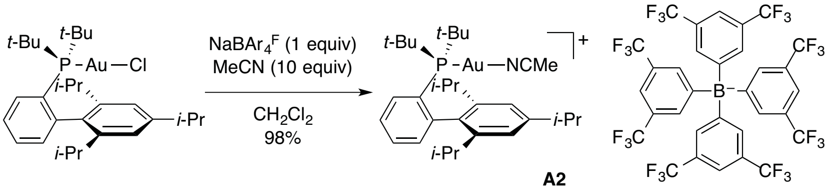

Scheme 11 Synthesis of complex [(*t*-BuXPhos)AuNCMe]BAr_4^F.

Reactivity of Complex A2 in Intermolecular Gold(I)-Catalyzed Reactions

We then sought to study the counterion effect in the [2+2] cycloaddition of phenylacetylene and α-methylstyrene, by varying the catalyst counterion. A remarkable improvement in the yield was observed by changing the optimized catalyst [(*t*-BuXPhos)AuNCMe]SbF_6 (**A1**) to the newly synthesized [(*t*-BuXPhos)AuNCMe]BAr_4^F (**A2**) (Table 1, entries 1 and 2).[106] The Au catalyst containing BF_4^- was less efficient giving the cyclobutene **3a** in 62% yield (Table 1, entry 3). Catalysts featuring PF_6^- and the coordinating NTf_2^- and OTf^- as counterions showed very poor reactivities (Table 1, entries 4, 5 and 6).

---

[105] Dr. David Leboeuf synthesized the analogue [(IPr)AuNCPh]BAr_4^F.

[106] Generating *in situ* **A2** by simple mixing [(*t*-BuXPhos)AuCl] and $NaBAr_4^F$ in the reaction media was as efficient as using [(*t*-BuXPhos)AuNCMe]BAr_4^F.

Table 1 Yield of cyclobutene **3a** formed according to the counterion in [(*t*-BuXPhos)AuNCMe]X.[a]

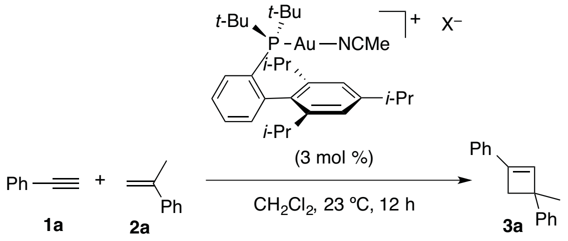

Entry	X$^-$	3a (Yield %)[b]
1	SbF$_6^-$	80
2	BAr$_4^{F-}$	95
3	BF$_4^-$	62
4	PF$_6^-$	19
5[c]	NTf$_2^-$	26
6[c]	OTf$^-$	18

[a] **1a** / **2a** = 2/1. [b] ^{1}H NMR yield determined using 1,4-diacetylbenzene as internal standard. [c] Catalysts generated *in situ* with [LAuCl] and the corresponding silver salts.

To prove whether the efficiency of catalyst **A2** could be extended to other substrates, we decided to screen different alkynes. The original methodology proceeded satisfactorily with terminal aryl alkynes containing substituents at the *meta*- and *para*- positions and with ethynylcyclopropane.[25] By using the same starting materials, catalyst **A2** proved to be more efficient improving the yields by 10 to 30% (Table 2). However, the yields were not significantly altered with the alkynes containing the electron-donating group OMe (**1c**, **1g** and **1l**). Catalyst **A2** proved to be less efficient for the formation of cyclobutene **3n** from cyclopropylethylene. Interestingly, 3-ethynylthiophene (**1m**) was found to be a competent alkyne in this [2+2] cycloaddition.

Table 2 Yield of cyclobutenes (**3**) formed according to the counterion in [(*t*-BuXPhos)AuNCMe]X.[a]

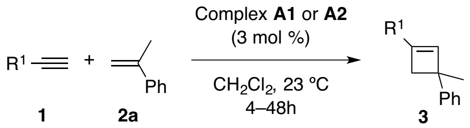

Entry	R	Catalyst	Product (Yield %)[b]
1	Ph (**1a**)	**A1**	**3a** (80)[c]
2		**A2**	**3a** (95)
3	*p*-Tol (**1b**)	**A1**	**3b** (74)[c]
4		**A2**	**3b** (86)
5	*p*-$MeOC_6H_4$ (**1c**)	**A1**	**3c** (68)[c]
6		**A2**	**3c** (64)
7	*p*-FC_6H_4 (**1d**)	**A1**	**3d** (75)[c]
8		**A2**	**3d** (84)
9	*p*-ClC_6H_4 (**1e**)	**A1**	**3e** (61)[c]
10		**A2**	**3e** (91)
11	*p*-BrC_6H_4 (**1f**)	**A1**	**3f** (74)[c]
12		**A2**	**3f** (97)
13	*m*-$MeOC_6H_4$ (**1g**)	**A1**	**3g** (80)
14		**A2**	**3g** (78)
15	*m*-Tol (**1h**)	**A1**	**3h** (78)[c]
16		**A2**	**3h** (91)
17	*m*-HOC_6H_4 (**1i**)	**A1**	**3i** (74)[c]
18		**A2**	**3i** (98)
19	*m*-FC_6H_4 (**1j**)	**A1**	**3j** (67)
20		**A2**	**3j** (77)
21	*m*-ClC_6H_4 (**1k**)	**A1**	**3k** (60)
22		**A2**	**3k** (83)
23	*o*-$MeOC_6H_4$ (**1l**)	**A1**	**3l** (30)
24		**A2**	**3l** (24)
25	3-Thienyl (**1m**)	**A1**	**3m** (84)
26		**A2**	**3m** (86)
27	Cyclopropyl (**1n**)	**A1**	**3n** (46)[c]
28		**A2**	**3n** (35)

[a] **1** / **2a** = 1:2. [b] Isolated yields. [c] Reference 25.

The reaction could not be extended to 2-ethynylpyridine. We hypothesize that the lone pair on the nitrogen coordinated too strongly to gold(I). Terminal alkyl alkynes could not be used as electrophilic counterparts. The reaction also failed with terminal alkynyl esters (which were expected to be attacked at the terminal position) (Figure 4).

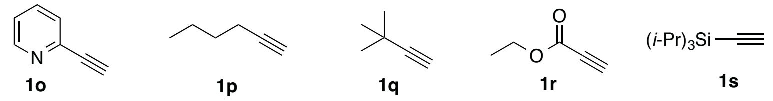

Figure 4 Terminal alkynes that failed to react in the [2+2] cycloaddition reaction.

Internal alkynes were found to be poor reaction partners as well. Only traces of cyclobutene were generated using diphenylethyne (**1t**) (< 5%) and acetylene dicarboxylate **1u** was totally unreactive. The non-symmetrical 1-phenylpropyne (**1v**) did not react either (Figure 5).

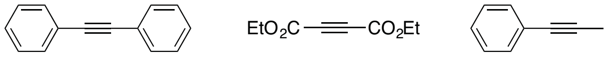

1t
(< 5% of cyclobutene)

1u

1v

Figure 5 Internal alkynes that failed to take part in the [2+2] cycloaddition reaction.

We next examined the scope of the alkene counterpart (Table 3). Again, catalyst **A2** proved to be much more efficient. Interestingly, the reaction could be extended to allyl silane **2d**, which gave the corresponding cyclobutene in good yield (Table 3, entries 5 and 6). Allyl ether **2e** and allyl silyl ether **2f** were less competent reaction partners due to their low nucleophilicity (Table 3, entries 7–10).

Table 3 Yield of cyclobutene **3** formed according to the counterion in [(*t*-BuXPhos)AuNCMe]X.[a]

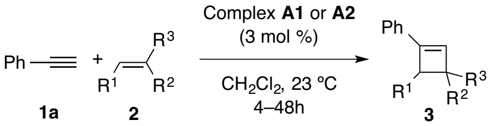

1a **2** **3**

Entry	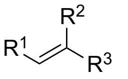	Catalyst	Product (Yield %)
1	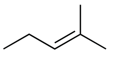 (**2b**)	**A1**	**3o** (74, 9:1 regioisomers)[b,c,d]
2		**A2**	**3o** (79)[b]
3	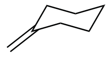 (**2c**)	**A1**	**3p** (53)[b,c]
4		**A2**	**3p** (69)[b]
5	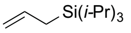 (**2d**)	**A1**	**3q** (48)[e]
6		**A2**	**3q** (71)[e]
7	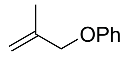 (**2e**)	**A1**	**3r** (26)[e]
8		**A2**	**3r** (31)[e]
9	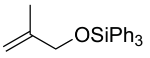 (**2f**)	**A1**	**3s** (21)[e]
10		**A2**	**3s** (31)[e]

[a] **1a** / **2** = 1:2. [b] Isolated yields. [c] Reference 25. [d] Minor regioisomer is 1,3,4,4-tetrasubstituted cyclobutenes. [e] Yield determined by ^{1}H NMR using 1,4-diacetylbenzene as internal standard.

Unfortunately, *cis*-diphenylethene (**2g**) and allyl methyl ether (**2h**) could not be used as nucleophilic counterparts. The strained molecules norbornene (**2i**) and pinene derivatives (**2j** and **2k**) did not afford any cyclobutene either. Finally, the functionalized substrate geraniol (**2l**) gave no reaction (Figure 6).

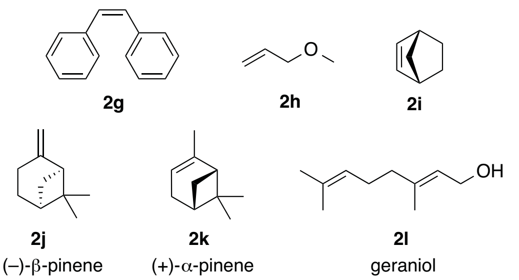

Figure 6 Alkenes that failed to partake in the [2+2] cycloaddition reaction.

We then explored if complex **A2** was more efficient in the [2+2+2] cycloaddition reaction between alkynes (**1**) and oxoalkenes (**4**) giving 8-oxabicyclo[3.2.1]oct-3-enes **5**.[73] We could indeed observe moderate improvement in this challenging cascade reaction (Table 4).

Table 4 Yield of 8-oxabicyclo[3.2.1]oct-3-enes **5** formed according to the counterion in [(*t*-BuXPhos)AuNCMe]X.[a]

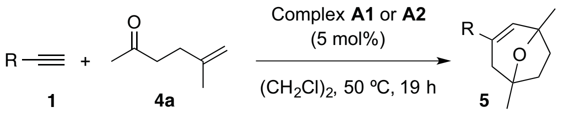

Entry	R	Catalyst	Product (Yield %)[b]
1	Ph (**1a**)	**A1**	**5a** (68)[c]
2		**A2**	**5a** (72)
3	*p*-ClC_6H_4 (**1e**)	**A1**	**5b** (51)[c]
4		**A2**	**5b** (62)
5	*m*-HOC_6H_4 (**1i**)	**A1**	**5c** (65)[c]
6		**A2**	**5c** (81)
7	*m*-Tol (**1h**)	**A1**	**5d** (70)[c]
8		**A2**	**5d** (72)

[a] **1** / **4a** = 3.5:1. [b] Isolated yields. [c] Reference 73.[107]

The use of BAr_4^{F-} as counterion was also generally beneficial in the synthesis of phenols. Yields were improved up to 31% reacting different alkynes with 2,5-dimethylfuran in the presence of complex [IPrAu(NCPh)] BAr_4^F (**B2**) (Table 5).

---

[107] Experiments performed by Carla Obradors.

Table 5 Yield of phenols **7** formed according to the counterion in [IPrAuNCPh]X. [a]

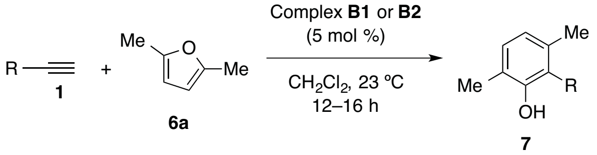

Entry	R	Catalyst	Product (Yield %)[b]
1	Ph (**1a**)	**B1**	**7a** (70)
2		**B2**	**7a** (85)
3	*p*-Tol (**1b**)	**B1**	**7b** (55)
4		**B2**	**7b** (67)
5	*o*-BrC_6H_4 (**1w**)	**B1**	**7c** (45)
6		**B2**	**7c** (76)

[a] **1** / **6a** = 1:2. [b] Isolated yields.[108]

Interestingly, the use of $NaBAr_4^F$ as a chloride abstracter for gold(I) complexes in different intramolecular reactions[109] did not improve the yields. Therefore, we decided to study how this bulky counterion affected the intermolecular gold(I)-catalyzed reactions, specifically the [2+2] cycloaddition.

Monitoring the [2+2] Cycloaddition Reaction and DFT Modeling

Monitoring this reaction by ^1H NMR using complexes containing SbF_6^-, BAr_4^{F-} and BF_4^- showed that the counterion not only affected the final yield of the cyclobutene but also the reaction rate (Figure 7). Interestingly, the cycloadduct product was generated faster and in higher yield with bulkier and softer counterions. Thus, BAr_4^{F-} was the most efficient anion, followed by SbF_6^- and BF_4^-.

---

[108] Experiments performed by Núria Huguet and Dr. David Leboeuf.

[109] In addition to intramolecular gold(I)-catalyzed cycloadditions, we also included different cycloisomerizations of 1,6-enynes.

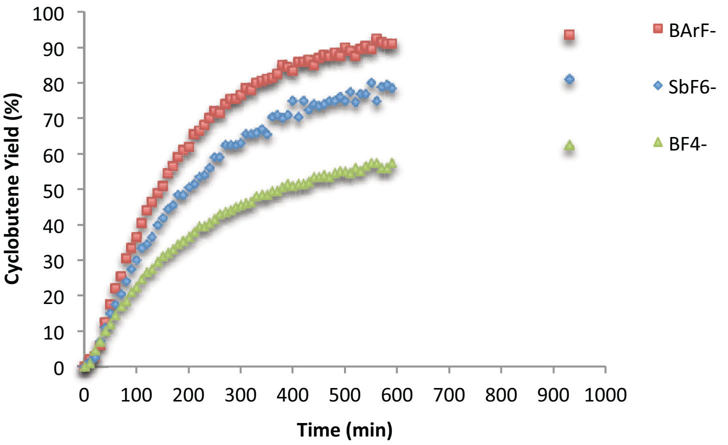

Figure 7 Kinetics of the [2+2] cycloaddition between phenylacetylene and α-methylstyrene with [(*t*-BuXPhos)AuNCMe]X (X = BAr_4^{F-}, SbF_6^-, BF_4^-).

To explain the results obtained we then examined if the formation of ion pairs was feasible. Thus, we studied the anion–cation interaction combining nOe NMR measurements and theoretical modeling following the methodology reported by the group of Macchioni.[103,110] The ^1H, ^{19}F, ^{31}P and HOESY NMRs at 23 ºC and –60 ºC of complexes **A1** or **A2** alone and with phenylacetylene and α-methylstyrene were first examined. Despite our efforts, no correlation was observed between the fluorine atoms of the counterion and any of the substrates. Our efforts to calculate the radius of the ionic complexes using DOESY experiments were also unsuccesful. Then, we modeled the behavior of the complexes [(*t*-BuXPhos)Au(η^2-phenylacetylene)]X (X = BF_4^-, SbF_6^- and BAr_4^{F-}) in solution using DFT calculations [M06, 6-31G(d) (C, H, P, B, F) and SDD (Au, Sb), CH_2Cl_2].[111]

We analyzed the charge distribution by determining the electron density from total SCF density mapped with ESP (ρ = 0.03 e/Å^3) (Figure 8). Interestingly, the positive charge was significantly redistributed on the ligands and not concentrated only in the metal center. By determining the Mulliken atomic charges, we could observe that the acidity of terminal alkyne changed moderately with the bulkiness of the counterion. The electron density of the proton decreased with the anion size; 0.250 for BF_4^-, 0.243 for SbF_6^- and 0.237 for BAr_4^{F-}. Furthermore, there is a considerable steric congestion around the substrate with BAr_4^{F-}, which presumably hampers the deprotonation of the alkyne and therefore, the formation of σ,π-digold(I) alkyne.

---

[110] Macchioni, A. *Eur. J. Inorg. Chem.* **2003**, *19*, 195–205.

[111] DFT calculations performed by Carla Obradors.

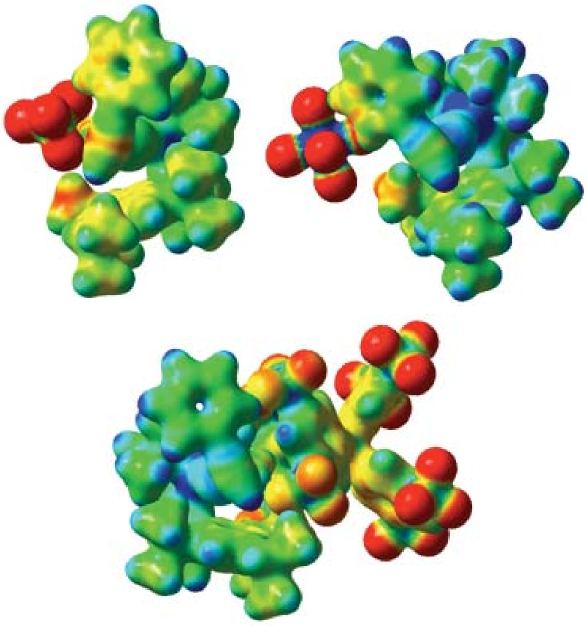

Figure 8 Views of the Coulomb potential of [(η^2-phenylacetylene)Au(I)]X (X = BF_4^-, SbF_6^- and BAr_4^{F-}) mapped in an electronic isodensity surface ρ = 0.03 e/Å^3.

Mechanistic Studies

The mechanism proposed for the gold(I)-catalyzed [2+2] cycloaddition reaction between alkynes and alkenes was based on previous theoretical work (Scheme 11).[23b,d,73] Accordingly, it proceeded through an initial attack of the alkene onto [(*t*-BuXPhosAu(η^2-phenylacetylene)]$^+$. This nucleophilic attack was proposed to be the rate-limiting step of the reaction. The cyclopropyl gold(I) carbene **II** generated subsequently underwent ring expansion, giving rise to the benzylic carbocation **III** that after demetalation, afforded cyclobutenes. The active species were regenerated after associative ligand exchange between [(η^2-cyclobutene)gold(I)]$^+$ species and phenylacetylene.

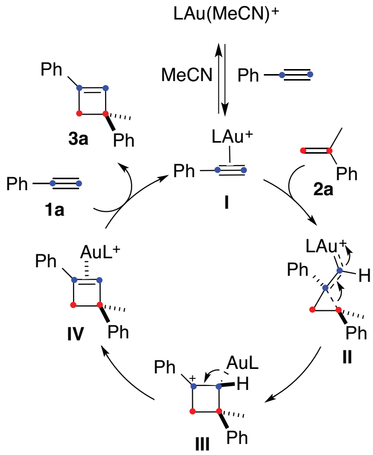

Scheme 11 Proposed mechanism for the [2+2] cycloaddition between alkynes and alkenes.

Order of Reagents

To study experimentally this reaction, we calculated the order of the reagents in the rate equation of the reaction by using the method of initial rates. The initial rate in a given reaction is the instantaneous rate determined right after the reaction begins, and before the initial concentration of reagents changes significantly. In a given reaction, the general rate equation is:

$$A + B \rightarrow C$$
$$rate = k \cdot [A]^a \cdot [B]^b$$

a and b are the order of reagents

Equation 1.

The method of initial rates allows determining the orders of the reagents by running the reaction multiple times under certain conditions and measuring the initial rate of the reaction in each case. In each experiment, all the variables remain constant from one run to the next except for the concentration of one reactant. Thus, the order a reagent can be determined by comparing the reaction rates as the concentration of this particular reagent varies.

We screened different methods (IR, HPLC and GC-MS) to perform this kinetic study. However, since none of them proved to be reliable enough, we decided to study the reaction by ^{1}H NMR varying the quantities of phenylacetylene, α-methylstyrene and finally gold(I) complex **A2** (Scheme 12). We considered that the concentration of reagents had not changed significantly until 10–15% of cyclobutene was formed.

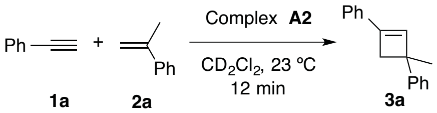

Scheme 12 Intermolecular [2+2] cycloaddition reaction performed.

Thus, we performed the intermolecular gold(I)-catalyzed [2+2] cycloaddition reaction using 0.5 mmol of α-methylstyrene and 7.2 μmol of complex **A2** and incrementing the amounts of phenylacetylene from 0.05 to 0.50 mmol. The amount of cyclobutene generated increased by increasing the amount of phenylacetylene (Figure 9).

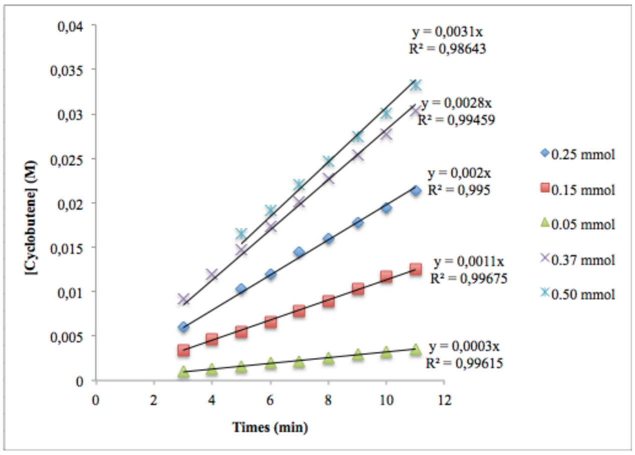

Figure 9 ^{1}H NMR monitoring of the [2+2] cycloaddition reaction changing the amounts of phenylacetylene (**1a**).

Monitoring of the reaction maintaining the amounts of phenylacetylene (0.25 mmol) and complex **A2** (7.2 μmol) constant whilst varying the quantities of α-methylstyrene from 0.25 to 1.25 mmol gave a different behavior. The formation of cyclobutenes when vaying the amount of alkene utilized did not increase (Figure 10).

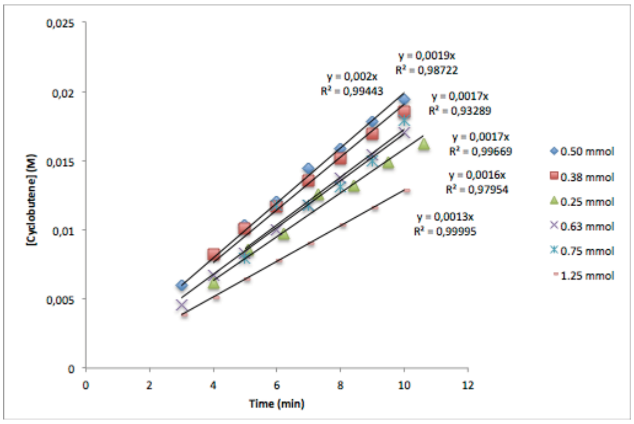

Figure 10 ^{1}H NMR monitoring of the [2+2] cycloaddition reaction varying the amounts of α-methylstyrene (**2a**).

The trend observed after monitoring the reaction when changing the amount of catalyst was analogous to the one depicted in Figure 9. The amount of cyclobutene generated was higher when 13 μmol of catalyst were used with 0.25 mmol of phenylacetylene and 0.50 mmol of α-methylstyrene. Using 2.5 μmol of complex under the same conditions afforded less product (Figure 11).

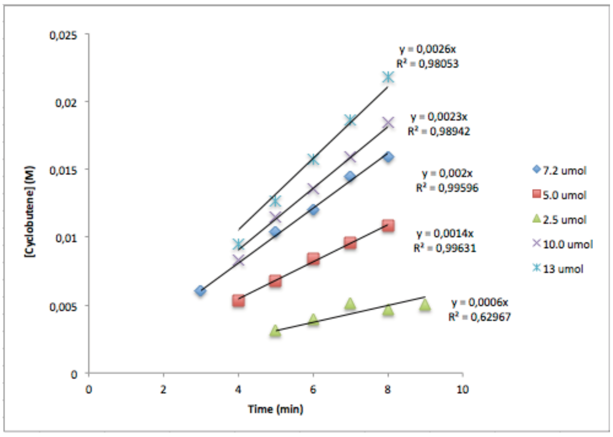

Figure 11 ^{1}H NMR monitoring of the [2+2] cycloaddition reaction changing the amounts of catalyst **A2**.

Finally, the initial rates were plotted against the initial concentration on a logarithmic scale according to the method of initial rates (Figure 12). The positive slope for phenylacetylene (**1a**) and the catalyst **A2** was an evidence of first order. Remarkably, the "horizontal" line (close to zero slope) observed for α-methylstyrene indicated 0 order for the alkene. Hence, the more reasonable rate determining step would be the generation of the active species [LAu(η^2-phenylacetylene)]$^+$ (**I**).

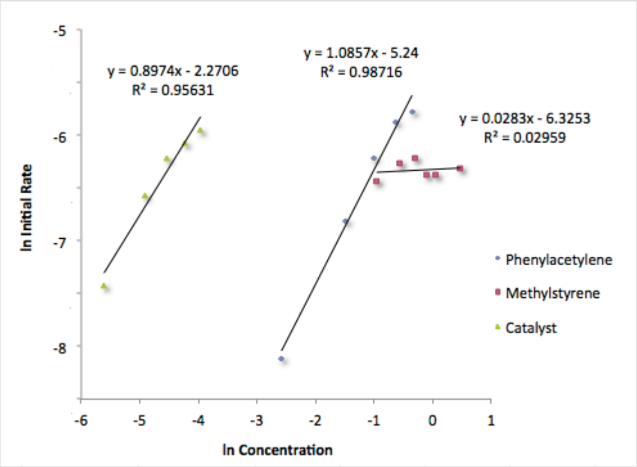

Figure 12 Order of the reagents in the [2+2] cycloaddition between phenylacetylene (**1a**) and α-methylstyrene (**2a**) with complex **A2**.

We hypothesized that the orders of reagents do not change when other counterions are used in the reaction. Thus, to get further insight into the counterion effect, we decided to examine the species formed in the reaction mixture.

Species Formed in the Reaction Mixture: Counterion Differences

In the [2+2+2] cycloaddition of alkynes with oxoalkenes[73] we observed that the formation of [LAu(η^2-phenylacetylene)]$^+$ species was more complex than expected due to the competition with the formation of σ,π-digold(I) alkynes complexes. In this reaction, σ,π-digold(I) alkyne species are known to be dead-ends of the catalytic cycle. In order to probe whether these species were also formed in the [2+2] cycloaddition reaction, we carefully examined the ^{31}P NMR at the very beginning of the reaction using the three different catalysts [LAu(NCMe)]X (X = BAr_4^{F-}, SbF_6^-, BF_4^-). Interestingly, two different species could be observed in all the spectra, which were later determined to be [LAu(η^2-α-methylstyrene)]$^+$ (**C**) and σ,π-digold(I) alkyne complex **D** (Figure 13).

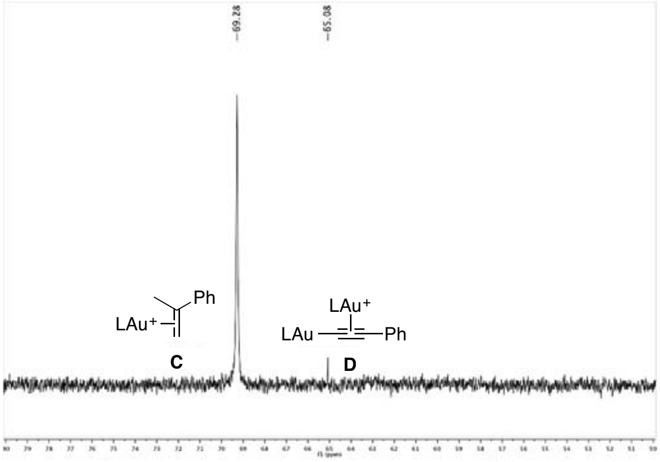

Figure 13 Initial ^{31}P NMR spectrum of the intermolecular gold(I)-catalyzed [2+2] cycloaddition of phenylacetylene and α-methylstyrene with complex **A2** in CD_2Cl_2 at 23 ºC (L = *t*-BuXPhos).

Remarkably, the ratio between these two species increased following the same trend observed for the effectiveness of the counterion: 115 for BAr_4^{F-}, 30 for SbF_6^- and 4 for BF_4^-. To assess the role of these species in the reaction medium, we decided to examine their reactivity in the [2+2] cycloaddition reaction. Thus, following the reported procedures, we synthetized both complexes (containing BAr_4^{F-} as counterion).[73,86] No reaction took place at all when stoichiometric amounts of **D** and α-methylstyrene (**2a**) were used as starting materials with or without catalyst **A2** (Scheme 13).

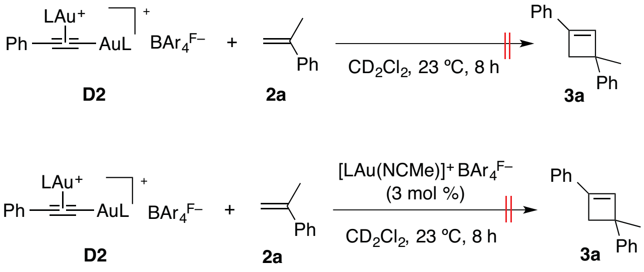

Scheme 13 Unreactivity of **D2** as substrate in the [2+2] cycloaddition reaction (L = *t*-BuXPhos).

The reaction proceeded very poorly using 1.5 mol % of of digold complex **D2**, indicating again that these species are not catalytically active. The same result was obtained for complex **D1** containing SbF_6^- as counterion (Scheme 14).

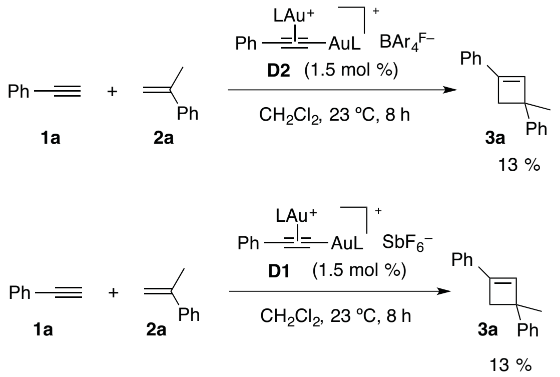

Scheme 14 [2+2] Cycloaddtion reaction between phenylacetylene (**1a**) and α-methylstyrene (**2a**) using **D** as catalyst (L = *t*-BuXPhos).

The reaction only was effective using [LAu(η^2-α-methylstyrene)]BAr$_4^F$ (**C2**) as the cycloaddition partner with phenylacetylene. In this case, cyclobutene **3a** was isolated in 72% yield (Scheme 15). These results led us to consider whether these were the actual catalytically active species. Although it was less likely, the mechanism could start with the activation of α-methylstyrene with a cationic gold(I) complex (**C**), that could be attacked by phenylacetylene. To exclude this mechanism, we performed the gold(I)-catalyzed reaction of α-methylstyrene and different nucleophiles. No reaction took place using carbon nucleophiles, specifically allyltrimethylsilane, indole, 1,3,5-trimethoxybenzene or 1,3-diphenylpropane-1,3-dione that had been used as nucleophiles in reactions with 1,5- or 1,6-enynes.[53b] Thus, we concluded that [LAu(η^2-α-methylstyrene)]BAr$_4^F$ (**C2**) acts as a reservoir of cationic gold(I) species (resting state), whilst σ,π-digold(I) alkyne complex is a dead-end of the catalytic cycle.

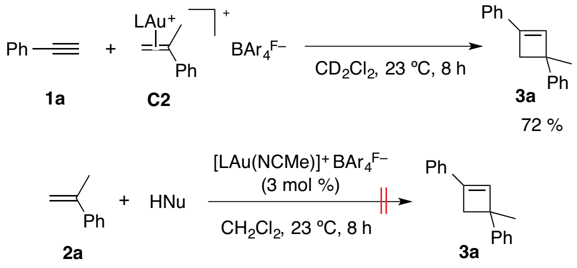

Scheme 15 [2+2] Cycloaddition reaction between stoichiometric **C2** and phenylacetylene and reaction between α-methylstyrene (**2a**) and different nucleophiles (L = *t*-BuXPhos).

We postulated that the same outcome would have been observed using [LAu(η^2-α-methylstyrene)]X (**C**) and σ,π-digold(I) alkyne complexes with SbF_6^- and BF_4^- as counterions. Thus, we could explain the efficiencies of the reaction with [LAu(NCMe)]X featuring the different counterions. The ratio between reservoir species [LAu(η^2-α-methylstyrene)]X (**C**) / σ,π-digold(I) alkyne (**D**) was considerably higher for BAr$_4^{F-}$ than for the less bulky SbF_6^- and BF_4^-.

To get further mechanistic insight, we then decided to calculate the equilibrium constants K_{eq} for the formation of [LAu(η^2-α-methylstyrene)] and σ,π-digold(I) alkyne containing BAr$_4^{F-}$ and SbF_6^-.

Equilibrium Constants

The equilibrium constants between catalyst **A1** and **A2** and their related LAu(η^2-α-methylstyrene)] (**C1** and **C2**) and σ,π-digold(I) alkyne (**D1** and **D2**) were determined using the van't Hoff equation (Equation 2).

$$\ln(K_{eq}) = -\frac{\Delta H^{\ddagger}}{\mathrm{RT}} + \frac{\Delta S^{\ddagger}}{\mathrm{R}}$$

Equation 2.

0.5 M solutions containing different ratios of **A**:**2a** (1:2, 1:1, 2:1, 3.5:1 and 5:1) in CD_2Cl_2 (0.5 mL) were analyzed immediately at temperatures ranging from –10 ºC to 35 ºC (15 ºC increments) by ^{1}H- and ^{31}P NMR.

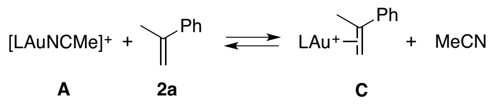

$$K_{eq} = \frac{[\boldsymbol{C}] \cdot [MeCN]}{[\boldsymbol{A}] \cdot [\boldsymbol{2a}]} = \frac{[\boldsymbol{C}]^2}{([\boldsymbol{A}]_O - [\boldsymbol{C}]) \cdot ([\boldsymbol{2a}]_O - [\boldsymbol{C}])}$$

$$\text{Integrals ratio} = \frac{[\boldsymbol{C}]}{([\boldsymbol{A}]_O - [\boldsymbol{C}])}$$

Equation 3.

Plotting the acquired datapoints, we obtained the correlation between the equilibrium constant of complexes **A1** or **A2** and [LAu(η^2-α-methylstyrene)] (**C**) and the temperature (Figure 14 and Figure 15).

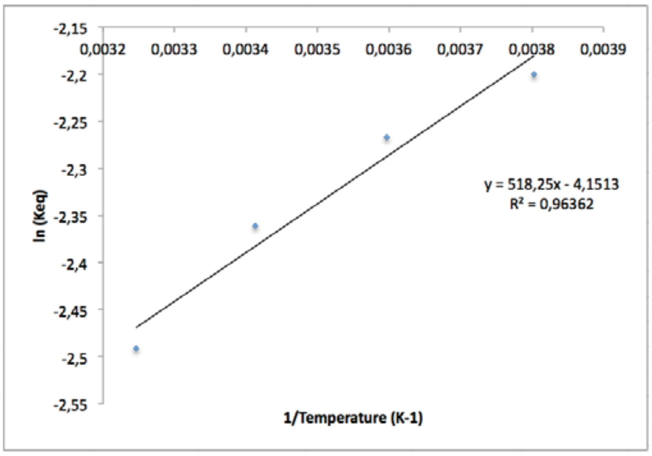

Figure 14 van't Hoff plot of **A1** and **C1** against temperature.

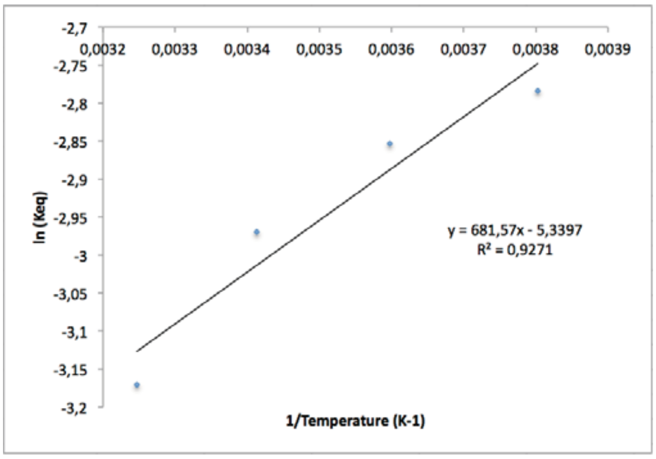

Figure 15 van't Hoff plot of **A2** and **C2** against the temperature.

In both cases, the equilibrium showed a positive slope, which corresponds to an exothermic process. An analogous experiment was performed to study the equilibrium between catalyst **A2** and σ,π-digold(I) alkyne. In this case, the equilibrium proved more complicated since more species had to be considered. The study with catalyst **A1** had already been performed for the [2+2+2] cycloaddition reaction.[73]

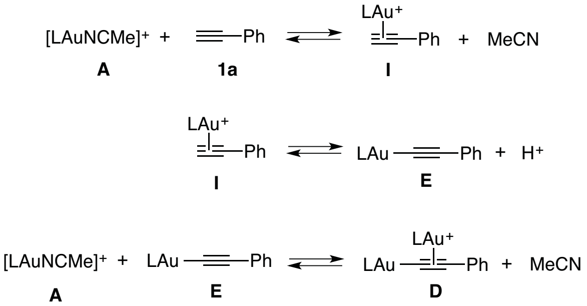

$$K_{eq} = \frac{[\boldsymbol{D}]\cdot[H^{+}]\cdot[MeCN]^{2}}{[\boldsymbol{A}]^{2}\cdot[\boldsymbol{1a}]} = \frac{4\cdot[\boldsymbol{D}]^{4}}{([\boldsymbol{A}]_{O}-2\cdot[\boldsymbol{D}])^{2}\cdot([\boldsymbol{1a}]-[\boldsymbol{D}])}$$

$$Integrals\ ratio = \frac{[\boldsymbol{D}]}{([\boldsymbol{A}]_{0}-2\cdot[\boldsymbol{D}])}$$

Equation 4.

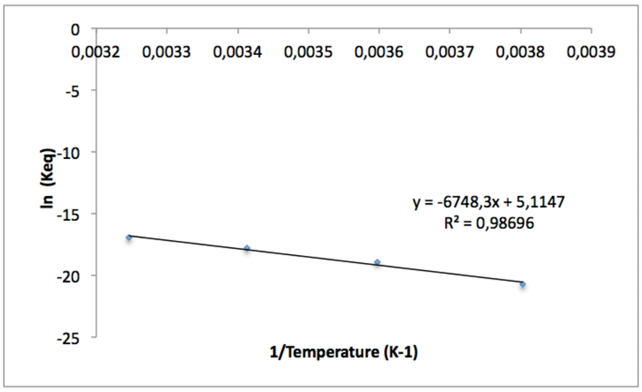

Figure 16 van’t Hoff plot of **A2** and the alkyne complex with the temperature.

In contrast with the previous equilibrium, the generation of σ,π-digold(I) complexes (**D**) was found to be an endothermic process (negative slope, Figure 16). Finally, we calculated the K_{eq} at 23 ºC, the temperature at which the reaction was performed. The equilibrium constants obtained were in accordance with the ratio of [LAu(η^2-α-methylstyrene)]X (**C**) / σ,π-digold(I) alkyne complex **D** observed at the very beginning of the reaction. Thus, **A2** binded more strongly to the alkene than **A1**, whereas the formation of σ,π-digold(I) alkyne complex was more favorable for **A1** (Scheme 16). Based on these results, we postulated that the concentration of the catalytically active species for BAr_4^{F-} as counterion was higher than that for SbF_6^-.

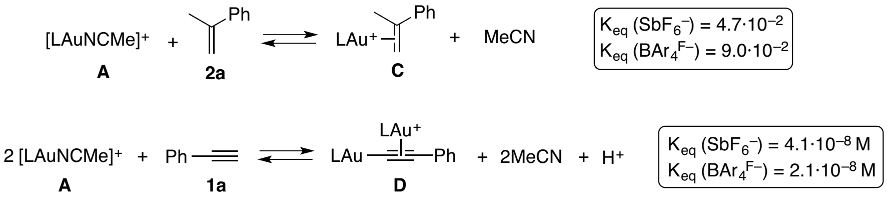

Scheme 16 Determination of the equilibrium constants from **A** to **C** and **D** at 23 ºC.

We reasoned that the acid released in the case of the bulky anion BAr_4^{F-} was less stable than $HSbF_6$ and therefore, the K_{eq} was smaller. In conclusion, we unambiguously proved the stability of the σ,π-digold(I) alkyne complex and its formation during the course of the reaction.

Formation of σ,π-Digold(I) Complex

To evaluate the formation of σ,π-digold(I) complexes, we studied the evolution of the ^{31}P NMR of the mixture of **A1** or **A2** with phenylacetylene (10:1 ratio respectively) from –60 ºC to 20–25 ºC. [LAu(η^2-phenylacetylene)]SbF_6 (**I1**) had previously been characterized at –60 ºC through the correlation observed in the ^{1}H-^{31}P HMBC spectrum at –60 ºC between the terminal proton of the phenylacetylene (doublet) and the phosphorous atom of the ligand.[73]

For **A1**, the monogold species **I** are clearly observed at –60 ºC as well as σ,π-digold **D1** and **A1**. However, only traces of the active species can be observed at temperatures higher than –40 ºC (Figure 17). On the contrary, when **A2** is utilized the only species observed at

–60 ºC are [LAu(η^2-phenylacetylene)]BAr_4^F (**I2**) and **A2**. In this case, the monogold species **I2** is present at higher temperatures, up to 0 ºC, which is also the temperature at which σ,π-digold **D2** is observed (see experimental section for further information) (Figure 18).

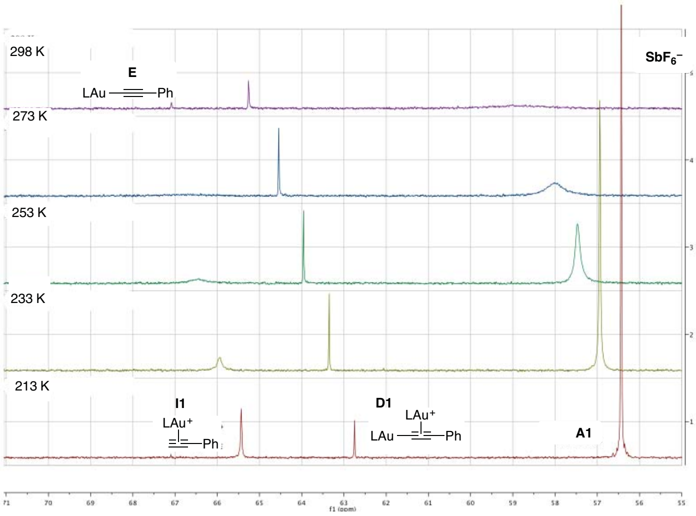

Figure 17 ^{31}P NMR spectrum of phenylacetylene and complex **A1** from –60 ºC to 25 ºC.

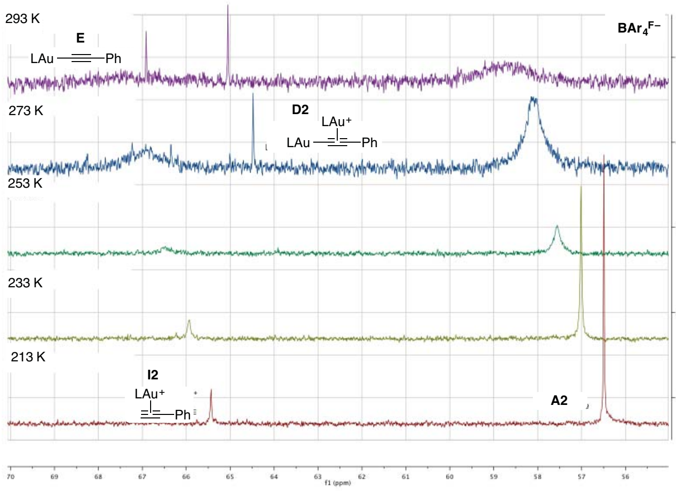

Figure 18 ^{31}P NMR spectrum of phenylacetylene and complex **A2** from –60 ºC to 20 ºC.

These results proved again the difference of stability of the σ,π-digold complexes formed depending on the counterion utilized (Scheme 17). Therefore, in the case of BAr_4^{F-}, the formation of the unreactive dinuclear species is less favored than for SbF_6^-, explaining the higher efficiency of complexes featuring this counterion in various transformations.

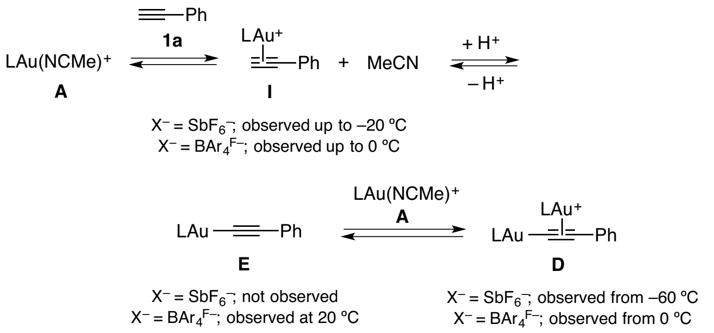
Ph
1a
LAu(NCMe)+
A
LAu+
Ph
I
+ MeCN
+ H+
– H+
X− = SbF6−; observed up to –20 °C
X− = BAr4F−; observed up to 0 °C
LAu(NCMe)+
A
LAu
Ph
E
LAu+
LAu
Ph
D
X− = SbF6−; not observed
X− = BAr4F−; observed at 20 °C
X− = SbF6−; observed from –60 °C
X− = BAr4F−; observed from 0 °C

Scheme 17 Gold(I) species formed between phenylacetylene and **A1** or **A2** from –60 ºC to 20 ºC.

Finally, in order to account for all the observations gathered in study, it was necessary to propose a more complex mechanistic picture than the one previously put forward (Scheme 18). We postulated an initial rate-determining step involving the formation of (η^2-phenylacetylene)gold(I) complex **I** through the ligand exchange between complex **C** and phenylacetylene (**1a**). These electrophilic species undergo nucleophilic attack by α-methylstyrene (**2a**) generating cyclopropylgold(I) carbene **II**. Then, ring expansion occurs forming benzylic carbocation intermediate **III**, that upon demetalation gives (η^2-cyclobutene)gold(I) complex **IV**. A final associative ligand exchange between **IV** and α-methylstyrene (**2a**) closes the catalytic cycle. (η^2-Phenylacetylene)gold(I) complex (**I**) has been shown to be in equilibrium with unreactive σ,π-digold(I) alkyne complex **D**, which is a dead-end outside the catalytic cycle. The generation of these species is more difficult when the complex initially used contains BAr_4^{F-} as counterion.

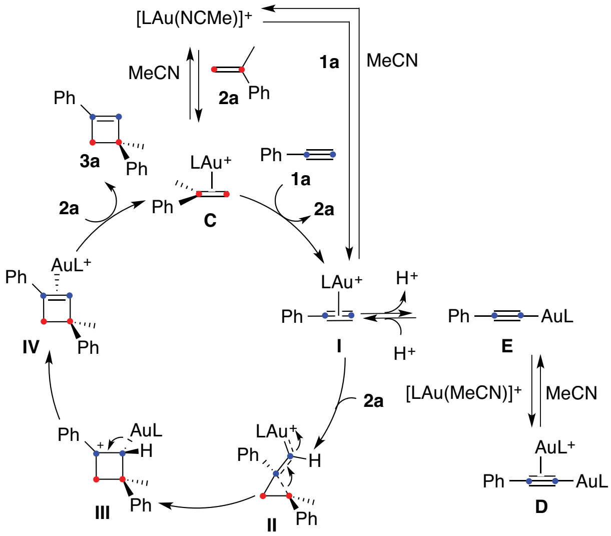
[LAu(NCMe)]+
MeCN
2a
Ph
1a
MeCN
Ph
3a
Ph
LAu+
Ph
C
Ph
1a
2a
2a
Ph
AuL+
IV
Ph
LAu+
H+
Ph
I
H+
Ph
AuL
E
2a
[LAu(MeCN)]+
MeCN
AuL+
Ph
AuL
D
Ph
AuL
H
III
Ph
LAu+
Ph
H
II
Ph

Scheme 18 Proposed revised mechanism for the [2+2] cycloaddition reaction between phenylacetylene and α-methylstyrene.

To exclude the occurrence of any other possible pathways, we performed several additional control experiments (Scheme 19). (σ-Phenylacetylene)gold(I) complex **E** proved to be an unreactive partner when it was treated with α-methylstyrene (**2a**). No traces of cyclobutene were observed either when 3 mol % of **A2** were added to the reaction mixture. Another evidence for complex **E** to be out of the catalytic cycle was its inability to mediate the reaction between phenylacetylene and α-methylstyrene.

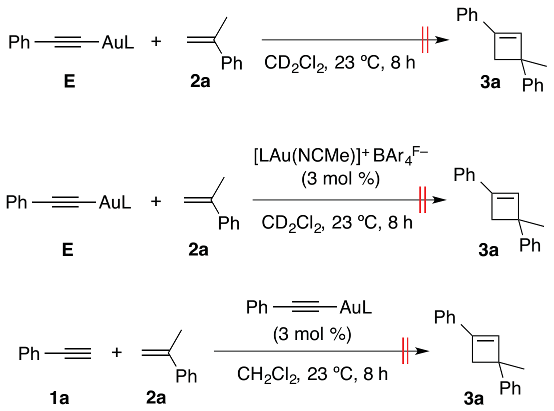
Ph—≡—AuL
+
Ph
E
2a
CD_2Cl_2, 23 °C, 8 h
Ph
Ph
3a
$[LAu(NCMe)]^+ BAr_4^{F-}$
(3 mol %)
Ph—≡—AuL
(3 mol %)
CH_2Cl_2, 23 °C, 8 h
Ph—≡
1a

Scheme 19 Unreactivity of **E** as substrate or catalyst in the [2+2] cycloaddition.

Importantly, the lack of reactivity of both complexes (σ-phenylacetylene)gold(I) **E** and (σ,π-phenylacetylene)gold(I) **D** could be restored upon addition of $HSbF_6 \cdot 6H_2O$ (Scheme 20). The presence of the acid shifted the equilibrium of (σ,π-phenylacetylene)gold(I) **D** towards (π-phenylacetylene)gold(I) **I**, by cleaving the Au–C bond. Thus, cyclobutene **3a** could be obtained in 75–79% yield.

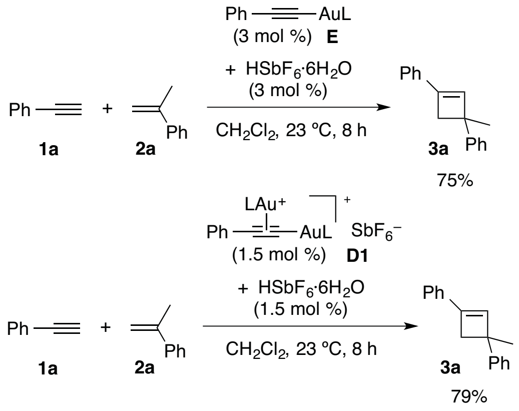
Ph—≡—AuL
(3 mol %) E
+ $HSbF_6 \cdot 6H_2O$
(3 mol %)
Ph—≡
+
Ph
1a
2a
CH_2Cl_2, 23 °C, 8 h
Ph
Ph
3a
75%
LAu^+
Ph—≡—AuL
SbF_6^-
(1.5 mol %) D1
+ $HSbF_6 \cdot 6H_2O$
(1.5 mol %)
79%

Scheme 20 Catalytically activity recovery from **D1** and **E** by addition of $HSbF_6$.

Conclusions

A new generation of catalysts containing BAr_4^{F-} [BAr_4^{F-} = tetrakis [3,5-bis(trifluoromethyl) phenylborate] as counterion have been developed (Figure 19). These complexes have proven to be more efficient in several gold(I)-catalyzed transformations since yields are improved up to 30% in the reactions of alkynes and alkenes, oxoalkenes and furans.

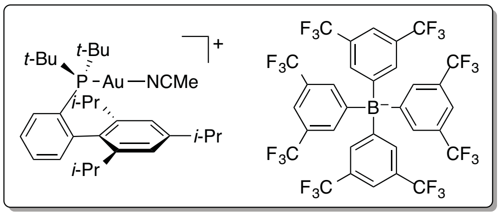

Figure 19 Complex [*t*-BuXPhosAu(NCMe)]BAr_4^F.

An extensive mechanistic study on the [2+2] cycloaddition reaction between phenylacetylene and α-methylstyrene has been performed. By calculating the orders of the reagents, we have been able to determine the rate-determining step of the reaction, which has been found to be ligand exchange between complex **C** and phenylacetylene to form (η^2-phenylacetylene)gold(I) complex **I**. The mechanism has been revised and a clear and well-supported mechanistic picture has been proposed.

(η^2-Phenylacetylene)gold(I) species **I** are very unstable and are in equilibrium with the unreactive (σ,π-phenylacetylene)gold(I) complexes **D**. However, the formation of these species with the bulky counterion BAr_4^{F-} is less favored than with its analogue SbF_6^- as observed when calculating the K_{eq} constant between [*t*-BuXPhosAu(NCMe)]X (X = BAr_4^{F-} and SbF_6^-) and phenylacetylene These results have been supported by monitoring of the reaction of phenylacetylene and [*t*-BuXPhosAu(NCMe)]X (X = BAr_4^{F-} and SbF_6^-) by ^{31}P NMR at low temperature, and explain the higher efficiency of the catalysts featuring the bulky and less basic counterion BAr_4^{F-}.

Experimental part

General Information

The general information is provided in the experimental part of the first chapter.

Synthesis of Gold(I) Complexes

(Acetonitrile)[(2′,4′,6′-triisopropyl-1,1′-biphenyl-2-yl)di-*tert*-butylphosphine]gold(I) tetrakis[3,5-bis(trifluoromethyl)phenyl] borate (A2)

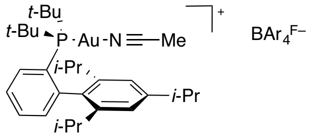

Chloro[(2’,4’,6’-triisopropyl-1,1’-biphenyl-2-yl)di-*tert*-butylphosphine]gold(I) (100.0 mg, 0.152 mmol) and acetonitrile (9.5 μL, 0.183 mmol) were dissolved in CH_2Cl_2 (6.6 mL). Then, sodium tetrakis[3,5-bis(trifluoromethyl) phenyl] borate (135.0 mg, 0.152 mmol) was added and the reaction mixture was stirred at 23 ºC for 30 min. The crude was filtered through celite and concentrated. Finally, it was filtered through Teflon 0.22, washed with CH_2Cl_2 and the solvent was removed to afford a white powder.

224 mg of **A2** (0.147 mmol) were obtained in 97%.

^{1}H NMR (400 MHz, CD_2Cl_2) δ_H 7.92 – 7.85 (m, 1H), 7.75 – 7.70 (m, 8H), 7.66 – 7.58 (m, 2H), 7.56 (s, 4H), 7.32 (m, 1H), 7.16 (s, 2H), 2.94 (p, *J* = 6.9 Hz, 1H), 2.33 (dt, *J* = 13.4, 6.7 Hz, 2H), 2.25 (broad s, 3H), 1.41 (d, *J* = 16.3 Hz, 18H), 1.32 (d, *J* = 6.9 Hz, 6H), 1.25 (d, *J* = 6.8 Hz, 6H), 0.93 (d, *J* = 6.6 Hz, 6H). **^{13}C NMR** (101 MHz, CD_2Cl_2) δ_C 162.3 (q, *J* (^{13}C-^{11}B) = 50.1 Hz), 150.4, 148.0, 147.6 (d, *J* (^{13}C-^{31}P) = 12.8 Hz), 136.7 (d, *J* (^{13}C-^{31}P) = 6.1 Hz), 135.5, 135.4, 134.7 (d, *J* (^{13}C-^{31}P) = 4.6 Hz), 132.1 (d, *J* (^{13}C-^{31}P) = 2.6 Hz), 129.5 (q, *J* (^{13}C-^{19}F) = 28.6 Hz), 128.1 (d, *J* (^{13}C-^{31}P) = 8.1 Hz), 126.0 (d, *J* (^{13}C-^{31}P) = 50.2 Hz), 125.2 (q, *J* (^{13}C-^{19}F) = 272.3 Hz), 122.5, 118.1 (p, *J* (^{13}C-^{19}F) = 4.0 Hz), 39.2 (d, *J* (^{13}C-^{31}P) = 29.3 Hz), 34.6, 31.5 (d, *J* (^{13}C-^{31}P) = 4.3 Hz), 31.5, 26.3, 24.5, 23.4, 3.3 and one carbon is missing probably because of overlapping. **^{31}P {^{1}H} NMR** (162 MHz, CD_2Cl_2) δ_P 58.7. **^{19}F {^{1}H} NMR** (376 MHz, CD_2Cl_2) δ_F –62.97. **^{11}B{^{1}H} NMR** (128 MHz, CD_2Cl_2) δ_B –6.7. **HRMS** (MALDI) calculated for $[C_{31}H_{48}AuNP]^+$ (M^+– $C_{32}H_{12}BF_{24}$): 662.3184, found *m/z* 662.3175. **Elemental Analysis** calculated for $C_{63}H_{60}AuBF_{24}NP$: C, 49.59; H, 3.97; N, 0.92; found: C, 49.56; H, 3.94; N, 0.97.

(Acetonitrile)[(2′,4′,6′-triisopropyl-1,1′-biphenyl-2-yl)di-*tert*-butylphosphine]gold(I) tetrafluoroborate

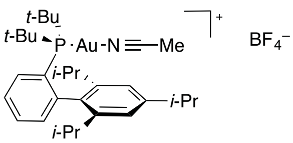

Chloro[(2’,4’,6’-triisopropyl-1,1’-biphenyl-2-yl)di-*tert*-butylphosphine]gold(I) (100.0 mg, 0.152 mmol) and acetonitrile (9.5 μL, 0.183 mmol) were dissolved in CH_2Cl_2 (6.6 mL). Then, silver tetrafluoroborate (29.6 mg, 0.152 mmol) was added and the reaction mixture was stirred at 23 ºC for 20 min. The crude was filtered through celite and concentrated. Finally, it was filtered through Teflon 0.22, washed with CH_2Cl_2 and the solvent was removed to afford a white powder.

114 mg of (acetonitrile)[(2′,4′,6′-triisopropyl-1,1′-biphenyl-2-yl)di-*tert*-butylphosphine]gold(I) tetrafluoroborate (0.152 mmol) were isolated in 100%.

^{1}H NMR (400 MHz, CD_2Cl_2) δ_H 7.90 (td, J = 8.9, 8.1, 2.3 Hz, 1H), 7.69 – 7.54 (m, 2H), 7.32 (ddd, J = 6.9, 4.9, 2.5 Hz, 1H), 7.17 (s, 2H), 2.97 (hept, J = 6.8 Hz, 1H), 2.39 (s, 3H), 2.33 (hept, J = 6.7 Hz, 2H), 1.43 (d, J = 16.3 Hz, 18H), 1.33 (d, J = 6.9 Hz, 6H), 1.27 (d, J = 6.8 Hz, 6H), 0.93 (d, J = 6.6 Hz, 6H). **^{13}C NMR** (101 MHz, CD_2Cl_2) δ_C 150.5, 147.8, 147.7 (d, J (^{13}C-^{31}P) = 12.7 Hz), 136.6 (d, J (^{13}C-^{31}P) = 6.0 Hz), 135.4 (d, J (^{13}C-^{31}P) = 8.1 Hz), 134.8 (d, J (^{13}C-^{31}P) = 4.3 Hz), 132.0, 128.0 (d, J (^{13}C-^{31}P) = 7.8 Hz), 126.3 (d, J (^{13}C-^{31}P) = 47.8 Hz), 122.5, 120.0 (d, J (^{13}C-^{31}P) = 4.4 Hz), 39.2 (d, J (^{13}C-^{31}P) = 28.2 Hz), 34.5, 31.6 (d, J (^{13}C-^{31}P) = 5.8 Hz), 31.5, 26.4, 24.5, 23.4, 3.3. **^{31}P {^{1}H} NMR** (162 MHz, CD_2Cl_2) δ_P 58.6. **^{19}F NMR** (376 MHz, CD_2Cl_2) δ_F –153.1. **^{11}B {^{1}H} NMR** (128 MHz, CD_2Cl_2) δ_B –1.23. **HRMS** (MALDI) calculated for $[C_{31}H_{48}AuNP]^+$ (M^+– BF_4): 662.3184, found *m/z* 662.3180. **Elemental Analysis** calculated for $C_{63}H_{60}AuBF_{24}NP$: C, 49.68; H, 6.46; N, 1.87; found: C, 48.89; H, 6.20; N, 1.64.

(Acetonitrile)[(2′,4′,6′-triisopropyl-1,1′-biphenyl-2-yl)di-*tert*-butylphosphine]gold(I) hexafluorophosphate

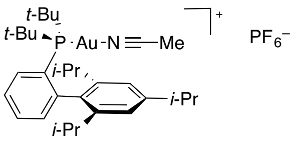

Chloro[(2’,4’,6’-triisopropyl-1,1’-biphenyl-2-yl)di-*tert*-butylphosphine]gold(I) (350.0 mg, 0.533 mmol) and acetonitrile (33.0 µL, 0.639 mmol) were dissolved in CH_2Cl_2 (23 mL). Then, silver hexafluorophosphate (135.0 mg, 0.533 mmol) was added and the reaction mixture was stirred at 23 ºC for 20 min. The crude was filtered through celite and concentrated. Finally, it was filtered through Teflon 0.22, washed with CH_2Cl_2 and the solvent was removed to afford a white powder.

221 mg of (acetonitrile)[(2′,4′,6′-triisopropyl-1,1′-biphenyl-2-yl)di-*tert*-butylphosphine] gold(I) hexafluorophosphate (0.152 mmol) were isolated in 51%.

^{1}H NMR (400 MHz, CD_2Cl_2) δ_H (ppm) 7.90 (ddd, J = 9.0, 7.1, 2.2 Hz, 1H), 7.60 (dq, J = 7.1, 2.0 Hz, 2H), 7.33 (td, J = 6.6, 5.7, 3.2 Hz, 1H), 7.17 (s, 2H), 2.95 (hept, J = 6.9 Hz, 1H), 2.38 – 2.27 (m, 6H), 1.43 (d, J = 16.3 Hz, 18H), 1.33 (d, J = 6.9 Hz, 6H), 1.27 (d, J = 6.7 Hz, 6H), 0.93 (d, J = 6.6 Hz, 6H). **^{13}C NMR** (101 MHz, CD_2Cl_2) δ_C 149.9, 147.8, 136.6 (d, J (^{13}C-^{31}P) = 7.1 Hz), 135.3 (d, J (^{13}C-^{31}P) = 9.3 Hz), 134.8 (d, J (^{13}C-^{31}P) = 4.2 Hz), 132.0, 128.0 (d, J (^{13}C-^{31}P) = 7.2 Hz), 122.4, 117.9, 39.2 (d, J (^{13}C-^{31}P) = 29.2 Hz), 34.55, 31.56 (d, J = 5.6 Hz), 26.35, 24.47, 23.39, 3.23. Two signals are missing due to overlapping. **^{31}P {^{1}H} NMR** (162 MHz, CD_2Cl_2) δ_P 58.53, –139.23 (hept, J (^{31}P-^{19}F) = 715.0 Hz). **^{19}F NMR** (376 MHz, CD_2Cl_2) δ_F –73.46 (d, J (^{19}F-^{31}P) = 710.3 Hz). **HRMS** (MALDI) calculated for $[C_{31}H_{48}AuNP]^+$ (M^+– PF_6): 662.3184, found *m/z* 662.3182.

[(2′,4′,6′-Triisopropyl-1,1′-biphenyl-2-yl)di-*tert*-butylphosphine](2-phenylethynyl) gold(I) (E)

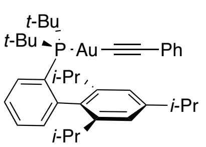

Lithium bis(trimethylsilyl)amide (54 mg, 0.320 mmol) was dissolved in THF (4.0 mL) and cooled to 0 ºC. Phenylacetylene (35 µL, 0.320 mmol) was added and the solution was stirred for 30 min. Afterwards, chloro[(2’,4’,6’-triisopropyl-1,1’-biphenyl-2-yl)di-*tert*-butylphosphine]gold(I) (200 mg, 0.304 mmol) dissolved in THF (3.0 mL) was added and the solution was stirred overnight at 23 ºC. The crude was concentrated, dissolved in CH_2Cl_2, filtered through Teflon 0.22 and the solvent was removed to afford a white powder.

219 mg of **E** (0.303 mmol) were obtained in 99% yield.

^{1}H NMR (500 MHz, CD_2Cl_2) δ_H 7.92 (td, J = 7.4, 1.8 Hz, 1H), 7.53 – 7.46 (m, 2H), 7.30 – 7.28 (m, 3H), 7.21 – 7.18 (m, 2H), 7.15 – 7.12 (m, 3H), 2.93 (p, J = 6.9 Hz, 1H), 2.40 (p, J = 6.7 Hz, 2H), 1.43 (d, J = 14.8 Hz, 18H), 1.36 (d, J = 6.8 Hz, 6H), 1.27 (d, J = 6.9 Hz, 6H), 0.92 (d, J = 6.7 Hz, 6H). **^{13}C NMR** (126 MHz, CD_2Cl_2) δ_C 150.0, 148.7 (d, J (^{13}C-^{31}P) = 15.6 Hz), 146.4, 137.3 (d, J (^{13}C-^{31}P) = 133.1 Hz), 136.6 (d, J (^{13}C-^{31}P) = 5.1 Hz), 136.1 (d, J (^{13}C-^{31}P) = 1.6 Hz), 135.2 (d, J (^{13}C-^{31}P) = 7.9 Hz), 132.2, 130.4 (d, J (^{13}C-^{31}P) = 2.2 Hz), 129.9 (d, J (^{13}C-^{31}P) = 37.0 Hz), 128.3, 127.4 (d, J (^{13}C-^{31}P) = 2.7 Hz), 126.9 (d, J (^{13}C-^{31}P) = 6.0 Hz), 126.0, 122.3, 101.5 (d, J (^{13}C-^{31}P) = 23.9 Hz), 38.5 (d, J (^{13}C-^{31}P) = 23.2 Hz), 34.5, 31.7 (d, J (^{13}C-^{31}P) = 6.8 Hz), 31.4, 26.5, 24.4, 23.2. **^{31}P {^{1}H} NMR** (202 MHz, CD_2Cl_2) δ_P 66.9. **HRMS** (MALDI) calculated for $[C_{37}H_{50}AuPNa]^+$ (M^++Na): 745.3208, found *m/z* 745.3216.

(α-Methylstyrene)[(2′,4′,6′-triisopropyl-1,1′-biphenyl-2-yl)di-*tert*-butylphosphine] gold(I) tetrakis[3,5-bis(trifluoromethyl)phenyl] borate (C)

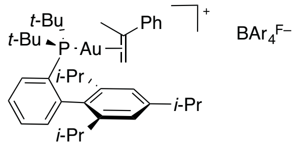

Chloro[(2’,4’,6’-triisopropyl-1,1’-biphenyl-2-yl)di-*tert*-butylphosphine]gold(I) (100.0 mg, 0.152 mmol) and α-methylstyrene (30 μL, 0.228 mmol) were dissolved in CH_2Cl_2 (10.0 mL). Then, sodium tetrakis[3,5-bis(trifluoromethyl)phenyl] borate (135.0 mg, 0.152 mmol) was added and the reaction mixture was stirred at 23 ºC for 30 min. The crude was filtered through celite and concentrated. Finally, it was filtered through Teflon 0.22, washed with CH_2Cl_2 and the solvent was removed to afford a white powder.

210 mg of **C** (0.131 mmol) were obtained in 86% yield.

^{1}H NMR (400 MHz, CD_2Cl_2) δ_H 7.82 (td, J = 7.8, 1.6 Hz, 1H), 7.76 – 7.70 (m, 8H), 7.63 – 7.53 (m, 6H), 7.50 – 7.39 (m, 5H), 7.29 (s, 2H), 7.21 (ddd, J = 7.3, 3.7, 1.7 Hz, 1H), 4.27 (dd, J = 4.5, 0.8 Hz, 1H), 3.95 (d, J = 4.5 Hz, 1H), 3.12 (p, J = 6.9 Hz, 1H), 2.50 (s, 3H), 2.42 – 2.19 (m, 2H), 1.43 (d, J = 6.9 Hz, 6H), 1.39 – 1.03 (m, 24H), 0.92 (d, J = 6.6 Hz, 6H). **^{13}C NMR** (101 MHz, CD_2Cl_2, 213 K): it was not possible to properly assign all the signals due to the broadening of some peaks because of the weak coordination of the metal to the alkene combined with the complexity of the heterocouplings with ^{31}P, ^{19}F and ^{11}B; δ_C 162.95, 162.55, 162.16, 161.76, 155.99, 151.76, 149.09, 147.08, 146.97, 135.95, 135.75, 135.47, 135.32, 135.04, 133.40, 132.93, 132.61, 132.26, 130.29, 129.79, 129.61, 129.36, 129.07, 128.44, 127.14, 126.67, 126.27, 124.11, 123.63, 123.12, 121.94, 118.55, 118.21, 117.88, 117.55, 89.01, 88.68, 38.61, 38.41, 34.76, 31.64, 31.42, 31.11, 26.27, 26.04, 25.90, 25.02, 24.82, 24.64, 24.45, 23.82. **^{31}P {^{1}H} NMR** (162 MHz, CD_2Cl_2) δ_P 69.3. **^{19}F {^{1}H} NMR** (376 MHz, CD_2Cl_2) δ_F –62.8. **^{11}B {^{1}H} NMR** (128 MHz, CD_2Cl_2, 298 K) δ_B –6.7. **HRMS** (ESI+) calculated for $[C_{29}H_{45}AuP]^+$ (M^+– $C_{41}H_{22}BF_{24}$): 621.2919, found *m/z* 621.2916.

{Phenylethynyl[(2′,4′,6′-triisopropyl-1,1′-biphenyl-2-yl)di-*tert*-butylphosphine] gold(I)}[(2′,4′,6′-triisopropyl-1,1′-biphenyl-2-yl)di-*tert*-butylphosphine]gold(I) tetrakis[3,5-bis(trifluoromethyl)phenyl] borate (D)

Chloro[(2’,4’,6’-triisopropyl-1,1’-biphenyl-2-yl)di-*tert*-butylphosphine]gold(I) (68.2 mg, 0.104 mmol) and [(2′,4′,6′-triisopropyl-1,1′-biphenyl-2-yl)di-*tert*-butylphosphine](2-phenylethynyl)gold(I) (75 mg, 0.104 mmol) were dissolved in CH_2Cl_2 (9.4 mL). Then, sodium tetrakis[3,5-bis(trifluoromethyl)phenyl] borate (92 mg, 0.104 mmol)was added and

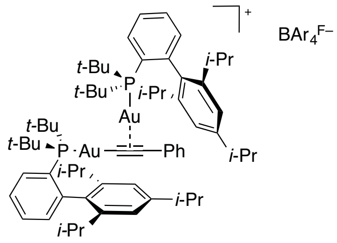

the reaction mixture was stirred at 23 ºC for 30 min. The crude was filtered through celite and concentrated. Finally, it was filtered through Teflon 0.22, washed with CH_2Cl_2 and solvent was removed to afford a white powder.

223 mg of **D** (0.101 mmol) were isolated in 97% yield. **^{1}H NMR** (400 MHz, CD_2Cl_2) δ_H 7.95 – 7.87 (m, 2H), 7.73 (dd, *J* = 4.2, 2.0 Hz, 8H), 7.57 (broad s, 4H), 7.56 – 7.49 (m, 4H), 7.48 – 7.42 (m, 1H), 7.42 – 7.37 (m, 2H), 7.34 – 7.30 (m, 2H), 7.26 – 7.22 (m, 2H), 6.84 (s, 4H), 2.39 – 2.29 (m, 6H), 1.42 (d, *J* = 15.6 Hz, 36H), 1.14 (d, *J* = 6.8 Hz, 12H), 1.09 (d, *J* = 6.9 Hz, 12H), 0.85 (d, *J* = 6.6 Hz, 12H). **^{13}C NMR** (101 MHz, CD_2Cl_2) δ_C 162.3 (q, *J* (^{13}C-^{11}B) = 50.0 Hz), 150.0, 148.1 (d, *J* (^{13}C-^{31}P) = 14.3 Hz), 147.1, 136.2 (d, *J* (^{13}C-^{31}P) = 5.6 Hz), 135.5, 135.4, 135.0 (d, *J* (^{13}C-^{31}P) = 1.2 Hz), 133.1, 131.4, 130.6, 130.0 – 129.0 (m), 129.0, 127.7 (d, *J* (^{13}C-^{31}P) = 42.5 Hz), 127.6, 127.5, 125.2 (q, *J* (^{13}C-^{19}F) = 272.6 Hz), 122.2, 121.3, 118.2 – 118.0 (m), 39.3 (d, *J* (^{13}C-^{31}P) = 24.6 Hz), 34.0, 31.9 (d, *J* (^{13}C-^{31}P) = 6.8 Hz), 31.4, 26.4, 24.3, 23.6 and one carbon is missing probably because of overlapping. **^{31}P {^{1}H} NMR** (162 MHz, CD_2Cl_2) δ_P 65.1. **^{19}F {^{1}H} NMR** (376 MHz, CD_2Cl_2) δ_F –62.9. **^{11}B {^{1}H} NMR** (128 MHz, CD_2Cl_2) δ_B –6.7. **HRMS** (MALDI) calculated for $[C_{66}H_{95}Au_2P_2]^+$ (M^+–$C_{32}H_{12}BF_{24}$): 1343.6235, found *m/z* 1343.5751.

General Procedure for the Preparation of Cyclobutenes

Alkyne (1 equiv.) and alkene (2 equiv.) were dissolved in CH_2Cl_2 (0.48 M) and the cationic gold (I) catalyst (3 mol %) was added. The reaction mixture was stirred at 23 ºC until no alkyne was observed by TLC. Then, it was quenched by adding a drop of a solution of Et_3N in cyclohexane (1M) and the solvent was removed. Preparative TLC was used to purify the resulting cyclobutenes.

1-Methoxy-3-(3-methyl-3-phenylcyclobut-1-en-1-yl)benzene (3g)

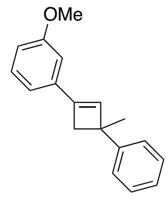

Cyclobutene **3g** was synthetized following the general procedure starting from 1-ethynyl-3-methoxybenzene (**1g**) (21 μL, 0.169 mmol) and α-methylstyrene (**2a**) (44 μL, 0.338 mmol) with catalyst **A2** (7.7 mg, 0.05 mmol). The reaction time was 8 h and a mixture of pentane and diethyl ether (9:1) was used as eluent in the separation.

33 mg (0.132 mmol) of **3g** were isolated as a colorless oil in 78% yield. **^{1}H NMR** (500 MHz, $CDCl_3$) δ_H 7.47 – 7.43 (m, 2H), 7.40 – 7.35 (m, 2H), 7.33 – 7.28 (m, 1H), 7.25 (td, *J* = 7.2, 1.4 Hz, 1H), 7.05 (dt, *J* = 7.7, 1.2 Hz, 1H), 7.00 – 6.95 (m, 1H), 6.87 (dd, *J* = 7.8, 3.2 Hz, 1H), 6.78 (s, 1H), 3.87 (s, 3H), 3.02 (d, *J* = 12.7 Hz, 1H), 2.95 (d, *J* = 12.5 Hz, 1H), 1.68 (s, 3H). **^{13}C NMR** (126 MHz, $CDCl_3$) δ_C 159.8, 147.7, 143.9, 136.2, 134.3, 129.5, 128.3, 126.0, 125.8, 117.4, 113.8, 110.0, 55.4, 46.1, 44.5, 27.7. **HRMS** (APCI) calculated for $[C_{18}H_{18}O]^+$ (M^++ H): 251.1430, found *m/z* 251.1434.

1-Fluoro-3-(3-methyl-3-phenylcyclobut-1-en-1-yl)benzene (3j)

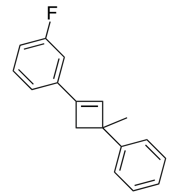

Cyclobutene **3j** was synthetized following the general procedure starting from 1-ethynyl-3-fluorobenzene (**1j**) (21 μL, 0.169 mmol) and α-methylstyrene (**2a**) (44 μL, 0.338 mmol) with catalyst **A2** (7.7 mg, 0.05 mmol). The reaction time was 24 h and a mixture of pentane and diethyl ether (90:1) was used as eluent in the separation.

31 mg (0.130 mmol) of **3j** were isolated as a yellowish oil in 77% yield.

^{1}H NMR (500 MHz, CDCl$_3$) δ_H 7.40 – 7.35 (m, 2H), 7.34 – 7.29 (m, 2H), 7.29 – 7.24 (m, 1H), 7.21 – 7.17 (m, 1H), 7.14 (dt, *J* = 7.7, 1.2 Hz, 1H), 7.05 (ddd, *J* = 9.8, 2.6, 1.5 Hz, 1H), 6.94 (tdd, *J* = 8.3, 2.6, 1.0 Hz, 1H), 6.75 (s, 1H), 2.95 (d, *J* = 12.6 Hz, 1H), 2.88 (d, *J* = 12.5 Hz, 1H), 1.62 (s, 3H). **^{13}C NMR** (126 MHz, CDCl$_3$) δ_C 163.2 (d, *J* = 245.8 Hz), 147.5, 143.0 (d, *J* = 2.5 Hz), 137.1 (d, *J* = 7.6 Hz), 135.4, 130.0 (d, *J* = 8.3 Hz), 128.3, 126.0, 125.9, 120.5 (d, *J* (^{13}C-^{19}F) = 2.8 Hz), 114.8 (d, *J* (^{13}C-^{19}F) = 21.4 Hz), 111.5 (d, *J* (^{13}C-^{19}F) = 21.4 Hz), 46.29, 44.34, 27.68. **HRMS** (APCI) calculated for $[C_{17}H_{15}F]^+$ (M^++ H): 239.1234, found *m/z* 239.1231.

1-Chloro-3-(3-methyl-3-phenylcyclobut-1-en-1-yl)benzene (3k)

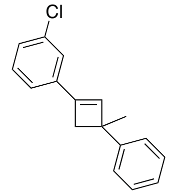

Cyclobutene **3k** was synthetized following the general procedure starting from 1-ethynyl-3-chlorobenzene (**1k**) (21 μL, 0.169 mmol) and α-methylstyrene (**2a**) (44 μL, 0.338 mmol) with catalyst **A2** (7.7 mg, 0.05 mmol). The reaction time was 24 h and a mixture of pentane and diethyl ether (90:1) was used as eluent in the separation.

36 mg (0.141 mmol) of **3k** were isolated as a yellowish oil in 83% yield.

^{1}H NMR (500 MHz, CDCl$_3$) δ_H 7.40 – 7.35 (m, 3H), 7.35 – 7.30 (m, 2H), 7.27 – 7.17 (m, 4H), 6.77 (s, 1H), 2.96 (d, *J* = 12.5 Hz, 1H), 2.89 (d, *J* = 12.5 Hz, 1H), 1.63 (s, 3H). **^{13}C NMR** (126 MHz, CDCl$_3$) δ_C 147.4, 142.7, 136.6, 135.6, 134.6, 129.7, 128.3, 127.9, 125.9, 124.9, 122.9, 46.4, 44.3, 27.7. **HRMS** (APCI) calculated for $[C_{17}H_{15}Cl]^+$ (M^++ H): 255.0935 found *m/z* 255.0935.

1-Methoxy-3-(3-methyl-3-phenylcyclobut-1-en-1-yl)benzene (3l)

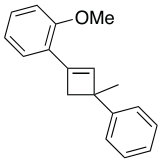

Cyclobutene **3l** was synthetized following the general procedure starting from 1-ethynyl-2-methoxybenzene (**1l**) (22 μL, 0.169 mmol) and α-methylstyrene (**2a**) (44 μL, 0.338 mmol) with catalyst **A2** (7.7 mg, 0.05 mmol). The reaction time was 48 h and a mixture of pentane and diethyl ether (9:1) was used as eluent in the separation.

11 mg (0.044 mmol) of **3l** were isolated as a colorless oil in 24% yield.

^{1}H NMR (300 MHz, CDCl$_3$) δ_H 7.47 – 7.39 (m, 2H), 7.36 – 7.28 (m, 2H), 7.25 – 7.14 (m, 3H), 6.98 – 6.86 (m, 2H), 6.80 (s, 1H), 3.92 (s, 3H), 3.03 (d, *J* = 12.4 Hz, 1H), 2.95 (d, *J* = 12.3 Hz, 1H), 1.65 (s, 3H). **^{13}C NMR** (75 MHz, CDCl$_3$) δ_C 158.6, 148.2, 140.3, 138.7, 128.9, 128.2, 127.2, 126.0, 125.6, 123.6, 120.3, 110.5, 55.3, 46.9, 45.4, 27.9. **HRMS** (APCI) calculated for $[C_{18}H_{18}O]^+$ (M^++ H): 251.1430, found *m/z* 251.1433.

3-(3-Methyl-3-phenylcyclobut-1-en-1-yl)thiophene (3m)

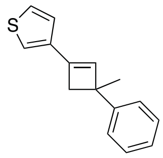

Cyclobutene **3m** was synthetized following the general procedure starting from 3-ethynylthiophene (**1m**) (17 µL, 0.169 mmol) and α-methylstyrene (**2a**) (44 µL, 0.338 mmol) with catalyst **A2** (7.7 mg, 0.05 mmol). The reaction time was 24 h and a mixture of pentane and diethyl ether (90:1) was used as eluent in the separation.

33 mg (0.146 mmol) of **3m** were isolated as a brownish oil in 86% yield.

^{1}H NMR (500 MHz, CDCl$_3$) δ_H 7.43 – 7.39 (m, 2H), 7.36 – 7.31 (m, 2H), 7.30 (dd, *J* = 5.0, 2.9 Hz, 1H), 7.23 – 7.19 (m, 2H), 7.17 (dd, *J* = 3.0, 1.2 Hz, 1H), 6.51 (s, 1H), 2.97 (d, *J* = 12.5 Hz, 1H), 2.91 (d, *J* = 12.4 Hz, 1H), 1.65 (s, 3H). **^{13}C NMR** (126 MHz, CDCl$_3$) δ_C 147.8, 139.4, 137.9, 132.7, 128.2, 126.0, 125.9, 125.8, 125.1, 121.1, 47.2, 45.2, 27.7. **HRMS** (APCI) calculated for $[C_{15}H_{14}S]^+$ (M^++ H): 239.0889, found *m/z* 239.0896.

Triisopropyl((1-methyl-3-phenylcyclobut-2-en-1-yl)methyl)silane (3q)

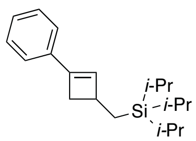

Cyclobutene **3q** was synthetized following the general procedure starting from phenylacetylene (**1a**) (19 µL, 0.169 mmol) and allyltriisopropylsilane (**2d**) (81 µL, 0.338 mmol) with catalyst **A2** (7.7 mg, 0.05 mmol). The reaction time was 72 h and a mixture of pentane 100% was used as eluent in the separation. **3q** was isolated as a colorless oil.

^{1}H NMR (400 MHz, CDCl$_3$) δ_H 7.38 – 7.28 (m, 4H), 7.25 – 7.20 (m, 1H), 6.39 (d, *J* = 1.1 Hz, 1H), 3.07 – 2.94 (m, 2H), 2.31 (dd, *J* = 12.4, 1.4 Hz, 1H), 1.08 (s, 23H). **^{13}C NMR** (101 MHz, CDCl$_3$) δ_C 143.8, 135.2, 133.8, 128.4, 127.5, 124.5, 38.6, 35.5, 19.0, 15.3, 11.4. **HRMS** (APCI) calculated for $[C_{20}H_{32}Si]^+$ (M^++H): 301.2346, found *m/z* 301.2352.

(3-Methyl-3-(phenoxymethyl)cyclobut-1-en-1-yl)benzene (3r)

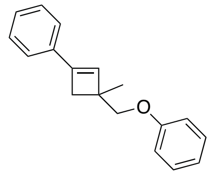

Cyclobutene **3r** was synthetized following the general procedure starting from phenylacetylene (**1a**) (19 µL, 0.169 mmol) and ((2-methylallyl)oxy)benzene (**2e**) (52 µL, 0.338 mmol) with catalyst **A2** (7.7 mg, 0.05 mmol). The reaction time was 72 h and a mixture of pentane and diethyl ether (20:1) was used as eluent in the separation in a preparative TLC in Alumina oxide.

3r was isolated as a colorless oil.

^{1}H NMR (500 MHz, CDCl$_3$) δ_H 7.39 – 7.36 (m, 2H), 7.36 – 7.31 (m, 2H), 7.30 – 7.26 (m, 3H), 6.96 – 6.91 (m, 3H), 6.47 (s, 1H), 3.98 (d, *J* = 8.7 Hz, 1H), 3.95 (d, *J* = 8.7 Hz, 1H), 2.74 (d, *J* = 12.8 Hz, 1H), 2.56 (d, *J* = 12.8 Hz, 1H), 1.42 (s, 3H). **^{13}C NMR** (126 MHz, CDCl$_3$) δ_C 159.6, 144.3, 134.8, 133.0, 129.5, 128.5, 128.0, 124.7, 120.7, 114.8, 75.5, 42.9, 38.9, 21.8. **HRMS** (APCI) calculated for $[C_{18}H_{18}O]^+$ (M^++ H): 251.1426, found *m/z* 251.1430.

((1-methyl-3-phenylcyclobut-2-en-1-yl)methoxy)triphenylsilane (3s)

Cyclobutene **3s** was synthetized following the general procedure starting from phenylacetylene (**1a**) (19 µL, 0.169 mmol) and ((2-methylallyl)oxy)triphenylsilane (**2f**) (112 mg, 0.338 mmol) with catalyst **A2** (7.7 mg, 0.05 mmol). The reaction time was 72 h

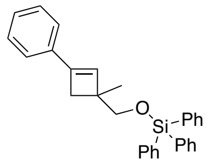

and a mixture of pentane and diethyl ether (20:1) was used as eluent in the separation in a preparative TLC in Alumina oxide. **3s** was isolated as a colorless oil. **^{1}H NMR** (300 MHz, $CDCl_3$) δ_H 7.68 – 7.57 (m, 6H), 7.46 – 7.28 (m, 14H), 6.29 (s, 1H), 3.80 (s, 2H), 2.61 (d, *J* = 12.7 Hz, 1H), 2.40 (d, *J* = 12.7 Hz, 1H), 1.30 (s, 3H). **^{13}C NMR** (75 MHz, $CDCl_3$) δ_C 143.9, 135.6, 135.1, 134.6, 133.5, 130.1, 128.4, 127.9, 127.7, 124.6, 71.1, 44.6, 38.3, 21.5. **HRMS** (APCI) calculated for $[C_{30}H_{28}OSi]^+$ (M^++H): 433.1982, found *m/z* 433.1984.

General Procedure for the Preparation of [3.2.1]-Oxabicycles

Alkyne (3.5 equiv.) and oxoalkene (1 equiv.) were dissolved in $(CH_2Cl)_2$ (0.50 M) and the cationic gold (I) catalyst (5 mol %) was added. The reaction mixture was stirred at 50 ºC untill no oxoalkene was observed by TLC. Then, it was quenched by adding a drop of of Et_3N and the solvent was removed. Preparative TLC was used to purify the [3.2.1]-oxabicycle product.

General Procedure for the Preparation of Phenols

Alkyne (1 equiv.) and furan (2 equiv.) were dissolved in $(CH_2Cl)_2$ (0.50 M) and the cationic gold (I) catalyst (3 mol %) was added. The reaction mixture was stirred at 23 ºC untill no alkyne was observed by TLC. Then, it was quenched by adding a drop of of Et_3N and the solvent was removed. Chromatography column with SiO_2 was used to purify the phenols.

Monitoring the [2+2] Cycloaddition Reaction

^{1}H NMR monitoring of the intermolecular gold(I)-catalyzed [2+2] cycloaddition of phenylacetylene and α-methylstyrene with [LAuNCMe]X (3 mol %, L = *t*-BuXPhos, X = BAr_4^{F-}, SbF_6^-, BF_4^-) in CD_2Cl_2 at 23 ºC and using diphenylmethane as internal standard (Figure S1).

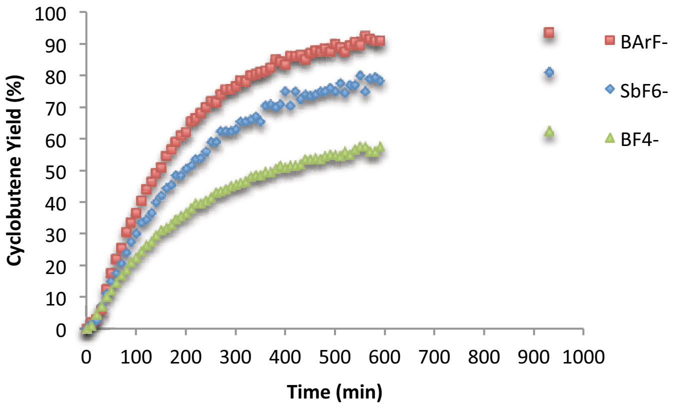

Figure S1 Monitoring the [2+2] cycloaddition reaction using [LAuNCMe]X (L = *t*-BuXPhos, X = BAr_4^{F-}, SbF_6^-, BF_4^-).

Electrondensity Surfaces

Total SCF density mapped with ESP (r = 0.03 e/Å^3). Structures calculated with Gaussian 09 using M06 with 6-31G(d) (C, H, P, B, F) and SDD (Au, Sb) in CH_2Cl_2 (Figure S2).

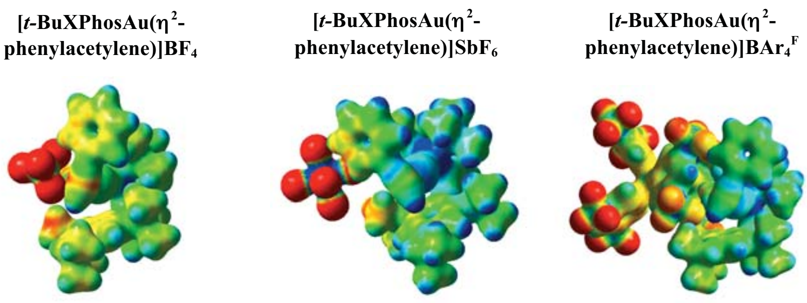

[*t*-BuXPhosAu(η^2-phenylacetylene)]BF_4 **[*t*-BuXPhosAu(η^2-phenylacetylene)]SbF_6** **[*t*-BuXPhosAu(η^2-phenylacetylene)]BAr_4^F**

Figure S2 Coloumb potential of [(η^2-phenylacetylene)Au(I)]X (X = BF_4^-, SbF_6^- and BAr_4^{F-}) mapped in an electronic isodensity surface.

Mechanistic Studies

Order of Reagents

^{1}H NMR monitoring of the intermolecular gold(I)-catalyzed [2+2] cycloaddition of α-methylstyrene (0.50 mmol) and changing quantities of phenylacetylene with catalyst **A2** (7.2 μmol) in CD_2Cl_2 (0.56 mL) at 23 ºC and using diphenylmethane as internal standard (Figure S3).

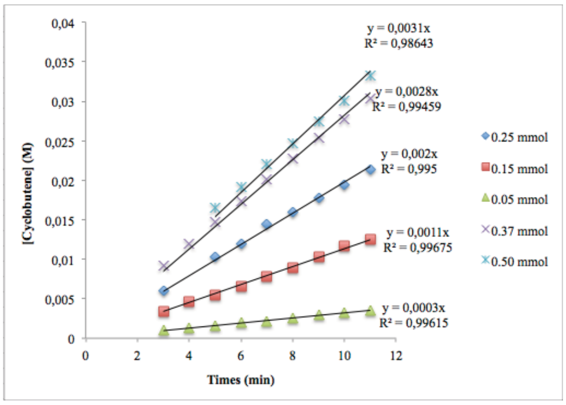

Figure S3 Correlation between [cyclobutene] and time by changing the quantities of phenylacetylene.

^{1}H NMR monitoring of the intermolecular gold(I)-catalyzed [2+2] cycloaddition of phenylacetylene (0.25 mmol) and changing quantities of α-methylstyrene with catalyst **A2** (7.2 μmol) in CD_2Cl_2 (0.56 mL) at 23 ºC and using diphenylmethane as internal standard (Figure S4).

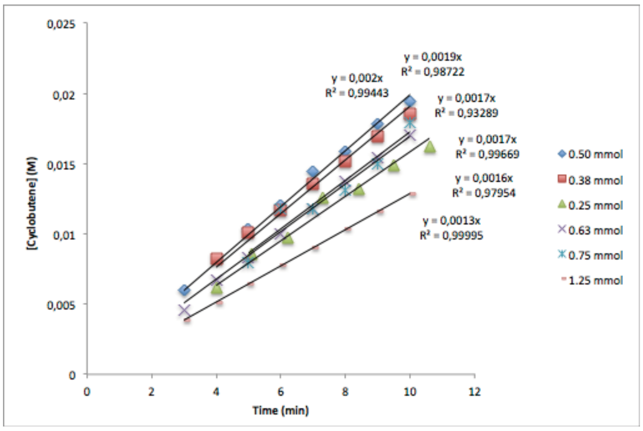

Figure S4 Correlation between [cyclobutene] and time by of changing the quantities of α-methylstyrene.

^{1}H NMR monitoring of the intermolecular gold(I)-catalyzed [2+2] cycloaddition of phenylacetylene (0.25 mmol) and α-methylstyrene (0.50 mmol) with changing quantities of catalyst **A2** in CD_2Cl_2 (0.56 mL) at 23 ºC and using diphenylmethane as internal standard (Figure S5).

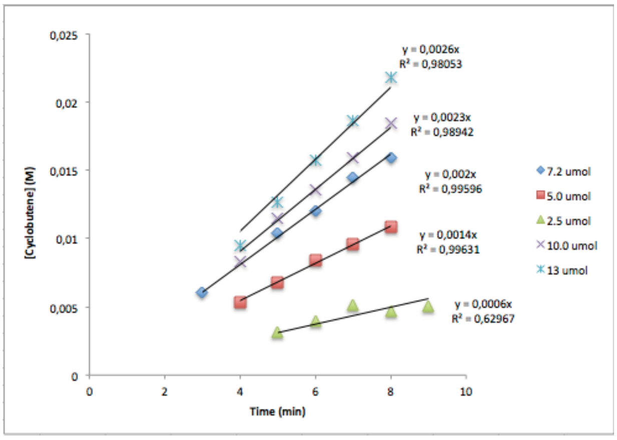

Figure S5 Correlation between [cyclobutene] and time by changing the quantities of **A2**.

According to the method of the initial rates, it is possible to determine the order of the reagents by the logarithmic graph of the initial formation of the product and the concentration of the varying reagent (Figure S6).

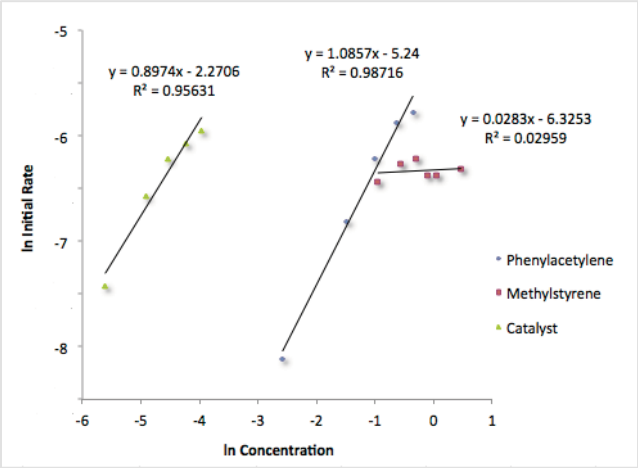

Figure S6 Correlation between ln [initial rate] and ln [product].

Species Formed in the Reaction Mixture

Initial ^{31}P NMR spectrum of the intermolecular gold(I)-catalyzed [2+2] cycloaddition of phenylacetylene and α-methylstyrene with **A2** (3 mol %) in CD_2Cl_2 at 23 ºC (Figure S7).

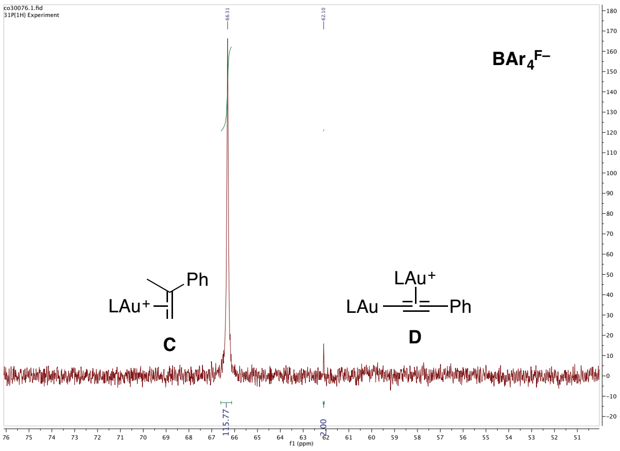

Figure S7 Initial ^{31}P NMR of the [2+2] cycloaddition reaction using **A2**.

Initial ^{31}P NMR spectrum of the intermolecular gold(I)-catalyzed [2+2] cycloaddition of phenylacetylene and α-methylstyrene with **A1** (3 mol %) in CD_2Cl_2 at 23 ºC (Figure S8).

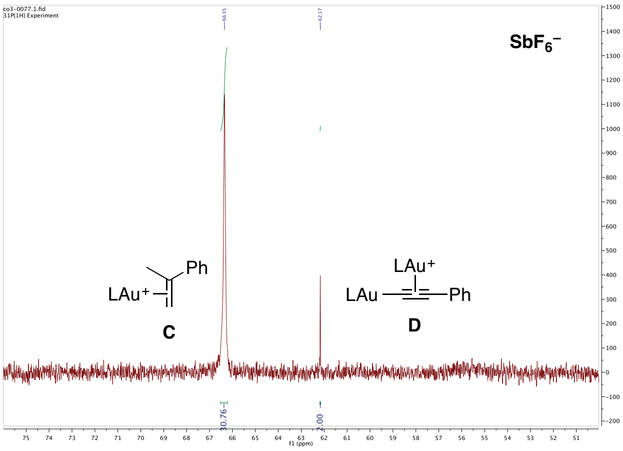

Figure S8 Initial ^{31}P NMR of the [2+2] cycloaddition reaction using **A1**.

Initial ^{31}P NMR spectrum of the intermolecular gold(I)-catalyzed [2+2] cycloaddition of phenylacetylene and α-methylstyrene with (acetonitrile)[(2′,4′,6′-triisopropyl-1,1′-biphenyl-2-yl)di-*tert*-butylphosphine]gold(I) tetrafluoroborate (3 mol %) in CD_2Cl_2 at 23 ºC (Figure S9).

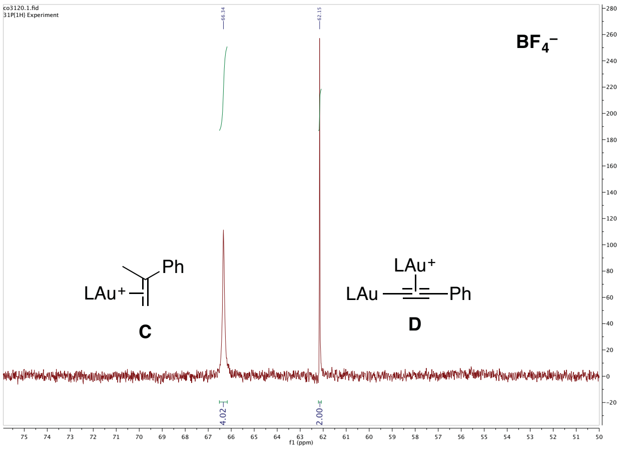

Figure S9 Initial ^{31}P NMR of the [2+2] cycloaddition reaction using (acetonitrile)[(2′,4′,6′-triisopropyl-1,1′-biphenyl-2-yl)di-*tert*-butylphosphine]gold(I) tetrafluoroborate.

Additional Experiments

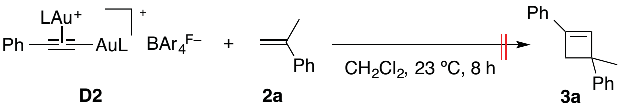

D2 (40 mg, 0.018 mmol) and α-methylstyrene (2.35 μL, 0.018 mmol) were dissolved in CD_2Cl_2 (40 μL) and the mixture was stirred for 8 h at 23 °C. No reaction took place.

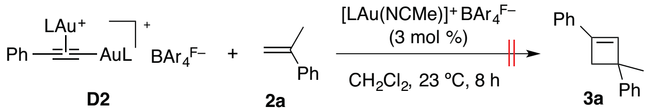
LAu+
+
Ph
AuL
BAr4F−
+
Ph
[LAu(NCMe)]+ BAr4F−
(3 mol %)
CH2Cl2, 23 °C, 8 h
Ph
Ph
D2
2a
3a

D2 (40 mg, 0.018 mmol), α-methylstyrene (2.35 μL, 0.018 mmol), and **A2** (0.8 mg, 0.54 μmol) were dissolved in CD_2Cl_2 (40 μL) and the mixture was stirred for 8 h at 23 °C. No reaction took place.

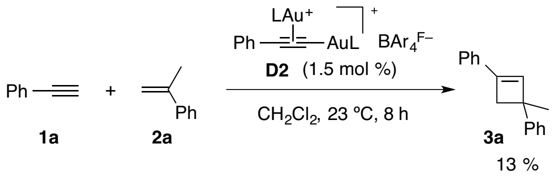
LAu+
+
Ph
AuL
BAr4F−
D2 (1.5 mol %)
CH2Cl2, 23 °C, 8 h
Ph
+
Ph
Ph
Ph
1a
2a
3a
13 %

Phenylacetylene (29 μL, 0.263 mmol), α-methylstyrene (68 μL, 0.526 mmol) and **D2** (8 mg, 3.9 μmol) were dissolved in CH_2Cl_2 (0.6 mL) and the mixture was stirred for 8 h at 23 °C. Solvent was finally evaporated. 13% of cyclobutene **3a** was observed by ^{1}H NMR using diphenymethane as internal standard.

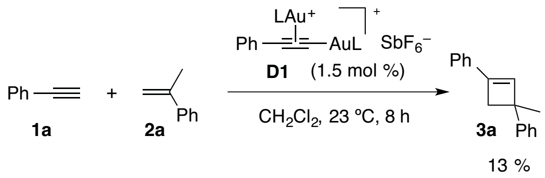
LAu+
+
Ph
AuL
SbF6−
D1 (1.5 mol %)
CH2Cl2, 23 °C, 8 h
Ph
+
Ph
Ph
Ph
1a
2a
3a
13 %

Phenylacetylene (29 μL, 0.263 mmol), α-methylstyrene (68 μL, 0.526 mmol) and **D1** (6 mg, 3.9 μmol) were dissolved in CH_2Cl_2 (0.6 mL) and the mixture was stirred for 8 h at 23 °C. Solvent was finally evaporated. 13% of cyclobutene **3a** was observed by ^{1}H NMR using diphenylmethane as internal standard.

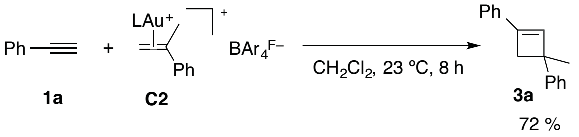
Ph
+
LAu+
+
Ph
BAr4F−
CH2Cl2, 23 °C, 8 h
Ph
Ph
1a
C2
3a
72 %

Phenylacetylene (3.5 μL, 0.031 mmol) and **C2** (50 mg, 0.031 mmol) were dissolved in CD_2Cl_2 (69 μL) and the mixture was stirred for 8 h at 23 °C. 72% of cyclobutene **3a** was observed by ^{1}H NMR using diphenylmethane as internal standard.

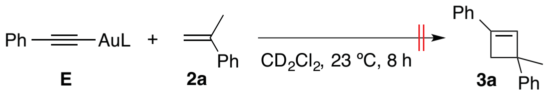
Ph
AuL
+
Ph
CD2Cl2, 23 °C, 8 h
Ph
Ph
E
2a
3a

E (20 mg, 0.028 mmol) and α-methylstyrene (3.59 μL, 0.028 mmol) were dissolved in CD_2Cl_2 (62 μL) and the mixture was stirred for 8 h at 23 ºC. No reaction took place.

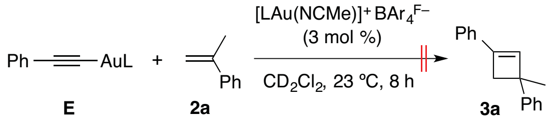
Ph—≡—AuL
+
Ph
[LAu(NCMe)]+ BAr4F−
(3 mol %)
CD2Cl2, 23 °C, 8 h
Ph
Ph
E
2a
3a

E (20 mg, 0.028 mmol), α-methylstyrene (3.59 μL, 0.028 mmol) and **A2** (1.3 mg, 0.83 μmol) were dissolved in CD_2Cl_2 (62 μL) and the mixture was stirred for 8 h at 23 ºC. No reaction took place.

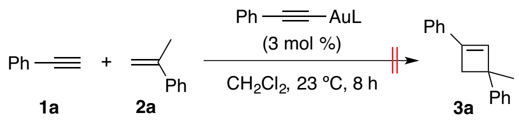
Ph—≡
+
Ph
Ph—≡—AuL
(3 mol %)
CH2Cl2, 23 °C, 8 h
Ph
Ph
1a
2a
3a

Phenylacetylene (23 μL, 0.211 mmol), α-methylstyrene (55 μL, 0.422 mmol) and **E** (4.6 mg, 6.3 μmol) were dissolved in CH_2Cl_2 (0.5 mL) and the mixture was stirred for 8 h at 23 ºC. Solvent was finally evaporated. No reaction took place.

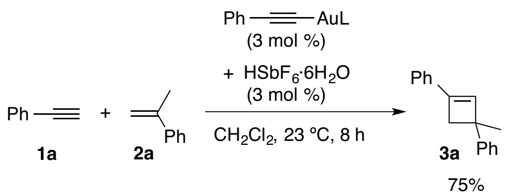
Ph—≡
+
Ph
Ph—≡—AuL
(3 mol %)
+ HSbF6·6H2O
(3 mol %)
CH2Cl2, 23 °C, 8 h
Ph
Ph
1a
2a
3a
75%

Phenylacetylene (23 μL, 0.211 mmol), α-methylstyrene (55 μL, 0.422 mmol), **E** (4.6 mg, 6.3 μmol) and $HSbF_6·6H_2O$ (2.1 mg, 6.3 μmol) were dissolved in CH_2Cl_2 (0.5 mL) and the mixture was stirred for 8 h at 23 ºC. Solvent was finally evaporated. 75% of cyclobutene **3a** was observed by ^1H NMR using diphenylmethane as internal standard.

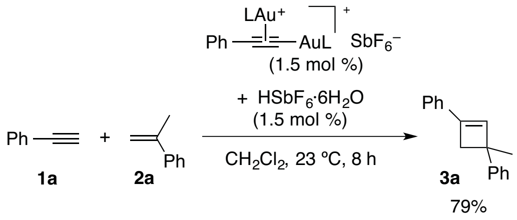
Ph—≡
+
Ph
LAu+
Ph—≡—AuL SbF6−
+
(1.5 mol %)
+ HSbF6·6H2O
(1.5 mol %)
CH2Cl2, 23 °C, 8 h
Ph
Ph
1a
2a
3a
79%

Phenylacetylene (23 μL, 0.211 mmol), α-methylstyrene (55 μL, 0.422 mmol), **D2** (5 mg, 3.2 μmol) and $HSbF_6·6H_2O$ (1.1 mg, 3.2 μmol) were dissolved in CH_2Cl_2 (0.5 mL) and the mixture was stirred for 8 h at 23 ºC. Solvent was finally evaporated. 79% of cyclobutene **3a** was observed by ^1H NMR using diphenylmethane as internal standard.

Equilibrium Constants

The equilibrium constants between catalysts **A1** and **A2** and their related alkene (**C**) and digold (**D**) complexes were determined using the van't Hoff equation. Therefore, several samples (substrate:complex = 1:2, 1:1, 2:1, 3.5:1 and 5:1) in CD_2Cl_2 were analyzed at 263, 278, 293 and 308 K by ^{1}H and ^{31}P NMR.

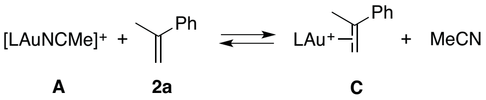

$$K_{eq} = \frac{[\boldsymbol{C}] \cdot [MeCN]}{[\boldsymbol{A}] \cdot [\boldsymbol{2a}]} = \frac{[\boldsymbol{C}]^2}{([\boldsymbol{A}]_O - [\boldsymbol{C}]) \cdot ([\boldsymbol{2a}]_O - [\boldsymbol{C}])}$$

$$\text{Integrals ratio} = \frac{[\boldsymbol{C}]}{([\boldsymbol{A}]_O - [\boldsymbol{C}])}$$

Substrate:sample	263 K	278 K	293 K	308 K
1:2	4.84	4.90	4.97	5.05
1:1	3.01	3.03	3.32	3.53
2:1	1.85	1.98	2.04	2.19
3.5:1	1.32	1.36	1.46	1.57
5:1	0.98	1.06	1.12	1.32

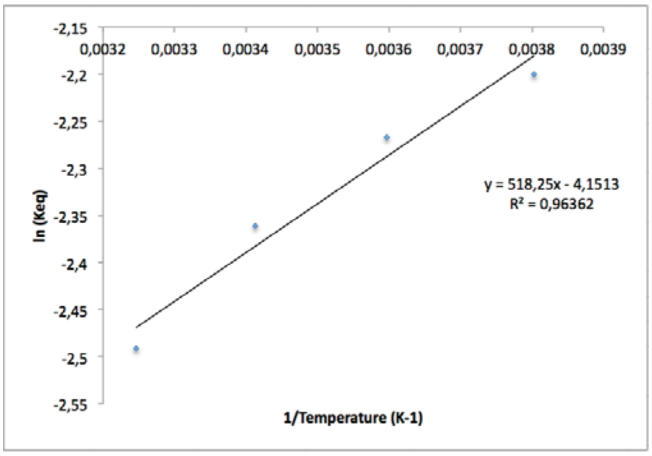

Figure S10 Correlation between the equilibrium constant of **A1** and **C1** with the temperature.

Substrate:sample	263 K	278 K	293 K	308 K
1:2	5.93	5.96	6.41	6.90
1:1	4.01	-	4.77	5.91
2:1	2.76	2.78	2.77	3.63
3.5:1	1.78	1.96	2.00	1.97
5:1	1.49	1.57	1.70	1.75

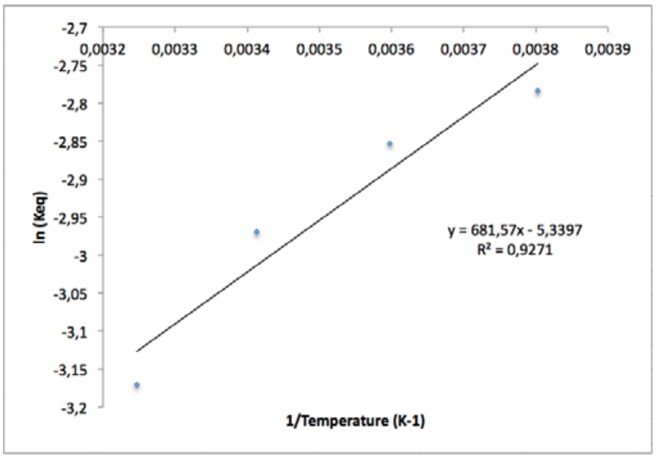

Figure S11 Correlation between the equilibrium constant of **A2** and **C2** with the temperature.

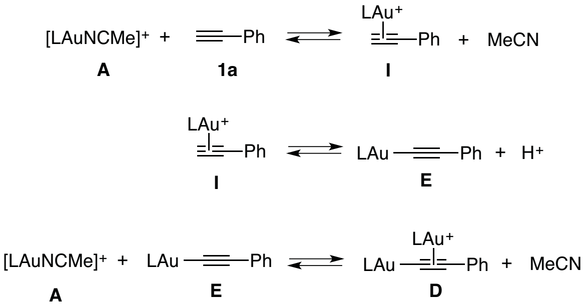
[LAuNCMe]⁺ + ≡—Ph ⇌ LAu⁺ ≡—Ph + MeCN
A
1a
I
LAu⁺ ≡—Ph ⇌ LAu—≡—Ph + H⁺
I
E
[LAuNCMe]⁺ + LAu—≡—Ph ⇌ LAu—LAu⁺ ≡—Ph + MeCN
A
E
D

$$K_{eq} = \frac{[\boldsymbol{D}] \cdot [H^+] \cdot [MeCN]^2}{[\boldsymbol{A}]^2 \cdot [\boldsymbol{1a}]} = \frac{4 \cdot [\boldsymbol{D}]^4}{([\boldsymbol{A}]_O - 2 \cdot [\boldsymbol{D}])^2 \cdot ([\boldsymbol{1a}] - [\boldsymbol{D}])}$$

$$Integrals\ ratio = \frac{[\boldsymbol{D}]}{([\boldsymbol{A}]_0 - 2 \cdot [\boldsymbol{D}])}$$

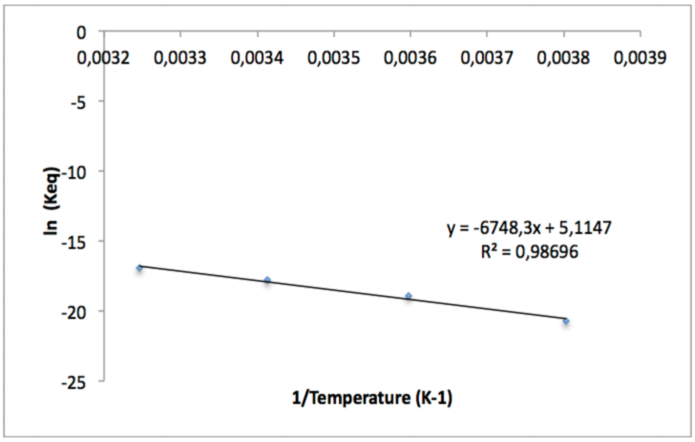

Figure S12 Correlation between the equilibrium constant of **A1** and **D1** with the temperature (reported in [73]).

Substrate:sample	263 K	278 K	293 K	308 K
1:2	160.29	103.04	86.90	56.60
1:1	155.16	97.66	78.90	59.71
2:1	113.30	79.36	49.29	46.04
3.5:1	107.32	65.03	46.26	39.33
5:1	82.45	52.90	42.26	35.38

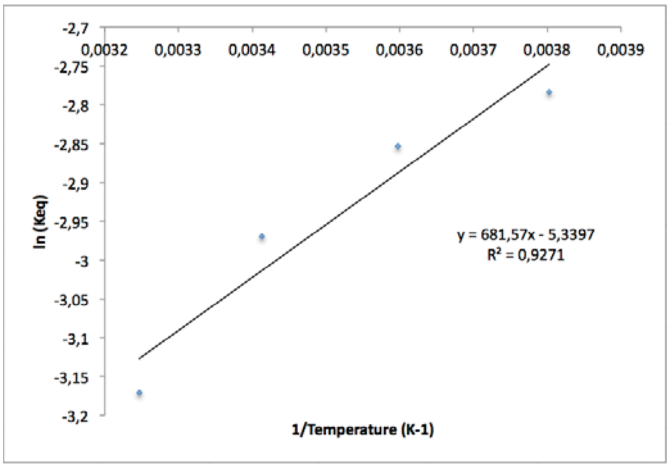

Figure S13 Correlation between the equilibrium constant of **A2** and **D2** with the temperature.

Chapter 3: Total Synthesis of Nardoaristolone B and an Approach to the Synthesis of (–)-Aristolone and Kanshone H

Introduction

Natural products, a group of organic compounds isolated from plants, microorganisms and marine creatures, possess chemical or biological activities that could potentially benefit the human life. It is not surprising that a large number of major drugs nowadays are natural products or their derivatives. Therefore, studies on the synthesis of natural products are an area of great importance. Not only does it allow the access to these biologically potent molecules but also opens new opportunities for the discovering of new transformations.

Nardoaristolone B

Nardoaristolone B is a novel terpenoid isolated in 2013 from the underground parts of *Nardostachys chinensis* Batal,[112] a perennial herb that grows around the Himalayas mountain areas.[113] While the plant has been used as a sedative and analgesic agent in traditional Chinese medicine for centuries,[114] the isolated molecule presented protective effects on the injury of neonatal rat cardiomyocytes. This novel aristolane-type sesquiterpenoid possesses an unusual 6/5/3 fused tricyclic skeleton. It was isolated from *N. chinensis*, first along with nardoaristolone A, and later with another seven new sesquiterpenes[115] and two other already isolated ((–)-aristolone[116] and kanshone F[117]) (Figure 1).

---

[112] Liu, M.-L.; Duan, Y.-H.; Hou, Y.-L.; Li, C.; Gao, H.; Dai, Y.; Yao, X.-S. *Org. Lett.* **2013**, *15*, 1000–1003.

[113] Qiu, L. Q. *Flora Reipublicae Popularis Sinicae (Zhongguo Zhiwu Zhi)*; Science Press: Beijing, China, **1986**, *73*, 224–225.

[114] Chinese Pharmacopoeia; State Pharmacopoeia Committee; China Medical Pharmaceutical Science and Technology Publishing House: Beijing, **2010**, *1*, 79.

[115] Liu, M.-L.; Duan, Y.-H.; Zhang, J.-B.; Yang, Y.; Dai, Y.; Yao, X.-S. *Tetrahedron* **2013**, *69*, 6574–6578.

[116] (a) Harrigan, G. G.; Ahmad, A.; Baj, N.; Glass, T. E.; Gunatilaka, A. A. L.; Kingston, D. G. I. *J. Nat. Prod.* **1993**, *56*, 921–925. (b) Buchi, G.; Greuter, F.; Tokoroyama, T. *Tetrahedron Lett.* **1962**, *18*, 827–833.

[117] Tanitsu, M. A.; Takaya, Y.; Akasaka, M.; Niwa, M.; Oshima, Y. *Phytochemistry*, **2002**, *59,* 845–849.

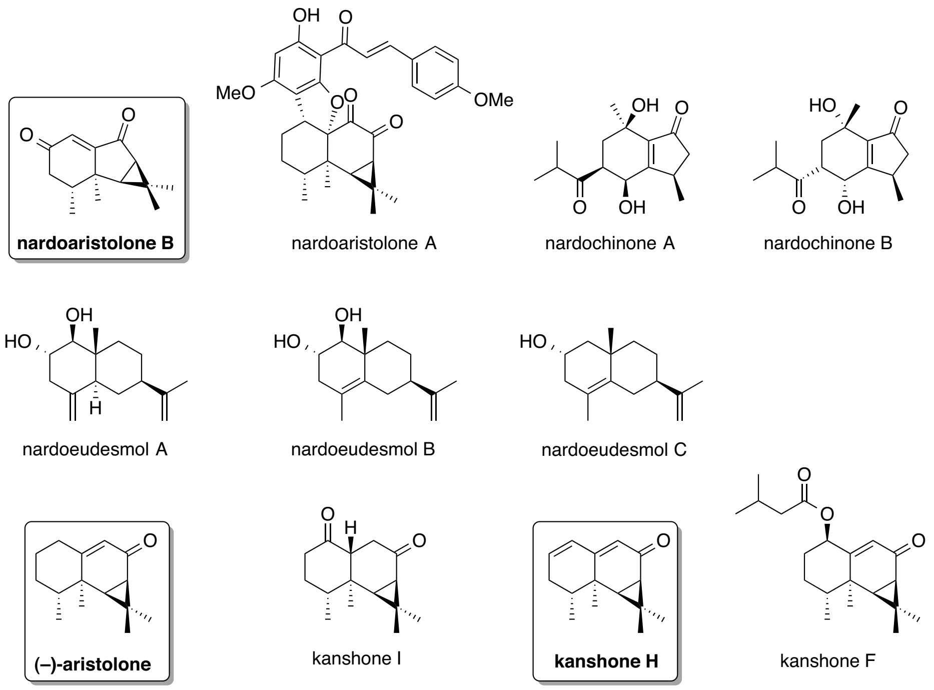
nardoaristolone B
MeO
OH
O
OMe
nardoaristolone A
OH
nardochinone A
HO
nardochinone B
OH
HO
H
nardoeudesmol A
nardoeudesmol B
nardoeudesmol C
(–)-aristolone
H
kanshone I
kanshone H
kanshone F

Figure 1 Structures of different sesquiterpenes isolated from *Nardostachys chinesis*.

Extraction of 5 kg of the air-dried medicinal plant *Nardostachys chinesis* at reflux in EtOH (x2) followed by several chromatography columns over macroporous resin HP-20 or silica gel let to the isolation of 89.2 mg of nardoaristolone B, which could be fully characterized and whose absolute configuration could be unambiguously established by X-ray diffraction (Figure 2).

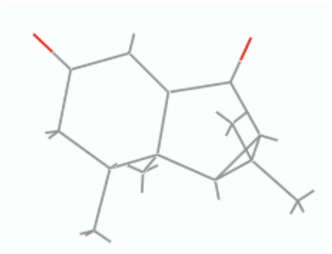

Figure 2 X-ray crystal structure of nardoaristolone B.

The proposed biogenetic pathway proposed is showed in Scheme 1. Kanshone C was presumed to be the biosynthetic precursor that could evolve through an initial epoxide ring-opening reaction followed by a benzilic acid rearrangement giving access to the quadricycle intermediate **3**. Subsequent decarboxylation, dehydration and oxidation would produce nardoaristolone B.

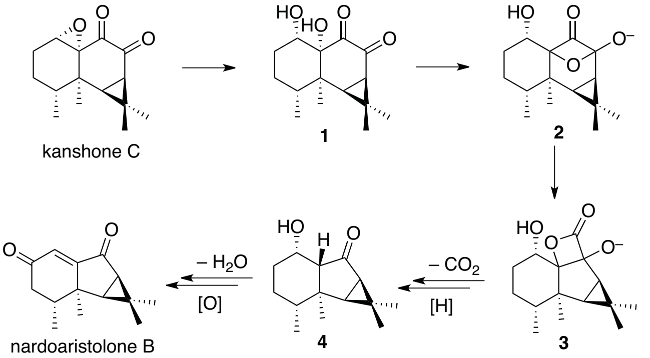

Scheme 1 Biogenetic pathway for nardoaristolone B.

The first total synthesis of (±)-nardoaristolone B was reported at the very end of July 2014.[118] The racemic mixture of the natural product could be accessed after a cyclopropanation of bicylic intermediate **5** that could be synthesized from a double allylic oxidation of **6**. The starting points of the synthesis were diene **7** and tiglic aldehyde (**8**) that were coupled following a three step-sequence of Nobel prize reactions; Diels-Alder (DA), Wittig olefination and ring-closing metathesis (RCM) (Scheme 2).

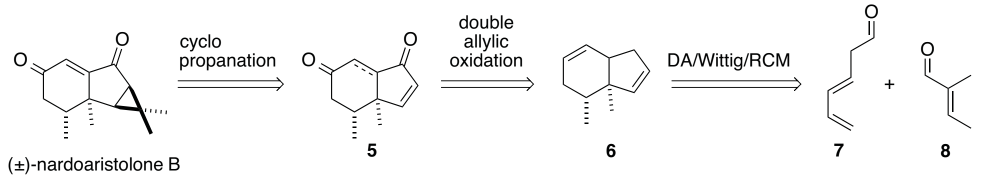

Scheme 2 Retrosynthetic analysis of (±)-nardoaristolone B.

Although the racemic natural product could be synthesized in 5 steps, the overall yield of the synthesis was very low (1.4%). Nevertheless, adding two more steps to the synthesis the overall yield could be increased to 5.8%. Tiglic aldehyde (**8**) and diene **7** were exposed to a boron trifluoride-mediated Diels-Alder cycloaddition followed by a Wittig reaction. The resulting diene **6** could be isolated in 8-10% yield as a 9:1 mixture of diastereomers. Diene **6** could be obtained in higher yield (41%) and the same diastereoselectivity after being replaced by its more stable ester analogue **9**. Nevertheless, two more steps (DIBAL-H reduction and Wittig reaction) were required to reach the desired intermediate **10**. Ring-closing metathesis using Grubbs-II catalyst, followed by a double allylic oxidation gave the doubly oxidized diene **5** in 44% yield over 2 steps. A final cyclopropanation using diphenylisopropyl sulfinium tetrafluoroborate under basic conditions[119] gave the desired racemic natural product albeit in low yield (32%) (Scheme 3).

---

[118] Handore, K. L.; Reddy, D. S. *Org. Lett.* **2014**, *16*, 4252–4255.

[119] Zhang, R.; Mamai, A.; Madalengoitia, J. S. *J. Org. Chem.* **1999**, *64*, 547–555.

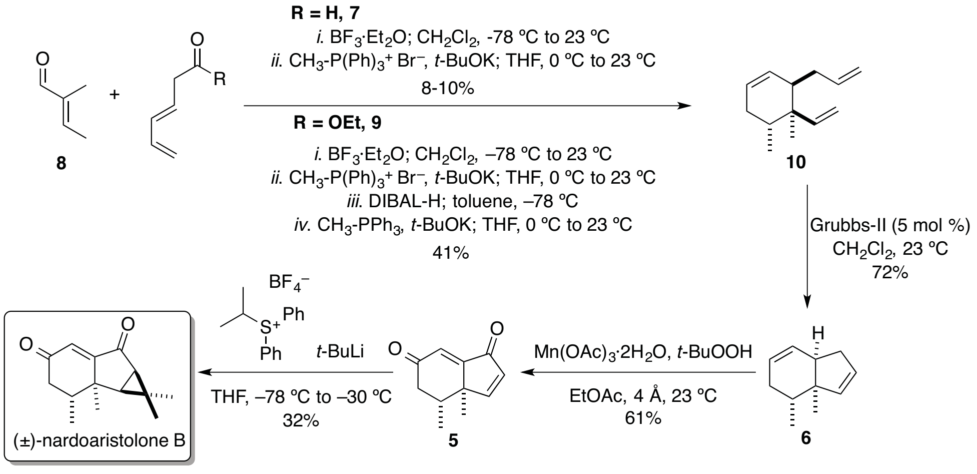
R = H, 7
i. BF3·Et2O; CH2Cl2, -78 °C to 23 °C
ii. CH3-P(Ph)3+ Br−, t-BuOK; THF, 0 °C to 23 °C
8-10%
R = OEt, 9
i. BF3·Et2O; CH2Cl2, −78 °C to 23 °C
ii. CH3-P(Ph)3+ Br−, t-BuOK; THF, 0 °C to 23 °C
iii. DIBAL-H; toluene, −78 °C
iv. CH3-PPh3, t-BuOK; THF, 0 °C to 23 °C
41%
O
R
8
10
Grubbs-II (5 mol %)
CH2Cl2, 23 °C
72%
H
6
Mn(OAc)3·2H2O, t-BuOOH
EtOAc, 4 Å, 23 °C
61%
5
BF4−
S+
Ph
Ph
t-BuLi
THF, −78 °C to −30 °C
32%
(±)-nardoaristolone B

Scheme 3 Total synthesis of (±)-nardoaristolone B.[118]

The *endo*-stereochemistry of the last reaction was consistent with an approach of the sulfur ylide reagent from the opposite side of the methyl groups. Interestingly, the *exo*-cyclopropanation could be obtained using the same conditions as for nardoaristolone B after a reduction of the trisubstituted olefin of the dioxidized diene **5** followed by the selective protection of the cyclohexanone moiety as an acetal. The convex shape of the new bicyclic product formed (**11**), favored the attack of the ylide from the *exo* face (same side as the methyl groups) (Scheme 4).

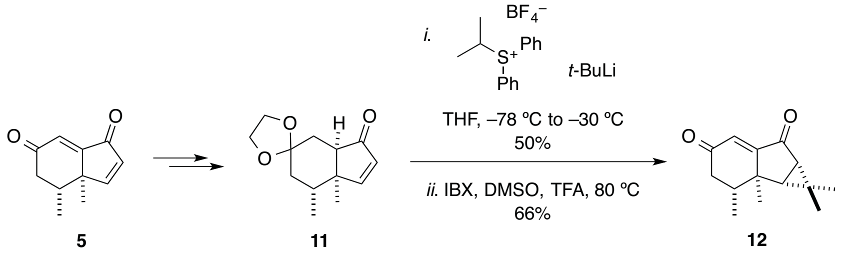
i.
BF4−
S+
Ph
Ph
t-BuLi
THF, −78 °C to −30 °C
50%
ii. IBX, DMSO, TFA, 80 °C
66%
O
H
5
11
12

Scheme 4 Synthesis of *exo*-cylopropanated (±)-nardoaristolone B analogue.

(–)-Aristolone

As it has already mentioned, (–)-aristolone was isolated from the roots of *Nardostachys chinensis*,[112] the sesquiterpene was isolated for the first time from the roots and the fruits of *Aristolochia debilis* Sieb. et Zucc. in 1955.[120] However, its structure was not determined until the early 60s, when the groups of Furukawa and Büchi could establish the absolute configuration of the natural product.[121] Since then, three different total syntheses of (±)-aristolone have been reported in the literature.

---

[120] Kariyone, T.; Naito, S. *J. Pharm. Soc. Japan* **1955**, *75*, 1511–1516.

[121] (a) Furukawa, S.; Oyamada, K.; Soma, N. *J. Pharm. Soc. Japan* **1961**, *81*, 565-570. (b) Büchi, G.; Greuter, F.; Tokoroyama, T. *Tetrahedron Lett.* **1962**, 827–833.

The Robinson annulation of methyl vinyl ketone with 2,3-dimethylcyclohexanone was the starting point of the first synthesis.[122] Treatment of the conjugated bicyclic ketone **13**, obtained as a 2:3 mixture of diastereomers (in disfavor of the desired one), with Li-NH_3 gave the *trans*-2-decalone that was brominated after the addition of AcOH and Br_2. Elimination of the halogen upon addition of HMPA (**14**) followed by the addition of 2-diazopropane led to the formation of the pyrazoline ring of **15** by a 1,3-dipolar cycloaddition. Its photolysis gave the formation of (±)-*trans*-dihydroaristolone **16**, which after a bromination / elimination sequence let to the isolation of (±)-aristolone for the first time (Scheme 5).

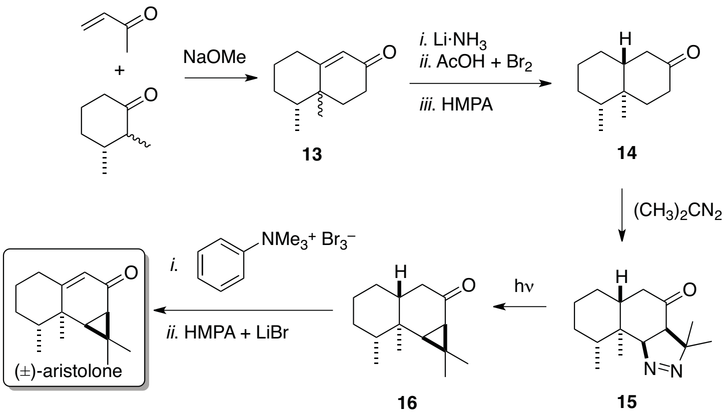

Scheme 5 First total synthesis of (±)-aristolone.[123]

The second synthesis relied on a copper-catalyzed cyclization of diazoketone **23** bearing a pendant olefin to construct the cyclopropyl ring as the key step (Scheme 6).[124] The 6-position of 2,3-dimethylcyclohexanone was blocked using ethyl formate and further converted to its 6-*n*-butylthiomethylene derivative **17**. Alkylation using methallyl chloride followed by the alkaline hydrolysis of the thiomethylene group gave the trialkylated ketone **18** as a 4:1 ratio of diastereomers. Isomerization of **18a** using *p*-toluenesulfonic acid gave the internal olefin **19** along with hemiacetal **20** as a 1.2:1 mixture of products. The diazoketone-containing side chain was introduced using cyanomethylphosphonate giving a mixture of α,β- and β,γ-unsaturated nitriles **21** and **22** in a 2:1 ratio. Hydrolysis of both isomers gave the β,γ-unsaturated carboxylic acid as the sole product that was further converted into its acyl chloride analogue and finally to the corresponding diazoketone **23**. Heating diazoketone **23** at reflux in the presence of $CuSO_4$ gave 42% yield of (±)-aristolone and 20% of (±)-6,7-epi-aristolone.

---

[122] Berger, C.; Franck-Neumann, M.; Ourisson, G. *Tetrahedron Lett.* **1968**, 3451–3452.

[123] Detailed conditions were missing in the original report.

[124] Piers, E.; Britton, R. W.; De Waal, W. *Can. J. Chem.* **1968**, *47*, 831–840.

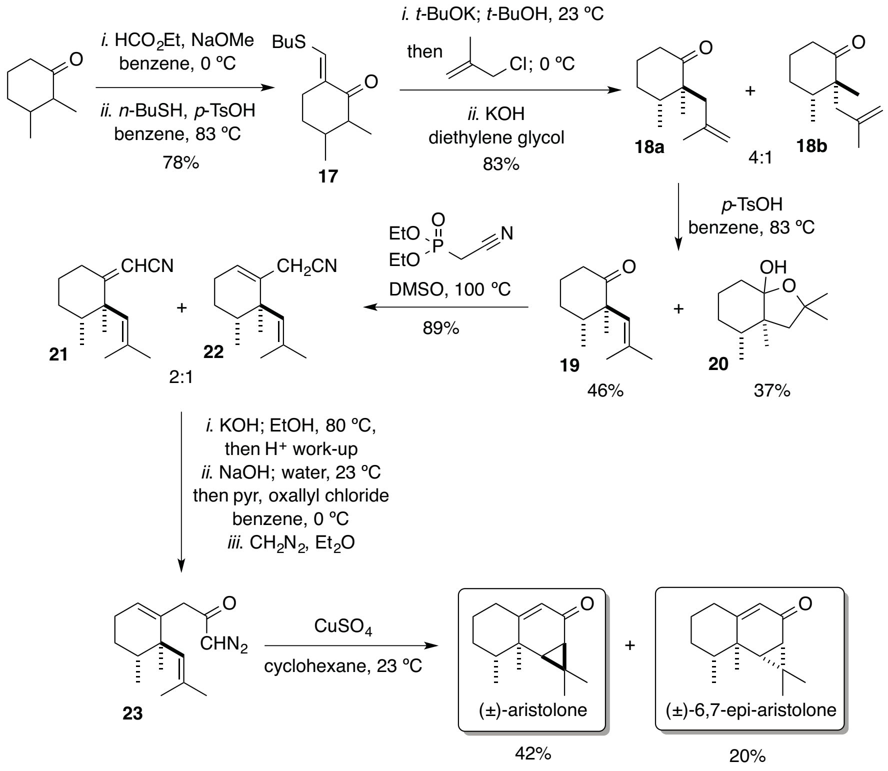
i. HCO2Et, NaOMe benzene, 0 °C
ii. n-BuSH, p-TsOH benzene, 83 °C
78%
BuS
17
i. t-BuOK; t-BuOH, 23 °C
then
Cl; 0 °C
ii. KOH diethylene glycol
83%
18a
4:1
18b
p-TsOH benzene, 83 °C
OH
19
46%
20
37%
EtO
EtO
P
N
DMSO, 100 °C
89%
CHCN
CH2CN
21
22
2:1
i. KOH; EtOH, 80 °C, then H+ work-up
ii. NaOH; water, 23 °C then pyr, oxallyl chloride benzene, 0 °C
iii. CH2N2, Et2O
CHN2
23
CuSO4
cyclohexane, 23 °C
(±)-aristolone
42%
(±)-6,7-epi-aristolone
20%

Scheme 6 Second total synthesis of (±)-aristolone.

The last synthesis was reported by the group of Chan[125] and was based on a methodology disclosed by the same group.[126] 3-(Phenylthio)-1-(trimethylsiloxy)-1-methoxy-1,3-butadienes (**24**) was found to participate in Michael additions with α,β-unsaturated ketones under Lewis acid conditions. Subsequently, a Claisen condensation took place. Interestingly, the annulation could be controlled to give the *trans*- or *cis*- fused compounds stereoselectively. This procedure gave access to the 9-methyldecalin scaffold with a *trans*-junction **25** that was used as the starting point. Treatment with methylmagnesium bromide gave a mixture of isomeric alcohols **26** that were dehydrated using H_2SO_4 yielding **27**. Transformation of the thioether to the enolether followed by hydrogenation in the presence of $Pd/CaCO_3$ conditions delivered **28**. Reduction of **28** using $LiAlH_4$ gave intermediate **14**, which was converted to the final product after following the same synthetic sequence used in the synthesis presented above (Scheme 7).

---

[125] Prasad, C. V. C.; Chan, T. H. *J. Org. Chem.* **1987**, *52*, 120–124.

[126] Chan, T. H.; Prasad, C. V. C. *J. Org. Chem.* **1987**, *52*, 110–119.

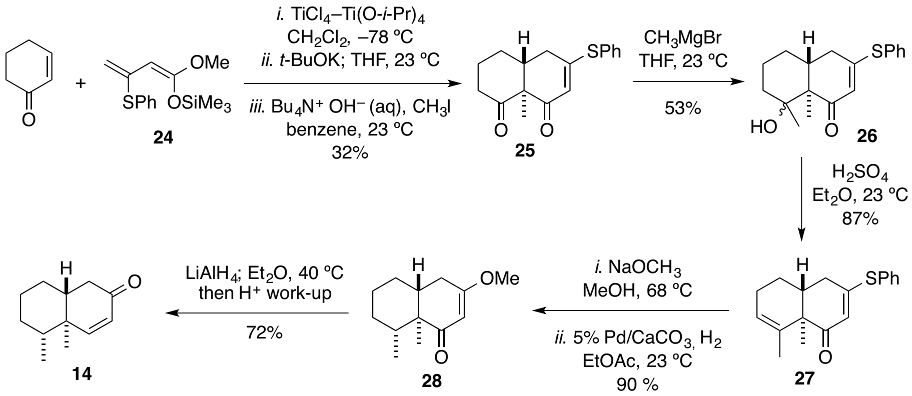
i. TiCl4–Ti(O-i-Pr)4
CH2Cl2, –78 °C
ii. t-BuOK; THF, 23 °C
iii. Bu4N+ OH– (aq), CH3I
benzene, 23 °C
32%
24
25
26
27
28
14
CH3MgBr
THF, 23 °C
53%
H2SO4
Et2O, 23 °C
87%
i. NaOCH3
MeOH, 68 °C
ii. 5% Pd/CaCO3, H2
EtOAc, 23 °C
90 %
LiAlH4; Et2O, 40 °C
then H+ work-up
72%
SPh
OMe
OSiMe3
HO
H
O

Scheme 7 Third total synthesis of (±)-aristolone.

The synthesis of Kanshone H has never been accomplished.

Gold(I) Catalysis in Total Synthesis

As mentioned in the general introduction, the exceptional ability that gold(I) has to activate π-bonds creating complex ring systems has drawn significant attention towards its application in the synthesis of natural products. The high stability of gold catalysts to air and moisture as well as the mild conditions usually required, explain the increasing number of total syntheses involving a gold-catalyzed transformation.[127]

Our group has contributed to the field significantly, first by reporting the syntheses of pubinernoid B (originally proposed structure), orientalol F[91] and englerins A and B.[92] These three molecules share an oxatricyclic skeleton that could originate from a gold(I)-catalyzed [2+2+2] cycloaddition reaction. The key step for the synthesis of (+)-schisanwilsonene A involved a tandem gold(I)-catalyzed cyclization of a 1,6-enyne followed by 1,5-acyloxy migration with a final trapping of the resulting carbene by an intermolecular cyclopropanation.[128] More recently, the synthesis of three aromadendranes ((–)-epiglobulol, (–)-4β,7α-aromadendranediol, and (–)-4α,7α-aromadendranediol) has been completed using a stereodivergent gold(I)-catalyzed cascade reaction (Scheme 8).[129]

---

[127] (a) Zhang, Y.; Luo, T.; Yang, Z. *Nat. Prod. Rep.* **2014**, *31*, 489–503. (b) Rudolph, M.; Hashmi, A. S. K. *Chem. Soc. Rev.* **2008**, *37*, 1766-1775. (c) Rudolph, M.; Hashmi, A. S. K. *Chem. Soc. Rev.* **2012**, *51*, 2448–2462.

[128] Gaydou, M.; Miller, R. E.; Delpont, N.; Ceccon, J.; Echavarren, A. M. *Angew. Chem. Int. Ed.* **2013**, *52*, 6396–6399.

[129] Carreras, J.; Livendahl, M.; McGonigal, P. R.; Echavarren, A. M. *Angew. Chem. Int. Ed.* **2014**, *53*, 4896–4899.

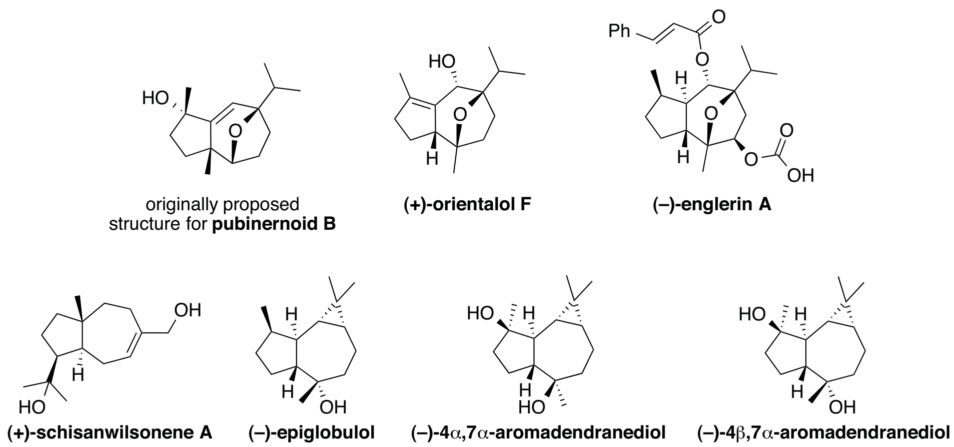
originally proposed structure for pubinernoid B
(+)-orientalol F
(–)-englerin A
(+)-schisanwilsonene A
(–)-epiglobulol
(–)-4α,7α-aromadendranediol
(–)-4β,7α-aromadendranediol

Scheme 8 Total synthesis reported by our group using gold(I)-catalyzed cascade reactions.

However, the use of oxidative gold(I)-catalyzed transformations in total synthesis still remains an untapped opportunity to built-up complexity in a single step.

So far, (±)-cermizine C has been the only natural product synthesized using an intramolecular oxidative gold(I)-catalyzed cyclization (Scheme 9).[130] *Cis*-2,4-dimethylpiperidine (**24**), prepared from 4-methylpiperidine in five steps, was alkylated and converted into quinolizidinone **31** upon addition of *m*-CPBA and the Au(I) source. Final deoxygenation let to the isolation of the desired natural product.

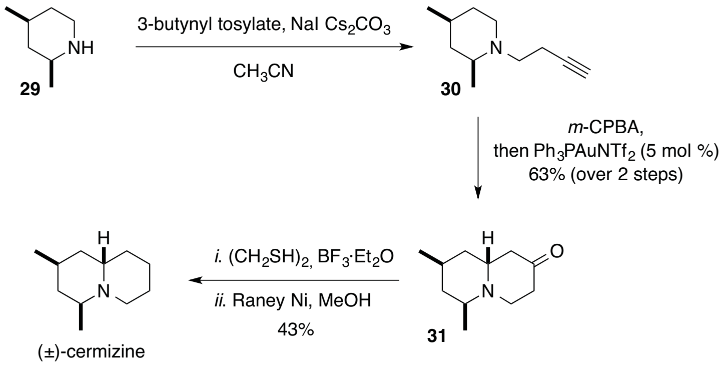
29
3-butynyl tosylate, NaI Cs_2CO_3
CH_3CN
30
m-CPBA,
then $Ph_3PAuNTf_2$ (5 mol %)
63% (over 2 steps)
31
i. $(CH_2SH)_2$, $BF_3·Et_2O$
ii. Raney Ni, MeOH
43%
(±)-cermizine

Scheme 9 Total synthesis of (±)-cermizine C using an oxidative gold(I)-catalyzed cyclization.

The key step involved an initial formation of the tertiary aliphatic amine *N*-oxide that underwent gold-catalyzed intramolecular alkyne oxidation leading to α-oxo gold carbene **I**. Migration of the amine α-hydrogen giving **III** followed by cylization provided the quinolizidinone **31** (Scheme 10).

---

[130] Cui, L.; Peng, Y.; Zhang, L. *J. Am. Chem. Soc.* **2009**, *131*, 8394–8395.

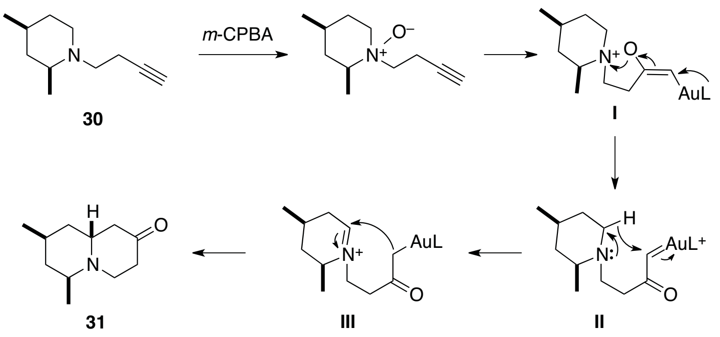

Scheme 10 Au(I)-catalyzed transformation in the synthesis of (±)-cermizine C.

Gold(I)-Catalyzed Oxidative Cyclization of Enynes

As described in the general introduction, in 2011, the group of Liu contributed with a new methodology involving a gold(I) mediated oxidative cycloisomerization of 1,5-enynes (Scheme 11).[35a] The outcome of the reaction could be tuned by the use of terminal or non-terminal alkynes. Products of 5-*exo*-dig cyclization were obtained using 2-aminoalkynylstyrenes analogues, whereas the corresponding 5-*endo*-dig derivatives were isolated with terminal alkynes. 8-Methylquinoline-*N*-oxide and IPrAuNTf$_2$ were found to be the oxidant and gold source of choice, respectively.

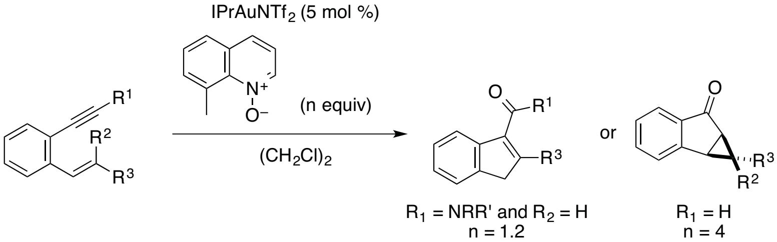

Scheme 11 Oxidative cycloisomerization of 1,5-enynes.

One of the most relevant examples, due to its structural similarity with nardoaristolone B and (–)-aristolone, is the transformation of substrate **32** whose structure is not based on an arene and which gave the cyclopentanone derivative **33** in 78% yield (Scheme 12). Additionally, 1,6-enyne **34** could also be cyclized in 61% yield, although it required a longer reaction time.

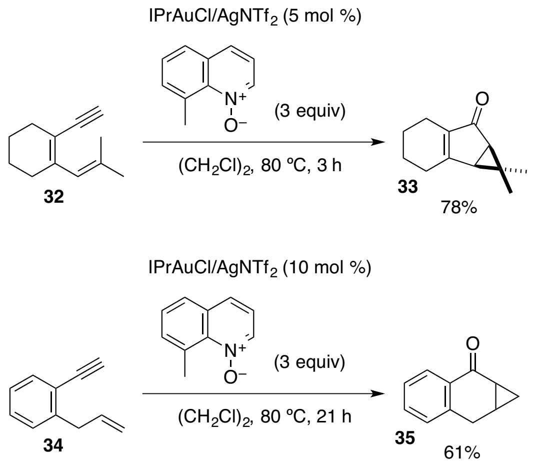
IPrAuCl/AgNTf2 (5 mol %)
N+
O−
(3 equiv)
(CH2Cl)2, 80 °C, 3 h
32
33
78%
O
IPrAuCl/AgNTf2 (10 mol %)
N+
O−
(3 equiv)
(CH2Cl)2, 80 °C, 21 h
34
35
61%
O

Scheme 12 Selected examples of oxidative cyclization of 1,5- and 1,6-enynes.

The authors proposed two different pathways for the cylcloisomerization of terminal alkynes. After the activation of the alkyne by the metal, a 6-*endo*-dig cyclization can take place followed by the oxidation of the resulting carbene giving the tricyclic product **VII**. However, several control experiments supported an alternative mechanism involving the initial oxidation of **IV** giving the α-oxo gold carbene **V** that could further be trapped with the alkene moiety (Scheme 13).

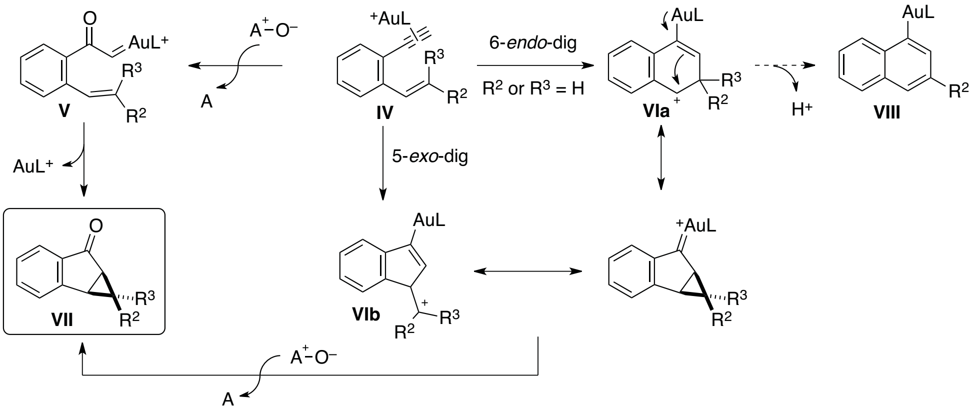
O
AuL+
R3
R2
V
A+–O−
A
+AuL
R3
R2
IV
6-endo-dig
R2 or R3 = H
AuL
R3
R2
VIa
AuL
R2
VIII
H+
AuL+
5-exo-dig
O
R3
VII
R2
AuL
VIb
R2
R3
+AuL
R3
R2
A+–O−
A

Scheme 13 Proposed mechanisms for the formation of tricyclic ketones **VII**.

Nonetheless, we suspect that the first mechanism proposed only applies to non- or monosubstituted alkenes. When the alkene bears two substituents, a 5-*exo*-dig cyclization is favored, since the resulting tertiary carbocation **VIb** is presumably more stable than the benzylic one (**VIa**). In all cases, whether the transformation proceeds via one or the other pathway, ultimately, it leads to the formation of the same product **VII**.

The oxidation / cyclization sequence was the one favored by the authors since **36** was only cyclized under Au-catalyzed conditions when the oxidant was present in the reaction media. Furthermore, **38** was converted to **39** after a proposed α-oxo carbene formation followed by C–H insertion (Scheme 14). Finally, the authors were expecting the rearomatization of hypothetical benzyl cation **VIa** (starting from monosubstituted alkenes) to give naphthalenes **VIII** rather than the oxidized product (Scheme 13).

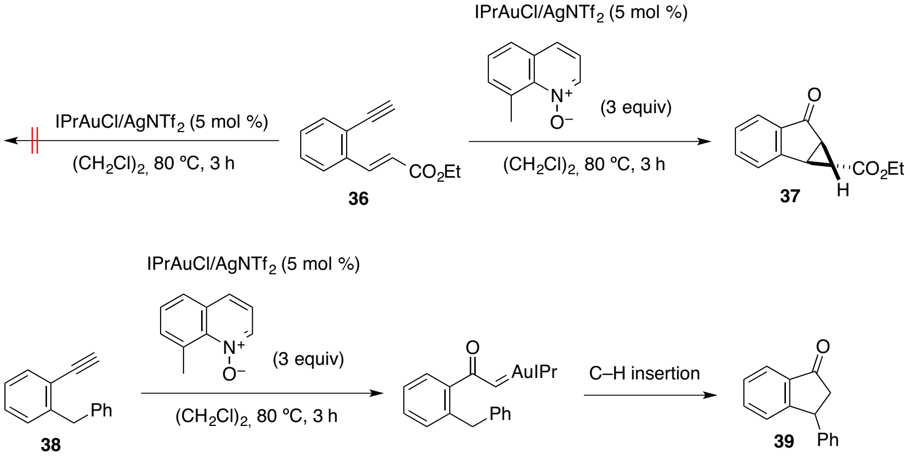
IPrAuCl/AgNTf2 (5 mol %)
(CH2Cl)2, 80 °C, 3 h
CO2Et
36
IPrAuCl/AgNTf2 (5 mol %)
N+
O−
(3 equiv)
(CH2Cl)2, 80 °C, 3 h
O
CO2Et
H
37
IPrAuCl/AgNTf2 (5 mol %)
N+
O−
(3 equiv)
(CH2Cl)2, 80 °C, 3 h
Ph
38
O
AuIPr
Ph
C–H insertion
O
39
Ph

Scheme 14 Control experiments of the Au(I)-catalyzed oxidative cyclization of **36** or **38**.

Objectives

Inspired by the easy accessibility of 6/5/3 tricyclic compounds through the gold(I)-catalyzed oxidative cyclization of terminal 1,5-enynes,[35a] we decided to synthesize for the first time nardoaristolone B in an enantioenriched form (Figure 3).

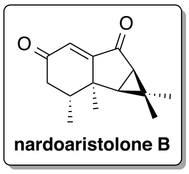

Figure 3 Structure of nardoaristolone B.

Following a parallel approach, we decided to expand the cyclization to 1,6-enynes towards the first asymmetric synthesis of (–)-aristolone and kanshone H (Figure 4).

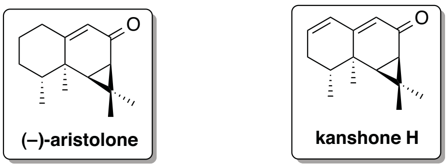

Figure 4 Structures of (–)-aristolone and kanshone H.

Results and Discussion

The retrosynthetic plan envisioned for the synthesis of all the natural products featured an oxidative gold(I)-catalyzed cyclization of a 1,5- or a 1,6-enyne as a key step, inspired by the methodology reported by Liu (Scheme 15).[35a]

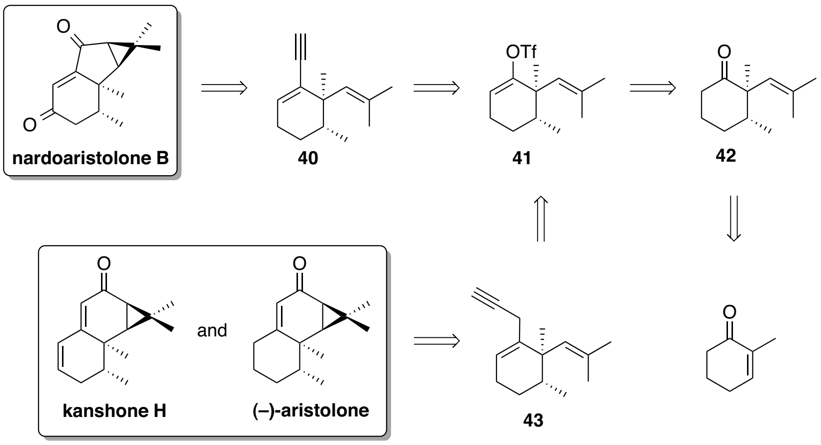

Scheme 15 Convergent retrosynthetic analyses of nardoaristolone B, (–)-aristolone and kanshone H.

The three tricyclic natural products could be accessed from the above-mentioned cyclization of the corresponding 1,5- (**40**) or 1,6-enynes (**43**). These enynes could arise from a common vinyl triflate intermediate **41**, which could be used as the electrophilic coupling partner of a cross coupling reaction. Compound **41** would be formed from its ketone analogue **42** that could be obtained by double alkylation of 2-methylcyclohexenone. Although 2-methylcylohexenone is a commercially available starting material, the price of its precursor 2-methylcyclohexanone is much more attractive (60 €/g vs 0.8 €/g).[131] Therefore, we prepared 2-methylcyclohexenone by bromination of 2-methylcyclohexanone followed by elimination of HBr under basic conditions (Scheme 16). Despite the high yields reported in the literature procedures, under the best conditions 2-methylcylohexenone was obtained in 55%.

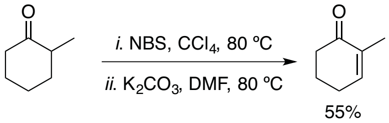

Scheme 16 Synthesis of 2-methylcyclohexenone.

---

[131] Prices checked in Sigma-Aldrich website on 04/11/2014.

Synthesis of trialkylated ketone 42

In order to reach the trialkylated ketone **42**, we studied in parallel two different approaches: a more challenging one pot procedure and the dialkylation through a two (or three)-step process. In both cases, the use of phosphoramidite was crucial to induce enantioselectivity at C-3.[132]

One-step dialkylation reaction

The dialkylation in one step encompassed a copper-catalyzed enantioselective Michael addition of 2-methylcyclohexenone followed by enolate trapping.[133] This reaction had been studied by the group of Alexakis[134] and, later, by the groups of Cramer[135] and Maldonado[136] (Scheme 17). The aluminium enolate could be formed in 90% *ee* after treating 2-methylcyclohexenone with a mixture of a copper source, Feringa's phoshoramidite ligand and $AlMe_3$. The resulting metal enolate could then be trapped with different benzyl and propargyl iodides, whereas the corresponding bromides were unreactive.[135] The addition of MeLi was crucial for this alkylation to proceed, by enhancing the nucleophilic character of the ate-complex,[137] while the use of HMPA as solvent was essential as well. The trapping of the metal-enolate could also be performed using 4-methyl-3-furaldehyde forming the corresponding aldol product.[136] The similar procedure using Grignard reagents was also developed, forming the corresponding magnesium-enolate intermediates that could react with propargyl bromides, activated alkyl or allyl halides and benzyl bromides.[134b] However, in this latter case, Mauduit-type NHC ligand had to be employed since phosphoramidites did not induce enantioselectivity.[138] Besides, addition of MeLi was not required to enhance the nucleophilic character of the enolate. In all the cases, the trisubstitued ketones were isolated as a mixture of diastereomers in favor to the depicted one. The electrophile always approaches from the least hindered face, which is the one opposite the substituent at C-3.[139]

---

[132] For selected reviews in asymmetric conjugate addtions see: (a) Alexakis, A.; Benhaim, C.; *Eur. J. Org. Chem.* **2002**, 3221–3236. (b) Alexakis, A.; Bäckvall, J. E.; Krause, N.; Pàmies, O.; Diéguez, M. *Chem. Rev.* **2008**, *108*, 2796–2823. (c) Haerutyunyan, S. R.; (den) Hartog, T.; Geurts, K.; Minnaard, A. J.; Feringa, B. L. *Chem. Rev.* **2008**, *108*, 2824–2852.

[133] For key pioneering studies on Cu(I)-catalyzed enantioselective conjugate additions of various organometallic reagents see: (a) Alexakis, A.; Mutti, S.; Normant, J. F. *J. Am. Chem. Soc.* **1991**, *113*, 6332–6334. (b) Alexakis, A.; Frutos, J.; Mangeney, P. *Tetrahedron: Asymmetry*, **1993**, *4*, 2427–2430. (c) Feringa, B. L.; Badorrey, R.; Peña, D.; Harutyunyan, S. R.; Minnaard, A. J. *Proc. Natl. Acad. Sci.* **2004**, *101*, 5834–5838. (d) d'Augustin, M.; Palais, L.; Alexakis, A. *Angew. Chem. Int. Ed.* **2005**, *44*, 1376–1378.

[134] (a) Vuagnoux-d'Augustin, M.; Alexakis, A. *Chem.–Eur. J.* **2007**, *13*, 9647–9662. (b) Germain, N.; Guénée, L.; Mauduit, M.; Alexakis, A. *Org. Lett.* **2014**, *16*, 118–121.

[135] Ngoc, D. T.; Albicker, M.; Schneider, L.; Cramer, N. *Org. Biomol. Chem.* **2010**, *8*, 1781–1784.

[136] (a) Guzmán, J. A.; García, E.; Mendoza, V.; De Jesús, D.; Maldonado, L. A. *Rev. Soc. Quim. Mex.* **2004**, *48*, 250−255. (b) Silva, A. L.; Toscano, R. A.; Maldonado, L. A. *J. Org. Chem.* **2013**, *78*, 5282–5292.

[137] Tsuda, T.; Satomi, H.; Hayashi, T.; Saegusa, T. *J. Org. Chem.* **1987**, *52*, 439–443.

[138] Magrez, M.; Le Guen, Y.; Baslé, O.; Crévisy, C.; Mauduit, M. *Chem.–Eur. J.* **2013**, *19*, 1199–1203.

[139] The ranges of diastereoselectivities depended on the methodology used and the bulkyness of the group introduced at C-3.

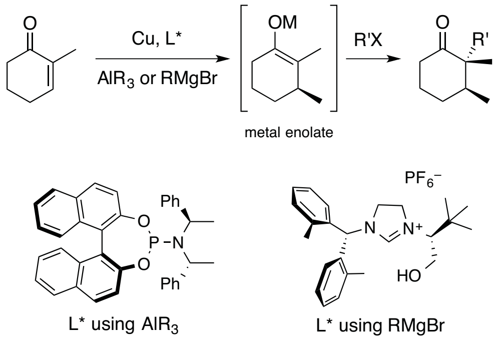

Scheme 17 Cu-catalyzed Michael addition followed by enolate trapping.

We started examining the reaction generating aluminium enolate complexes that were trapped with methallyl bromide. Very low yields were obtained in the firsts attempts recovering mainly the starting material even increasing the reaction times or raising the temperature (Table 1, entry 1). Encouragingly, full conversion was not achieved until we added the phosphoramidite ligand to the reaction mixture: such ligand acceleration has been previously demonstrated.[140] Ketone **45** was always isolated as a byproduct (Table 1, entry 2). In order to have a more reactive electrophile, we decided to generate *in situ* methallyl iodide synthesized from its bromide analogue and NaI. Although only traces of trialkylated ketone **44** were isolated (Table 1, entry 3), the yield was substantially improved using the previously synthesized and isolated electrophile (Table 1, entry 4). Ketone **44** was isolated as a 3:1 mixture of separable diastereomers with a 91–92% *ee*.[141] Other attempts to improve this yield were unsuccessful. Remarkably, when MeLi was not added, the desired product **44** was not formed, leading mainly to the isolation of ketone **45** (Table 1, entry 5). In order to improve the levels of *dr*, we tried to use methally triflate. However, its synthesis proved to be unsuccessful (the neat product decomposed spontaneously). Substituting $AlMe_3$ to $ZnMe_2$ did not give the Michael addition product, and only starting material was recovered.

Table 1 Optimization of the conditions for the Cu(I)-catalyzed conjugate addition followed by Al-enolate trapping.

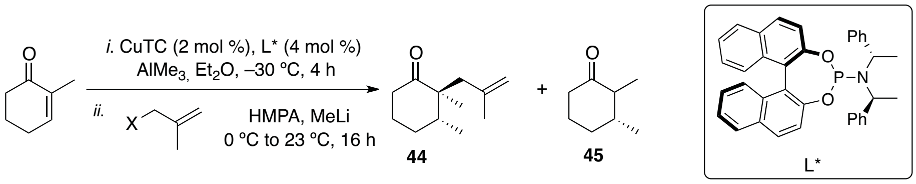

---

[140] Berrisford, D.; Bolm, C.; Sharpless, K. B. *Angew. Chem. Int. Ed.* **1994**, *34*, 1059–1070.

[141] 3:1 *dr* determined by ^{1}H NMR; 91–92% *ee* (IC column, Hex:IPA 99:1, 0.85 mL/min, [sample] = 5 mg/mL, 5 mL injection, 310 nm).

Entry	Electrophile	Yield 44 and 45	Change from standard conditions
1	X = Br	7% [a]	No ligand added
2	X = Br	18% and 24%	-
3	X = I	6% and 20%	Electrophile generated *in situ* from methallyl bromide and NaI
4	**X = I**	**45% and 15-20%**	**-**
5	X = I	9% and 62%	MeLi not added
6	X = I	No reaction	$ZnMe_2$ instead of $AlMe_3$

[a] 60% conversion.

We then further optimized these reaction conditions decreasing the amount of electrophile used as well as solvent without any drop in the yield, *dr* or *ee* (Table 2). Although this transformation was performed with the utmost precautions, yields ranged from 45–52% obtaining between 15–20% of **45** as byproduct. The yield of **44** could finally be improved up to 55% upon addition of THF as solvent in the second step whilst the amount of **45** was reduced.

Table 2 Optimization of the conditions for the Cu(I)-catalyzed conjugate addition followed by Al-enolate trapping.

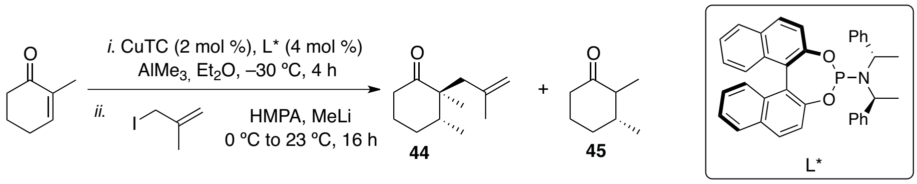

Entry	Change from standard conditions	Yield 44
1	1 mmol scale; 2 mL Et_2O and 2 mL HMPA 2 equiv electrophile	48%
2	7 mmol scale; 3 mL Et_2O and 3 mL HMPA 2 equiv electrophile	52%
3	9 mmol scale; 4 mL Et_2O and 4 mL HMPA 1.3 equiv electrophile	45%
4	**18 mmol scale; 15 mL Et_2O, 15 mL THF and 12 mL HMPA** **1.7 equiv electrophile**	**55%**

Since this reaction was performed several times, the amount of byproduct **45** was significant. We then decided to convert it into the trialkylated ketone **44** by using a slightly modification of Piers' procedure.[124,142] Reaction of **45** with ethyl formate blocked the position at C-6 forming hydroxymethylene ketone **46**. Addition of *n*-butanethiol gave intermediate **47**, which could easily be alkylated using methallyl bromide. Final hydrolysis of the protecting thiomethylene group led to the isolation of ketone **44** as a 4:1 mixture of diastereomers (Scheme 18).

---

[142] Mace, L. H.; Shanmugham, M. S.; White, J. C.; Drew, M. G. B. *Org. Biomol. Chem.* **2006**, *4*, 1020–1031.

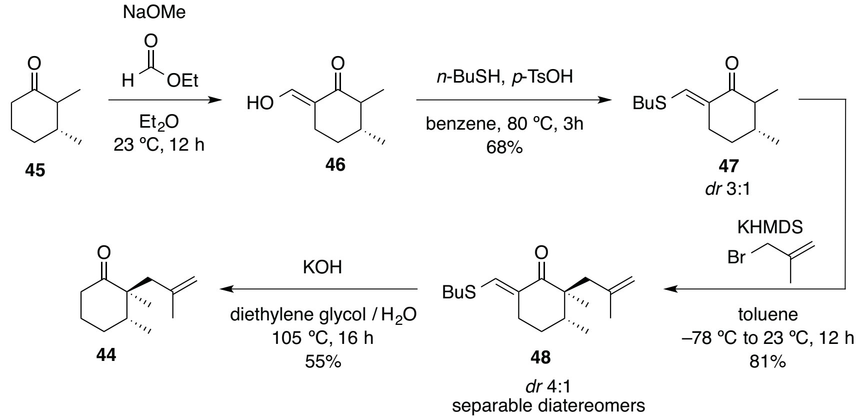
NaOMe
H OEt
Et2O
23 °C, 12 h
45
HO
46
n-BuSH, p-TsOH
benzene, 80 °C, 3h
68%
BuS
47
dr 3:1
KHMDS
Br
toluene
–78 °C to 23 °C, 12 h
81%
48
dr 4:1
separable diatereomers
KOH
diethylene glycol / H2O
105 °C, 16 h
55%
44

Scheme 18 Recycling hydrolyzed ketone **45** to trialkylated ketone **44**.

When isobutyraldehyde was the electrophile, the resulting aldol product **49** could only be obtained in 6% yield. Trying to change the conditions by adding MeLi to the enolate or HMPA did not give any product (Scheme 19).

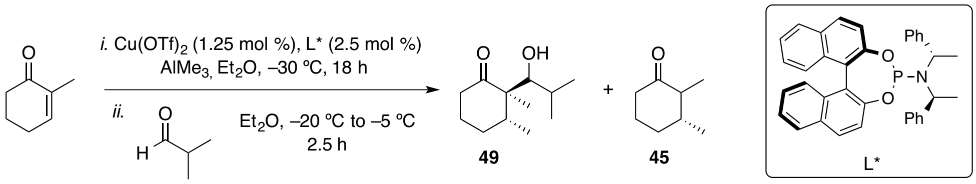
i. Cu(OTf)2 (1.25 mol %), L* (2.5 mol %)
AlMe3, Et2O, –30 °C, 18 h
ii.
H
Et2O, –20 °C to –5 °C
2.5 h
OH
49
+
45
Ph
O
P-N
O
Ph
L*

Scheme 19 Enantioselective Cu(I)-catalyzed conjugate addition followed by Al-enolate trapping.

We then switched to the magnesium-enolate approach. Since the synthesis of the Mauduit-type NHC ligand involves 5 steps,[134b] we initially screened the reaction conditions using a simpler and commercially available carbene. The improved yield observed with the trapping of methallyl bromide (compared to the one obtained from the aluminium-enolate trapping) was attributed to the higher nucleophilicity of the resulting metal-enolate. When methallyl iodide was utilized instead, the desired product **44** was obtained in 51% in a 3.6:1 mixture of diastereomers along with 20% of 2,3-dimethylcyclohexanone (**45**) (Table 3).

Table 3 Optimization of the conditions for the Cu(I)-catalyzed conjugate addition followed by Mg-enolate trapping.

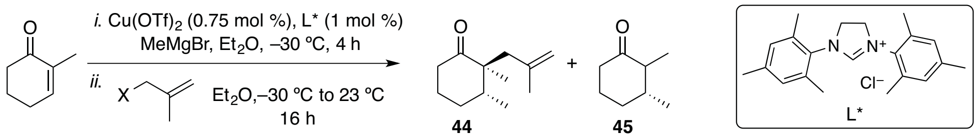
i. Cu(OTf)2 (0.75 mol %), L* (1 mol %)
MeMgBr, Et2O, –30 °C, 4 h
ii. X
Et2O,–30 °C to 23 °C
16 h
44
+
45
N
N+
Cl–
L*

Entry	Electrophile	Yield 44 and 45
1	X = Br	30% and 5% [a]
2	**X = I**	**51% and 20%**

[a] 90% conversion.

The use of the NHC-Maudit carbene gave moderate levels of enantioselectivities in the described methodology (80% *ee* in all the examples)[134b] and its synthesis was complex. Therefore, we decided to use the aluminium-enolate procedure.

Two or three-steps dialkylation reaction

For this approach we sought to perform an enantioselective conjugate addition of the methyl group at C-3 following the procedure described by Alexakis.[134a] However, we decided to initially focus on the more difficult second alkylation. Early attempts to alkylate 2,3-dimethyl-1-trimethyloxycyclohexene gave a mixture of mono- and doubly alkylated products in very low yields although the base used was MeLi, which is known to favor the formation of thermodynamic enolates (Scheme 20).[143]

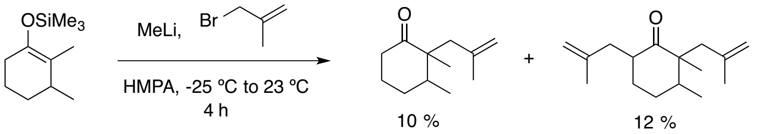

Scheme 20 Alkylation of 2,3-dimethyl-1-trimethyloxycyclohexene with MeLi.

To avoid the polyalkylation, we converted the thermodynamic controlled lithium-enolate to its manganese analogue. The resulting Mn-enolates had been found to give monoalkylated ketones regioselectively.[144] Despite our efforts, only traces of the desired alkylated ketone were observed.

The group of Yamamoto designed a new protocol in which the enolate formed under kinetically controlled conditions was resulting in the alkylation at the more hindered α-position. [145] The combination of the bulky aluminium tris(2,6-diphenylphenoxide) (ATPH) and LDA was essential to make the reaction proceed. This new procedure provides an entry for the highly selective alkylation at the more-substituted α-carbon of unsymmetrical ketones. However, this approach was not successful in our case, recovering most of the starting material (Scheme 21).

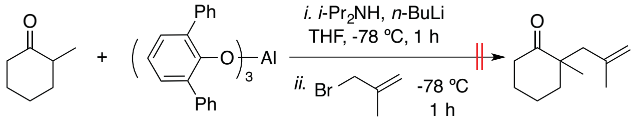

Scheme 21 Failure to alkylate 2-methylcyclohexanone with LDA and ATPH.

The low reactivity of the methallyl bromide used as electrophile made us turn our attention to another highly regioselective protocol. Different aldehydes could be added to the encumbered α-position of unsymmetrical ketones, including 2-methylcyclohexane, upon addition of catalytic quantities of $TiCl_4$.[146] When we tried to reproduce the reaction between 2-methylcyclohexanone and isobutyraldehyde under the conditions reported, only decomposition of starting materials was observed (Scheme 22).

---

[143] Posner, G. H.; Sterling, J. J.; Whitten, C. E.; Lentz, C. M.; Brunelle, D. J. *J. Am. Chem. Soc.* **1975**, *97*, 107–118.

[144] Cahiez, G.; Chau, K.; Cléry, P. *Tetrahedron Lett.* **1994**, *35*, 3069–3072.

[145] Saito, S.; Ito, M.; Yamamoto, H. *J. Am. Chem. Soc.* **1997**, *119*, 611–612.

[146] Mahrwals, R.; Gündogan, B. *J. Am. Chem. Soc.* **1998**, *120*, 413–414.

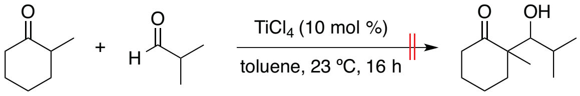

Scheme 22 Failure to add isobutyraldehyde to 2-methylcyclohexanone in the presence of TiCl$_4$.

We finally tried the coupling of silyl enol ether **50** and dimethallyl carbonate **51** using a Pd-catalyzed decarboxylative alkylation reaction based on a reported methodology.[147] The reaction was initiated by the presence of tetra-*n*-butylammonium difluorotriphenylsilicate (TBAT) generating the enolate that could be coupled to the {Pd^{II}(allyl)} species formed during the course of the reaction by decarboxylation of **51**. Although the reaction proceeded very efficiently (79% reported yield) using 2-methyl-1-trimethyloxycyclohexene (**50**) and **51**, the yield dropped to 10% using the same enol ether with a methyl group at C-3. Starting material was also recovered (Scheme 23). It is worth mentioning that none of the reported examples feature a tertiary or quaternary carbon at C-3.

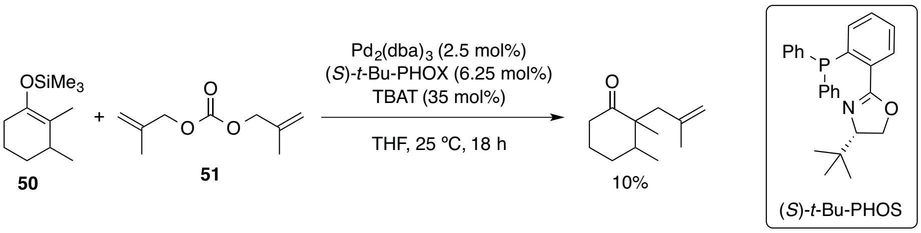

Scheme 23 Pd-catalyzed decarboxylative alkylation of 2,3-dimethyl-1-trimethyloxycyclohexene.

Since none of the reactions among this two-step processes were effective, we focused on the straightforward one-pot procedure using AlMe$_3$ and methallyl iodide.

We then focused our attention on the isomerization of the terminal double bond of **44**. The group of Piers had performed this transformation under acid-catalyzed conditions obtaining a mixture of isomerized trisubstituted ketone **19** and the hemiacetal **20** in 46% and 37% yield, respectively (Scheme 6).[124] The byproduct could be avoided protecting the ketone as its ethylene acetal form (**52**). Despite the fact that the isomerization then proceeded quantitatively, the poor-yielding transacetalization was a major drawback (Scheme 24).[142]

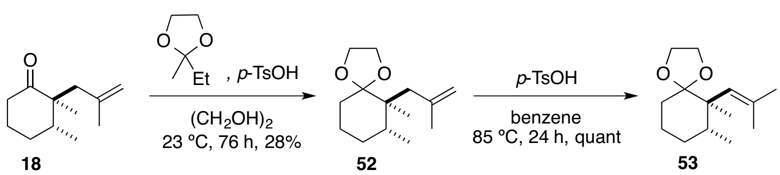

Scheme 24 Transacetalization of trisubstituted ketone **18** followed by isomerization of the alkene.

---

[147] Behenna, D. C.; Mohr, J. T.; Sherden, N. H.; Marinescu, S. C.; Harned, A. M.; Tani, K.; Seto, M.; Ma, S.; Novák, Z.; Krout, M. R.; McFadden, R. M.; Roizen, J. L.; Enquist, Jr., J. A.; White, D. E.; Levine, S. R.; Petrova, K. V.; Iwashita, A.; Virgil, S. C.; Stoltz, B. M. *Chem–Eur. J.* **2011**, *17*, 14199–14223.

$RhCl(PPh_3)_3$ was also found to isomerize the terminal double bond after refluxing **18** in EtOH for 72 h.[142] Although the reported yield was 55%, when we tried to reproduce these conditions, the desired product was not formed (Table 4, entry 1). We then decided to screen different metal complexes and acids capable of isomerizing olefins. Whilst $PdCl_2(PhCN)_2$ gave only traces of product in our system (Table 4, entry 2),[148] $RhCl_3{\cdot}nH_2O$ showed greater efficiency (Table 4, entry 3).[149] The use of Crabtree's iridium(I) catalyst had shown migration abilities under H_2 pressure,[150] although in our system, the method only afforded the reduction of the olefin (Table 4, entry 4). Trisubstituted ketone **44** decomposed upon addition of triflic acid (Table 4, entry 5).[151]

Table 4 Screening of conditions to isomerize the terminal olefin.

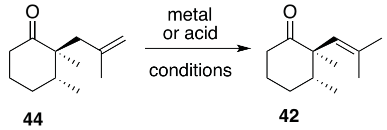

44 **42**

Entry	Metal or acid	Conditions	Outcome[a]
1	$RhCl(PPh_3)_3$	EtOH, reflux, 52 h	No reaction
2	$PdCl_2(PhCN)_2$	$(CH_2Cl)_2$, reflux, 20 h	Traces of **42**
3	$RhCl_3{\cdot}nH_2O$[b]	EtOH, sealed tube 115 ºC, 1 h	42% of **42** + 10% **44**
4	Crabtree's Ir catalyst	H_2, CH_2Cl_2, 0 ºC to 23 ºC, 12 h	Hydrogenated **42**
5	CF_3SO_3H	dioxane, 95 ºC, 30 h	Decomposition

[a] All these reactions were performed using a 3:1 mixture of diastereomers. [b] Rh source from Stream Chemicals.

The mechanism of migration varies according to the metal (or acid) and the conditions used. Our system could not tolerate acid-catalyzed conditions, and the formation of π-allyl complexes (formed using $PdCl_2(PhCN)_2$ that would evolve through 1,3-hydrogen migrations) was difficult.[152] Thus, we decided to focus on the most promising result obtained when using $RhCl_3$.

Surprisingly, when we reproduced the migration using $RhCl_3{\cdot}nH_2O$ under the same isomerization conditions the reaction failed. Examining the experimental setup more closely, we discovered that the Rh source used was purchased from Sigma-Aldrich whereas in the first experiment it was supplied by Stream Chemicals. We then examined the optimal reaction conditions using a 3:1 mixture of diasteromers (**44** and **44'**). The conversion could be increased by reducing the temperature to 70 ºC (Table 5, entry 1) and increasing the reaction time (Table 5, entry 2). Surprisingly, the desired diasteromer was reacting preferentially. When the reaction was left for prolonged time, full conversion could never be reached, while both, starting material and product were decomposed to some extend (Table 5, entry 3). Only traces of product were observed under refluxing conditions (Table 5, entry 4). The reaction could also be performed under MW irradiation reducing the reaction time (Table 5, entries 5, 6 and 7). The use of other solvents did not improve the reaction efficiency (Table 5, entries 8 and 9).

---

[148] Hatanaka, N.; Ozaki, O.; Matsumoto, M. *Tetrahedron Lett.* **1986**, *27*, 3169–3172.

[149] Nickel, A.; Maruyama, T.; Tang, H.; Murphy, P. D.; Greene, B.; Yusuff, N.; Wood, J. L. *J. Am. Chem. Soc.* **2004**, *126*, 16300–16301.

[150] Krel, M. K.; Lallemand, J.-Y.; Guillou, C. *Synlett* **2005**, 2043–4046.

[151] (a) Kozikowski, A. P.; Campiani, G.; Aagaard, P.; McKinney, M. *J. Chem. Soc. Chem. Commun.* **1993**, 860–862. (b) Campiani, G.; Sun, L.-Q., Kozikowski, A. P.; Aagaard, P.; Mckinney, M. *J. Org. Chem.* **1993**, *58*, 7660–7669.

[152] (a) Harrod, J. F.; Chalk, A. J. *J. Am. Chem. Soc.* **1966**, *88*, 3491–3497. (b) Sen, A.; Lai, T.-W. *Inorg. Chem.* **1984**, *23*, 3257–3258.

Table 5 Optimization of the conditions for the $RhCl_3$-catalyzed isomerization.

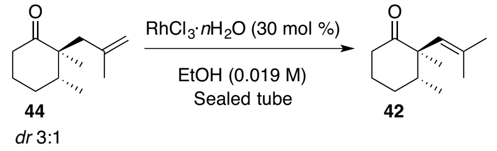

Entry	Time	Temp	Yield (42 + 44)[a]	*dr*	Change from standard conditions
1	1 h	70 ºC	51% + 20%	12:1	-
2	**4 h**	**70 ºC**	**60% + 14%**	**6:1**	**-**
3	13 h	70 ºC	40% + 3%	3:1	-
4	4 h	80 ºC	8% + 70%	-	Reflux
5	1.5 h	70 ºC	60% + 14%	7:1	MW irradiation
6	1.5 h	80 ºC	45% + 16%	6:1	MW irradiation
7	2 h	60 ºC	25% + 55%	13:1	MW irradiation
8	1.5 h	70 ºC	0 + 55%	-	MeOH as solvent MW irradiation
9	1.5 h	70 ºC	46% + 9%	4:1	*i*-PrOH as solvent MW irradiation

[a] Yield determined by ^1H NMR using diphenylmethane as internal standard.

The proposed mechanism features an initial coordination of the metal to the olefin that undergoes hydride insertion through a hydride-transfer mechanism, where the hydride originates from the solvent.[153] $RhCl_3$ is believed to undergo an initial reduction to Rh(I) under the isomerization conditions.

Considering the reaction as an equilibrium and therefore knowing that full conversion would not be attained, we set up the reaction using pure diastereomer **44** at 75 ºC for 4.5 h. We were then delighted to isolate **42** in 75% yield, containing traces of the unreacted ketone **44**. We could further optimize the reaction conditions by reducing the amount of catalyst to 5 mol % and increasing the concentration to 0.078 M without a significant drop in yield (Scheme 25).

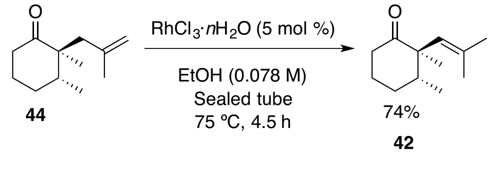

Scheme 25 $RhCl_3$-catalyzed isomerization of **44**.

---

[153] (a) Harrod, J. F.; Chalk, A. J. *J. Am. Chem. Soc.* **1964**, *86*, 1776–1779. (b) Hubert, A. J.; Reimlinger, H. *Synthesis* **1969**, 405–430.

Synthesis of 1,5-Enyne Towards Nardoaristolone B

For the synthesis of 1,5-enyne precursor, we envisioned two different strategies. The first one involved the formation of the enol triflate **41** from ketone **42** followed by a cross coupling reaction. In parallel, reacting **42** with ethynyl magnesium bromide followed by elimination of the hydroxyl group could also give access the desired enyne.

Ketone **42** could be converted into **41** using LDA and the triflating reagent 2-[*N*,*N*-bis(trifluoromethylsulfonyl)amino]pyridine in 82% yield (Scheme 26).

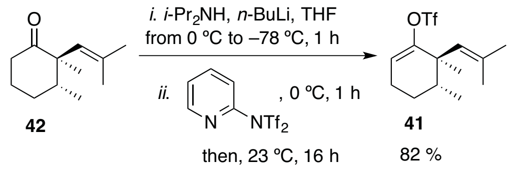
O
42
i. i-Pr$_2$NH, *n*-BuLi, THF
from 0 °C to –78 °C, 1 h
ii.
N
NTf$_2$
, 0 °C, 1 h
then, 23 °C, 16 h
OTf
41
82 %

Scheme 26 Triflation of the isomerized ketone **42**.

Enol triflate **41** could then be coupled to ethynyltrimethylsilane using standard Sonogashira cross coupling conditions. Upon methanolysis of the TMS group, 1,5-enyne **40** was isolated in 74% yield over two steps (Scheme 27). All the attempts to access to the 1,5-enyne in one step from triflate **41** using a Kumada cross coupling were unsuccessful. Different Ni, Pd and Co[154] catalysts were screened but **40** was not observed.

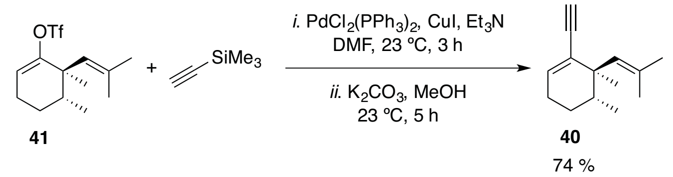
OTf
41
+
SiMe$_3$
i. PdCl$_2$(PPh$_3$)$_2$, CuI, Et$_3$N
DMF, 23 °C, 3 h
ii. K$_2$CO$_3$, MeOH
23 °C, 5 h
40
74 %

Scheme 27 Sonogashira cross coupling reaction followed by deprotection of TMS group.

Isomerized ketone **42** could be converted into its propargylated alcohol **54** upon addition of ethynyl magnesium bromide in 43% yield. Its dehydration under acidic conditions let to the undesired cyclic ether **55** (Scheme 28).

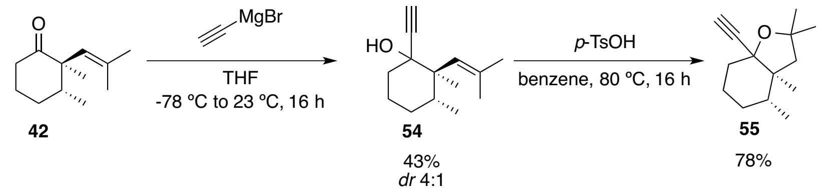
O
42
MgBr
THF
-78 °C to 23 °C, 16 h
HO
54
43%
dr 4:1
p-TsOH
benzene, 80 °C, 16 h
O
55
78%

Scheme 28 Generation of propargyl alcohol **54** followed by formation of cyclic enol ether **55**.

---

[154] Shirakawa, E.; Sato, T.; Imazaki, Y.; Kimura, T.; Hayashi, T. *Chem. Commun.* **2007**, *47*, 4513–4515.

Gold(I)-Catalyzed Cyclization to Access to Nardoaristolone B

The first trial for the gold(I)-catalyzed oxidative cyclization was done using the reported optimized conditions.[35a] Full conversion was obtained after heating **40** with IPrAuNTf$_2$ as catalyst and 8-methylquinoline-*N*-oxide at 80 ºC for 4 h (Scheme 29). The tricyclic oxidized compound **56** could be isolated in 20% yield along with the cycloisomerized product **57** arising from the 5-*endo*-dig cyclization.

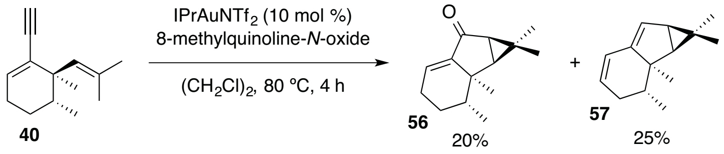

Scheme 29 Oxidative Au(I)-catalyzed cyclization of 1,5-enyne **40**.

In order to increase the yield of the oxidized product, we decided to screen the most common oxidants used in this type of oxidative cyclizations (Table 6).[155]

Table 6 Screening of different oxidants in the Au(I)-catalyzed reaction.

Entry	Oxidant	Yield 56	Yield 57
1	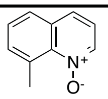	20%	25%
2	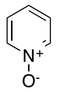	31%	5%
3	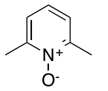	20%	36%
4	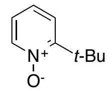	0%	44%
5	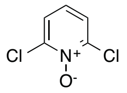	0%	55%
6	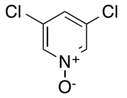	74%	10%
7	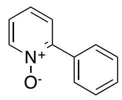	21%	9%[b]
8	No oxidant[c]	-	-

[a] Yield determined by ^{1}H NMR using diphenylmethane as internal standard. [b] 12% of unreacted starting material left. [c] Only decomposition was observed.

While the use of simple pyridine-*N*-oxide gave almost only the desired product albeit in low yield (Table 6, entry 2), 2,6-dimethylpyridine-*N*-oxide gave a 1:2 mixture of the oxidized and non-oxidized products (Table 6, entry 3), respectively. Interestingly, tricyclic compound **57** was obtained exclusively using 2-*tert*-butyl- or 2,6-dichloropyridine-*N*-oxide (Table 6, entries 4 and 5). The optimal oxidant proved to be 3,5-dichloropyridine-*N*-oxide, which gave **56** in 74% yield (Table 6, entry 6). The use of 5 mol % of Au in this last case did not result in any drop in the yield. Remarkably, the 1,5-enyne was fully decomposed when no oxidant was added (Table 6, entry 8).

---

[155] (a) Kawade, R. K.; Liu, R.-S. *Org. Lett.* **2013**, *15*, 4094–4097. (b) Henrion, G.; Chavas, T. E. J.; Goff, X. L.; Gagosz, F. *Angew. Chem. Int. Ed.* **2013**, *52*, 6277–6282.

To explain the generation of the cycloisomerized product **57**, the initial formation of α-oxo gold carbene has to be ruled out. However, the use of the pyridine-*N*-oxide is required since the reaction does not take place in the absence of the additive. It is likely that a 5-*endo*-dig cyclization initially takes place to form **IX**, followed by a proton abstraction at the α-position of the unsaturated carbon to give **XI**. Oxidation of carbene **IX** would lead to **X**, which finally gives **56** (Scheme 30).

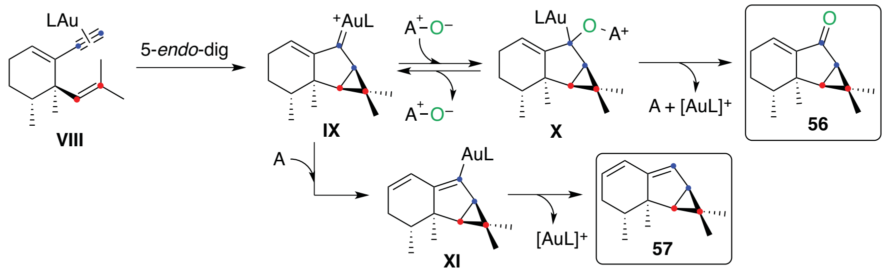

Scheme 30 Plausible mechanism for the gold(I)-catalyzed step.

The outcome of the reaction seems complex and no simple rationale can be proposed. No trend is observed between the ratio of cycloisomerized product **57** and the pK_a of the corresponding pyridine (Table 7). This supports that several factors such as the nucleophilicity of the *N*-oxide, basicity of the pyridine and/or pyridine *N*-oxide, nucleofugacity of the pyridine or/and steric hindrance of the pyridine-*N*-oxide might be at play.

Table 7 pK_a of the pyridine precursors of the additives used as oxidants.

Oxidant	pK_a
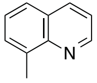	4.9
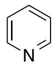	5.2
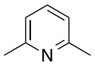	6.6
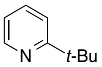	5.8
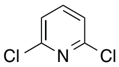	–3.8
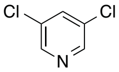	0.4
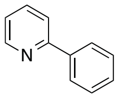	4.9

A final screening of different ligands in the gold(I) catalyzed transformation was carried out (Table 8). Interestingly, the two Buchwald-type phosphines employed gave substantially different results despite their structural similarity (Table 8, entries 1 and 2). The use of the two most electronically distinct gold complexes (phosphite and NHC carbenes) gave the same outcome (Table 8, entreies 3, 4 and 5). Finally, IPrAuNTf_2 remained the most efficient catalyst. We could not observe any correlation between the electrophilicity of the ligand used and the preferent formation of the cycloisomerized product **57** or the oxidized tricycle **56**.

Table 8 Screening of different Au(I) catalysts.

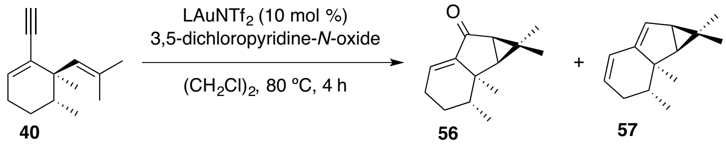

Entry	L	Yield 56	Yield 57
1	JohnPhos	43%	15%
2	*t*BuXPhos	18%	15%
3	tris(2,4-di-*tert*-butylphenyl)phosphite	55%	2%
4	IMes	55%	2%
5	IPr	74%	15%

Allylic Oxidation: Nardoaristolone B

The end-game of the synthesis was accomplished by allylic oxidation of **56**. The use of excess of CrO_3 and 3,5-dimethylpyrazole gave only traces of product.[156] We decided to switch to another methodology avoiding the use of Cr, by following the procedure described by Yu and Corey.[157] Nardoaristolone B was obtained in 93% yield treating **56** with $Pd(OH)_2/C$ and *t*-BuOOH under basic conditions (Scheme 31).

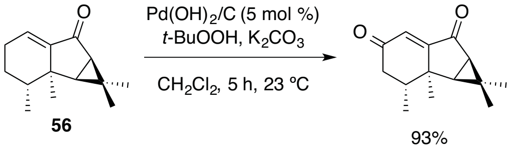

Scheme 31 Allylic oxidation of **56** using Pearlmann's catalyst and *t*-BuOOH.

---

[156] Salmond, W. G.; Barta, M. A.; Havens, J. L. *J. Org. Chem.* **1978**, *43*, 2057–2059.

[157] Yu, J.-Q.; Corey, E. J. *J. Am. Chem. Soc.* **2003**, *125*, 3232–3233.

Approach to the Synthesis of (–)-Aristolone and Kanshone H: Synthesis of 1,6-Enyne

For the synthesis of the 1,6-enyne we considered six different approaches: propargylation and regioselective elimination, Horner-Emmons reaction and other classical transformations, vinyl bromide formation followed by alkylation, Shapiro reaction and propargylation, homologation reaction and finally, cross-coupling reaction (Scheme 32). Some of these reactions were first studied using methylcyclohexanone derivatives as model systems.

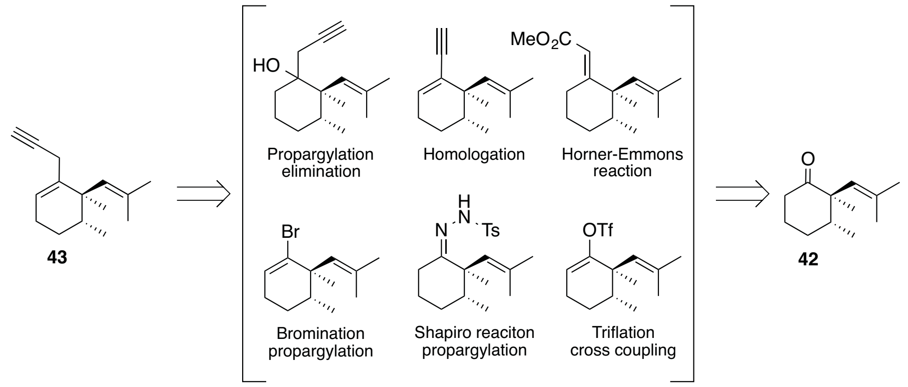
HO
Propargylation elimination
Homologation
MeO2C
Horner-Emmons reaction
43
42
O
Br
Bromination propargylation
H
N
N
Ts
Shapiro reaciton propargylation
OTf
Triflation cross coupling

Scheme 32 Different approaches to access the 1,6-enyne **43**.

Propargylation and Regioselective Elimination

2-Methylcyclohexanone could be easily propargylated using a Grignard reaction in 85% yield as a mixture of diastereomers. However, the elimination under dehydrating conditions gave rise to a mixture of different *endo* and *exo* isomers.[158] The different components obtained could not be separated by chromatography due to their very similar polarities (Scheme 33).

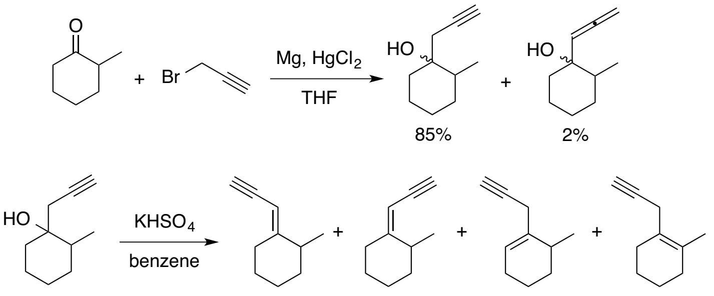
O
+
Br
Mg, HgCl2
THF
HO
+
HO
85%
2%
HO
KHSO4
benzene
+
+
+

Scheme 33 Propargylation of 2-methylcyclohexanone followed by dehydration.

Despite the difficulties to find the appropriate conditions to get a regioselective elimination of the hydroxyl moiety, we decided to propargylate the trialkylated ketone. The resulting tertiary alcohol was generated as a mixture of diastereomers that could be separated by chromatography. They were later subjected to oxidative gold(I)-catalyzed conditions

---

[158] Mondon, A. *Justus Liebigs Annalen der Chemie,* **1952**, 181–201.

(Scheme 34). No product was observed, although the starting materials were fully consumed.

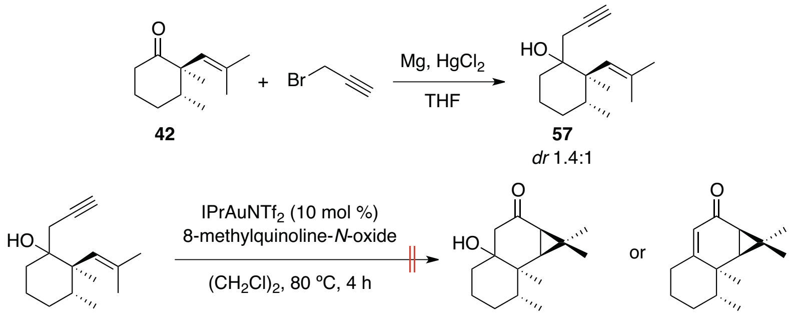
42
Br
Mg, HgCl$_2$
THF
HO
57
dr 1.4:1
IPrAuNTf$_2$ (10 mol %)
8-methylquinoline-N-oxide
(CH$_2$Cl)$_2$, 80 °C, 4 h
O
or

Scheme 34 Propargylation of trialkylated ketone **42** followed by oxidative gold(I)-catalyzed reaction.[159]

We decided to protect the alcohol using a group that would not give migration during the cyclization product.[160] Treatment of **57** with 2,6-dimethylpyridine and TMSOTf gave the corresponding protected tertiary alcohol (Scheme 35).

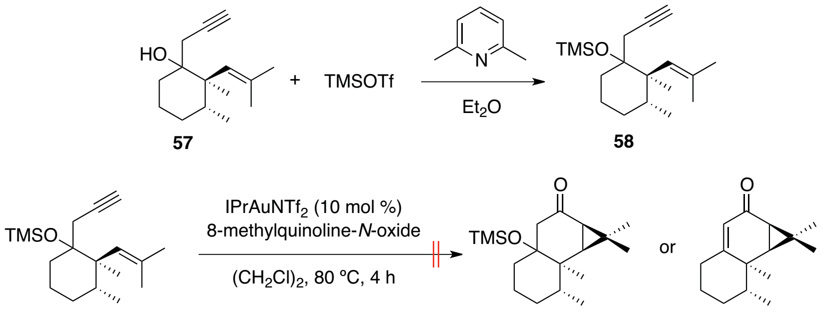
HO
57
TMSOTf
N
Et$_2$O
TMSO
58
IPrAuNTf$_2$ (10 mol %)
8-methylquinoline-N-oxide
(CH$_2$Cl)$_2$, 80 °C, 4 h
O
or

Scheme 35 Silylation of tertiary alcohol **57** with TMS group followed by oxidative gold(I)-catalyzed reaction.[159]

Again, oxidative gold(I)-catalyzed reaction did not prove to be successful. Starting material was still observed in the reaction mixture as well as a range of other different products. In some of them, the OTMS group was still present in the final compound whereas some other showed several olefinic protons. Unfortunately, we were not able to separate them by chromatography and to characterize them. However they presumably arise form the simple cycloisomerization of the starting enyne with or without elimination of the OTMS group.

Homologation

The first homologation process involved the anti-Markovnikov hydration of the 1,5-enyne previously synthesized. Several methods have been reported in the literature constituting a redox-neutral entry to aldehydes. Ruthenium had shown to be the most efficient catalyst to carry out this reaction. However, the reaction usually requires harsh conditions.[161] We initially tried the use of dppm as ligand at 120 ºC, but decomposition of the 1,5-enyne was observed (Scheme 36). Considering that the substrate contained both an alkyne and alkene moieties, it is likely that under Ru catalysis, cycloisomerization has taken place.

---

[159] Experiments carried out by Dr. Michael Muratore.

[160] Jiménez-Núñez, E.; Raducan, M.; Lauterbach T.; Molawi, K.; Solorio, C. R.; Echavarren, A. M. *Angew. Chem. Int. Ed.* **2009**, *33*, 6152–6155.

[161] (a) Tokunaga, M.; Wakatsuki, Y. *Angew. Chem. Int. Ed.* **1998**, *37*, 2867–2869. (b) Suzuki, T.; Tokunaga, M.; Wakatsuki, Y. *Org. Lett.* **2001**, *3*, 735–737. (c) Grotjahn, D. B.; Incarvito, C. D; Rheingold, A. L. *Angew. Chem.*

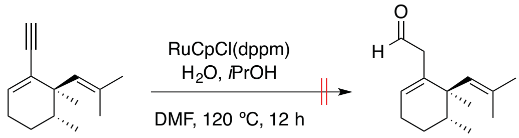

Scheme 36 Attempt of hydration of 1,5-enyne **40** in an anti-Markovnikov fashion.

Horner-Wadsworth-Emmons Reaction

All the attempts to perform a Horner-Wadsworth-Emmons reaction proved to be unsuccessful. Ketone **42** was reacted with phosphorous ylide **59** in the presence of NaH, but the desired product could not be observed even after heating the mixture for 20 h (Scheme 37).

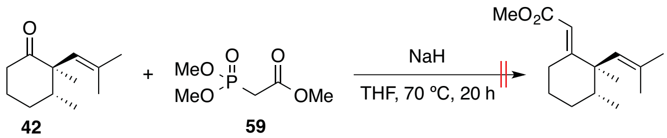

Scheme 37 Failure of the Horner-Wadsworth-Emmons reaction to trialkylated ketone **42**.

In order to verify if the ylide was indeed formed, we used cyclohexanone. Full conversion to the corresponding α,β-unsaturated ester was observed within 30 min (Scheme 38). We reasoned that the high steric hinderance around ketone **42** did not allow the reaction to take place.

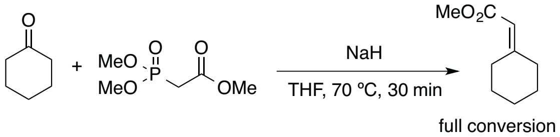

Scheme 38 Horner-Wadsworth-Emmons reaction of cyclohexanone.

Our subsequent synthetic plan was an initial base-catalyzed deconjugation of the ester.[162] Reduction to its alcohol and oxidation to the aldehyde using Swern conditions would have provided to the non-conjugated aldehyde that upon treatment with Bestmann-Ohira reagent would have afforded the desired enyne (Scheme 39).

Int. Ed. **2001**, *40*, 3884–3887. (d) Grotjahn, D. B.; Lev, D. A. *J. Am. Chem. Soc.* **2004**, *126*, 12232–12233. (e) Labonne, A. L.; Kribber, T.; Hintermann, L. *Org. Lett.* **2006**, *8*, 5853–5856. (f) Hintermann, L.; Dang, T. T.; Labonne, A.; Kribber, T.; Xiao, L.; Naumov, P. *Chem.–Eur. J.* **2009**, *15*, 7167–7179. (g) Boeck, F.; Kribber, T.; Xiao, L.; Hintermann, L. *J. Am. Chem. Soc.* **2011**, *133*, 8138–8141. (h) Chevallier, F.; Breit, B. *Angew. Chem. Int. Ed.* **2006**, *45*, 1599–1602.

[162] Fehr, C.; Winter, B.; Mahpantay, I. *Chem.–Eur. J.* **2009**, *15*, 9773–9784.

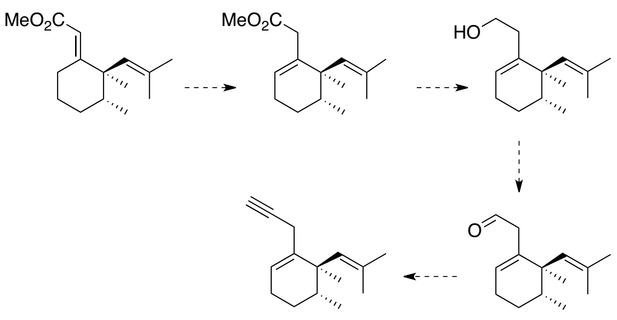

Scheme 39 Synthetic plan towards the 1,6-enyne.

Vinyl Bromide Formation and Propargylation

The direct formation of vinyl bromides from ketones is a known procedure.[163] Enolizable ketones can be converted into their halogen analogues in good to excellent yields applying $(PhO)_3P$–halogen based reagents. Under those conditions, we could convert 4-*tert*-butylcyclohexanone into 1-bromocyclohexene in 85% yield (Scheme 40).

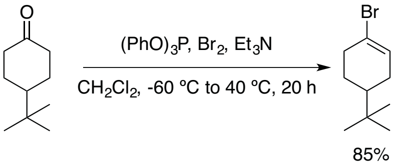

Scheme 40 Conversion of 4-*tert*-butylcyclohexanone into 1-bromocyclohexene.

Unfortunately, trying these conditions on our more substituted substrate **42** gave only traces of the desired compound (Scheme 41). We thought that the steric environment of our system was the cause of the lack of reactivity. Therefore, triphenylphosphite was replaced by the less bulky trimethylphosphite. However, in this case, no traces of product could be observed. To assess whether the problem was still the steric bulk of the substituted ketone, we performed the bromination of 4-*tert*-butylcyclohexanone with trimethylphosphite. No reaction took place. We reason that the brominating reagent $(MeO)_3P^+Br$ / Br^- was either not formed or it was not reactive enough. Changing the phosphite brominating reagent for 2,4,4,6-tetrabromo-2,5-cyclohexadienone in the presence of triphenylphosphine was also known to promote this transformation.[164] However, no reaction was observed with cyclohexanone.

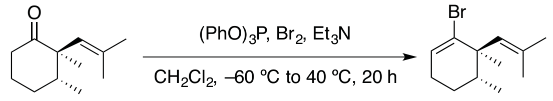

42

Scheme 41 Conversion of ketone **42** into its vinyl bromide analogue.

---

[163] Spaggiari, A.; Vaccari, D.; Davoli, P.; Torre, G.; Prati, F. *J. Org. Chem.* **2007**, *72*, 2216–2219.

[164] (a) Matveeva, E. D.; Feshin, D. B.; Zefirov, N. S. *Russ. J. Org. Chem.* **2001**, *37*, 52–55. (b) De Simone, F.; Andrès, J.; Torosantucci, R.; Waser, J. *Org. Lett.* **2009**, *11*, 1023–1026.

Enol triflates can also be converted into the corresponding vinyl bromide analogues under Ru catalysis and in the presence of lithium bromide.[165] Although this route would feature an extra synthetic step (triflation, bromination and alkylation), we decided to assess its viability. The addition of Zn to the reaction mixture had been found to be crucial in order to reduce the metal to Ru(I), then allowing the catalytic cycle to start. All the attempts to brominate cyclohex-1-en-1-yl trifluoromethanesulfonate following this procedure failed (Scheme 42).

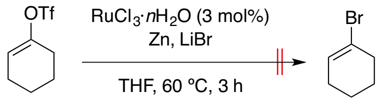

Scheme 42 Attempts to convert alkenyl triflate into alkenyl bromide.

Before optimizing the formation of vinyl bromide, we checked if the subsequent propargylation reaction would be viable. 1-Bromo-4-(*tert*-butyl)cyclohex-1-ene was treated with *t*-BuLi and 1-bromo-2-butyne was added as the model electrophile. However, no alkylation took place; the starting material was still observed in the crude NMR as well as a large amount of 4-(*tert*-butyl)cyclohex-1-ene (Scheme 43).

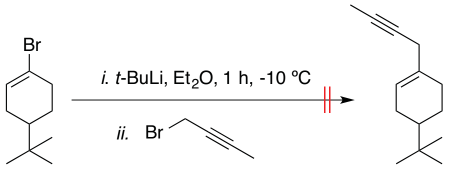

Scheme 43 Reactions that would have rendered the desired 1,6-enyne.

We also tried to convert the lithiated species to its copper counterpart and further react it with propargyl bromide but it also failed to provide the alkylated product. Starting material was partially consumed and the only product observed was the reduced starting material.[166] However, giving that the formation of the vinyl bromide from substituted cyclohexanone **42** failed, we decided to focus on a more direct approach.

Shapiro Reaction and Propargylation

4-*tert*-Butylcyclohexanone was converted into its tosylhydrazone analogue after addition of *p*-toluenesulfonyl hydrazide in 81% yield. However, all the attempts to carry out the Shapiro reaction trapping the resulting vinyl lithium intermediate with 1-bromo-2-butyne were unsuccessful.[167] As previously observed, attempts to transform the lithiated species to the organocuprate only furnished reduced product (Scheme 44).

---

[165] Shirakawa, E.; Imazaki, Y.; Hayashi, T. *Chem. Commun.* **2009**, 5088–5090.
[166] Majetich, G.; Hull, K.; Casares, A. M.; Khetani, V. *J. Org. Chem.* **1991**, *56,* 3958–3973.
[167] Chamberlin, A. R.; Liotta, E. L.; Bond, F. T. *Org. Synth.* **1990**, *Coll. Vol. 7*, 77–81.

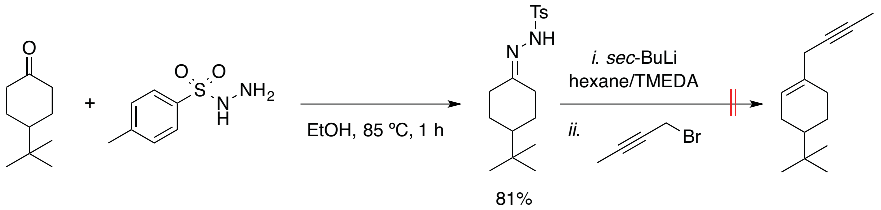

Scheme 44 Unsuccessful Shapiro reaction of 4-*tert*-butyltosylhydrazone.

Triflation and Cross Coupling

Cross coupling with allenylindium reagent

Interestingly, there is one single example in the literature that reports the cross coupling reaction between sp^2 carbons and propargyl moieties as nucleophilic counterpart.[168] Aryl or vinyl iodides and triflates could be coupled to allenylindium reagents (generated *in situ* from the reaction of In with propargyl bromide) using $Pd(PPh_3)_4$ (Scheme 45).

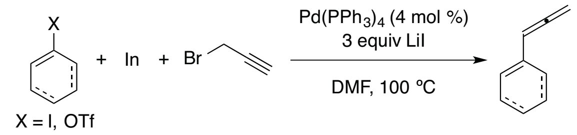

Scheme 45 Cross coupling between aryl or vinyl iodides and triflates with allenylindium.

Since Au(I) can also activate allenes towards the nucleophilic attack of alkynes, we decided to perform the reaction using enol triflate **41** as the electrophilic counterpart. Under the reaction conditions shown, full conversion of the starting material was observed towards a mixture of very apolar molecules with several olefinic protons. However, there were no evidences of the formation of the allene by GCMS analysis. Furthermore, the characteristic downfield signal of an allene in a ^{13}C NMR at around 210 ppm could not be observed (Scheme 46).

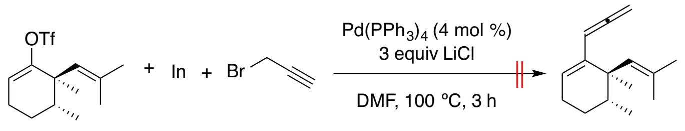

41

Scheme 46 Attempt of cross coupling of enol triflate **41** with allenylindium.

Suzuki cross coupling with propynyl boronic ester derivative

We then decided to try the coupling between the model cyclohexenyltriflate and a propynyl boronic ester derivative **60**, which could be easily synthesized following a known procedure.[169] A range of conditions was screened, as shown in Table 9.

---

[168] Lee, K.; Seomoon, D.; Lee, P. H. *Angew. Chem. Int. Ed.* **2002**, *41*, 3901–3903.

[169] Mszar, N. W.; Haeffner, F.; Hoveyda, A. H. *J. Am. Chem. Soc.* **2014**, *136*, 3362–3365.

Table 9 Conditions screened for the cross coupling between cyclohexenyltriflate and **60**.

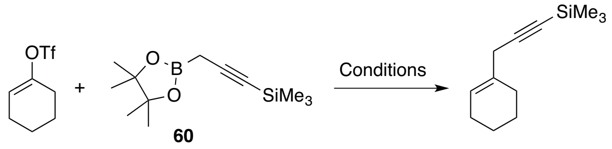

Entry	Conditions	Outcome
1	5 mol % $Pd(PPh_3)_4$, 4 equiv CsF THF, 65 ºC, 2 h	Conversion to unknown products
2	5 mol % $Pd_2(dba)_3$, 10 mol % PPh_3, 3 equiv K_3PO_4 H_2O/DMF, 55 ºC, 6 h	Some conversion to unknown products
3	5 mol % $PdCl_2(dppf)$, 3 equiv K_3PO_4 H_2O/DMF, 55 ºC, 6 h	No reaction, starter recovered
4	5 mol % $Pd(OAc)_2$, 10 mol % SPhos, 3 equiv K_3PO_4 H_2O/THF, 55 ºC, 6 h	No reaction, starter recovered

Among the conditions screened, only the first two gave some conversion to unidentified products. Indeed, the boronic ester **60** had never been used in a cross coupling reaction. We hypothesized that the transmetalation step was not viable.

Stille Cross Coupling with Allenyltributyltin

We also tried the coupling between a model enol triflate and allenyltributyltin through a Stille coupling. Both the alkylated and allenylated products would have been suitable for a further Au(I)-catalyzed reaction. 4-*tert*-Butylcyclohexene enol triflate reacted quantitatively with the stannane reagent under standard Stille conditions.[170] However, analysis of the NMR spectroscopic data revealed that an undesired 1,3-enyne (internal alkyne) had been formed (Scheme 47).

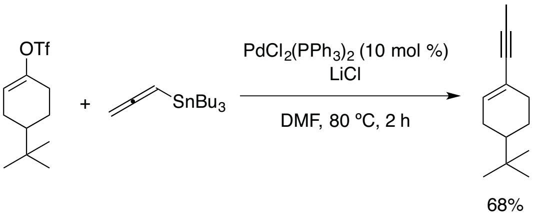

Scheme 47 Coupling of 4-*tert*-butylcyclohexene enol triflate with allenyltributyltin.

We postulated that under the reaction conditions or after the coupling, allenylstannane was isomerized to 1-propynyltributyltin. Thus, we decided to change the strategy and try the same coupling using an enol stannane as one of the reagents.

---

[170] Scott, W. J.; Stille, J. K. *J. Am. Chem. Soc.* **1986**, *108*, 3033–3040.

Stille and Suzuki Cross Couplings with Enol Ether Tin or Enol Ether Boronate

We decided to change the strategy and try the coupling using stannane **61** as the reagent. In this case, the reaction would produce an alkenyl enol ether that under acidic conditions, should be hydrolyzed to the corresponding aldehyde. A subsequent Seyferth-Gilbert homologation would afford the terminal alkyne giving rise to the desired 1,6-enyne. Under the conditions previously described followed by an acidic work-up, 4-*tert*-butylcyclohexenetriflate was converted into its α,β-unsaturated aldehyde analogue **62** in 68% yield (Scheme 48).

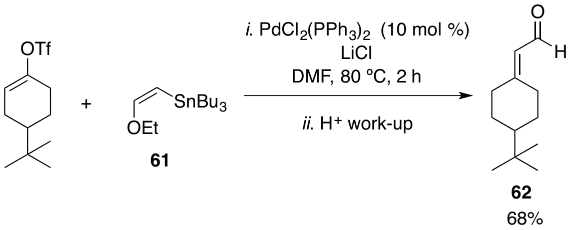
OTf
+
SnBu3
OEt
61
i. PdCl2(PPh3)2 (10 mol %)
LiCl
DMF, 80 °C, 2 h
ii. H+ work-up
O
H
62
68%

Scheme 48 Stille cross coupling between 4-*tert*-butylcyclohexenetriflate and enol ether stannane **61**.

When the same reaction was performed using the trialkylated enol triflate **41**, the corresponding aldehyde **63** was isolated in 54% yield (Scheme 49).

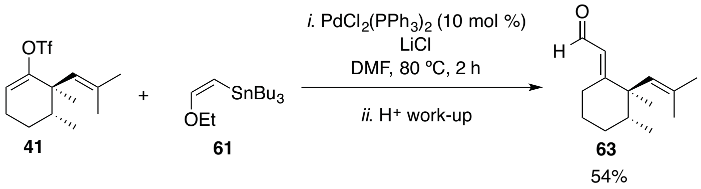
OTf
41
+
SnBu3
OEt
61
i. PdCl2(PPh3)2 (10 mol %)
LiCl
DMF, 80 °C, 2 h
ii. H+ work-up
O
H
63
54%

Scheme 49 Stille cross coupling between enol triflate **41** and enol ether stannane **61**.

Interestingly, the same reaction took place by the Suzuki cross coupling reaction using *trans*-enol ether boronate **64**, which was synthesized by the hydroboration of ethoxyethyne catalyzed by a zirconium complex.[171] Boronate **64** was coupled to enol triflate **41** using Pd_2dba_3/PPh_3 and K_3PO_4 as base. The amount of the metal needed could be reduced to 2.5 mol % and the yield was increased to 61% (Scheme 50). The *E*-configuration of **63** the *α,β*-unsaturated aldehyde was determined by nOe (Figure 5).

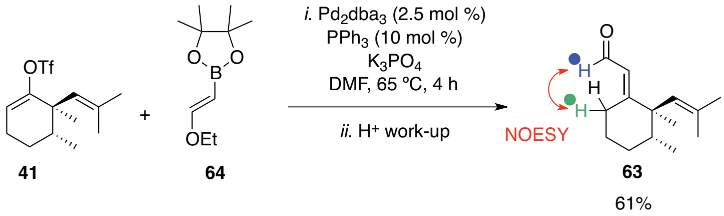
OTf
41
+
O
B
O
OEt
64
i. Pd2dba3 (2.5 mol %)
PPh3 (10 mol %)
K3PO4
DMF, 65 °C, 4 h
ii. H+ work-up
NOESY
O
H
H
H
63
61%

Scheme 50 Suzuki cross coupling between enol triflate **41** and enol ether boronate **64**.

---

[171] Cresteya, F.; Hooyberghsa, G.; Kristensen, J. L. *Tetrahedron* **2012**, *68*, 1417–1421.

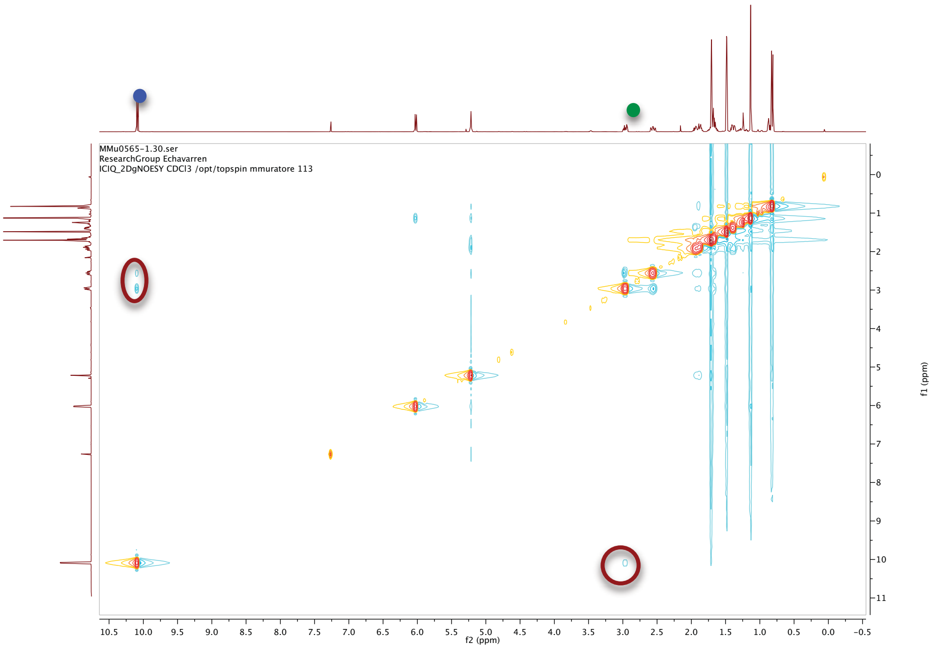

Figure 5 NOESY of α,β-unsaturated aldehyde **63**.

Reaction of α,β-unsaturated aldehyde **63** with the Bestmann-Ohira reagent in methanol led to enyne **65** in 70% yield (Scheme 51). Unfortunately, this substrate featured the undesired *E*-configuration, which was confirmed by nOe (Figure 6).

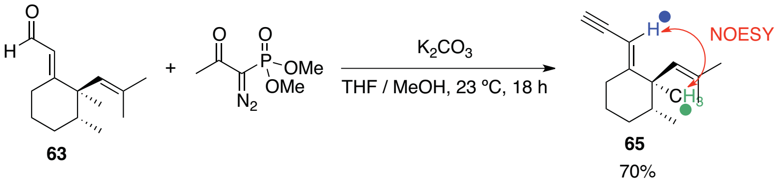
O
H
63
+
O
O
P
OMe
OMe
N2
K2CO3
THF / MeOH, 23 °C, 18 h
H
NOESY
CH3
65
70%

Scheme 51 Seyferth-Gilbert homologation of α,β-unsaturated aldehyde **63** giving 1,6-enyne **65**.

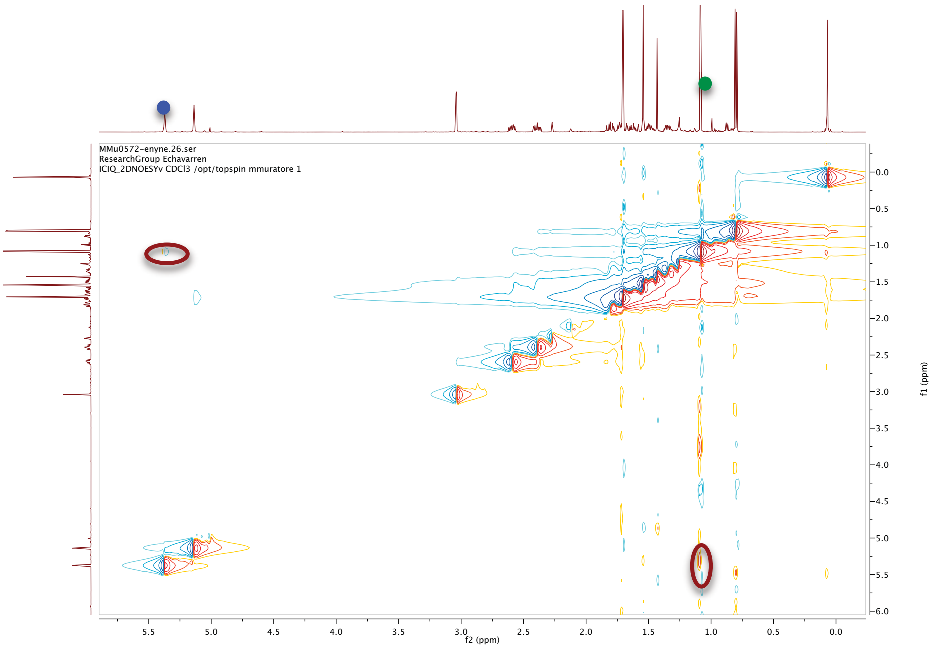

Figure 6 NOESY of 1,6-enyne **65**.

Although substrate **65** had the wrong *E*-configuration, under oxidative gold(I)-catalyzed conditions, traces of cyclization product of was observed. Presumably, the gold(I) catalyst is able to partially isomerize *E*-**65** to form a small amount of *Z*-**65**.

Kumada Cross Coupling with Propargyl Magnesium Bromide Derivatives

The first Kumada cross coupling reactions that we attempted with commercial reagents failed. Interestingly, 50% of conversion was observed after 6 h when reacting freshly prepared (and titrated) propargyl magnesium bromide with the model enol triflate 4-*tert*-butylcyclohexenetriflate using $NiCl_2$dppp as catalyst. However, the product that was isolated proved to be 4-*tert*-butyl-1-propynylcyclohexene, reminiscent of what was observed in the coupling with allenyltributyltin (Scheme 52).

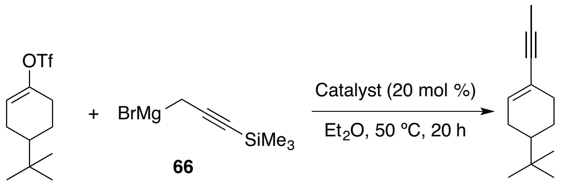

Scheme 52 Kumada cross coupling between 4-*tert*-butylcyclohexenetriflate and propargyl magnesium bromide.

The reaction of propargyl bromide with activated magnesium tunings gives the corresponding allenylmagnesium bromide, which isomerizes to the more thermodynamically stable 1-propynylmagnesium bromide (Scheme 53).[172]

---

[172] Hopf, H.; Böhm, I.; Kleinschroth, J. *Org. Synth.; Coll. Vol. 7*, **1990**, 485–490.

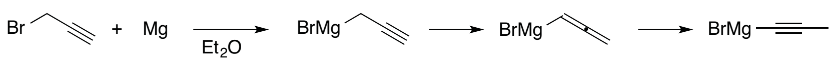

Scheme 53 Isomeriztion of propargyl magnesium bromide to 1-propynylmagnesium bromide.

Interestingly, the substituted enol triflate **41** gave no coupling under those conditions (Scheme 54).

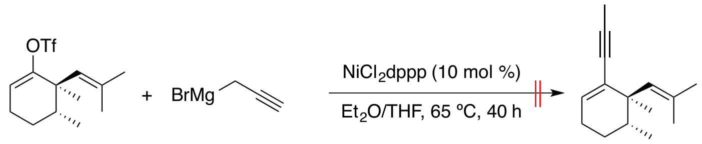

41

Scheme 54 Failure of the Kumada cross coupling between enol triflate **41** and propargyl magnesium bromide.

In order to avoid the isomerization of the resulting nucleophile, we decided to use its analogue protected with a TMS group. Different Ni sources containing phosphines or carbenes ligands were screened (Table 10). After heating the reaction at 50 ºC for more than 20 h, no desired coupling was observed, but only the formation of homocoupled Grignard reagent. Finally, swapping the metal to Pd(PPh$_3$)$_4$ the resulting coupling product was generated. Remarkably, the corresponding allene was not formed.

Table 10 Screening of different conditions for the Kumada cross coupling.

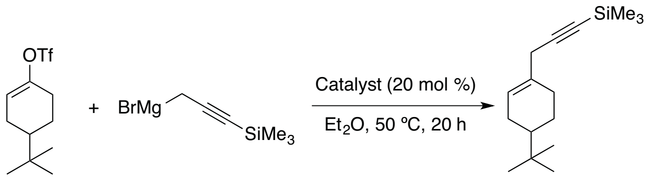

Entry	Catalyst	Outcome
1	NiCl$_2$(PPh$_3$)$_2$	Homocoupling of nucleophile. Starter recovered
2	NiCl$_2$(dppp)	Homocoupling of nucleophile. Starter recovered
3	NiCl$_2$(dppe)	Homocoupling of nucleophile. Starter recovered
4	NiCl$_2$ + 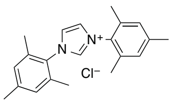	Homocoupling of nucleophile. Starter recovered
5	Pd(PPh$_3$)$_4$	Full conversion to the desired product. Homocoupling of nucleophile.

After optimizing the conditions for this reaction we obtained the coupled product in 63% yield using 2 mol % of Pd(PPh$_3$)$_4$ and 2.1 equiv of the Grignard reagent **66**. However, subjecting our trialkylated enol triflate **41** under these conditions gave very poor conversion. The catalyst loading had to be increased to 20 mol % and an excess of the

Gridnard reagent was used. Upon methanolysis, the silyl group was finally cleaved affording the desired 1,6-enyne **43** in 77% yield (Scheme 55).

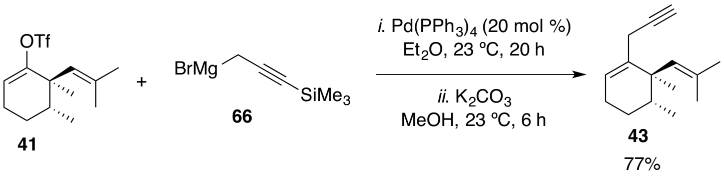
OTf
41
+
BrMg
SiMe3
66
i. Pd(PPh3)4 (20 mol %)
Et2O, 23 °C, 20 h
ii. K2CO3
MeOH, 23 °C, 6 h
43
77%

Scheme 55 Kumada cross coupling reaction between enol trilfate **41** and TMS-protected propargyl magnesium bromide **66**.

Gold(I)-Catalyzed Cyclization to Access to (–)-Aristolone and Kanshone H

For the oxidative gold(I)-catalyzed cyclization, we initially screened the optimized conditions for the 1,5-enyne cyclization reaction. Full conversion of the 1,6-enyne **43** was observed when it was treated with 3,5-dichloropyridine-*N*-oxide and IPrAuNTf$_2$ in 1,2-dichloroethane at 23 ºC. The reaction was very clean although the tricyclic product formed was not the desired one. Cyclization took place in the undesired 5-*exo*-dig fashion (Scheme 56).

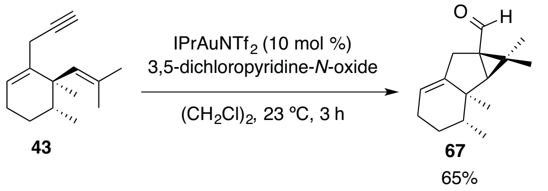
43
IPrAuNTf2 (10 mol %)
3,5-dichloropyridine-N-oxide
(CH2Cl)2, 23 °C, 3 h
O
H
67
65%

Scheme 56 Oxidative gold(I)-catalyzed cyclization of 1,6-enyne **43**.

The formation of the *exo*-cyclized product was also favored when 8-methylquinoline-*N*-oxide or 2-*tert*-butylpyridine-*N*-oxide were used. The final configuration of the molecule could not be confirmed by NOESY but by GOESY (Figure 7). Specifically irradiating the cyclopropyl proton, we could observe correlation with the three methyl groups pointing down as well as the correlation with the aldehydic proton.

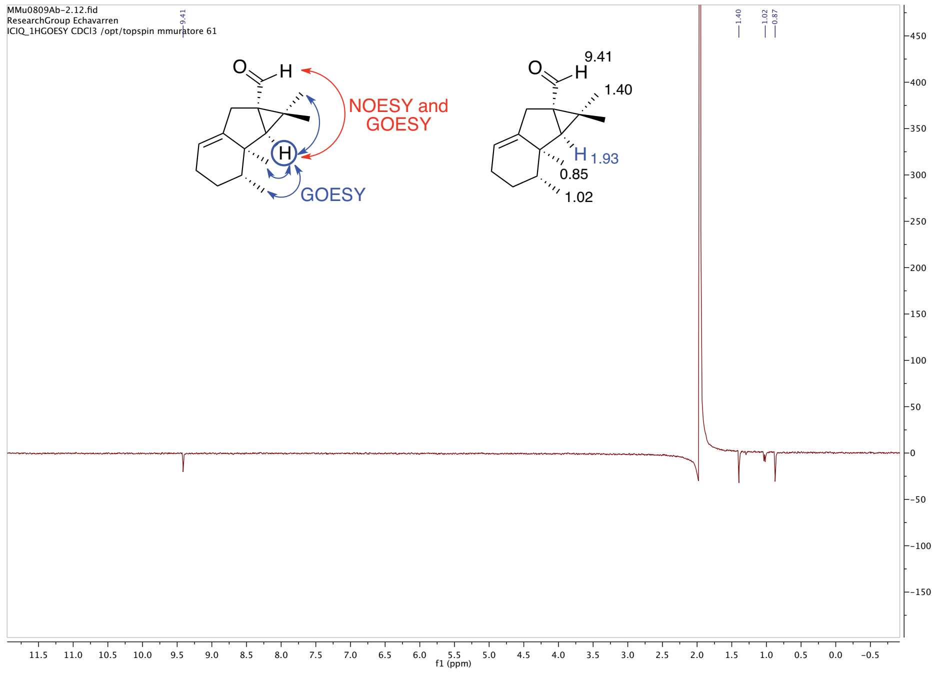

Figure 7 GOESY of compound **67** irradiating the pending proton in the cyclopropyl ring.

Indeed, 1,6-enynes bearing disubstituted groups at the alkene moiety usually react by *exo* pathways.[173] We also tried the gold(I)-catalyzed cyclization using the TMS protected enyne. However, the same 5-*exo*-dig product **67** was obtained. Finally, decided to use platinum(II) complexes that could also activate π-bonds in a manner different from gold.[174] However, subjecting 1,6-enyne **43** to $PtCl_2$ and 3,5-dichloropyridine-*N*-oxide gave again tricyclic product **67** in 70% NMR yield as well as 20% of the cycloisomerized product. Remarkably, it is the first example of an oxidative Pt-catalyzed reaction.

---

[173] (a) Nieto-Oberhuber, C.; Muñoz, M. P.; Buñuel, E.; Nevado, C.; Cárdenas, D. J.; Echavarren, A. M. *Angew. Chem. Int. Ed.* **2004**, *43*, 2402–2406. (b) Nieto-Oberhuber, C.; Muñoz, M. P.; López, S.; Jiménez-Núñez, E.; Nevado, C.; Herrero-Gómez, E.; Raducan, M.; Echavarren, A. M. *Chem.–Eur. J.* **2006**, *12*,1677–1693.

[174] (a) Fang, R.; Wei, X.; Yang, L. *Org. Biomol. Chem.* **2014**, *12*, 8433–8441. (b) Mokar, B. D.; Liu, R.-S. *Chem. Commun.* **2014**, *50*, 8966–8969.

Outlook

To complete the synthesis of (–)-aristolone and kanshone H, other strategies could be envisioned, either using bicyclic ketone **56** or 1,6-enyne **43**.

Use of Bicyclic Ketone 56

The most direct approach would involve the homologation of the precursor **56**. A Tiffeneau-Demjanov reaction[175] or a Lewis-acid promoted diazomethane addition[176] to **56** could afford the desired 6/6/3 framework (Scheme 57). We expect the 5-membered ring to be expanded rather than the 6, although the migratory preference of the methylene group is not very clear. A final isomerization of the olefin towards the conjugated α,β-unsaturated ketone would afford the natural product (–)-aristolone.

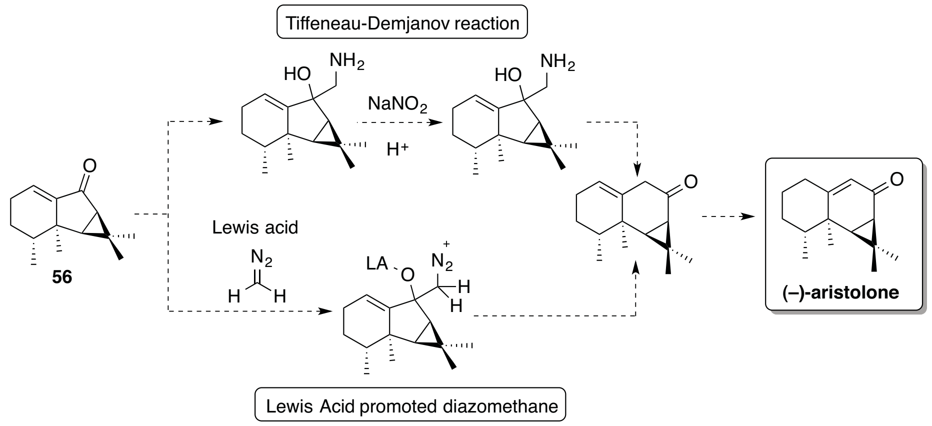

Scheme 57 First approach towards the synthesis of (–)-aristolone.

Use of 1,6-Enyne 43

The formation of the desired 6-*endo*-dig cyclized product could be favored by using the 1,6-enyne with the terminal alkyne containing an electron-withdrawing functional group. We hypothesize that the formation of 6/6/3 desired framework would be favored since the gold carbene formed is more stable than its 5-*exo*-dig analogue. Enynes bearing esters in the terminal position have been shown to cyclize under gold(I) catalyzed oxidative conditions.[177] The synthesis of the natural product could be accomplished after a decarboxylation and an isomerization of the olefin (Scheme 58).

---

[175] (a) Demjanov, N. J.; Luschnikov, M. *J. Russ. Phys. Chem. Soc.* **1901**, *33*, 279 –283. (b) Tiffeneau, M.; Tchoubar, B.; *Compt. Rend.* **1937**, *205*, 1411–1413. (c) Smith, P. A. S.; Baer, D. R. *Org. React.* **1960**, *11*, 157–188. (d) Dave, V.; Stothers, J. B.; Warnhoff, E. W. *Can. J. Chem.* **1979**, *57*, 1557–1568. (e) Coveney, D. J. *Comp. Org. Syn.* **1991**, *3*, 781–782. (f) Fattori, D.; Henry, S.; Vogel, P. *Tetrahedron* **1993**, *49*, 1649–1664.

[176] (a) Krow, G. R. *Tetrahedron* **1987**, *43*, 3–38. (b) Dauben, H. J. Jr.; Ringold, H. J.; Wade, R. H.; Pearson, D. L.; Anderson, A. G. Jr. *Org. Synth. Coll.* **1963**, *4*, 221–227.

[177] Uetake, Y.; Niwa, T.; Nakada, M. *Tetrahedron Lett.* **2014**, *55*, 6847–6850.

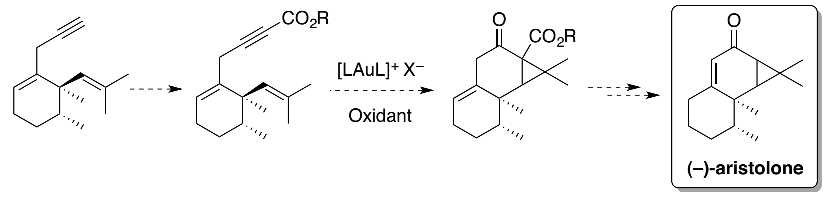
CO$_2$R
[LAuL]$^+$ X$^-$
Oxidant
O
CO$_2$R
O
(–)-aristolone

Scheme 58 Second approach towards the synthesis of (–)-aristolone.

Conclusions

The total synthesis of nardoaristolone B has been accomplished in 7 steps featuring a Cu-catalyzed conjugate addition/α-alkylation tandem transformation and a gold(I)-catalyzed oxidative cyclization as key steps (Scheme 59). The 13% overall yield obtained and short synthetic sequence give access to a straightforward synthesis of a molecule that can be an important target due to its interesting biological activities. Furthermore, it is the first time that a gold(I)-catalyzed oxidative cyclization is used in the synthesis of a natural product.

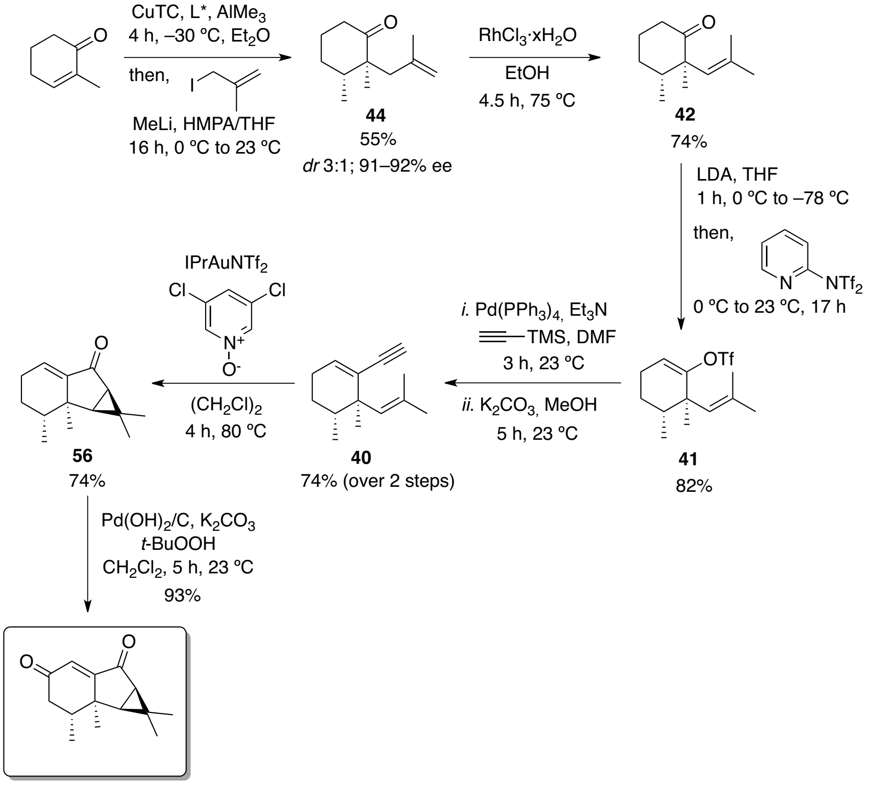
CuTC, L*, AlMe3
4 h, –30 °C, Et2O
then,
I
MeLi, HMPA/THF
16 h, 0 °C to 23 °C
44
55%
dr 3:1; 91–92% ee
RhCl3·xH2O
EtOH
4.5 h, 75 °C
42
74%
LDA, THF
1 h, 0 °C to –78 °C
then,
N
NTf2
0 °C to 23 °C, 17 h
OTf
41
82%
i. Pd(PPh3)4, Et3N
TMS, DMF
3 h, 23 °C
ii. K2CO3, MeOH
5 h, 23 °C
40
74% (over 2 steps)
IPrAuNTf2
Cl
Cl
N+
O-
(CH2Cl)2
4 h, 80 °C
56
74%
Pd(OH)2/C, K2CO3
t-BuOOH
CH2Cl2, 5 h, 23 °C
93%
O

Scheme 59 Total synthesis of nardoaristolone B.

Following an analogous strategy, a 1,6-enyne has been prepared through a challenging Kumada cross coupling with TMS-protected propargylmagnseium bromide. Interestingly, no traces of allene are generated during the course of the reaction. The oxidative gold(I)-catalyzed reaction of the resulting enyne gives rise to a 5-*exo*-dig cyclization instead of the desired 6-*endo*-dig (that would have afforded the core of (–)-aristolone and kanshone H). The 6/5/3 framework of the new compound obtained corresponds to a nardoaristolone B derivative (Scheme 60).

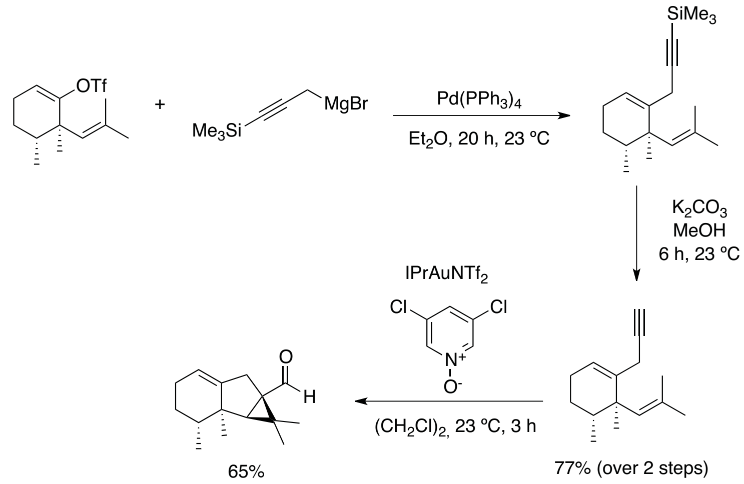
OTf
+
Me3Si
MgBr
Pd(PPh3)4
Et2O, 20 h, 23 °C
SiMe3
K2CO3
MeOH
6 h, 23 °C
IPrAuNTf2
Cl
Cl
N+
O-
(CH2Cl)2, 23 °C, 3 h
O
H
65%
77% (over 2 steps)

Scheme 60 Approach towards the synthesis of (–)-aristolone and kanshone H from a Au(I)-catalyzed cyclization of a 1,6-enyne.

Experimental Part

General Information

The general information is provided in the experimental part of the first chapter. Regarding the HPLC analysis, it was carried out in an Agilent Tehcnologies instrument HPLC 1100 series with VWD detector or HPLC 1200 series with DAD detector. The column used was a Chiralpack IC (4.6 mm x 250 mm) eluting with hexane:isopropanol (99:1), 0.85 mL/ min flux, 5 mL injection and λ = 210 nm.

Synthesis of Substrates

2-Bromo-2-methylcyclohexanone

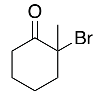

To a solution of *N*-bromosuccinimide (5.34 g, 30 mmol) in 100 mL CCl_4 was dropwise added 2-methylcyclohexanone (3.64 mL, 30 mmol). After stirring the mixture under reflux for 2.5 h, it was cooled down to 23 ºC and concentrated providing a yellow solid. Pentane (25 mL) was added and the resulting solution was filtrated through Celite. Organic layers were concentrated again affording 2-bromo-2-methylcyclohexanone, which was used in the next step without purifying it.

^{1}H NMR (400 MHz, $CDCl_3$) δ_H 3.21 (td, *J* = 15.8, 7.8 Hz, 1H), 2.36 (m, 2H), 2.06 (m, 2H), 1.82 (s, 3H), 1.77 (m, 2H), 1.62 (m, 1H).

2-Methylcyclohexenone

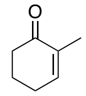

The crude 2-bromo-2-methylcyclohexanone was dissolved in 50 mL DMF and K_2CO_3 was added. The mixture was stirred at 80 ºC for 3 h and cooled to 23 ºC while stirring for 12 h. The reaction was hydrolyzed with water (50 mL) and extracted with Et_2O (3 × 50 mL). The combined organic layers were successively washed with aq. HCl 0.5 M (30 mL), water (2 × 50 mL), sat. brine (2 × 50 mL) and dried over Na_2SO_4. Chromatography column was done eluting with a gradient of pentane/Et_2O 40:1 to 20:1.

1.80 g (16.34 mmol) of 2-methylcyclohex-2-enone were isolated in 55% yield.

^{1}H NMR (400 MHz, $CDCl_3$) δ_H 6.76 – 6.72 (bs, 1H), 2.44 – 2.39 (m, 2H), 2.32 (m, 2H), 2.03 – 1.92 (m, 1H), 1.76 (q, *J* = 1.8 Hz, 3H). **^{13}C NMR** (101 MHz, $CDCl_3$) δ_C 200.2, 145.7, 135.9, 38.5, 26.2, 23.4, 16.1.

(11b*R*)-4-Chlorodinaphtho[2,1-*d*:1',2'-*f*][1,3,2]dioxaphosphepine

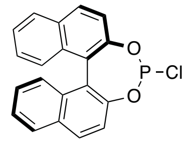

(R)-BINOL (10 g, 35 mmol) was introduced in a dry round bottom flask filled with Ar and PCl_3 (27.4 mL, 314 mmol) were added. The mixture was placed in a pre-heaterd oil bath (85 ºC) and refluxed for 16 h. After cooling to 23 ºC, the excess of PCl_3 was removed under vacuum until the oil solidified. Anhydrous Et_2O was used to wash the solid, and then it was removed under vacuum. This procedure was repeated twice. The resulting solid was placed immediately in the glovebox.

12 g of (11b*R*)-4-chlorodinaphtho[2,1-*d*:1',2'-*f*][1,3,2]dioxaphosphepine (34 mmol) were isolated in 98% yield (although not 100% pure).

^{1}H NMR (400 MHz, CDCl$_3$) δ$_H$ 8.02 (d, *J* = 6.6 Hz, 2H), 7.96 (d, *J* = 8.2 Hz, 2H), 7.54 (dd, *J* = 9.0, 2.6 Hz, 1H), 7.51 – 7.45 (m, 3H), 7.44 – 7.37 (m, 2H), 7.31 (q, *J* = 7.7 Hz, 2H). **^{31}P NMR** (162 MHz, CDCl$_3$) δ$_P$ 181.4.

(11b*R*)-*N*,*N*-Bis((*S*)-1-phenylethyl)dinaphtho[2,1-*d*:1',2'-*f*][1,3,2]dioxaphosphepin-4-amine

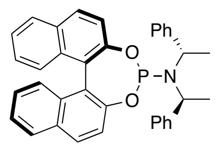

(-)-bis[(*S*)-phenylethyl]amine (3.43 mL, 15 mmol) was dissolved in 150 mL anhydrous THF. The solution was cooled to –78 ºC and *n*-BuLi (2.5 M in hexanes, 6 mL, 15 mmol) was added dropwise over 10 min (syringe pump). The mixture was left at this temperature for 1 h. A solution of chlorophosphite (11b*R*)-4-chlorodinaphtho[2,1-*d*:1',2'-*f*][1,3,2]dioxaphosphepine (5.9 g, 16.8 mmol) in 75 mL anhydrous THF was added dropwise over 30 min at –78 ºC and the resulting mixture stirred for additional 2 h in the cold bath. It was then allowed to warm to 23 ºC and stirring was continued for 1.5 h.

The solvent was removed in vacuum and the residue purified by column chromatography eluting with pentane/dichloromethane 4:1 to 1:1 to afford 5.5 g of (11b*R*)-*N*,*N*-bis((*S*)-1-phenylethyl)dinaphtho[2,1-*d*:1',2'-*f*][1,3,2]dioxaphosphepin-4-amine (10.2 mmol) were isolated (68% over 2 steps).

^{1}H NMR (400 MHz, CDCl$_3$) δ$_H$ 7.93 (d, *J* = 8.8 Hz, 2H), 7.88 (dd, J = 7.8, 4.2 Hz, 2H), 7.58 (d, *J* = 8.8 Hz, 1H), 7.43 (d, *J* = 8.8 Hz, 1H), 7.41 – 7.35 (m, 3H), 7.28 (d, *J* = 8.0 Hz, 1H), 7.26 – 7.17 (m, 2H), 7.15 – 7.06 (m, 10H), 4.49 (m, 2H), 1.72 (d, *J* = 6.8 Hz, 6H). **^{13}C NMR** (101 MHz, CDCl$_3$) δ$_C$ 150.1, 150.0, 149.5, 142.8, 132.8, 132.7, 131.4, 130.4, 130.2, 129.4, 128.3, 128.1, 127.9, 127.7, 127.1, 127.07, 126.6, 126.0, 125.9, 124.7, 124.4, 124.1, 124.0, 122.4, 122.3, 121.73, 121.71, 52.3, 52.2, 21.9. **^{31}P NMR** (162 MHz, CDCl$_3$) δ$_P$ 145.6

Methallyl iodide

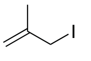

Metallyl chloride (44.1 mL, 450 mmol) was dissolved in 150 mL acetone and a solution of NaI (88 g, 585 mmol) dissolved om 600 mL actone was added by portions. The mixture was stirred at 23 ºC for 24 h with exclusion of light. The reaction was poured over water and extracted with pentane. The resulting organic layers were washed with Na$_2$SO$_3$ (x2), dried over Na$_2$SO$_4$ and filtrated. The product was isolated upon distillation (90 ºC, 200 mbar).

55 g of metallyl iodide (0.302 mmol) were isolated in 67% yield.

^{1}H NMR (300 MHz, CDCl$_3$) δ$_H$ 5.17 (m, 1H), 4.87 (m, 1H), 3.92 – 3.82 (m, 2H), 1.88 (m, 3H).

(2*S*,3*R*)-2,3-Dimethyl-2-(2-methylallyl)cyclohexan-1-one (44)

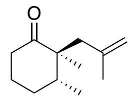

To a stirred suspension of copper(I)-thiophene-2-carboxylate (69 mg, 0.36 mmol, 0.02 equiv) in 15 mL Et$_2$O was added (*R*,*S*,*S*)-(+)-(3,5-dioxa-4-phospha-cyclohepta[2,1-a;3,4-a']dinaphthalen-4-yl)bis(1-phenylethyl) amine (392 mg, 0.72 mmol, 0.04 equiv). After stirring for 15 min at 23 ºC, the resulting suspension was cooled to –35 ºC and 2-methylcyclohex-2-en-1-one (2.1 mL, 18.2 mmol, 1 equiv) was added. Subsequently, AlMe$_3$ (2M in heptane, 10.4 mL, 20.9

mmol, 1.15 equiv) was added slowly over a period of 15 min and allowed to react for 4 h at –35 ºC (the mixture turns milky bright yellow upon addition of $AlMe_3$).

After 4 h at –35 ºC, dry THF (15 mL) and HMPA (12 mL) were added and the mixture allowed to warm to –5 ºC. MeLi (1.6 M in Et_2O, 12.7 mL, 20.3 mmol, 1.07 equiv) was added dropwise over 5 min from –5 ºC to 0 ºC (the reaction turns greenish upon addition of MeLi). After 20 min stirring, methallyl iodide (3.5 mL, 32.7 mmol, 1.7 equiv) was slowly added over 5 min. The reaction mixture was left at 0 ºC for 30 min and slowly warmed to 23 ºC and left stirring at this temperature for 16 h. The reaction was then quenched with a saturated aqueous solution of potassium sodium tartrate and extracted with dichloromethane (5 × 100 mL). The combined organic layers were washed with saturated aqueous NH_4Cl (200 mL) and brine (200 mL) and finally dried over Na_2SO_4. The volatiles were removed under vacuum and the crude mixture was purified by column chromatography on silica gel eluting with pentane/Et_2O 100:1 to 30:1 to afford a colorless liquid (3:1 mixture of diastereomers **44** and **44’**, 1.8 g, 10 mmol, 55% yield, 91-92% ee). The desired diastereomer **44** could be separated after several chromatography columns eluting with pentane/Et_2O 80:1 in essentially pure form (> 30:1 *dr*).

The *dr* was determined by integrating the olefinic protons in the ^{1}H NMR of both diastereomers. The *ee* was determined by HPLC.

Major diastereomer: ^{1}H NMR (400 MHz, $CDCl_3$) δ_H 4.81 – 4.77 (m, 1H), 4.67 – 4.63 (m, 1H), 2.65 (d, J = 13.9 Hz, 1H), 2.50 (dddd, J = 15.1, 7.0, 5.8, 1.5 Hz, 1H), 2.41 – 2.28 (m, 2H), 2.00 – 1.84 (m, 3H), 1.80 – 1.68 (m, 1H), 1.60 (s, 3H), 1.57 – 1.45 (m, 1H), 0.98 (s, 3H), 0.91 (d, J = 6.8 Hz, 3H). **^{13}C NMR** (100 MHz, $CDCl_3$) δ_C 215.7, 142.9, 114.5, 52.0, 44.3, 38.4, 38.3, 28.8, 24.2, 23.5, 19.7, 15.8. **$[\alpha]_D$** ($CHCl_3$, *c* 1.02, 26 ºC) = –10.0 º.

HPLC Chiralpack IC (4.6 mm × 250 mm); hexane:IPA 99:1; 0.85 mL/min; λ = 210 nm, 5 µL injection; t_R (major) 7.5–7.6 min, t_R (minor) 7.8–8.0 min, 91–92% *ee*.

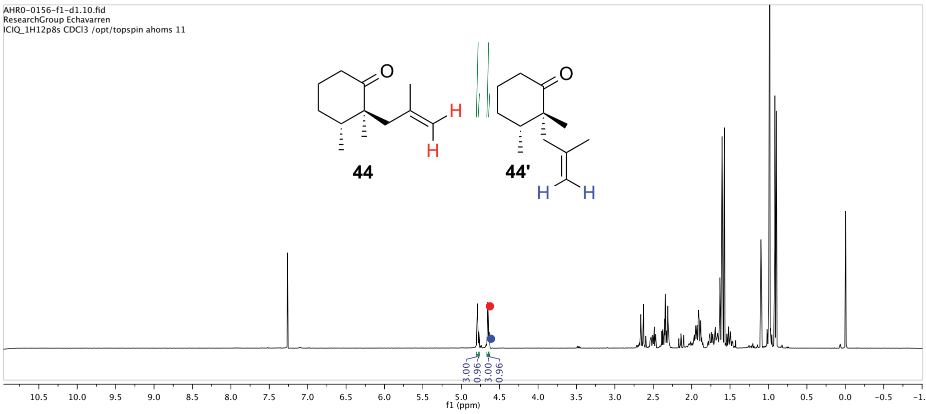

Figure S1 Diastereomeric mixture of **44** + **44´**: *ca.* 3:1 *dr*

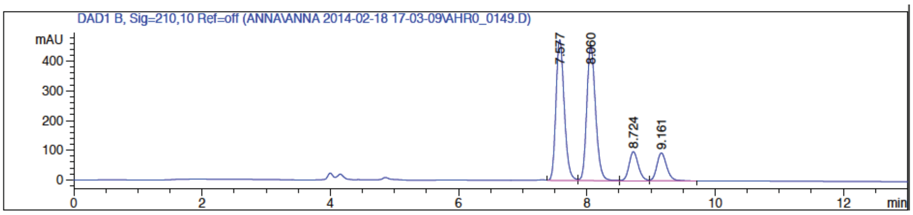

```
Peak RetTime Type  Width     Area      Height     Area
  #   [min]        [min]   [mAU*s]     [mAU]        %
----|-------|----|-------|----------|----------|--------|
  1   7.577 VV    0.1410 4277.24756  475.08759  40.3521
  2   8.060 VV    0.1498 4332.19971  452.15582  40.8706
  3   8.724 VV    0.1534  986.34308   98.01797   9.3053
  4   9.161 VB    0.1624 1004.01105   94.13841   9.4720
```

Figure S2 HPLC chromatogram of racemic **44** + **44´**

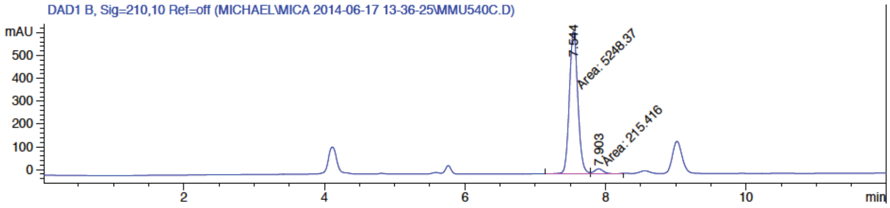

```
Peak RetTime Type  Width     Area      Height     Area
  #   [min]        [min]   [mAU*s]     [mAU]        %
----|-------|----|-------|----------|----------|--------|
  1   7.544 MF    0.1400 5248.36621  625.01849  96.0574
  2   7.903 FM    0.1609  215.41559   22.31853   3.9426

Totals :                 5463.78180  647.33702
```

Figure S3 Enantioenriched mixture of **44** + **44´**: *ca.* 92% *ee*

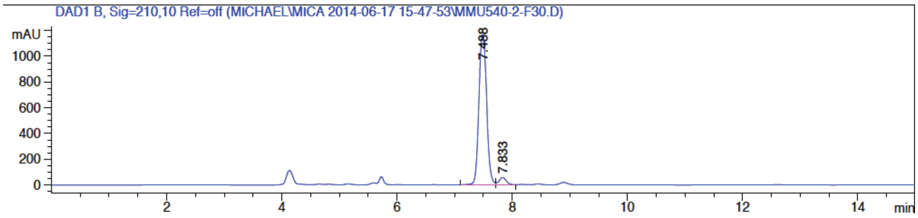

```
Peak RetTime Type  Width     Area      Height     Area
  #   [min]        [min]   [mAU*s]     [mAU]        %
----|-------|----|-------|----------|----------|--------|
  1   7.488 BV    0.1488 1.09079e4  1169.62219  95.5011
  2   7.833 VV    0.1332  513.85321   58.07860   4.4989

Totals :                 1.14218e4  1227.70079
```

Figure S4 Enantioenriched pure **44**: *ca.* 91% *ee*

(3*R*)-6-(Hydroxymethylene)-2,3-dimethylcyclohexan-1-one (46)

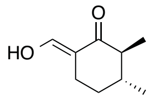

To a suspension of NaOMe (2.08 g, 38.63 mmol) in 30 mL Et$_2$O under Ar at 0 ºC was added 2,3-dimethylcyclohexanone **45** (1.95 g, 15.45 mmol) (as a 3:1 mixture of diastereomers) and the mixture was stirred for 10 min. Ethyl formate (2.12 mL, 26.27 mmol) was added and the mixture was allowed to warm to 23 ºC and stirred for 12 h. The reaction was diluted in water, and the ethereal layer was extracted with a solution of NaOH (10% aq). The aqueous layer and alkaline extract were cooled, acidified with a solution of HCl 6M and extracted with Et$_2$O (x3). Combined org. layers were washed with sat. brine, dried over Na$_2$SO$_4$ and concentrated to reduced pressure. The crude (3:1 mixture of diasteromers in favour to the depicted one) was used for the subsequent reaction without prior purification.

Major diastereomer: ^{1}**H NMR** (500 MHz, CDCl$_3$) δ_H 14.62 (bs, 1H), 8.65 (bs, 1H), 2.40 – 2.30 (m, 2H), 2.07 – 1.99 (m, 1H), 1.81 – 1.76 (m, 1H), 1.53 – 1.41 (m, 1H), 1.35 – 1.28 (m, 1H), 1.23 (d, *J* = 7.8 Hz, 3H), 1.05 – 1.01 (d, *J* = 6.5 Hz, 3H). ^{13}**C NMR** (126 MHz, CDCl$_3$) δ_C 187.8, 187.7, 108.0, 43.3, 35.2, 29.9, 22.4, 20.3, 15.9.

(3*R*,*E*)-6-((Butylthio)methylene)-2,3-dimethylcyclohexan-1-one (47)

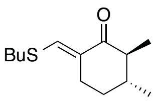

A solution of **46** (2.40 g, 15.45 mmol) (as a 3:1 mixture of diastereomers), butanethiol (2.16 mL, 20.09 mmol) and *p*-toluenesulfonic acid (10 mg, 0.05 mmol) were dissolved in 32 mL dry benzene and heated to 85 ºC using a Dean-Stark separator. After 3 h, the solution was allowed to warm to 23 ºC, diluted in Et$_2$O, washed with sat. NaHCO$_3$ and sat. brine, dried over Na$_2$SO$_4$ and concentrated under reduced pressure. A final chromatography column of the residue on SiO$_2$ eluting with pentane/Et$_2$O 20:1 let to the isolation of 2.40 g of **47** (3:1 mixture of diastereomers in favour to the depicted one) in 68% yield.

Major diastereomer: ^{1}**H NMR** (500 MHz, CDCl$_3$) δ_H 7.54 – 7.49 (m, 1H), 2.84 (t, *J* = 7.5 Hz, 2H), 2.57 – 2.48 (m, 1H), 2.48 – 2.35 (m, 1H), 2.35 – 2.23 (m, 1H), 1.93 – 1.84 (m, 1H), 1.76 – 1.60 (m, 3H), 1.47 – 1.38 (m, 3H), 1.17 (d, J = 6.9 Hz, 2H), 1.04 (d, *J* = 6.6 Hz, 3H), 0.93 (t, J = 7.4 Hz, 3H), 0.91 (d, *J* = 7.0 Hz, 1H). ^{13}**C NMR** (126 MHz, CDCl$_3$) δ_C 199.0, 141.9, 130.4, 50.2, 36.3, 34.4, 32.8, 30.4, 26.7, 21.7, 20.9, 14.5, 13.7.

(2*S*,3*R*,*E*)-6-((butylthio)methylene)-2,3-dimethyl-2-(2-methylallyl)cyclohexan-1-one (48)

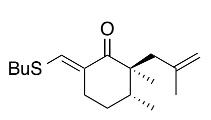

To a solution of **47** (2.00 g, 8.83 mmol) in 13 mL dry THF at –78 ºC was added a solution of potassium hexamethyldisilazide (1.56 g, 7.84 mmol) in 16 mL dry toluene and the resulting mixture was stirred at 0 ºC for 1 h. The reddish solution was cooled to –78 ºC and methallyl bromide (1.65 mL, 16.40 mmol) was added. The mixture was allowed to slowly warm to 23 ºC, after which it was quenched with sat. NH$_4$Cl, extracted with Et$_2$O (x3), dried over Na$_2$SO$_4$ and purified by column chromatography eluting with pentane/Et$_2$O 40:1.

1.60 g of **48** (5.71 mmol) were isolated in 65% yield as well as 405 mg (1.44 mmol) of the undesired diastereomer (**48'**) in 16% yield.

Major diastereomer: ^{1}**H NMR** (500 MHz, CDCl$_3$) δ_H 7.57 – 7.55 (m, 1H), 4.76 – 4.72 (m, 1H), 4.64 (dq, *J* = 1.7, 0.9 Hz, 1H), 2.90 – 2.81 (m, 3H), 2.52 – 2.45 (m, 1H), 2.33 – 2.23 (m, 1H), 2.12 (d, *J* = 13.9, 0.7 Hz, 1H), 2.00 – 1.91 (m, 1H), 1.70 – 1.54 (m, 4H), 1.51

(t, J = 0.5 Hz, 3H), 1.44 – 1.38 (m, 2H), 0.97 (s, 3H), 0.94 – 0.90 (m, 6H). **^{13}C NMR** (126 MHz, CDCl$_3$) δ_C 201.1, 143.4, 143.3, 130.0, 114.2, 49.5, 45.3, 34.4, 33.9, 32.8, 26.9, 26.4, 24.1, 21.8, 20.8, 16.2, 13.7.

(2*R*,3*R*)-2-((*R*)-1-Hydroxy-2-methylpropyl)-2,3-dimethylcyclohexan-1-one (49)

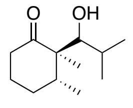

Bis(((trifluoromethyl)sulfonyl)oxy)copper (15 mg, 0.040 mmol) and (R,S,S)-(+)-(3,5-Dioxa-4-phospha-cyclohepta[2,1-a;3,4-a']dinaphthalen-4-yl)bis(1-phenylethyl) amine (43 mg, 0.080 mmol) were charged in a Schlenk filled with Ar and dissolved in 10 mL anhydrous Et$_2$O. The suspension was stirred at 23 ºC for and cooled to –30 ºC. AlMe$_3$ (2.9 mL, 6.4 mmol, 2.2 M in hexane) was then added and the mixture stirred at –30 ºC for 15 min. A solution of 2-methylcyclohexenone (363 μL, 3.20 mmol) in 4 mL Et$_2$O was added and the resulting mixture was stirred at –30 ºC for 18 h. Freshly distilled isobutyraldehyde (419 μL, 3.84 mmol) were added and the mixture was stirred at –20 ºC for 2 h and at –5 ºC for 30 min. The green solution was poured into a sat. solution of NH$_4$Cl and stirred for 4 h at 23 ºC. Extractions with Et$_2$O (x3) were done drying the combined organic layers over Na$_2$SO$_4$. After evaporating the solvent, the crude was purified using chromatography column eluting with a gradient of pentane/Et$_2$O 20:1 to 5:1.

53 mg of **49** (0.27 mmol) were isolated in 9% yield.

^{1}H NMR (500 MHz, CDCl$_3$) δ_H 4.07 (d, J = 10.5 Hz, 1H), 3.49 (dd, J = 10.4, 3.3 Hz, 1H), 2.43 – 2.32 (m, 2H), 2.13 – 2.02 (m, 1H), 1.95 – 1.86 (m, 2H), 1.79 – 1.66 (m, 3H), 1.25 (s, 3H), 1.01 (d, J = 6.9 Hz, 3H), 0.89 (d, J = 6.8 Hz, 3H), 0.80 (d, J = 6.9 Hz, 3H). **^{13}C NMR** (101 MHz, CDCl$_3$) δ_C 176.4, 81.3, 54.1, 39.7, 37.3, 35.9, 29.7, 29.1, 23.7, 21.8, 17.7, 15.1.

((5,6-Dimethylcyclohex-1-en-1-yl)oxy)trimethylsilane

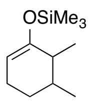

A solution of CuBr·Me$_2$S (180 mg, 0.88 mmol) dissolved in 3 mL anhydrous HMPA and 14 mL THF was cooled to –40 ºC and dropwise added a solution of MeMgBr (5.85 mL, 17.54 mmol, 3 M in diethyl ether). After 30 min stirring, 2-methylcyclohexenone (966 mg, 8.77 mmol) and chlorotrimethylsilane (2.23 mL, 17.54 mmol) were added at –40 ºC and stirred for 1 h. Et$_3$N (2.32 mL, 16.77 mmol) was finally added followed by water (1.6 mL). The mixture was extracted with Et$_2$O (x3) and the combined organic layers were washed with water and dried over Na$_2$SO$_4$. After solvent evaporation, the crude was purified by column chromatography eluting with pentane.

890 mg of ((5,6-dimethylcyclohex-1-en-1-yl)oxy)trimethylsilane (4.49 mmol) were isolated in 51% yield.

^{1}H NMR (300 MHz, CDCl$_3$) δ_H 2.11 (q, J = 6.4 Hz, 1H), 1.99 (dp, J = 5.6, 1.9 Hz, 2H), 1.77 – 1.62 (m, 2H), 1.55 (m, 4H), 1.27 (m, 1H), 0.98 (d, J = 6.9 Hz, 3H), 0.16 (s, 9H). **^{13}C NMR** (101 MHz, CDCl$_3$) δ_C 143.4, 116.6, 33.7, 31.5, 30.7, 20.6, 20.1, 14.4, 0.8.

(2*S*,3*R*)-2-Isobutyl-2,3-dimethylcyclohexan-1-one

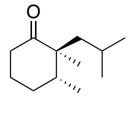

44 (100 mg, 0.56 mmol) was introduced in a dried Schlenk and dissolved in 5.4 mL. The solution was then degassed and the flask was purged with H$_2$ using a balloon and bubbled through the solution for 10 min. The Schlenk was cooled to 0 ºC and Crabtree's catalyst (4 mg, 5.5 μmol) was added in one portion. The reaction was allowed to stir under H_2 pressure at 23 ºC for 12 h. Solvent was evaporated and the resulting solid was diluted with Et_2O and filtered through SiO_2. Column chromatography was done eluting with pentane/Et_2O 40:1.

62 mg of (2*S*,3*R*)-2-isobutyl-2,3-dimethylcyclohexan-1-one (0.34 mmol) were isolated in 61% yield.

^{1}H NMR (300 MHz, $CDCl_3$) δ_H 2.53 – 2.27 (m, 2H), 2.03 – 1.84 (m, 3H), 1.74 – 1.48 (m, 3H), 0.97 (s, 3H), 0.94 (d, J = 6.4 Hz, 1H), 0.90 (d, J = 6.8 Hz, 3H), 0.85 (dd, J = 6.3, 3.3 Hz, 6H), 0.79 (d, J = 6.6 Hz, 1H). **^{13}C NMR** (75 MHz, $CDCl_3$) δ_C 216.7, 52.6, 45.5, 39.1, 38.6, 28.8, 25.1, 24.8, 24.2, 23.8, 19.7, 16.0. **HRMS** (APCI+) calculated for $[C_{12}H_{23}O]^+$ ($M+H^+$) *m/z* 183.1743, found *m/z* 183.1743.

(2*R*,3*R*)-2,3-Dimethyl-2-(2-methylprop-1-en-1-yl)cyclohexan-1-one (42)

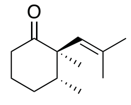

420 mg of **44** (2.33 mmol) (placed in 6 different MW vials) were dissolved in 120 mL of EtOH (20 mL each) and 384 mg $RhCl_3{\cdot}nH_2O$ (0.70 mmol, 38% Rh) (64 mg each) were added. The sealed vials were heated to 75 ºC for 4.5 h. After cooling to 23 ºC, the reactions were filtered through Celite. 400 mL of sat. brine were then added and extractions with pentane (5 x 400 mL) were done. After drying over Na_2SO_4, solvent was evaporated and the crude was purified by column chromatography eluting with pentane/Et_2O 50:1.

314 mg of **42** (1.74 mmol) were isolated in 75% yield containing traces of unreacted starting material.

The reaction was also performed decreasing the amount of catalyst to *ca.* 5% and increasing the concentration. Thus, **44** (58 mg, 0.322 mmol, 1 equiv) was placed in a 5 mL microwave vial and dissolved in HPLC analytical grade EtOH (5 mL) and $RhCl_3{\cdot}xH_2O$ (10 mg, 0.019 mmol, 38% Rh, 0.056 equiv) was added. The vial was sealed and heated at 75 ºC for 4.5 h. The work-up and purification were the same as previously stated.

43 mg of **42** were isolated as a colorless oil (0.238 mmol, 74% yield).

^{1}H NMR (400 MHz, $CDCl_3$) δ_H 5.37 (p, *J* = 1.4 Hz, 1H), 2.73 – 2.60 (m, 1H), 2.21 – 2.11 (m, 2H), 2.11 – 2.03 (m, 1H), 1.91 – 1.78 (m, 2H), 1.71 (d, *J* = 1.4 Hz, 3H), 1.45 – 1.38 (m, 1H), 1.42 (d, *J* = 1.3 Hz, 3H), 1.07 (s, 3H), 0.83 (d, *J* = 6.9 Hz, 3H). **^{13}C NMR** (100 MHz, $CDCl_3$) δ_C 216.5, 133.8, 132.4, 54.6, 45.0, 39.3, 28.8, 27.1, 23.9, 20.7, 18.5, 14.4. **[α]$_D$** ($CHCl_3$, *c* 0.50, 26 ºC) = 60.5 º.

(5*R*,6*R*)-5,6-Dimethyl-6-(2-methylprop-1-en-1-yl)cyclohex-1-en-1-yl trifluoromethane sulfonate (41)

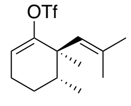

A solution of distilled diisopropylamine (0.35 mL, 2.50 mmol) in anhydrous THF (10 mL) was cooled to 0 ºC and *n*-BuLi (2.5 M in hexane, 1.0 mL, 2.50 mmol) was added dropwise. After 10 min at 0 ºC, the solution was cooled to –78 ºC and **4** (240 mg, 1.33 mmol) was added as a solution in anhydrous THF (2 mL). After 1 h stirring at –78 ºC, a solution of *N*-(2-pyridyl)bis(trifluoromethanesulfonimide) (800 mg, 2.24 mmol) in anhydrous THF (1 mL) was added. The resulting mixture was allowed to warm to 0 ºC for 1 h and then stirred at 23 ºC for 16 h. It was then poured on brine (100 mL) and extracted with pentane (5 × 50 mL). The combined organic layers were washed with brine (2 × 50 mL), dried over Na_2SO_4 and the solvent removed *in vacuo*. The crude mixture was purified by column chromatography on silica gel eluting with pentane.

340 mg of **41** were isolated as a colorless oil (1.09 mmol, 82% yield).
^{1}H NMR (400 MHz, $CDCl_3$) δ_H 5.71 (dd, J = 5.2, 3.1 Hz, 1H), 4.94 (app. pent, J = 1.5 Hz, 1H), 2.32 – 2.14 (m, 2H), 2.05 (app. dqd, J = 11.9, 6.9, 3.1 Hz, 1H), 1.71 (d, J = 1.4 Hz, 3H), 1.68 (d, J = 1.3 Hz, 3H), 1.58 – 1.37 (m, 2H), 1.14 (s, 3H), 0.92 (d, J = 6.9 Hz, 3H). **^{13}C NMR** (100 MHz, $CDCl_3$) δ_C 154.7, 135.0, 127.7, 118.3 (q, $J_{C\text{-}F}$ 319.2 Hz), 115.4, 43.1, 39.2, 27.4, 26.1, 23.8, 21.0, 18.4, 16.2. **^{19}F NMR** (376 MHz, $CDCl_3$) δ_F –75.4. **HRMS** (ESI+) calculated for $[C_{13}H_{19}F_3O_3SNa]^+$ (M+Na$^+$) *m/z* 335.0899, found *m/z* 335.0899. **[α]$_D$** ($CHCl_3$, *c* 0.67, 25 ºC) = –7.2 º.

(((5*R*,6*R*)-5,6-Dimethyl-6-(2-methylprop-1-en-1-yl)cyclohex-1-en-1-yl)ethynyl) trimethylsilane

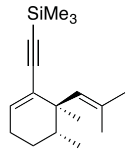

$PdCl_2(PPh_3)_2$ (9 mg, 0.013 mmol, 0.02 equiv) and CuI (6 mg, 0.032 mmol, 0.05 equiv) were suspended in degassed Et_3N (1.43 mL, 10.2 mmol, 16 equiv). To this suspension was added **41** (200 mg, 0.64 mmol, 1 equiv) dissolved in 1 mL of degassed DMF immediately followed by addition of TMS-acetylene (0.11 mL, 0.77 mmol, 1.2 equiv). The mixture was stirred at 23 ºC for 3 h, then poured on brine (50 mL) and extracted with pentane (3 × 30 mL). The combined organic layers were washed with brine (30 mL) and concentrated under reduced pressure. The crude material was used in the following reaction without further purification.
Note: alternatively this enyne can be purified by column chromatography on silica gel eluting with pentane to afford analytically pure material.
^{1}H NMR (400 MHz, $CDCl_3$) δ_H 6.11 (dd, J = 4.3, 3.4 Hz, 1H), 5.06 (app. pent, J = 1.2 Hz, 1H), 2.16 – 2.09 (m, 2H), 1.89 – 1.78 (m, 1H), 1.69 (d, J = 1.4 Hz, 3H), 1.65 (d, J = 1.3 Hz, 3H), 1.53 – 1.36 (m, 2H), 1.09 (s, 3H), 0.88 (d, J = 6.8 Hz, 3H), 0.13 (s, 9H). **^{13}C NMR** (101 MHz, $CDCl_3$) δ_C 134.6, 132.6, 132.4, 131.2, 107.1, 91.0, 42.3, 37.6, 27.5, 26.6, 26.1, 22.9, 18.5, 17.2, 0.2. **HRMS** (APCI+) calculated for $[C_{17}H_{29}Si]^+$ (M+H$^+$) *m/z* 261.2033, found *m/z* 261.2033. **[α]$_D$** ($CHCl_3$, *c* 0.75, 25 ºC) = –17.5 º.

(5*R*,6*R*)-1-Ethynyl-5,6-dimethyl-6-(2-methylprop-1-en-1-yl)cyclohex-1-ene (40)

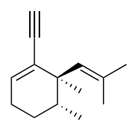

The crude material obtained previously was dissolved in MeOH (2 mL) and K_2CO_3 (177 mg, 1.28 mmol, theor. 2 equiv) was added. The resulting suspension was stirred at 23 ºC for 5 h (monitored by GC-MS) and poured on half-saturated brine (100 mL) and extracted with pentane (5 × 50 mL). The combined organic layers were dried over Na_2SO_4 and the solvent was concentrated. Purification by column chromatography on silica gel eluting with pentane afforded **6** as a pale yellow oil (90 mg, 0.48 mmol, 74% over 2 steps).
^{1}H NMR (400 MHz, $CDCl_3$) δ_H 6.17 (dd, J = 4.8, 3.4 Hz, 1H), 5.12 (app. pent, J = 1.4 Hz, 1H), 2.67 (app. s, 1H), 2.17 – 2.10 (m, 2H), 1.86 (dqd, J = 11.9, 6.8, 3.1 Hz, 1H), 1.72 (d, J 1.5 Hz, 3H), 1.66 (d, J 1.4 Hz, 3H), 1.54 – 1.47 (m, 1H), 1.45 – 1.36 (m, 1H), 1.11 (s, 3H), 0.89 (d, J 6.8 Hz, 3H). **^{13}C NMR** (100 MHz, $CDCl_3$) δ_C 135.5, 133.0, 132.0, 130.0, 84.9, 74.2, 41.9, 37.5, 27.4, 26.5, 26.0, 22.8, 18.2, 17.0. **HRMS** (APCI+) calculated for $[C_{14}H_{21}]^+$ (M+H$^+$) *m/z* 189.1638, found *m/z* 189.1645. **[α]$_D$** ($CHCl_3$, *c* 0.60, 26 ºC) = 19.0 º.

(2*R*,3*R*)-1-Ethynyl-2,3-dimethyl-2-(2-methylprop-1-en-1-yl)cyclohexan-1-ol (54)

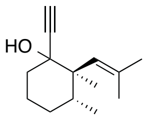

A solution of **54** (59 mg, 0.33 mmol) in 3 mL THF was cooled to –78 ºC and ethynylmagnesium bromide (1.6 mL, 1.64 mmol, 1 M in THF) was added over a period off 10 min. The reaction was stirred at –78 ºC for 10 min and stirred continued for 3 h at –15ºC. The reaction was warmed to 23 ºC for 16 h. Sat. aq. NH_4Cl was added and the mixture was extracted with Et_2O (x3). The combined organic layers were dried over Na_2SO_4, filtered and concentrated to reduced pressure. The crude was purified it by column chromatography eluting with pentane/Et_2O 50:1.

29 mg of **42** (0.14 mmol) were isolated in 43% yield as a 4:1 mixture of diastereomers.

^{1}H NMR (300 MHz, $CDCl_3$) (major diastereomer) δ_H 5.34 – 5.21 (m, 1H), 2.47 (s, 1H), 2.23 (s, 1H), 1.94 – 1.87 (m, 1H), 1.81 (d, *J* = 1.4 Hz, 3H), 1.80 (d, *J* = 1.4 Hz, 3H), 1.75 – 1.63 (m, 3H), 1.25 (s, 2H), 1.14 (s, 3H), 0.80 (d, *J* = 6.8 Hz, 3H). **^{13}C NMR** (101 MHz, $CDCl_3$) (major diastereomer) δ_C 147.9, 131.9, 77.4, 75.9, 74.0, 48.4, 39.5, 33.1, 29.4, 28.3, 22.7, 19.7, 17.0, 11.9.

(3a*S*,4*R*)-7a-Ethynyl-2,2,3a,4-tetramethyloctahydrobenzofuran (55)

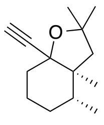

To a solution of *p*-toluenesulfonic acid (3.73 mg, 0.020 mmol) in 5 mL benzene was added **54** (27 mg, 0,131 mmol) and the mixture was stirred for 16 h at 80ºC. Water was added and the mixture was extracted with Et_2O (x3), washed with brine and drying over Na_2SO_4. Chromatography column was done eluting with pentane/Et_2O 70:1.

21 mg of **55** (0.102 mmol) were isolated in 78% yield.

^{1}H NMR (400 MHz, $CDCl_3$) δ_H 2.56 (s, 1H), 2.18 (ddd, *J* = 11.7, 6.9, 4.8 Hz, 1H), 2.03 (dd, *J* = 11.8, 1.2 Hz, 1H), 1.95 – 1.67 (m, 4H), 1.64 (d, *J* = 11.9 Hz, 1H), 1.58 (s, 3H), 1.45 – 1.38 (m, 2H), 1.35 (s, 3H), 0.95 (d, *J* = 0.9 Hz, 3H), 0.83 (d, *J* = 6.8 Hz, 3H). **^{13}C NMR** (101 MHz, $CDCl_3$) δ_C 88.1, 84.0, 81.7, 76.7, 49.9, 49.5, 37.0, 31.3, 30.7, 30.3, 28.2, 22.1, 17.2, 16.1. **HRMS** (APCI+) calculated for $[C_{14}H_{23}O]^+$ $(M+H^+)$ *m/z* 207.1743, found *m/z* 207.1739.

(1,3-Bis(2,6-diisopropylphenyl)-2,3-dihydro-1*H*-imidazol-2-yl)((1,1,1-trifluoro-*N*-((trifluoromethyl)sulfonyl)methyl)sulfonamido)gold

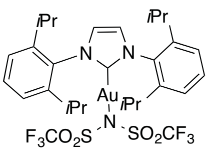

To IPrAuCl (200 mg, 0.32 mmol) dissolved in 1.6 mL CH_2Cl_2 was slowly added a solution of $AgNTf_2$ (125 mg, 0.32 mmol) in 1.6 mL CH_2Cl_2. After stirring for 1 h at 23 ºC, the mixture was filtrated through Celite and solvent was evaporated. The resulting solid was redissolved in CH_2Cl_2, filtered through Teflon filters and crystallized with pentane.

238 mg of $IPrAuNTf_2$ (0.274 mmol) were isolated in 85% yield.

^{1}H NMR (400 MHz, $CDCl_3$) δ_H 7.53 (t, *J* = 7.8 Hz, 2H), 7.31 (d, *J* = 7.9 Hz, 4H), 7.28 (s, 2H), 2.48 (sept, *J* = 6.9 Hz, 4H), 1.31 (d, *J* = 6.9 Hz, 12H), 1.23 (d, *J* = 6.9 Hz, 12H). **^{13}C NMR** (101 MHz, $CDCl_3$) 168.3, 145.7, 135.8, 133.6, 124.4, 123.7, 118.9 (q, $J_{C\text{-}F}$ = 320 Hz), 29.1, 14.4. 23.1. **^{19}F NMR** (376 MHz, $CDCl_3$) δ_F –75.7.

2-(*tert*-Butyl)pyridine

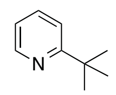

CuCN (1.44 g, 16.08 mmol) was dissolved in 250 mL THF and *tert*-butylmagnesium chloride (37.8 mL, 64.3 mmol) was added. After stirring the mixture at –78 ºC for 20 min, 2-bromopyridine (0.77 mL, 8,04 mmol) was added and the mixture was stirred for 3 h at –78 ºC and then at 23 ºC for 14 h. The reaction was quenched with a sat. solution of NH_4OH and the pH was adjusted to 10 upon addition of sat. solution NaOH. Extractions with Et_2O (x3) were done and the combined organic layers were dried over Na_2SO_4.

204 mg of 2-(*tert*-butyl)pyridine (1.51 mmol) were isolated in 19% yield.

^{1}H NMR (300 MHz, $CDCl_3$) δ_H 8.55 (dd, *J* = 4.0f, 1.2 Hz, 1H), 7.59 (td, *J* = 7.8, 1.9 Hz, 1H), 7.32 (d, *J* = 8.0 Hz, 1H), 7.06 (ddd, *J* = 7.5, 5.0, 0.7 Hz, 1H), 1.36 (s, 9H).

2-(*tert*-Butyl)pyridine-*N*-oxide

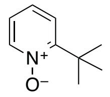

3-chlorobenzoperoxoic acid (296 mg, 1.71 mmol) was added portionwise to a 0 ºC solution of 2-(*tert*-butyl)pyridine (193 mg, 1.43 mmol) and 0.8 mL CH_2Cl_2. The mixture was allowed to warm to 23 ºC and stirred for 4 h. Sat. solution $NaHCO_3$ was added to the reaction mixture and the organic layers were extracted with CH_2Cl_2 (x3) and dried over Na_2SO_4. The crude was used without purifying it after evaporation of the solvent.

201 mg of 2-(*tert*-butyl)pyridine-*N*-oxide (1.33 mmol) were isolated in 93% yield.

^{1}H NMR (400 MHz, $CDCl_3$) δ_H 8.32 (dd, *J* = 6.4, 1.4 Hz, 1H), 7.37 (dd, *J* = 7.9, 1.4 Hz, 1H), 7.29 – 7.22 (m, 1H), 7.15 (ddd, *J* = 7.5, 6.4, 2.1 Hz, 1H), 1.53 (s, 9H). **^{13}C NMR** (101 MHz, $CDCl_3$) δ_C 158.3, 141.9, 126.8, 123.9, 123.7, 36.5, 27.1.

(1a*S*,1b*R*,2*R*,6a*R*)-1,1,1b,2-Tetramethyl-1a,1b,2,3,4,6a-hexahydrocyclopropa[*a*]inden-6(1*H*)-one (56)

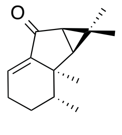

To a solution of **40** (65 mg, 0.345 mmol) in 1.5 mL $(CH_2Cl)_2$ were added 3,5-dichloropyridine-*N*-oxide (226 mg, 1.381 mmol) and $IPrAuNTf_2$ (15 mg, 0.017 mmol). The resulting mixture was stirred at 80 ºC for 4 h. After cooling to 23 ºC, the mixture was poured to a sat. sol. $CuSO_4$ and the extracted with CH_2Cl_2 (x3). The combined organic layers were dried over Na_2SO_4, solvent was evaporated and the crude was purified eluting with pentane/Et_2O 10:1.

52 mg of **56** (0.255 mmol) were isolated in 74% yield.

^{1}H NMR (500 MHz, $CDCl_3$) δ_H 6.43 (t, *J* = 3.5 Hz, 1H), 2.30 – 2.10 (m, 2H), 1.79 – 1.70 (m, 1H), 1.73 (d, *J* = 5.7 Hz, 1H), 1.61 (dd, *J* = 5.5, 0.7 Hz, 1H), 1.58 – 1.51 (m, 1H), 1.50 – 1.40 (m, 1H), 1.14 (s, 3H), 1.06 (s, 3H), 1.00 (d, *J* = 6.8 Hz, 3H), 0.96 (s, 3H). ^{13}C NMR (126 MHz, $CDCl_3$) δ_C 202.2, 146.8, 131.6, 42.4, 42.2, 39.2, 33.5 , 30.2, 28.9, 26.5, 25.9, 22.5, 16.9, 16.1. **HRMS** (APCI+) calculated for $[C_{14}H_{21}O]^+$ $(M+H^+)$ *m/z* 205.1587, found *m/z* 205.1590. **[α]$_D$** ($CHCl_3$, *c* 0.53, 26 ºC) = –39.0 º.

(1a*S*,1b*R*,2*R*,6a*R*)-1,1,1b,2-Tetramethyl-1,1a,1b,2,3,6a-hexahydrocyclopropa[*a*]indene (57)

As side product, 9 mg (0.048 mmol) of **57** were isolated in 15% yield containing around 10% of an unknown impurity.

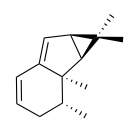

^{1}H NMR (500 MHz, $CDCl_3$) δ_H 6.14 (dd, *J* = 9.5, 2.4 Hz, 1H), 5.60 (ddd, *J* = 9.7, 5.4, 2.1 Hz, 1H), 5.33 (d, *J* = 1.4 Hz, 1H), 2.07 – 1.98 (m, 1H), 1.97 – 1.84 (m, 2H), 1.67 (dd, *J* = 6.0, 2.0 Hz, 1H), 1.03 (s, 3H), 1.01 (d, *J* = 6.5 Hz, 3H), 1.00 (d, *J* = 6.1 Hz, 1H), 0.95 (s, 3H), 0.90 (s, 3H). **^{13}C NMR** (126 MHz, $CDCl_3$) δ_C 147.5, 128.7 123.4, 121.8, 49.0, 37.1, 34.9, 33.0, 32.8, 27.8, 24.7, 21.2, 17.1, 16.7. **HRMS** (EI+) calculated for $[C_{14}H_{20}^{\bullet}]^+$ (M $^{\bullet+}$) *m/z* 188.1565, found *m/z* 188.1563.

Nardoaristolone B, ((1a*S*,1b*R*,2*R*,6a*R*)-1,1,1b,2-Tetramethyl-1,1a,1b,2,3,6a-hexahydro cyclopropa[*a*]indene-4,6-dione)

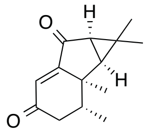

To a suspension of **56** (15 mg, 0.073 mmol) in 0.4 mL CH_2Cl_2 and K_2CO_3 (3 mg, 0.022 mmol) was added $Pd(OH)_2$ (5 mg, 0.007 mmol) and finally *t*-BuO_2H (6 μL, 0.037 mmol). The reaction was stirred for 5 h at 23 ºC. The crude was filtrated though Celite and solvent was evaporated. Column chromatography was done eluting with pentane/Et_2O 2:1.

15 mg (0.069 mmol) of **nardoaristolone B** were isolated in 93% yield.

^{1}H NMR (500 MHz, $CDCl_3$) δ_H 6.22 (s, 1H), 2.50–7.37 (m, 2H), 2.29 (dd, *J* 18.0, 13.5 Hz, 1H), 1.99 (d, *J* 5.5 Hz, 1H), 1.83 (dd, *J* 5.5, 0.8 Hz, 1H), 1.23 (s, 3H), 1.18 (s, 3H), 1.14 (s, 3H), 1.12 (d, *J* 6.7 Hz, 3H). **^{13}C NMR** (126 MHz, $CDCl_3$) δ_C 201.3, 199.7, 164.9, 123.3, 44.1, 42.1, 42.0, 40.0, 35.3, 31.9, 28.6, 20.6, 17.6, 15.6. **HRMS** (ESI+) calculated for $[C_{14}H_{19}O_2]^+$ (M+H$^+$) *m/z* 219.1380, found *m/z* 219.1371. **$[\alpha]_D$** (MeOH, *c* 0.5, 26 ºC) = –7.4 º.[178] **M.p.** 96–97 ºC.[179] Structure confirmed by **X-ray**.

2-Methyl-1-(prop-2-yn-1-yl)cyclohexan-1-ol

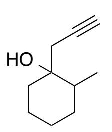

To a stirred suspension of Mg turnings (894 mg, 36.80 mmol), iodine (two crystals) and $HgCl_2$ (18 mg, 0.067 mmol) in 13.5 mL Et_2O under Ar equipped with a condenser was added dropwise a solution of 3-bromoprop-1-yne (3.17 mL, 36.80 mmol) in 6.5 mL Et_2O. The mixture was allowed to reflux for 30 min and then cooled down to 0 ºC. 2-methylcyclohexanone (1.62 mL, 13.37 mmol) was added and the reaction was stirred for 1 h 30 min at this temp. Sat. solution HCl (10%) were added to quench the reaction and extracted with Et_2O (x3). Org. layers were combined, dried over Na_2SO_4 and solvent was evaporated. Chromatography column was done eluting with pentane/Et_2O 30:1.

1.73 g of 2-methyl-1-(prop-2-yn-1-yl)cyclohexan-1-ol (11.40 mmol) were isolated in 85% yield as a 3.1:1 of diastereomers.

^{1}H NMR (500 MHz, $CDCl_3$) (major diastereomer) δ_H 2.46 (dd, *J* = 16.6, 2.7 Hz, 1H), 2.34 (dd, *J* = 16.6, 2.7 Hz, 1H), 2.04 (t, *J* = 2.7 Hz, 1H), 1.82 – 1.75 (m, 1H), 1.70 – 1.60 (m, 3H), 1.58 – 1.53 (m, 3H), 1.46 – 1.43 (m, 1H), 1.39 – 1.32 (m, 1H), 0.91 (d, *J* = 6.8 Hz, 3H) (proton from the OH group missing). **^{13}C NMR** (101 MHz, $CDCl_3$) (major diastereomer) δ_C 81.2, 72.5, 71.1, 37.9, 36.9, 31.3, 30.6, 25.7, 21.9, 15.1.

---

[178] The reported α_D of the isolated natural product is the following: $[\alpha]_D$ (MeOH, *c* 0.5, 26 ºC) = – 19.60º. See ref. 112.

[179] Melting point of the racemate: (60–62 ºC). See ref. 118.

1-Bromo-4-(*tert*-butyl)cyclohex-1-ene

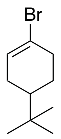

Triphenylphosphite (0.82 mL, 6.94 mmol) was dissolved in CH_2Cl_2 (15 mL) and the solution cooled to –60 ºC. Bromine (0.37 mL, 7.13 mmol) was added dropwise followed by addition of Et_3N (1 mL, 7.78 mmol) and 4-(*tert*-butyl)cyclohexanone (1 g, 6.48 mmol). The mixture was allowed to warm at 23 ºC for 16 h and then heated at 40 ºC for 2 h. After cooling to 23 ºC, water was added and extractions with pentane were done (x5). Organic layers were washed with sat. brine, dried over Na2SO4 and concentrated. The crude was purified by column chromatography on silica gel eluting with pentane.

1.2 g of 1-bromo-4-(*tert*-butyl)cyclohex-1-ene (5.52 mmol) were isolated in 85% yield.

^{1}H NMR (500 MHz, $CDCl_3$) δ_H 6.03 (ddd, J = 5.7, 3.5, 2.1 Hz, 1H), 2.48 – 2.44 (m, 2 H), 2.12 – 2.05 (m, 1H), 1.89 – 1.81 (m, 2H), 1.40 – 1.28 (m, 2H), 0.86 (s, 9H). **^{13}C NMR** (125 MHz, $CDCl_3$) δ_C 128.9, 121.9, 42.8, 36.4, 32.1, 29.0, 27.1, 25.9.

***N*'-(4-(*tert*-Butyl)cyclohexylidene)-4-methylbenzenesulfonohydrazide**

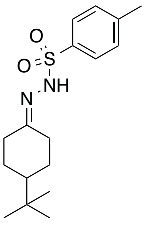

p-toluenesulfonyl hydrazide (500 mg, 3.24 mmol) was suspended in 1 mL EtOH and 4-*tert*-butylcyclohexanone was added. The mixture was heated at 85 ºC for 1 h. After cooling to 23 ºC, the suspension formed was dissolved in CH_2Cl_2, evaporated to dryness and the resulting white solid was washed with cold EtOH and Et_2O.

846 mg of *N*'-(4-(*tert*-butyl)cyclohexylidene)-4-methylbenzenesulfono hydrazide (2.62 mmol) were isolated in 81% yield.

^{1}H NMR (400 MHz, $CDCl_3$) δ_H 7.84 (d, J = 8.3 Hz, 2H), 7.58 (bs, 1H), 7.30 (d, J = 7.8 Hz, 2H), 2.77 – 2.68 (m, 1H), 2.48 – 2.42 (m, 1H), 2.41 (s, 3H), 2.12 – 2.01 (m, 1H), 1.93 – 1.84 (m, 2H), 1.74 (ddd, J = 14.5, 13.1, 5.3 Hz, 1H), 1.25 – 1.01 (m, 3H), 0.86 – 0.79 (m, 9H). **^{13}C NMR** (101 MHz, $CDCl_3$) δ_C 163.3, 144.0, 135.6, 129.6, 128.2, 47.2, 35.1, 32.6, 27.6, 27.5, 26.9, 26.5, 21.7.

4-(*tert*-Butyl)cyclohex-1-en-1-yl trifluoromethanesulfonate

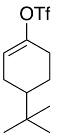

To a 0 ºC cold solution of distilled diisopropylamine (2.75 mL, 19.45 mmol) and 106 mL THF was dropwise added *n*-BuLi (2.5 M in hexane, 7.8 mL, 19.45 mmol). After 10 min, the solution was cooled to -50 ºC and 4-(*tert*-butyl)cyclohexanone in 22 mL THF was added. After 1 h stirring, a solution of *N*-phenyl-bis(trifluoromethanesulfonimide) (6.95 g, 19.45 mmol) in 3 mL THF were added. The resulting mixture was allowed to warm to 0 ºC for 1 h and quenched with sat. aq. NH_4Cl. The organic layers were extracted with pentane (x3), dried over Na_2SO_4 and purified by column chromatography eluting with pentane.

2.01 g (7.02 mmol) of 4-(*tert*-butyl)cyclohex-1-en-1-yl trifluoromethanesulfonate were isolated in 54% yield.

^{1}H NMR (500 MHz, $CDCl_3$) δ_H 5.74 (dt, J = 6.0, 2.3 Hz, 1H), 2.43 – 2.28 (m, 2H), 2.24 – 2.16 (m, 1H), 1.99 – 1.89 (m, 2H), 1.41 – 1.28 (m, 2H), 0.89 (s, 9H). **^{13}C NMR** (126 MHz, $CDCl_3$) δ_C 149.4, 118.7 (q, $J_{C\text{-}F}$ 320.7 Hz), 118.6, 43.1, 32.2, 28.7, 27.4, 25.5, 24.2.

4-(*tert*-Butyl)-1-(prop-1-yn-1-yl)cyclohex-1-ene

To a solution of 4-*tert*-butylcyclohexene enol triflate (25 mg, 0.087 mmol) in 1 mL DMF was added LiCl (11 mg, 0.261 mmol) and N_2 was bubbled through the mixture for 10 min

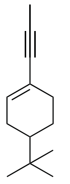

and bis(triphenylphosphine)palladium(II) dichloride (6 mg, 8.6 μmol) added. The mixture was heated at 70 ºC and allenyltributyltin (31 μL, 0.096 mmol) was finally added. The reaction was stirred for 2 h at 70 ºC, after which was allowed to cooled to 23 ºC, filtered through Celite and added to sat. brine. The org. layers were extracted with CH_2Cl_2 (x3) and solvent was concentrated. The crude was dissolved again with CH_2Cl_2 and extracted with HCl 10% (x5). The aq. layers were extracted with CH_2Cl_2 (x2), dried over Na_2SO_4 and solvent evaporated. Column chromatography eluting with pentane gave 11 mg of 4-(*tert*-butyl)-1-(prop-1-yn-1-yl)cyclohex-1-ene (0.059 mmol) in 68% yield.

^{1}H NMR (500 MHz, $CDCl_3$) δ_H 6.02 – 5.98 (m, 1H), 2.20 – 2.05 (m, 3H), 1.93 (s, 3H), 1.87 – 1.76 (m, 2H), 1.28 – 1.10 (m, 2H), 0.85 (s, 9H). **^{13}C NMR** (126 MHz, $CDCl_3$) δ_C 133.6, 120.9, 83.1, 81.4, 43.4, 31.2, 27.4, 27.3, 27.3, 24.0, 4.3.

2-(4-(*tert*-Butyl)cyclohexylidene)acetaldehyde (62)

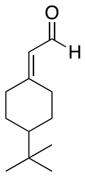

To a solution of 4-*tert*-butylcyclohexenetriflate (100 mg, 0.349 mmol) in 2 mL DMF was added LiCl (44 mg, 1.05 mmol) and N_2 was bubbled through the mixture for 10 min and bis(triphenylphosphine)palladium(II) dichloride (12 mg, 17 μmol) added. The mixture was heated at 70 ºC and cis-tributyl(2-ethoxyethenyl)stannane (128 μL, 0.384 mmol) dissolved in 2 mL DMF was finally added. The reaction was stirred for 6 h at 70 ºC, after which was allowed to cooled to 23 ºC, filtered through Celite and added to sat. brine. The org. layers were extracted with CH_2Cl_2 (x3) and solvent was concentrated. The crude was dissolved again with CH_2Cl_2 and extracted with HCl 10% (x5). The aq. layers were extracted with CH_2Cl_2 (x2), dried over Na_2SO_4 and solvent evaporated. Column chromatography eluting with pentane/Et_2O 25:1 gave 43 mg of isolated aldehyde **62** (0.239 mmol) in 68% yield.

^{1}H NMR (400 MHz, $CDCl_3$) δ_H 9.96 (d, J = 8.2 Hz, 1H), 5.77 (d, J = 8.2 Hz, 1H), 3.38 (d, J = 13.6 Hz, 1H), 2.38 (d, J = 13.6 Hz, 1H), 2.20 (dt, J = 13.0, 4.6 Hz, 1H), 2.10 – 1.92 (m, 3H), 1.36 – 1.10 (m, 3H), 0.83. **^{13}C NMR** (MHz, $CDCl_3$) δ_C 190.4, 167.7, 124.8, 47.7, 37.8, 32.4, 29.2, 29.0, 28.8, 27.4.

(*E*)-2-((2*R*,3*R*)-2,3-Dimethyl-2-(2-methylprop-1-en-1-yl)cyclohexylidene)acetaldehyde (63)

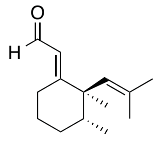

Stille cross coupling

To a solution of **41** (54 mg, 0.173 mmol) in 1 mL DMF was added LiCl (22 mg, 0.518 mmol) and N_2 was bubbled through the mixture for 10 min and bis(triphenylphosphine)palladium(II) dichloride (6 mg, 8.6 μmol) added. The mixture was heated at 70 ºC and cis-tributyl(2-ethoxyethenyl)stannane (64 μL, 0.190 mmol) dissolved in 1 mL DMF was finally added. The reaction was stirred for 6 h at 70 ºC, after which was allowed to cooled to 23 ºC, filtered through Celite and added to sat. brine. The org. layers were extracted with CH_2Cl_2 (x3) and solvent was concentrated. The crude was dissolved again with CH_2Cl_2 and extracted with HCl 10% (x5). The aq. layers were extracted with CH_2Cl_2 (x2), dried over Na_2SO_4 and solvent evaporated. Column chromatography eluting with pentane/Et_2O 25:1 gave 19 mg of isolated aldehyde **63** (0.092 mmol) in 54% yield.

Suzuki cross coupling

To a solution of **41** (144 mg, 0.461 mmol) and boronic ester **61** (122 mg, 0.616 mmol) in 0.75 mL degassed DMF was added a solution of tripotassium phosphate (293 mg, 1.383 mmol) in 0.75 mL degassed water. Pd_2dba_3 (10 mg, 11.5 μmol) and triphenylphosphine (12 mg, 46.1 μmol) were finally added and the resulting mixture was stirred at 65 ºC for 2 h. After cooling to 23 ºC, the reaction was quenched with sat. brine and the org. layers were extracted with CH_2Cl_2 (x3) and concentrated in vacuum. The crude was dissolved again with CH_2Cl_2 and extracted with HCl 10% (x5). The aq. layers were extracted with CH_2Cl_2 (x2), dried over Na_2SO_4 and solvent evaporated. Column chromatography eluting with pentane/Et_2O 25:1 gave 58 mg of isolated aldehyde **63** (0.281 mmol) in 61% yield

^{1}H NMR (400 MHz, $CDCl_3$) δ 10.09 (d, *J* = 8.1 Hz, 1H), 6.03 (d, *J* = 8.1 Hz, 1H), 5.22 (app. pent, *J* = 1.4 Hz, 1H), 2.96 (dt, *J* = 13.2, 4.9 Hz, 1H), 2.61 – 2.52 (m, 1H), 2.00 – 1.83 (m, 2H), 1.71 (d, *J* = 1.4 Hz, 3H), 1.70 – 1.61 (m, 3H), 1.49 (d, *J* = 1.3 Hz, 3H), 1.14 (s, 3H), 0.82 (d, *J* = 7.0 Hz, 3H). **^{13}C NMR** (101 MHz, $CDCl_3$) δ 191.2, 173.1, 133.6, 133.1, 126.4, 47.9, 44.0, 29.5, 27.5, 26.7, 24.8, 22.6, 19.0, 14.9. **HRMS** (ESI+) calculated for $[C_{14}H_{22}ONa]^+$ $(M + Na^+)$ *m/z* 229.1563, found *m/z* 229.1562.

Trimethyl(3-(4,4,5,5-tetramethyl-1,3,2-dioxaborolan-2-yl)prop-1-yn-1-yl)silane (60)

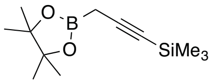

To a flame dried bottom flask was added 1-trimethylsilylpropyne (1.65 mL, 14.85 mmol) in 10 mL and cooled to -25 ºC under Ar. *n*-BuLi (5.66 mL, 14.14 mmol) was slowly added and the resulting yellow solution was stirred for 1 h at -25 ºC. Another flame-dried flask containing $MgCl_2$ (1.31 g, 13.78 mmol) and 2-isopropoxy-4,4,5,5-tetramethyl-1,3,2-dioxaborolane (2.81 mL, 13.78 mmol) was cooled to -25 ºC after which it was charged with the solution containing the lithiopropyne. The resulting suspension was allowed to stir at -20 ºC for 2 h and a solution of acetyl chloride (1.08 mL, 15.15 mmol) in 0.8 mL MTBE was added. The mixture was stirred for 1 h at -20 ºC, then allowed to warm to 23 ºC over 1 h and concentrated in vacuum. The resulting yellow gummy solid residue was added 20 mL hexanes and the suspension was filtered. The resulting solid was washed further with hexanes (2 × 10 mL) and the volatiles removed in vacuum.

1.80 g of **60** (7.56 mmol) were isolated in 51% yield.

^{1}H NMR (400 MHz, $CDCl_3$) δ_H 1.87 (s, 2H), 1.27 (s, 12H), 0.13 (s, 9H). **^{13}C NMR** (101 MHz, $CDCl_3$) δ_C 103.4, 84.2, 83.3, 24.8.

(*E*)-2-(2-Ethoxyvinyl)-4,4,5,5-tetramethyl-1,3,2-dioxaborolane (64)

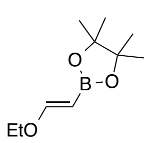

In a dry Scklenk tube under Ar, ethoxyehyne (4 mL, 16.76 mmol) and pinacolborane (2.67 mL, 18.38 mmol) were introduced ad dissolved in 40 mL CH_2Cl_2. Bis(cyclopentadienyl)zirconium(IV) chloride hydride (259 mg, 1.00 mmol) was introduced while a gentle argon overpressure was applied. The tube was sealed and stirred under argon at 23 ºC for 16 h after which the crude was filtered through neutral alumina, washed with Et_2O and the filtrated was collected in fractions. The fractions containing the product were combined and evaporated to give the desired boronate **64** in 94% yield (3.1 g, 15.65 mmol).

^{1}H NMR (500 MHz, $CDCl_3$) δ_H 7.05 (d, *J* = 14.4 Hz, 1H), 4.45 (d, *J* = 14.4 Hz, 1H), 3.86 (q, *J* = 7.1 Hz, 2H), 1.30 (t, *J* = 7.1 Hz, 3H), 1.27 (s, 12H).

4-Methylbenzenesulfonyl azide

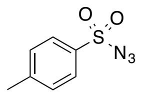

A solution of sodium azide (312 mg, 4.8 mmol) in water (1.3 mL) was quickly added to a suspension of 4-methylbenzenesulfonyl chloride (762 mg, 4.0 mmol) in 2.3 mL *i*-PrOH and stirred for 1 h at 23 ºC. Then, water (25 mL) was added and the mixture was stirred for another hour. Extractions were done with EtOAc (x3), the combined organic layers were dried over Na_2SO_4 and solvent was evaporated. The crude was used without any further purification in the next step.

^{1}H NMR (400 MHz, $CDCl_3$) δ 7.84 (d, *J* = 8.3 Hz, 2H), 7.41 (d, *J* = 8.0 Hz, 2H), 2.48 (s, 3H). **^{13}C NMR** (101 MHz, $CDCl_3$) δ 146.2, 135.5, 130.3, 127.6, 21.8.

Bestmann-Ohira reagent (Dimethyl (1-diazo-2-oxopropyl)phosphonate)

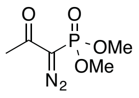

A solution of dimethyl (2-oxopropyl)phosphonate (631 mg, 3.8 mmol) in benzene (3.7 mL) was slowly added to a suspension of NaH (160 mg, 4 mmol, 60% in oil) in THF (2.4 mL) and benzene (19 mL). The reaction was stirred at 0 ºC for 1 h before the addition of 4-methylbenzene sulfonyl azide (789 mg, 4 mmol) in benzene (3.7 mL). The resulting solution was stirred for 2 h, filtered over Celite and the solvent was removed. Column chromatography in SiO2 was done eluting with hexanes/ EtOAc 1:1.

300 mg of Bestmann-Ohira reagent (1.56 mmol) were isolated in 40% yield.

^{1}H NMR (500 MHz, $CDCl_3$) δ_H 3.86 (s, 3H), 3.83 (s, 3H), 2.27 (s, 3H). **^{13}C NMR** (125 MHz, $CDCl_3$) δ_C 190.1, 189.1, 53.7 (d, *J* = 5.6 Hz), 27.3.

(1*R*,2*R*,*E*)-1,2-dimethyl-1-(2-methylprop-1-en-1-yl)-6-(prop-2-yn-1-ylidene)cyclo hexane (65)

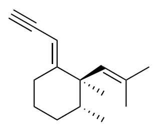

To **63** (19 mg, 0.092 mmol) dissolved in 0.3 mL THF, was added 0.3 mL MeOH followed by K_2CO_3 (23 mg, 0.166 mmol) and Bestmann-Ohira reagent (19 mg, 0.101 mmol). The reaction was stirred for 18 h at 23 ºC, after which sat. $NaHCO_3$ was added and extractions with CH_2Cl_2 (x3) were done. The org. layers were dried over Na_2SO_4, solvent was concentrated and the crude was purified in a chromatography column eluting with pentane.

13 mg of **65** (0.064 mmol) were isolated in 70% yield.

^{1}H NMR (500 MHz, $CDCl_3$) δ 5.37 (d, *J* = 2.3 Hz, 1H), 5.14 (app. pent, *J* = 2.6 Hz, 1H), 3.04 (d, *J* = 2.3 Hz, 1H), 2.64 – 2.54 (m, 1H), 2.50 – 2.35 (m, 1H), 1.85 – 1.77 (m, 1H), 1.75 – 1.71 (m, 1H), 1.71 (d, *J* = 1.4 Hz, 3H), 1.66 – 1.59 (m, 1H), 1.54 (d, *J* = 1.0 Hz, 3H), 1.52 – 1.46 (m, 1H), 1.39 – 1.33 (m, 1H), 1.09 (s, 3H), 0.80 (d, *J* = 6.9 Hz, 3H). **^{13}C NMR** (126 MHz, $CDCl_3$) δ 162.2, 133.3, 132.9, 102.0, 82.5, 79.9, 46.5, 43.0, 29.9, 29.2, 27.7, 24.1, 22.2, 18.9, 15.2. **HRMS** (EI+) calculated for $[C_{15}H_{22}^{\bullet}]^+$ ($M^{\bullet+}$) *m/z* 202.1722, found *m/z* 202.1721.

(3-((5*R*,6*R*)-5,6-Dimethyl-6-(2-methylprop-1-en-1-yl)cyclohex-1-en-1-yl)prop-1-yn-1-yl)trimethylsilane

A dry 2-neck round-bottom flask equipped with a condenser, was charged with activated magnesium tunings (315 mg, 13.0 mmol, 1.5 equiv) that were covered with anhydrous diethyl ether (8 mL). Dibromoethane (10 μL, 4.6 μmol, catalytic) was added followed by trimethylsilylpropargyl bromide (0.5 mL, 2.9 mmol, 0.33 equiv). The reaction was initiated

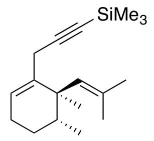

by warming to reflux. A gentle reflux was then maintained by slow addition of the remaining bromide (1 mL, 5.8 mmol, 0.66 equiv). After addition the mixture was heated to reflux for 20 additional min. The Grignard reagent was titrated and used in the following reaction.

A dry Schlenk tube was charged with Pd(PPh$_3$)$_4$ (148 mg, 0.128 mmol, 0.2 equiv) which was suepended in anhydrous Et$_2$O (8 mL). The suspension was stirred vigorously and **5** (200 mg, 0.64 mmol, 1 equiv) was added as a solution in anhydrous Et$_2$O (2 mL) immediately followed by addition of the solution of Grignard reagent freshly prepared (0.37 M, 6.9 mL, 2.56 mmol, 4 equiv) were added dropwise. The resulting reaction was stirred for 20 h at 23 ºC (monitored by GC-MS). The mixture was poured on brine (100 mL) and extracted with Et$_2$O (3 × 50 mL). The combined organic layers were dried over Na$_2$SO$_4$, filtered and the solvent concentrated. The crude material was used in the next step without further purification.

^{1}H NMR (500 MHz, CDCl$_3$) δ 5.93 – 5.87 (m, 1H), 5.04 (app. pent, *J* = 1.4 Hz, 1H), 2.94 (dq, *J* = 20.0, 2.7 Hz, 1H), 2.85 (dq, *J* = 20.0, 2.4 Hz, 1H), 2.15 – 2.09 (m, 2H), 1.90 – 1.83 (m, 1H), 1.67 (d, *J* = 1.4 Hz, 3H), 1.58 (d, *J* = 1.3 Hz, 3H), 1.50 – 1.37 (m, 2H), 0.99 (s, 3H), 0.87 (d, *J* = 7.0 Hz, 3H), 0.17 (s, 9H).

(5*R*,6*R*)-5,6-Dimethyl-6-(2-methylprop-1-en-1-yl)-1-(prop-2-yn-1-yl)cyclohex-1-ene (43)

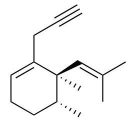

The crude material from the reaction described above (theor. 0.64 mmol, 1 equiv) was dissolved in MeOH (1.5 mL) and K$_2$CO$_3$ (177 mg, 1.28 mmol, 2 equiv) was added. The resulting suspension was stirred at 23 ºC for 6 h (monitored by GC-MS) and then poured on brine (50 mL) and extracted with pentane (5 × 30 mL). The combined organic layers were dried over Na$_2$SO$_4$, filtered and solvent was concentrated. Purification by column chromatography on silica gel eluting with pentane.

100 mg of **8** (0.494 mmol) were isolated as a colourless oil in 77% yield over 2 steps.

^{1}H NMR (400 MHz, CD$_2$Cl$_2$) δ$_H$ 6.20 – 6.12 (m, 1H), 5.57 (t, *J* = 1.2 Hz, 1H), 3.19 – 3.10 (m, 1H), 3.09 – 3.00 (m, 1H), 2.38 (t, *J* = 2.7 Hz, 1H), 2.38 – 2.33 (m, 2H), 2.19 – 2.04 (m, 1H), 1.93 (d, *J* = 1.4 Hz, 3H), 1.83 (d, *J* = 1.3 Hz, 3H), 1.74 – 1.66 (m, 2H), 1.24 (s, 3H), 1.12 (d, *J* = 6.9 Hz, 3H). **^{13}C NMR** (101 MHz, CD$_2$Cl$_2$) δ$_C$ 140.1, 133.5, 132.9, 123.4, 83.8, 71.0, 43.0, 39.1, 27.5, 27.3, 26.2, 22.5, 22.4, 18.2, 17.4. **HRMS** (EI+) calculated for $[C_{15}H_{22}^{\bullet}]^+$ (M$^{\bullet+}$) *m/z* 202.1722, found *m/z* 202.1721. **[α]$_D$** (CHCl$_3$, *c* 0.37, 23 ºC) = –2.3 º.

(1a*S*,1b*R*,2*R*,6a*S*)-1,1,1b,2-Tetramethyl-1a,1b,2,3,4,6-hexahydrocyclopropa[*a*]indene-6a(1*H*)-carbaldehyde (67)

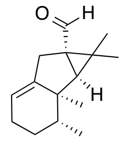

To a solution of **43** (10 mg, 0.049 mmol) in 0.5 mL (CH$_2$Cl)$_2$ was added 3,5-dichloropyridine-*N*-oxide (32 mg, 0.198 mmol) and IPrAuNTf$_2$ (4 mg, 4.9 μmol). The resulting mixture was stirred at 23 ºC for 3 h. After cooling to 23 ºC, the mixture was poured to a sat. sol. CuSO$_4$ and the extracted with CH$_2$Cl$_2$ (x3). The combined organic layers were dried over Na$_2$SO$_4$, solvent was evaporated and the crude was purified eluting with pentane/Et$_2$O 20:1.

7 mg of **67** (0.032 mmol) were isolated in 65% yield.

^{1}H NMR (500 MHz, CDCl$_3$) δ 9.39 (s, 1H), 5.29 (d, *J* = 3.1 Hz, 1H), 3.30 – 3.23 (m, 1H), 2.28 (dd, *J* = 16.6, 1.5 Hz, 1H), 2.07 – 2.00 (m, 2H), 1.93 (s, 1H), 1.63 – 1.55 (m, 1H), 1.58 (d, *J* = 1.3 Hz, 3H), 1.52 – 1.38 (m, 2H), 1.37 (s, 3H), 1.00 (d, *J* = 6.8 Hz, 3H), 0.85

(s, 3H). **^{13}C NMR** (126 MHz, $CDCl_3$) δ 202.3, 146.4, 119.0, 51.4, 46.4, 45.6, 35.0, 34.7, 29.8, 26.9, 25.6, 24.8, 21.1, 17.3, 17.1. **HRMS** (ESI+) calculated for $[C_{15}H_{22}NaO]^+$ $(M+Na^+)$ *m/z* 241.1563, found *m/z* 241.1555. **$[\alpha]_D$** ($CHCl_3$, *c* 0.57, 26 ºC) = –73.9 º.